DOCTOR OF PHILOSOPHY COMPUTER SCIENCE applied in GEOPHYSICS-ASTROPHYSICS2

SUPERVISORS

1.Dr. HORST HOLSTEIN

2.Dr. EDEL SHERRATT

The dissertation of Konstantinos P. Anastasiadis is approved:

Chair Date

Date

Date

Date

University of Wales at Aberystwyth

2010

To my daughter Katerina

ACKNOWLEDGEMENTS

Thanks to the people who made this dissertation possible, especially Horst Holstein my supervisor my wife Ramona who suffered with my absence from home, my mother and my daugter Katerina who inspired me.

NOTATION

Free-air anomaly To correct for variations in elevation, the vertical gradient of gravity (vertical rate of change of the force of gravity, 0.3086 mGalm-1) is multiplied by the elevation of the station and the result is added, producing the free-air anomaly.
$FA = g_o - g_t + (d_g/d_z)h$
where:
g_o = observed gravity (mGal)
g_t = theoretical gravity (mGal)
d_g/d_z = vertical gradient of gravity (0.3086 mGalm-1)
h = elevation above mean sea level (m).

Bouguer anomaly To isolate the effects of lateral variations in density on gravity, it is also necessary to correct for the gravitational attraction of the slab of material between the observation point and the mean sea level. This is the Bouguer gravity anomaly, which is given for static land measurements by the formula:
$BA = g_o - g_t + (d_g/d_z - 2\pi G\rho c)$
where:
g_o = observed gravity (mGal)
g_t = theoretical gravity (mGal)
d_g/d_z = vertical gradient of gravity $(0.3086 mGal \cdot m^{-1})$
G = gravitational constant $(6.672$ x $10^{-11} m\dot{k}g^{-1}s^{-2}$ or 6.672 x $10^{-6} m\dot{k}g^{-1} \cdot mGal$ or 6.672 x $10^{-11} N(m/kg)^2$
ρ_c = density of crustal rock $(kg \cdot m^{-3})$
h = elevation above mean sea level (m).

Isostatic correction The principle of isostasy states that mass excesses, represented by topographic loads at the surface, are compensated by mass deficiencies at depth which are referred to as isostatic roots. The effect of these mass deficiencies are not accounted for in the Bouguer reduction and there exists an inverse correlation between broad Bouguer anomaly lows and positive topography. The isostatic correction removes the gravity effect of the isostatic roots. The depth of the roots can be estimated based on the Airy-Heiskanen model (Simpson et al., 1986).

Terrain correction In areas of rough terrain, a correction for the effect of nearby masses above (mountains) or mass deficiencies below (valleys) the gravity measurement point can be calculated and applied. The final Bouguer gravity anomaly reflects lateral variations in rock density

Susceptibility Degree of magnetization.Susceptibility contrast, represents a geological surface.

Magnetic intensity The amount of magnetic flux in a unit area perpendicular to the direction of magnetic flow.

Matrix trace In linear algebra, the trace of an n-by-n square matrix A is defined to be the sum of the elements on the main diagonal (the diagonal from the upper left to the lower right)

LIST OF SYMBOLS

TABLE OF CONTENTS

Chapter 1

Introduction

1.1 Anomaly

An anomaly is any occurrence or object that is strange, unusual, or unique. It can also mean a discrepancy or deviation from an established rule or trend (http://en.wikipedia.org/wiki/Anomaly)

Gravi-magnetic anomaly

Living on planet earth we know that we are not living on a solid sphere whith uniform gravitation. A solid sphere could be an approximation of our earth. The shape of our planet spheroidal in shape, flatened in the poles makes the difference together with other physical effects like, water flow, movement of tectonic plates below crust, movement of stars and also various residing geophysical structures and minerals ,for the anomaly on gravity pull, thus hiding information about the terrestrial inside.
Anomaly is therefore the result of a different density contrast of earth's interior. Masses residing in the interior of different densities, transmit signals through gravity for their shape and density. People try to decode these signals using models of earth and the interior structures and computing the gravity using special aglorithms, the anomaly algorithms. The sensitivity of these algorithms depends on the order of the computed quantities, therefore at large distances the algorithms meet fixed precision problems. Gravity and magnetic anomalies of a particular source,cause small disturbances in earth's gravity and magnetism.When these are observed from a particular point they might give some significant information considered that the algorithm doesn't crush above critical distances.

The sources of the anomaly can be modelled with geometric 3D shapes. Maping of the anomalies can be done by airborn surveys using gravitometers. Differences in gravity can also be mapped by tracking the movement of two orbiting satellites, NASA says. As the Earths gravitational pull increases and decreases, the position of the satellites also change. In a Geophysical context, gravity anomaly of the geoid, is the difference between the observed and the predicted gravity, using as reference an attraction center of unified density and magnetization.

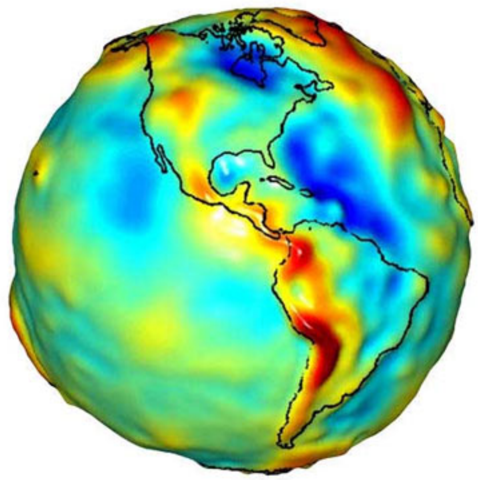

Figure 1.1: NASA image: maping of the Earth gravity, from satelite gravity pulls

Target modelling

To model the sources of the anomaly, target models are used. These are considered as geometric 3D shapes of unified density. Using models we try to approximate a specific geophysical structure The produced anomaly is computed and compared with the measurements, using inversion. Model targets must be valid objects, with closure and distinct interior and exterior.
In case of polygonal facets, the model will be a polyhedron convex or not convex, like in figure 1.21.3.

If the facets are triangles the shape formulated is a single tetrahedron or can be a tetrahedral model like in figure 1.4.

Anomaly algorithms

Is the class specific to the context, of algorithms computing numerically, gravity anomaly for a particular shape. To decode gravity signals to useful information of geophysical interest, particular algorithms have been developed based on the Newtonian Inverse Square Law of Universal Gravitation, called the anomaly algorithms. These algorithms compute the volume of a particular mass of unified density, from a distant point and they are formulated since 1960's. Most of them depend on a particular coordinate system resulting very complex computations. In contrast the use of a free from any particular coordinate system, vector derivation, relative to a local target origin, gains in decreased complexity lower the order of magnitude of the computed terms.

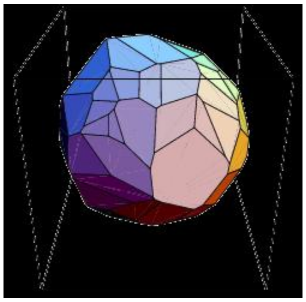

Figure 1.2: A convex polyhedron

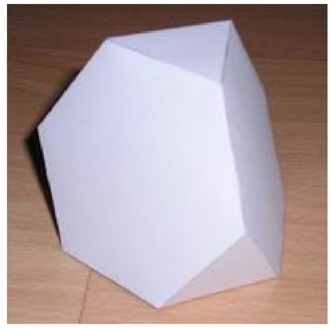

Figure 1.3: A not convex polyhedron

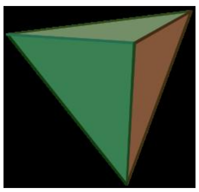

Figure 1.4: a tetrahedron

The formulation of the anomaly algorithms

Three error growth classes were depicted by the present research: The Vertex method, the Line method and the Surface method ordered by decreasing error growth.

Numerical instability of anomaly algorithms

Since the beginning of this project, anomaly algorithms suffered from numerical illnesses. Numerical inconsistencies arise as the observation point recedes from the target

Floating point finite precision of computer systems

Limited floating point precision double or single, cause the performance of the anomaly algorithms at far away distances from the target to be experience unstable behaviour, developing an error growth.This error growth bounds their operational horizon at pre-defined critical distances from the target up to the observation point.

The error growth

The work of Holstein et al.

The initiating trigger for this project, was the Holstein et al. work on the field. Since past years 1996 to 2005 the line of research had lead to improvements on numerical stability using mathematical analysis to cancell any high order evaluations, before programming. The research line was including the identification of any error growth patterns and development of theoretical trends, target modelling and migration, with new models of new shape but equal volumes and a detailed numerical analysis of all the algorithmic anomaly terms and contributions.

Since the beginning of this project a new method with decreased error growth was found, following the line method of the error growth invented by Strakhov et al.([40]), an improved version of Pohanka Vertex method, known as the Surface method by Holstein([26]). This method raised new issues for internal cancellation of dominant terms. It used differencing on arctan terms leading to a series evaluation of an exact number of terms, according to the available precision. This finding was firing a new era, overcoming all the past algorithms with one order of magnitude less, of the relative distance from the target local origin to the observation point.

The research and analysis of new methods, in the context of improving the performance of the anomaly algorithms by any means, triggered this thesis towards contributions for creating a clear master plan as a road map from the given state of the art, to another extend where the research will lead, until the completion of this project.

1.2 The thesis plan

The motivation that inspired the development of this project was emerged in 2005, when the need to create a road map to the future of the anomaly algorithms regarding the research horizon of Holstein et al., became apparent. The objectives were spread around a central point: The development of anomaly algorithms with improved range of operation and increased efficiency .

Due to the fact that the existed anomaly algorithms in the literature, suffered from inconsistencies and deficiencies due to the rounding error of order $\alpha\gamma^2\epsilon$ magnified with a γ^{-3} factor after the necessary integration steps to convert integrals from volume to vertex evaluations, limited precision was exhausted at far distances from the target with meaningless results to be delivered.

Methods of anomaly algorithms were classified according to their range of operation and at each class a particular critical point was assigned, beyond which the results were not any more enclosing any useful gravity and magnetic information about the source target.

This project followed a successful root to illustrate the solution of various problems on the way, and present the highlights of a complete research around gravity and magnetics since 2005.

The line of research before 2005 summarized in chapter 2 previous literature.

Chapter 3 explains the geometry of a target facet and an edge with all the associated quantities and vectors, before hand.

Anomaly algorithms compute very small differences between very large numbers as the target recedes from the observation point. These calculations at far distances (γs) become sources of instability as the computer precision is stressed to the limits(ϵ).

Stability issues for the anomaly algorithms are illustrated using the case of a receding edge chapter 4.

In this study we analyze the source of inconsistency as the target is getting far and analytical stabilization method is discussed canceling dominant terms before computation, offering convergent error growth.

In chapter 5, the physical problem for the calculation of the anomaly is derived in anomaly compact formulas of pre - estimated error growth, under a triangular concept, environment in which it was expected our 3D target models to experience decreased computational complexity, in contrast to their polyhedral counterparts.
Gravity and magnetic formulas are searched for invariable features, with a common term to emerge and can be used as the constructor quantity for all gravity and magnetic anomaly calculations and therefore express them in a single form.

As anomaly formulas involve calculation of small angles such as arctan and arctanh, Arctan arguments of lower complexity were searched in the literature.It was found that the Oesterom's formula for the solid angle of a facet([35]), suitably modified ([14])could replace the mathematically equivalent arctan counter parts in the Line and Surface methods. Because new term was evaluated at facets and not to edges,the result appeared of lower order of complexity initially. In fact the anomaly suffered from the higher order term and thus the error growth was maintained as in Line and Surface methods. As expected we had contribution, regarding efficiency.
This contribution is described with counting operations tests in chapter 6. The improved performance of the Oesterom formula gave us the motivation to step towards finding decreased efficiency on triangulated targets, with success. The new Oesterom version was tested in the most challenging representatives of algorithms the Line(Strakhov) and the Surface(Holstein) methods, under the lights of increased efficiency. We used the performed counted operations per observation point as our metrics. The results show superiority of the Oesterom variant at all cases of the anomaly comparing to the number of equivalent counts for any triangulated polyhedron. We used Euler's formula for polyhedra to establish a common measure. Only in the potential case the result involved a very small increase and we consider it as a singularity of the particular case. Field and gradient computations, found to be more efficient, because their process involve more complex edge-side operations , and so the Oesterom variants on these anomalies, appeared to have apparent superiority against their Strakhov counterparts. The results gave us the motivation to proceed to an article around the triangulation efficiency issues that we discovered during our research, with the title "'Gravimagnetic Anomaly Formulae for Triangulated Homogeneous Polyhedra"', presented in the EAGE London Conference during 2007.([22])
In chapter 7 we examine power series especially Taylor, for the contributions to the analytical approach of decreasing error growth of the anomaly methods before computation. An algorithm was implemented to choose a best fit of the infinite terms to include, analytically simplifying algorithms canceling dominant large terms before computation. This was experienced , in the Surface method, decreasing this way orders of complexity from γ^3 amplification factor.

The exactly to the precision computed series now, increase the number of the useful bits in favor of the distance of our observation.

In addition to this chapter, we describe the contributions of the power series and especially Taylor,with example and we explain why homogeneous polyhedra may usefully be augmented by Taylor series expansions around an observation point. Our research on this sub-objective ended successfully with an article titled "'Gravity potential series expansion for homogeneous polyhedra"', presented in Rome, in 2008.

Thereafter by obtaining the expansion coefficients in a way that allows rapid development competitive with the other expansion methods, the approach can be extended to include field and field gradients.
Inspired from the strategy to adopt one common to the facet observation vector, as in the surface method, to decrease L order differences of vertex computations, to α order differences from the local origin canceling dominant terms before computation, we developed a plan to explore targets not as 3D solids, but as stacks of plates of a limiting thickness,deriving a 2D evaluation. Integrating by parts the thin slices for the our thickness parameter, we resolve the initial 3D polyhedral solid.
The work was published in the article:
"'Gravity potential series expansion for homogeneous polyhedra"' presented at Rome in the EAGE conference in 2008.
In chapter 8 an attempt to explore the relation between the finite and limiting forms by exploring elongated prismatic targets was made.The target was viewed as a stack of thin plates of a finite number. In the context, stabilized algorithms were found and compared to unstabilized algorithms and the effects from the stabilization of the algorithms for this special case, were explored. Both algorithms were found to approach initially the limiting forms. For very long prismatic targets however, unstabilized algorithms lost control over numerical error and deviated more and more from the limiting forms. The stabilized algorithms using analytical cancellation of dominant terms, approached limiting forms, up to a point where only the finite precision prevented further approach.
The work was published by the article:
"'Gravimagnetic anomaly formulae for extended homogeneous Prisms"' presented at the EAGE conference at St.Petersbourg, Russia in 2008.
Next, the need for developing algorithms for thin planar sheet target models became apparent.
In chapter 9 based to the similarity concept to explore thin sheet variants for gravity and magnetic anomalies. The polyhedral approach was adapted successfully to the thin sheet case. Using the centroid approach of the surface method on the thin sheet case resulted a zero error growth stable algorithm.
The work was published in an article with the title:
"'Thin polygonal sheet anomaly"' presented at the SAGA conference in S.Africa, in 2009 winning the 1st prize for its presentation by H.Holstein.
In chapter 10,using the centroid of a target to combine anomalies of thin-sheet and a polyhedral target. Point source anomaly applied at the centroid of a polyhedral target, reflected a lower bound of the floating point precision.
Examining the relative difference between the thin-sheet and point source we demonstrate that the Line method initialy converges down to a point where the internal cancelation between dominant terms, undertakes and the error growth takes the lead, increasing the ratio

without bound. In the Surface method the decrease continues after the Line method breakdown, until it converges to the point source.
The work was published in article under the title:
"'Asymptotic anomalies of Thin Polygonal Sheets"' presented at the EAGE conference, St.Petersbourg, Russia in 2010.
In chapter 11, we combine thin-sheet formulas with the polyhedral presented under the similarity concept, a new stable algorithm namely Exact Finite Expansion was found to experience zero error growth. The derivation of an exact finite expansion for the uniform thin polygonal sheet gravitational anomaly, was given by separating the dominant equivalent point source term and an exact higher order perturbation term expressing the finite target geometry. The method was based to the fact that the polyhedral anomaly formulae may be regarded as a weighted sum of sheet formulae, it is anticipated that the point source contributions from each facet will combine, allowing a stable separation into a volume point source and perturbations from the finite geometry.
This work was published in the article:
"'Exact Finite Expansion method for thin sheets"', presented at the EAGE Conference Exhibition incorporating SPE EUROPEC 2010 in Barcelona, Spain.

Finally chapter 12 reflects the construction of a stable polyhedral magnetic anomaly formula. The formulation of a zero error growth method has not been achieved previously. On account of gravi-magnetic similarity, stable algorithms can be found for all the standard gravi-magnetic anomalies of uniform polyhedral targets.The formula was based to the fact that the dominant $O(\gamma^2)$ terms were captured entirely by a central term, the point source term, while all the target anomaly is now regarded as a sum of sheet contributions from the polygonal facets instead of vertex contributions around the edges.
The work in this chapter sealed the present research by publishing an article under the title:
"'A numerically stable magnetic anomaly formula for uniform polyhedra"', presented in SEG conference in Denver,Colorado,USA in 2010.

Chapter 2

Literature review

2.1 The research background

The gravity and magnetic field called hereafter in this thesis gravimagnetic, is the longest studied of all the geophysical properties of earth. Gravity and magnetic field measurements are consequences of the physical laws governing them(such as the Newtonian law) and of the subsurface structures.

Over the past 10 , years the line of research of Holstein et al. at the Universtity of Wales at Aberystwyth, proposed a new perception of gravity and magnetism.

Team work produced metrics to classify anomally algorithms according to their enhanced complexity.

Over the past 10 , years the line of research of Holstein et al. at the Universtity of Wales at Aberystwyth, proposed a new perception of gravity and magnetism.

Team work produced metrics to classify anomally algorithms according to their enhanced complexity.

It was proved that gravity and magnetism can be computed in one package, linked with a common computation quantity named b_{ij}, [33]. Therefore gravity and magnetism are linked together with same equations offering a wide field for further investigation.

A proposed geological model of the subsurface structures is tested for its observational consequences, provided the algorithms for doing this have been developed.

A target model is a generalization of a solid object of uniform density.

Forward strategies use model targets to compute all gravi-magnetic effects from several distances. Targets are modeled in closed form in order to be validated numerically.

A wide variety of geometrical shapes may serve as target models such as polyhedron,tetrahedron, sphere,cone, but the most representative target is the polyhedral target because its realistic complexity exersize the gravi-magnetic calculations stressing to the limits the computer system. For the purposes of the present thesis, a polyhedral target, called standard polyhedron,a tetrahedron and the standard polyhedron triangulated, vectorially represented were numerically evaluated from an observation point to the local origin of the particular target. Anomaly algorithms were implemented in Java and the results taken in double precision included the expected error growth for all different classes of anomaly methods and the output was validated using a 100 digits precision system, like MAPLE. For the purpose of inverse modelling, anomally computations , may have to be carried out many times. Therefore there is interest in developing efficient algorithms for the task.

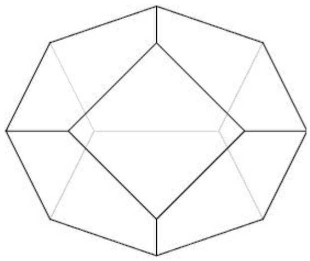

Figure 2.1: Polyhedron-9 facets

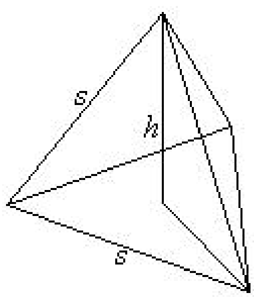

Figure 2.2: Tetrahedron-4 facets

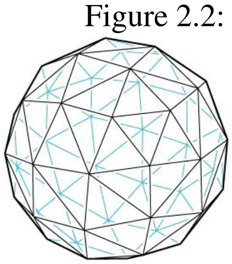

Figure 2.3: Polyhedron-16 facets

Backward strategies (reverse problem) use the results of the forward process to form predefined critical measurements and compare them with real-time geophysical surveys trying to establish relations and suggest candidate solutions. Many research lines of this type have being attended in the past, all leading to the problem of non-unique solution due to the actual target irregularities. So most of them lead to many types of targets, selecting at the very end a survivor solution, using artificial intelligence techniques like, genetic algorithms. Regular targets may form a collection of different types of models. For each different model gravity and magnetic calculations may be derived.
In the forward context the present research line uses Gravity and Magnetism in one package to investigate the computational error behavior over a wide range of remote observation points at long distances and different orientations above, in or on theoretical targets, represented by different models and orientations .

Gravimagnetic theory provides the important investigative structure in geophysical surveys for delineating subsurface structures.
Gravimetry relies upon the fact that subsurface density variations from place to place will affect the above ground acceleration due to gravity in a small but measurable way. Similarly, many rocks have a magnetic susceptibility that responds to the earth's magnetic field, and distorts it, again giving rise to above ground measurable effects. During the past 20 years, airborne gravity and magnetic surveys have become routine, allowing rapid surveys to be carried out even where there is an absence of accessibility on the ground. Thus gravimagnetic surveys are often the first to be carried out, with relevance to locating oil and mineral deposits. The aim is to image the earth's interior by scanning it above the surface where it is accessible.
Gravity and magnetics by themselves do not provide sufficient information to do this, but they do provide very valuable "signatures" that can often be interpreted in a meaningful way in the geological context of the survey site.
A development in the last 10 years is airborne gravity and magnetic field gradient measurement. In this case, the three spatial (x,y,z) rates of change of the field vector are measured, giving rise to a 9-component entity called a tensor. The interest in gradiometry lies in the fact that the boundaries of gravimagnetic sources are delineated much better in the gradient data, allowing better interpretation.
Current data acquisition techniques are still imperfect, and yield a lot of noise compared to the signal, necessitating compensation methods for removing far stronger signal sources (e.g. the aircraft's acceleration in the gravity case) than the geophysical source. There is then an issue of quality control: how can the signal be "cleaned up" before it is used in geophysical interpretation. There is an increasing merger of this science with techniques in image processing, in which sources of image degradation are "filtered out".
Because massive data sets can now be captured over relatively short periods, there is an ever increasing need to apply automated methods for data analysis.
My thesis will attempt to make contributions towards that aim both in the modeling of gravimagnetic effects, and in their interpretation. I have made a start with the former problem, and this will provide tools for generating synthetic data which I can then use in the latter interpretation problem and estimate the effect of noise on a particular interpretation procedure.[3]

2.2 The derivation of the analytical formulae for gravimagnetic anomalies

I shall first summarise the classification of algorithms that allows both gravity and magnetic algorithms to be classed into "Vertex", "Line" and "Surface" methods.
This work, published by Holstein and co-workers ([2]-[11]), forms the basis of the developments to be described in this thesis.This basis allows useful definitions of algorithm accuracy and efficiency to be made, and is the basis for software reliability control.
Physical calculations will require the appropriate physical constants (constant of universal gravitation, magnetic permeability of the medium) in order to produce results in SI units. These results are commonly described as the "anomaly", that is the disturbance produced

by the modelled target body that is the causative (or is the source) of the calculated field (or potential or field gradient, etc.). The calculations for a target body of homogenous properties can be regarded in two parts: the first is purely geometric (depending on the shape of the target and the location of the observation point), and the second is the conversion of the geometric-based calculations to SI units by multiplication by the relevant physical constants. At this stage I am concerned with obtaining a good understanding of the geometric-posed algorithms.
The concern in the thesis with computational efficiency is justified by noting that ”forward” anomaly algorithms are invariably used in an iterative context in problems of inversion, where a target model is to be delineated from observational data. Possibly hundreds of thousands of iterations are required. Any saving of time in the basic step is therefore a welcome improvement.

2.3 Classification of anomaly algorithms

Closed anomaly formulae for gravity and magnetics in the context of uniform polyhedral targets have been known for some time [25], and special cases for rectangular prismatic targets much earlier [11, 28]. These early approaches are characterized by formulating the physical problem in facet-oriented Cartesian coordinate systems. It meant that there was an artificial alignment with a facet normal and an edge. A choice of a different edge for alignment would involve a different formula, with different rounding error. Moreover, the related problems of finding gravity and magnetic formulae was treated in separate derivations, even though the resulting formulae had obvious similarities.
Strakhov and coworkers [40, 27, 34, 11] used complex variable theory to formulate the problems in a remarkably far-sighted way. The detailed derivation was difficult to follow, and these papers had a delayed impact in the western literature. The authors presented a polar form of the solution, in which the observation point played a fundamental role as reference point. The solution contained quantities that would be best described via the operations of the scalar dot product projection of one vector on another, but this was not explicitly used, making the details difficult to follow. The major contributions, however, were firstly to express the potential and field, whether of gravitational or magnetic origin, in terms of one set of functions, one per each edge of each facet, summed with geometric weighting factors appropriate to the particular problem. Commonality of the functions was seen to be theoretically demonstrable, and not an accident for some particular derivation. Secondly, they showed that different forms of anomaly formulae, mathematically equivalent, can have quite different rounding error growths with increasing distance of the observation point from the target, and they recommended one form as being superior to the one generally used.
In the western literature, [39, 10] first gave a fully vectorial formulation that was not linked to a specific choice of coordinate system, though in Goetze’s case the result was ”reverse engineered”, having first adopted specific coordinate systems and then eliminated them again.
The first truly vectorial derivation of the gravity field anomaly formulae was given by Hol-

stein and Ketteridge [16] This paper is seminal to the subsequent work on polyhedral target anomaly modeling, and is therefore discussed in some detail.

2.3.1 1996 H Holstein, B Ketteridge, "Gravimetric Analysis of Uniform Polyhedra",Geophysics, 61(2):357-364.

The authors were the first to appreciate that the original volume integral over the target interior could be treated, in successive steps, by Gauss' divergence theorem to convert the volume integral into a sum of surface integrals over the target facets, by Stokes' integral theorem to transform each surface integral to a sum of line integrals around the polygonal facet boundary, and finally the explicit evaluation of each line integral. Prior to this paper, there was a reluctance to employ Stokes' theorem - the approach was to treat the surface integral as a degenerate 2D volume integral and to use Gauss' divergence theorem a second time. This could only be achieved by abandoning coordinate independence and transforming a 2D coordinate system to lie in the facet plane. Use of Stokes'theorem allowed the formulation to maintain coordinate system independence. Hence all quantities in the formulae could be related directly to the geometric data defining the target and observation point location.

The dependence of all terms on the defining data made in possible for Holstein and Ketteridge to trace the numerical error growth inherent in the formulae. It allowed a powerful but simple theory for error growth to be stated, in which the critical quantities are the apparent angular size γ that the target subtends at the observation point, and the machine precision ϵ in which the calculations are made. For a target of a given linear size α, at a typical distance δ from the observation point, $\gamma \approx \alpha/\delta$, that is, γ decreases with increasing target distance. The relative error η in the calculated anomaly is then given by the relation $\eta \approx \gamma^{-(2+\phi-\kappa)}\epsilon$, where κ is algorithm dependent and ϕ is a number between 0 and 1 (like a foreshortening cosine: if the quantity sought is along the principal direction of the result (e.g. vertical gravity), then the factor ϕ is 1, if it is at right angles (e.g. the horizontal gravity component caused by a mountain when the principal field is vertical) then the factor is 1). Holstein and Ketteridge found that κ = -1 holds in the standard algorithms (such as given by Goetze). The worst case scenario is therefore $\eta \approx \gamma^{-(4)}\epsilon$, that is, the relative error grows as the 4th power of the target distance. When the target distance is sufficiently large to make $\gamma \approx \epsilon^{(1/4)}$, then $\eta \approx 1$, i.e. the relative error is of order unity, leaving no significant digit left in the solution. Effectively, the method has an operational horizon. When the target distance exceeds this critical distance from the observation point, all significance in the solution is lost. In single precision, $\epsilon \approx 10^{-7}$, so $\gamma \approx \alpha/\delta \approx 10^{-1.7} \approx$ 1/60. Thus, when the observation point is at 60 target diameters distance, the numerical algorithm fails. There will have been a steady degradation of solution quality up to that point.

Holstein and Ketteridge noted that to obtain lower error growth, we could work in a higher precision (e.g. double precision, $\epsilon \approx 10^{-17}$), or find an algorithm for which γ is lower (or both). They found the source of the error growth to be destructive cancellation during summation, in the sense that the more distant the target, the larger the terms to be summed, yet the smaller the final result. They therefore looked for ways in which the summation could in part be carried out, so as to cancel dominant terms analytically before computation. They found that the first integration of volume to surface integrals would have resulted in a formula with κ = 1, (leading to a notional "surface" method), the next integration from surface to line integrals would have resulted in a formula with κ = 0, (leading to a notional "line" method), and the final integration of line integrals to evaluation at the lower and upper limits (the line's end points at facet edge vertices) results in a formula with κ = -1, leading to the "vertex" method. Unfortunately, the "surface" and "line" methods derived in this way would not have given closed solution, and the integrals would have to be evaluated numerically. However, by reverse engineering the vertex method, they did find means to cancel the dominant terms, and thus achieved closed form "surface" and "line" methods. The arithmetic complexity of the line method is about the same as the vertex method, so it is arguable that the line method could replace the vertex method. The surface method, however, is more complex, and one would not use it unless one is working near the horizon limit for the line method. Holstein and Ketteridge claimed that all polyhedral target anomaly algorithms are bound by the error formula in normal usage. Thus, claims in the literature (see e.g.[26]) that one algorithm is superior to another could be quantitatively tested, first by comparing κ-values, and for the same κ-values, comparing arithmetic operation counts. The paper by Holstein and Ketteridge is primarily concerned with developing the theoretical and practical concepts for the vertex, line and surface methods. The next paper by Holstein et al. applies this classification to the main contributors of anomaly formulae in the literature. This paper is discussed next.

2.3.2 1999 H Holstein, P Schorholz, A J Starr, M Chakraborty, "Comparison of gravimetric formulas for uniform polyhedra",Geophysics, 64, 1438-1446.

This paper's agenda is to classify all previously published gravity algorithms for uniform polyhedra according to their error growths, into the vertex, line and surface methods. The great variety of published formulae is encompassed by this approach. A correctness test is provided, and two published solutions are shown to contain subtle errors. Objective comparison of gravity anomaly algorithms becomes feasible. Theoretical arguments are provided as to which class (vertex, line or surface) a given published algorithm belongs, and these classifications are verified computationally. The algorithms from the 1999 paper were updated by taking the best features of algorithms published in the literature into account. The algorithm presented by Strakhov and coworkers [34, 11] is found to be superior in arithmetic counts to that of Holstein and Ketteridge, and a hybrid version taking the best features of both is adopted. Also, a new analytical surface method is presented (the version in the 1996 paper presented a numerical surface method). The revised vertex, line and surface algorithms have a reduced arithmetic complexity compared to their predecessors. Particular attention is drawn to the concept of calculation reuse, in which quantities are identified that are used at multiple stages in the algorithm execution. This arises because the topology of the polyhedral target is such that each edge is shared by two facets. Certain calculations, associated with that edge, could therefore be shared. This implies either a certain order of computation (not immediately obvious), or a suitable data structure that allows previous results to be recalled. For example,Haroon and Lakshmi [9, 1] used doubly linked lists, and Sherratt [33] used a graph access technique of Dijkstra [5] A further distinction is made between quantities intrinsic to the polyhedron, (such as the area of a facet or the length of an edge), that are independent of the location of the observation point; and extrinsic quantities, which cannot be know until the observation point is chosen. Clearly, intrinsic quantities need only be calculated once, but must be available at subsequent stages, implying a suitable data structure with a retrieval mechanism. The previous two papers by Holstein and coworkers were specifically for gravitational anomaly calculations. The next papers generalise this work to encompass gravity and magnetic calculations into a single framework.

2.3.3 2001, H Holstein, Discussion on "An analytical expression for the gravity field of a polyhedral body with linearly varying density",R.O. Hansen, Geophysics, 66, 1327-1328.

The linearly varying density gravity anomaly is derived by Hansen (1999, [30]), but there is an error at an early stage of the derivation, raised in this discussion. Hansen's is one of two papers which have considered, before Holstein, the gravity field anomaly from a polyhedral target of linearly varying density. The other paper is by (1998, [39]). The Holstein paper (2003) greatly extends Pohanka's and Hansen's works, by
(a) including the magnetic case,
(b) deriving potentials and fields
(c) deriving two classes of algorithm (vertex and line)
(d) stating the appropriate error analysis for the algorithms
(e) stating the conditions for singularities
(f) computing model case studies, for algorithm verification

The extension to the surface method (with further reduced error growth) was not achieved in this paper, but the necessary extensions are outlined in Holstein (2003, [12]). During the past 30 years the closed analytical formulas for computing gravity and magnetic anomalies received wide attention but the numerical suitability across a computer based formulation did not received critical attention. Analytical formulas for computing gravity anomaly of a uniform polyhedral body are subject to numerical error that increases with distance from the target while the anomaly decreases [26]. A substantial part of the present research has being dedicated to the classification of all existing formulas for computing gravi-magnetic anomalies, according to a pre-defined error growth. This classification led to 3 classes of error growth namely Vertex, Line, and Surface.

2.3.4 2002a, H. Holstein, "Gravimagnetic similarity for uniform polyhedra",Geophysics, 67,1126-1133.

This paper generalises the previous gravity results to include the magnetic case, and embraces both potential and field calculations. The paper notes that gravity and magnetic solutions are expressible in terms of the same transcendental functions. The origins of such similarity are investigated mathematically, and the historical realisation of the similarity is chronicled. The paper puts forward a new scheme that embraces all the standard potential and field anomalies of gravitational and magnetic origin. The result is a schema in that is very suitable for implementation and for analysis.It includes a clear statement of singularities. By highlighting the similarities between the gravity and the magnetic cases, the correctness test and taxonomy (vertex, line, surface methods) of Holstein and coworkers (1996, 1999) become applicable to all published solutions in gravity and magnetics for uniform polyhedra. Gravity and magnetic anomaly algorithms, previously treated separately, become amenable to common construction and an identical error analysis, namely the error anlysis of Holstein and Ketteridge (1996,[16]), whether for potentials or fields. This is significant for the construction of software with a priori performance bounds. The paper notes the futility in providing distinct derivations of the gravity and magnetic cases. Each can be deduced from the other. Much of the history of anomaly formulae is saubject to this criticism. The paper acknowledges the retrospective debt to Strakhov and coworkers (1986, [34, 11]) that spelled out the similarity concept, without it having been understood in the subsequent literature until the appearance of the paper under discussion.

2.3.5 2002b H Holstein, ”Gravimagnetic invariance for uniform polyhedra”,Geophysics, 67, 1134-1137

The gravity and magnetic solutions are related through differentiation, as expressed by Poisson’s relation [20]. This means the magnetic anomaly formulae could be derived from the gravity formulae by a process of analytical differentiation. This would lead one to expect much more complicated magnetic formulae. The paper shows that the simplicity of the magnetic formulae, and the simplicity between the potenial and field formulae (again differentially related) is due to certain terms summing to zero. The effect, therefore, is as if certain terms are constant (since they differentiate to zero). In fact, the terms are not constant, but have zero sum. These terms are named ”invariants”, and they explain why the formula for potentials and fields, in gravity and magnetism, are so similar - differently weighted sum of the same functions. As pointed out above, this has a profound consequence on gravimagnetic anomaly formula programming - essentially all quantities can be computed in one program, with only the summations in the inner and outer loops (over facet edges and facets) having different weight factors applied. Another practical consequence is that, since gravity and magnetics have a differential relationship, this must be reflected in the computational results.Therefore, numerical differentiation of the gravity results should give values close to those obtained directly (and more accurately) by the corresponding magnetic formulae. Such numerical checks are demonstrated in the previous paper, and give a stringent test for correct implementation. A further powerful check is that at far distances from the target, polyhedral sources will act approximately like point sources, whose closed form solutions are known. For from the target, the error growth is best observed. Hence, a correct implementation must reproduce the differential relationship in the solutions at near and moderate target distances, and at large target distances must present the correct error growth for the method. This leads to a variety of powerful consistency checks that computed solutions must satisfy. These checks will be applied to the new anomaly formula to be developed under item iv section 2.

2.3.6 2003a, H Holstein, "Gravimagnetic anomaly formulas for polyhedra of spatially linear media",Geophysics, 68 No 1, January-February, 157-167.

The author used the methodology of the 2002 [15] paper, and found it was found ideal for extending the case of anomalies from uniform polyhedra to those of spatially linearly varying density or magnetisation. The gravity field case had been published in the recent past by two other authors (see below). This paper applies the similarity concepts of 2002a,b [**?** 15] to give the comprehensive gravimagnetic anomalies (gravity potential, gravity field, gravity field gradient, magnetic potential, magnetic field) for the linear medium case under one common approach, and provides the accompanying analysis concerning singularities and accurate computation. The classification of vertex and line algorithms is carried over to the linear medium case. In this way, an algorithm of superior error growth is constructed, and its theoretical properties are verified. The results are applicable to algorithms for all the gravimagnetic anomalies. The results are a substantial advance on previous work in the literature, which only deals with the gravity case.

2.3.7 2003b, H Holstein, EM Sherratt, "Performance of gravimagnetic anomaly algorithms for uniform polyhedra", International Geophysical Conference and Exhibition, Russia, Moscow, Sovincenter, September 1-4, 2003, OS9-1425 1-4.

This paper gives the algorithmic steps and finds close experimental error growth compared to that predicted by theory. Its relies heavily on the similarity formulation (2002a). grounds of absence of references (2002a/b not having appeared in print), length and specialisation. This is a shortened version of a much more comprehensive paper to be submitted to Geophysics. The paper presents a compact form of the anomaly formulas which allows the theoretical a priori templates to be derived. The computational results demonstrate automatic method selection to accomplish maintenance of rounding error to a specified level in magnetic field computations throughout an increasing target distance. A new vector term bij is being introduced. This term appears to be common to all gravimagnetic expressions namely the gravitational potential, field, field gradient and magnetic gradient, and represents a closed form expression of the gravity anomaly evaluated at each vertex. It appears both as a 3 dimensional vector and as a dimensionless scalar, easily computed in both forms for all different error growth methods namely vertex, line and surface, unifying the gravity and magnetic theory in one single package.

2.3.8 2003c, H Holstein "Asymptotically improved gravimagnetic anomaly formulas for linear medium polyhedra". SEG 2003 International Exposition and 73rd Annual Meeting, October 2003, Dallas. 1-4. Dallas, Texas October 26-31, 2003, http://www.seg.org

This paper extends Paper 2003a to the "Surface Method" for accurate distant target calculation. It completes the taxonomy for the Linear Medium polyhedral target, which now mirrors results for the uniform medium case in giving three algorithms (Vertex, Line, Surface) of successively improved error growth with target distance.

Chapter 3

Target geometry

3.1 Typing conventions

Target geometry is illustrated using 2D figures and expressed with typed quantities of vectors and scalars, manipulated with their related operations. We adapt our notation conventions to the related literature of the published papers starting from Gravimetric Analysis of Uniform Polyhedra, Holstein and Ketteridge,1996([16]).
Therefore we use the bold typed letters to denote vector quantities while the not bold typed letters to denote scalars.

Also we use the hat symbol above bold typed letters($\hat{\mathbf{n}}$), to express the unit vectors.

To express vector operations, we use the $\mathbf{a} \cdot \mathbf{b}$ and $\mathbf{a} \wedge \mathbf{b}$, to denote dot and cross products between two vectors $\mathbf{a}, \mathbf{b}$, respectively.

3.2 The quantity γ

$$\gamma = \frac{\alpha}{\delta} \tag{3.1}$$

where:
α= target dimension.
δ= the distance of the target(origin) to the observation point. The γ quantity is getting very small as the target recedes from the observation point. This is the cause of the numerical breakdown of the algorithms when the finite precision of the computer system is exceeded.
Order γ ($O(\gamma)$)is the order of an operation where γ quantity has to be computed.

3.3 Edge quantities

We start from figure 3.2, with an observation point P and a subobservation point P_i projected on to a facet plane.
In general, an orthonormal triad of unit vectors ($\hat{\mathbf{h}}_{\mathbf{ij}}$ the unit horizontal,$\hat{\mathbf{t}}_{\mathbf{ij}}$ the unit tangent,$\hat{\mathbf{n}}_{\mathbf{i}}$ the unit outward normal) is assigned to each edge in order to represent a x,y,z coordinate frame,unit normal being a vector vertical to the facet containing the edge, unit tangent being the vector across the edge and unit horizontal being the cross product of unit normal

and unit tangent vertical to their plane, taken all in an anticlockwise direction, with components, the projections of the position vector r on to the axes, represented by the quantities: u_i, l_{ij}, h_{ij}. The first being the component of r on to the normal $\mathbf{n}_i$, the second the component of r on to the tangent $\mathbf{t}_{ij}$, the third the component of r on to the horizontal vector $\mathbf{h}_{ij}$. More analytically, the quantities $\mathbf{r1}_{ij}, \mathbf{r2}_{ij}$ represent the position vectors of 2 successive target vertices of the edge dl, relative to the observation point P and its mirror subpoint P_i.(figure 3.2).

Quantities $l1_{ij}, l2_{ij}$ represent the projections of the position vectors on to the edge dl. Subscripts i,j define facet and edge respectively.
The vertical and horizontal components of the position vectors are represented by u_i, and h_{ij} respectively. The normal to the facet is expressed by $\mathbf{n}_i$ and is vertical to the plane of the facet S_i.With $\mathbf{R}$ being the position vector relative to P_i,(figure3.2) for any point on the facet S_i, quantities u, r, R must satisfy,

$$u_i = \mid \mathbf{r} \cdot \mathbf{n}_i \mid \tag{3.2}$$

$$r^2 = R^2 + u_i^2 \tag{3.3}$$

Consider figure 3.3 where the polygonal facet i belongs to a polyhedral target of unit density ρ and unit magnetization vector $\mathbf{M}$ consisting of straight line edges ∂S_{ij}. There are 3 subscripts k,i,j. Ijs target a particular facet-edge while k a particular vertex(k=1,2). For example $\boldsymbol{\rho_{1ij}}$ is the position vector of vertex 1, edge j and facet i relative to the local origin. Edge vector $\boldsymbol{\rho_{2ij}} - \boldsymbol{\rho_{1ij}}$ is directed in a right hand sense anticlockwise around the outward facet normal.

$\mathbf{A}_i, A_i$ are the vector and scalar facet areas while L_{ij} is the scalar edge length and the facet edge orthonormal triad is formed from $\mathbf{n_i}, \mathbf{\hat{t}_{ij}}, \mathbf{\hat{h}_{ij}}$ i.e the unit outward normal, the unit edge vector or tangent and the facet plane edge outward edge normal or horizontal. Primed quantities in equation **??** are the edge successors of the unprimed ones. The vertex position vectors $\boldsymbol{\rho_{kij}}$ are taken relative to an origin local to the target while a typical observation point is denoted by $\mathbf{r_{obs}}$

$$2\mathbf{A}_i = \sum (\boldsymbol{\rho_{2ij}} - \boldsymbol{\rho_{1ij}}) \wedge (\boldsymbol{\rho_{2ij}} - \boldsymbol{\rho_{1ij}}) \tag{3.4}$$

(ref.:Appendices A-cross product)

The scalar area is:

$$A_i = |\mathbf{A}_i| \tag{3.5}$$

The edge length:

$$L_{ij} = |\boldsymbol{\rho_{2ij}} - \boldsymbol{\rho_{1ij}}| \tag{3.6}$$

The unit normal:

$$\mathbf{\hat{n}_i} = \mathbf{A_i}/A_i \tag{3.7}$$

The unit edge vector:

$$\mathbf{\hat{t}_{ij}} = (\boldsymbol{\rho_{2ij}} - \boldsymbol{\rho_{1ij}})/L_{ij} \tag{3.8}$$

The unit horizontal:

$$\hat{\mathbf{h}}_{ij} = \hat{\mathbf{t}}_{ij} \wedge \mathbf{n}_i \tag{3.9}$$

The vertex position vector $\mathbf{r}_{kij}$ in relation with the local origin position vector $\mathbf{r}_{obs}$ and their projections on the facet-edge orthonormal system $(\hat{\mathbf{n}}_i, \hat{\mathbf{h}}_{ij}, \hat{\mathbf{t}}_{ij})$ can be expressed as:

$$\mathbf{r}_{kij} = \boldsymbol{\rho_{kij}} - \mathbf{r}_{obs}, k = 1, 2 \tag{3.10}$$

or

$$\mathbf{r}_{kij} = \boldsymbol{\rho_{kij}} - \mathbf{r}_{obs} + \boldsymbol{\rho_0}, k = 1, 2 \tag{3.11}$$

in case that $\boldsymbol{\rho_0}$ represents the absolute coordinates of the local origin. Their components are:
The normal component:

$$u_i = \mathbf{r}_{kij} \cdot \mathbf{n}_i, k = 1, 2 \tag{3.12}$$

The horizontal component:

$$h_{ij} = \mathbf{r}_{kij} \cdot \mathbf{h}_{ij}, k = 1, 2 \tag{3.13}$$

The edge component:

$$l_{kij} = \mathbf{r}_{kij} \cdot \mathbf{t}_{ij}, k = 1, 2 \tag{3.14}$$

The magnitudes of the position vectors can be expressed as:

$$r_{kij} = |\mathbf{r}_{kij}| = (u_i^2 + h_{ij}^2 + l_{kij}^2)^{\frac{1}{2}}, k = 1, 2 \tag{3.15}$$

The shortest distance to the line containing edge ij relative to the observation point (figure:3.2) is:

$$r_{0ij} = |\mathbf{r}_{kij} - (\mathbf{r}_{kij} \cdot \hat{\mathbf{t}}_{ij})\hat{\mathbf{t}}_{ij}| = (u_i^2 + h_{ij}^2)^{\frac{1}{2}}, k = 1, 2 \tag{3.16}$$

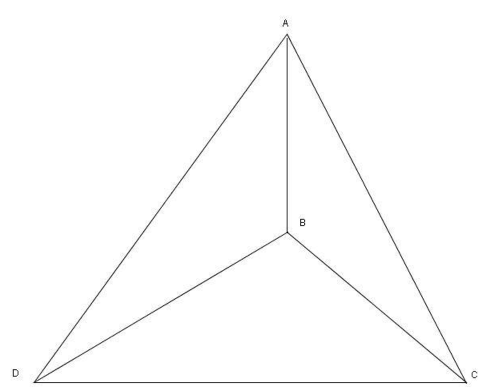

Figure 3.1: a tetrahedron with nose up

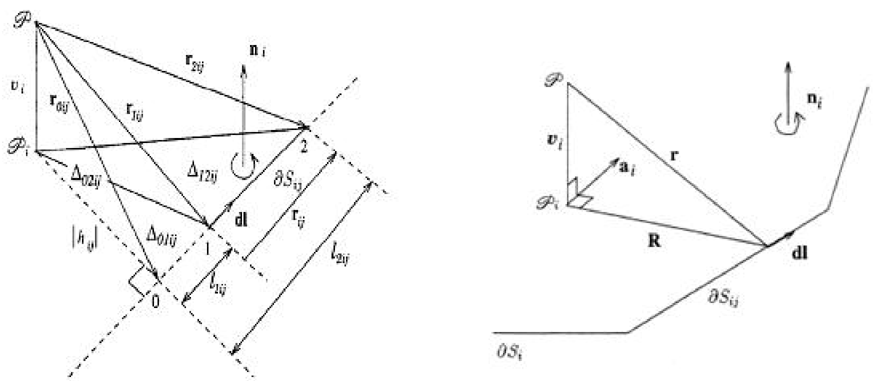

Figure 3.2: Quantities associated with an edge

3.4 Diversion of quantities to extrinsic-intrinsic

Quantities related with the observation point expressing long distance from the target, expressed as high order terms, are called extrinsic, while quantities related with the local origin and therefore expressing short distances expressing low order terms, are called intrinsic. Extrinsic quantities are computed once for every observation point while intrinsic only once per target stored to be reused for every observation point.

3.4.1 Order of magnitude of quantities involved in the anomaly algorithms

The geometric quantities assemble the structural components or terms for the anomally algorithms. All definitions employ vectors independent of any particular coordinate system. Physical invariances are preserved in the anomaly formulas, leading to a consistent theory. Target data are stored in vectors representing positions of vertices and we can distinguish 2 different data classes, the intrinsic class with quantities independent of the observation point and the extrinsic with quantities related to the observation point. In that way equations 3.10 - 3.16 are intrinsic to the target, while **??** - 3.9 are extrinsic. On the purpose of error analysis intrinsic quantities are ascribed order $O(\alpha)$ while extrinsic $O(\delta)$. The floating point truncation errors will be respectively $O(\alpha\epsilon)$ and $O(\delta\epsilon)$ respectively in a floating point precision 1/ϵ. The extrinsic difference $r_{2ij} - r_{1ij}$ with rounding error $O(\delta\epsilon)$ recomputed for each observation point and the intrinsic equivalent $\rho_{2ij} - \rho_{1ij}$ with rounding error $O(\alpha\epsilon)$ computed once for a target induce a reduction in error by a factor γ for every observation point. A naive anomaly formula can be expressed entirely in terms of extrinsic quantities the methods followed by prior solutions to Strakhov et al ([27]) and Pohanka ([39]), suffered from efficiency and accuracy penalties. This is due to the fact that intrinsic quantities need only to be calculated once per target adding negligible overhead, if we consider surveys on grids of 10^4 observation points and thus saving machine time([33]). On the same track efficiency gains can be arised from the recognition of arithmetic redundundy in an anomaly computation. For example the commonality of a vertex by 3 facets, induces redundundy by recomputing the same vertex for the 2 extra facets. Such invariances are known (Dijkstra [5],Weiler [21],Guibas and Stolfi [23],Ni [29])but the contribution to the

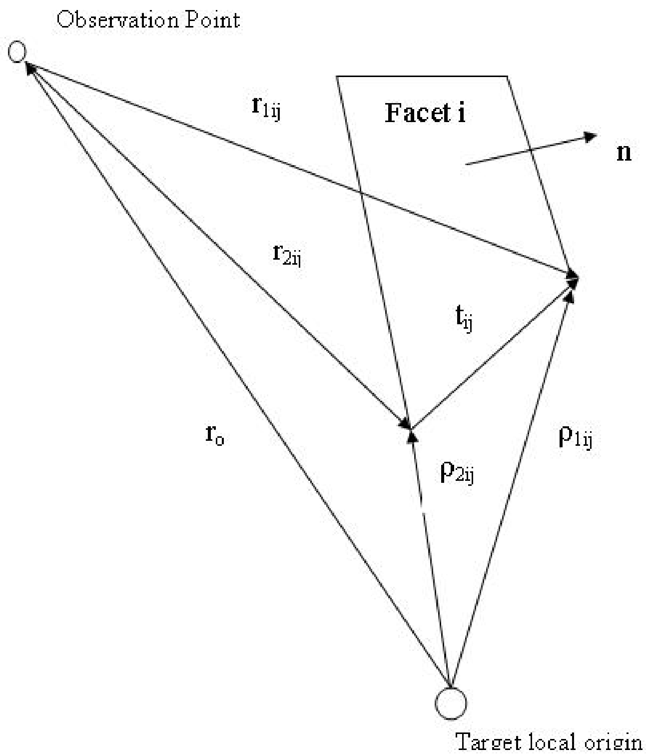

Figure 3.3: Facet related quantities

geophysical modeling has not been appreciated.Section 3.2.1.3 addresses these issues.

Chapter 4

Numerical instability for a receding edge

4.1 Introduction

The purpose of this chapter is to demonstrate the concept of numerical instability, arising from a formula evaluated in floating point arithmetic. For a fixed polygonal edge, the formula calculates the difference of vertex distances from an increasingly remote observer. We develop a theory that is able to describe the observed experimental instability.

Identification of the cause of numerical instability also gives the theoretical means of designing a form of the calculation to be free from numerical instability. We verify this experimentally.

Although the discussion concerns a very special idealized case, the approach is generic and relevant to the much more complicated situations encountered in gravi-magnetic anomaly calculation of polyhedral targets, to be discussed in future chapters.

We did note that for a number n expressible within the floating point range, the truncation error is $O(|n|\varepsilon)$, where ε is the floating point precision constant that expresses the finite information (approximately $\log_{10}(1/\varepsilon)$ decimal digits) that can be represented. The truncation error may be regarded as a rounding error. This error will feed into all the arithmetic operations, and in unfavorable circumstances can accumulate and significantly corrupt the calculated result. The robustness of an algorithm to accumulation of rounding error is a measure of its numerical stability.

4.2 Problem statement

Consider an edge, with vertex position vectors $\boldsymbol{\rho}_1$ and $\boldsymbol{\rho}_2$ relative to an origin local to the edge. The position vector of an observer relative to that origin is taken as $L\hat{\mathbf{L}}$, where $\hat{\mathbf{L}}$ is a unit vector and L is the scalar distance from the origin. As is evident form Figure 4.1, the position vectors $\mathbf{r}_1$ and $\mathbf{r}_2$ of the edge vertices relative to the observation point are given by

$$\mathbf{r}_1 = \boldsymbol{\rho}_1 - L\hat{\mathbf{L}},\ \mathbf{r}_2 = \boldsymbol{\rho}_2 - L\hat{\mathbf{L}} \tag{4.1}$$

We define the edge length E and the scalar distances r_1, r_2 of the edge vertices from the observation point, via 2-norms

$$E = ||\boldsymbol{\rho}_2 - \boldsymbol{\rho}_1||_2,\ \ r_i = ||\mathbf{r}_i||_2 = ||\boldsymbol{\rho}_i - L\hat{\mathbf{L}}||_2, i = 1, 2 \tag{4.2}$$

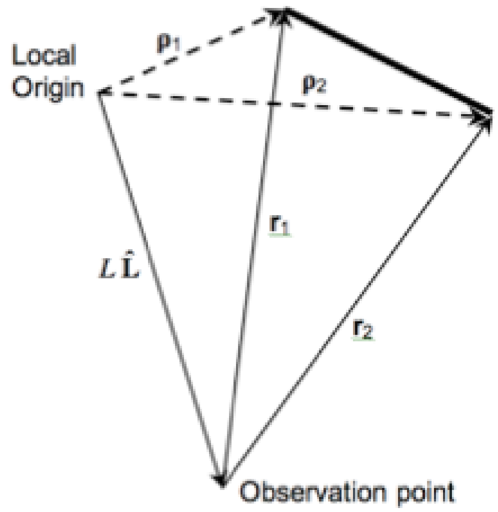

Figure 4.1: Reference systems for edge, displayed as a heavy line.

The problem under investigation is the computation of the vertex distance difference

$$\Delta = r_2 - r_1 \tag{4.3}$$

with increasing L as the observer recedes from the edge in a manner that keeps quantities $\boldsymbol{\rho}_1, \boldsymbol{\rho}_2, \hat{\mathbf{L}}$ constant. Distances r_1 and r_2 will then also increase with L. Their difference Δ, however, can never exceed the edge length E. The practical computation of equation (4.3) in floating point arithmetic will therefore, as L increases, succumb to successive degrees of destructive cancellation error until all significance in the result is lost.

An analysis of this problem, and its cure, are the subject of this chapter.

4.3 Experimental demonstration of the instability: the unstable formula $\Delta = r_2 - r_1$

Two parameter sets are given in Tables 4.1 and 4.2. For a first practical example we chose parameters as in Table 4.1. A straightforward plot of Δ for increasing values of L will show Δ approaching a limiting value Δ_{lim} before diverging again on account of floating point errors. The plot can be made more meaningful if we first obtain an expression for this limiting value. It will be shown below that

$$\Delta_{lim} = \lim_{L\to\infty}(r_2 - r_1) = (\boldsymbol{\rho}_2 - \boldsymbol{\rho}_1) \bullet \hat{\mathbf{L}} \tag{4.4}$$

The relative deviation d, of the vertex distance difference Δ from its limiting value Δ_{lim},

$$d = (\Delta - \Delta_{lim})/E\ , \tag{4.5}$$

can now be plotted against increasing dimensionless distance L/E of the observation point from the edge. Such a plot, on logarithmic scales, is shown in Figure 4.2. The dots are experimental values, and the solid and dashed lines are theoretical trend lines.

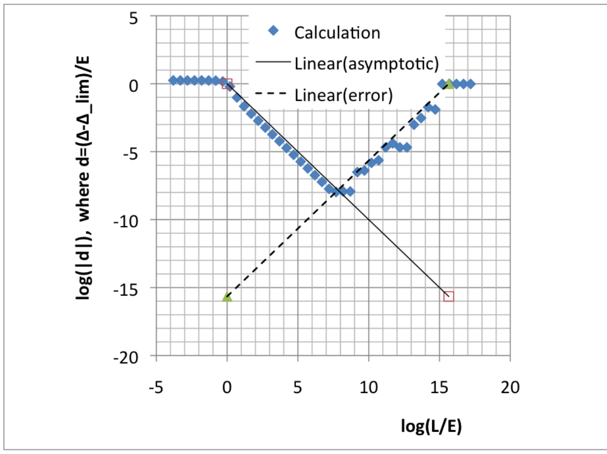

Figure 4.2: Unstabilized case

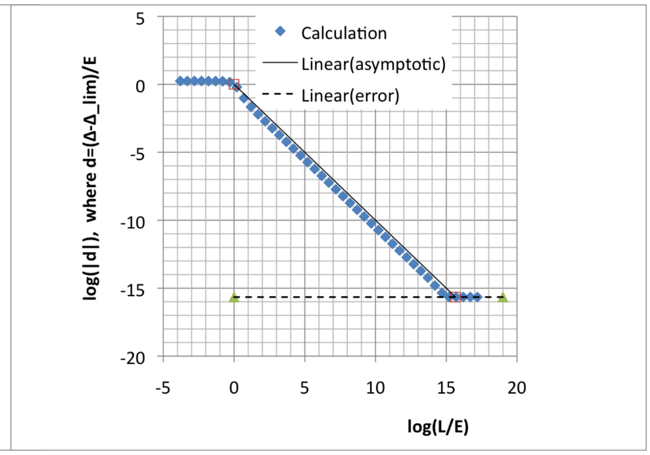

Figure 4.3: Stabilized case

Table 4.1: Receding edge parameters 1

vector	components x	y	z
$\boldsymbol{\rho}_1$	53.00	25.00	0
$\boldsymbol{\rho}_2$	109.00	-5.00	0
$\hat{\mathbf{L}}$	$1/\sqrt{2}$	$1/\sqrt{2}$	0

Table 4.2: Receding edge parameters 2

vector	components x	y	z
$\boldsymbol{\rho}_1$	53.00	25.00	0
$\boldsymbol{\rho}_2$	109.00	-5.00	0
$\hat{\mathbf{L}}$	$\frac{56}{\sqrt{4036}}$	$\frac{-30}{\sqrt{4036}}$	0

For very small values of L/E, corresponding to negative values of $\log_{10}(L/E)$, the observation point is essentially at the local origin, giving no change in the value of d/E. This leads to the initial horizontal trend.

As L/E increases, d/E decreases initially, indicating that Δ approaches Δ_{lim}. At about $L/E \approx 10^8$, this trend is reversed, and Δ increasingly diverges from Δ_{lim}. The divergence increases until $|d| \approx 1$, indicating 100% difference between Δ and Δ_{lim}. This is a direct indication of numerical instability, the consequence of cancellation of common digits from the difference of two increasingly large values of nearly equal magnitude, under finite floating point arithmetic.

The final horizontal run-out is a consequence of Δ from equation (4.3) being returned as zero from total cancellation. This leaves $|d|$ from equation (4.5) being computed as the constant $|-\Delta_{lim}/E|$, with a value $O(1)$, and hence a constant logarithmic value near zero.

Although this example is computed for the specific data in Table 4.1, the use of dimensionless variables means that the plots will be quite generic and not example specific.

4.4 Analysis of the unstable formula $\Delta = r_2 - r_1$

To understand the shape of the plot in Figure 4.2, we develop a series expansion of equation (4.5). The dominant expansion terms will indicate the power law by which d/E diminishes. As expansion parameter we use the dimensionless edge length to edge distance ratio, $\gamma = E/L$.

From equations (4.3) and (4.2), we can write

$$r_i = \left(L^2 - 2(\boldsymbol{\rho}_i \bullet \hat{\mathbf{L}})L + ||\boldsymbol{\rho}_i||^2\right)^{1/2} = L\left(1 - 2\frac{\boldsymbol{\rho}_i}{E} \bullet \hat{\mathbf{L}}\gamma + \left(\frac{||\boldsymbol{\rho}_i||}{E}\right)^2 \gamma^2\right)^{1/2}, i = 1, 2. \tag{4.6}$$

Since $\boldsymbol{\rho}_i/E = O(1)$ and the range of interest $L \gg E$ indicates $\gamma \ll 1$, we can use the binomial expansion of the form $(1 + x)^{1/2} = 1 + \frac{1}{2}x - \frac{1}{8}x^2 + O(x^3)$ and obtain from equation (4.6)

$$r_i = L\left\{1 + \tfrac{1}{2}\left(-2\frac{\boldsymbol{\rho}_i}{E} \bullet \hat{\mathbf{L}}\gamma + \left(\frac{||\boldsymbol{\rho}_i||}{E}\right)^2 \gamma^2\right) - \tfrac{1}{8}\left(-2\frac{\boldsymbol{\rho}_i}{E} \bullet \hat{\mathbf{L}}\gamma + \left(\frac{||\boldsymbol{\rho}_i||}{E}\right)^2 \gamma^2\right)^2 + O(\gamma^3)\right\}. \tag{4.7}$$

Regrouping and retaining terms below $O(\gamma^3)$ leads to

$$r_i = L\left\{1 + \alpha_i\gamma + \beta_i\gamma^2 + O(\gamma^3)\right\}, i = 1, 2, \tag{4.8}$$

where

$$\alpha_i = -\frac{\boldsymbol{\rho}_i}{E} \bullet \hat{\mathbf{L}},\ \beta_i = \tfrac{1}{2}||\frac{\boldsymbol{\rho}_i}{E} \times \hat{\mathbf{L}}||^2,\ i = 1, 2. \tag{4.9}$$

Equation (4.8) shows the expected result that $r_i = O(L)$. This means that the truncation error in computing r_i in floating point arithmetic with precision ε is $O(L\varepsilon)$. This enables us to express the floating point (fl) evaluation of r_i as

$$\mathrm{fl}(r_i) = L\left\{1 + \alpha_i\gamma + \beta_i\gamma^2 + O(\gamma^3) + O(\varepsilon)\right\}, i = 1, 2. \tag{4.10}$$

An estimate of $\mathrm{fl}(\Delta)$ of equation (4.3) can now be given as

$$\mathrm{fl}(\Delta) = \mathrm{fl}(r_2) - \mathrm{fl}(r_1) = L\left\{(\alpha_2 - \alpha_1)\gamma + (\beta_2 - \beta_1)\gamma^2 + O(\gamma^3) + O(\varepsilon)\right\}. \tag{4.11}$$

Here the dominant $O(L)$ terms have canceled, however, the full rounding error $O(L\varepsilon)$ has been inherited - this does not cancel. The floating point evaluation of the difference Δ of equation (4.3) can now be given, using $L = E\gamma^{-1}$, as

$$\mathrm{fl}(\Delta) = \mathrm{fl}(r_2) - \mathrm{fl}(r_1) = E\left\{(\alpha_2 - \alpha_1) + (\beta_2 - \beta_1)\gamma + O(\gamma^2) + O(\varepsilon/\gamma)\right\}. \tag{4.12}$$

In the absence of errors from finite precision, it is seen that

$$\Delta_{lim} = \lim_{L\to\infty}(r_2 - r_1) = \lim_{\gamma\to 0}(r_2 - r_1) = E(\alpha_2 - \alpha_1), \tag{4.13}$$

and this result justifies, via result (4.9), the previously used expression (4.4) for Δ_{lim}.

From equations (4.12) and (4.13), an estimate of the floating point value of d, equation (4.5), is

$$\mathrm{fl}(d) = \frac{\mathrm{fl}(\Delta) - \Delta_{lim}}{E} = (\beta_2 - \beta_1)\gamma + O(\gamma^2) + O(\varepsilon/\gamma). \tag{4.14}$$

Noting that $\beta_i = O(1)$), fl(d) , the first term on the right hand side exceeds the last provided

$$|(\beta_2 - \beta_1)\gamma| \gg \varepsilon/\gamma, \text{ or } \gamma^2 \gg \varepsilon. \tag{4.15}$$

In this regime, equation (4.14) is well approximated by the first right hand side term, leading to

$$\log_{10}(|\text{fl}(d)|) = \log_{10}|\beta_2 - \beta_1| - \log_{10}(1/\gamma). \tag{4.16}$$

The first term is small since $\beta_2 - \beta_1 = O(1)$. The trend line $\log_{10}|d| = -\log_{10} 1/\gamma = -\log_{10}(L/E)$ of theoretical slope -1 in log-log space has been added as a continuous line to Figure 4.2 , which the experimental points follow closely, until the point of divergence.

Equation (4.15) indicates that the first term on the right hand side of equation (4.14) no longer dominates when

$$\gamma \approx \varepsilon/\gamma, \text{ i.e. } 1/\gamma \approx \varepsilon^{-1/2} \,. \tag{4.17}$$

Using $\varepsilon = 2^{-52} \approx 2.2 \times 10^{-16}$ gives $1/\gamma \approx 10^8$ for the predicted distance when the floating point error prevents further approach of Δ to Δ_{lim}, and this is observed in Figure 4.2.

With the last term of equation (4.14) deominating, the relationship becomes essentially

$$\text{fl}(d) = \varepsilon/\gamma, \text{ or: } \log_{10}|d| = \log_{10}\varepsilon + \log_{10}(1/\gamma) \,. \tag{4.18}$$

This is a straight line in the log-log diagram, with an intercept on the vertical axis at $\log_{10}\varepsilon \approx -16$, and slope +1. The upward sloping dashed trend line in Figure 4.2 is this line. After $1/\gamma > \varepsilon^{-1/2}$, the scatter points are bounded by this line until $1/\gamma \approx 1/\varepsilon \approx 10^8$. Before this point the dashed line also gives an estimate of the growing rounding error, but it is small compared to the value of $|d|$, and so does not visibly affect the steadily decreasing value of $|d|$. However, at and beyond $L/E \approx \varepsilon^{-1/2}$, the finite precision error dominates and prevents fl$(|d|)$ getting smaller.

4.5 A stabilized formula for the difference $r_2 - r_1$ of vertex distances

The origin of the above instability lies in the direct calculation of the $O(L)$ vertex distances, r_i, and then taking their difference in floating point arithmetic. The truncation error in representing fl(r_i) is $O(L\varepsilon)$, which grows with increasing L, while the actual difference remains of the order of the edge length $O(E)$. When $L\varepsilon \approx E$, i.e. $L/E \approx \varepsilon$, the error is of the order of the quantity being sought, and all significant digits in the difference calculation is lost.

To calculate the difference $r_2 - r_1$ in a stable manner, we must cancel the dominant $O(L)$ terms analytically before numerical evaluation. This can be achieved in the following manner.

$$r_2 - r_1 = \frac{(r_2 - r_1)(r_2 + r_1)}{r_2 + r_1} = \frac{r_2^2 - r_1^2}{r_2 + r_1} = \frac{\mathbf{r}_2 \bullet \mathbf{r}_2 - \mathbf{r}_1 \bullet \mathbf{r}_1}{r_2 + r_1} = \frac{(\mathbf{r}_2 - \mathbf{r}_1) \bullet (\mathbf{r}_2 + \mathbf{r}_1)}{r_2 + r_1} \,. \tag{4.19}$$

The factor $(\mathbf{r}_2 - \mathbf{r}_1)$ in the right most term represents the difference of two $O(L)$ quantities, and will be subject to increasing floating point error of $O(L)$. Crucially, this difference equals, according to Figure 4.1, $\boldsymbol{\rho}_2 - \boldsymbol{\rho}_1$. This is the edge vector, calculated from $O(E)$ terms. Thus the stabilized difference Δ_s is calculated from formula

$$\Delta_s = r_2 - r_1 = \frac{(\boldsymbol{\rho}_2 - \boldsymbol{\rho}_1) \bullet (\mathbf{r}_2 + \mathbf{r}_1)}{r_2 + r_1} \; . \tag{4.20}$$

The ratio $(\mathbf{r}_2 + \mathbf{r}_1)/(r_2 + r_1)$ is of $O(1)$, making the whole expression (4.20) of $O(E)$. Thus an estimate of the floating point evaluation is

$$\mathrm{fl}(\Delta_s) = \frac{(\boldsymbol{\rho}_2 - \boldsymbol{\rho}_1) \bullet (\mathbf{r}_2 + \mathbf{r}_1)}{r_2 + r_1} + O(E\varepsilon) \; . \tag{4.21}$$

The error term $(E\varepsilon)$ is constant and does not grow as $L/E \to \infty$, or equivalently, $\gamma \to 0$. The formula is *stable*. This contrasts with the unbounded error growth from equation (4.3). Even though relations (4.20) show that the formulas are mathematically equivalent, their numerics are quite different.

Corresponding to equation (4.5), we plot relative the difference d_s of the stabilised expression Δ_s from its limiting value,

$$d_s = (\Delta_s - \Delta_{lim})/E \; , \tag{4.22}$$

for increasing values of L/E. As before, the absolute values are plotted on logarithmic axes. The result is shown in Figure 4.3.

4.6 Analysis of the stabilized formula (4.20) for Δ_s

The unstable and stabilized expressions for Δ and Δ_s are mathematically equivalent. Therefore they have the same power series expansion, allowing the previous results to be used at once to express the relative difference of Δ_s from the limit Δ_{lim}, as

$$\mathrm{fl}(d_s) = \frac{\mathrm{fl}(\Delta_s) - \Delta_{lim}}{E} = (\beta_2 - \beta_1)\gamma + O(\gamma^2) + O(\varepsilon). \tag{4.23}$$

in analogy with equation (4.14). The crucial difference between the two equations is that the floating point error is now constant, of $O(\varepsilon)$. In the regime where $\gamma \gg \varepsilon$, i.e. $L/E \ll \varepsilon^{-1}$, the first term on the right hand side of equation (4.23) dominates, and the logarithmic equation is

$$\log_{10} |\mathrm{fl}(d_s)| = \log |\beta_2 - \beta_1| - \log_{10}(1/\gamma) \; , \tag{4.24}$$

that is, a straight line relationship of slope -1, as shown by the continuous line in Figure 4.3.

When $L/E = \gamma^{-1} \approx \varepsilon^{-1}$ and beyond, that is $\gamma \lessapprox \varepsilon$, the dominant relationship is just

$$\log_{10} |\mathrm{fl}(d_s)| = \log_{10} \varepsilon \; , \tag{4.25}$$

that is, the dashed horizontal straight line at a vertical level of $\log_{10} \varepsilon \approx -15.95$ on the logarithmic scale of Figure 4.3. The computed points are seen to follow the two trend line regimes.

The limiting error does not grow with increasing L/E, and in this sense the formula for Δ_s is stable.

The term $O(\varepsilon)$ in equation (4.23) is an estimate of the maximum floating point error that can occur. In practical computation, the error is usually close to the maximum, as evidenced in the graphs where the scatter points closely follow the theoretical trend lines. However, the error can fall anywhere between zero and ε. To prevent the possibility of a zero relative error on a logarithmic scale, the practical calculation of equation (4.23) is carried out as $|d_s| \leftarrow \max(\mathrm{fl}(|d_s|), \varepsilon)$.

4.7 A case of super convergence

The above analyses for the unstabilised Δ and stabilised Δ_s expressions, particularly as used in equations (4.14) and (4.23), stated that $(\beta_2 - \beta_1)\gamma$ was the dominant term when γ is sufficiently large. This is true provided $\beta_2 - \beta_1 \neq 0$.

It is possible to construct non-trivial cases with $\beta_2 - \beta_1 = 0$. In that case the dominant term for non-small γ is of $O(\gamma^2)$, and the logarithmic relation for both d and d_s is

$$\log_{10} |\mathrm{fl}(d_{(s)})| = \log_{10} c - 2 \log_{10} 1/\gamma \,, \tag{4.26}$$

where $c\gamma^2 + O(\gamma^3)$ is taken as the expanded form of the $O(\gamma^2)$ term. Thus we expect to see a slope of -2 in the log-log graph, contrasting with the previous slope of -1.

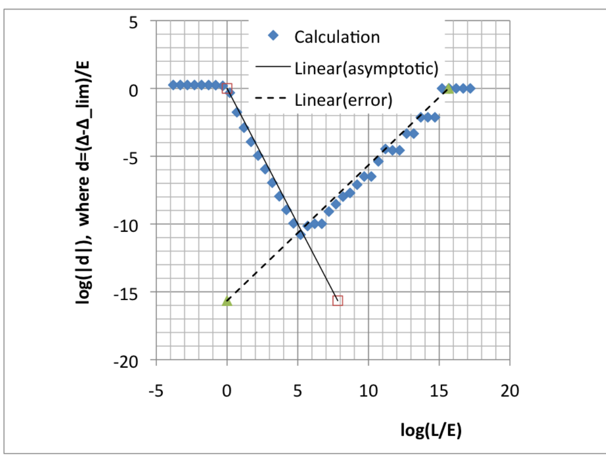

Figure 4.4: Super-convergent, unstabilized

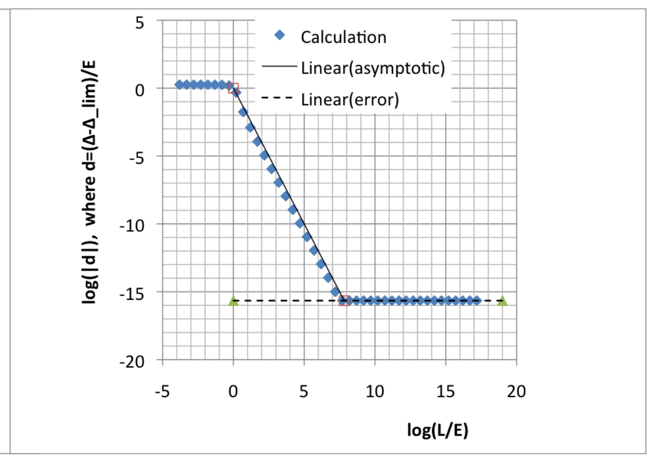

Figure 4.5: Super-convergent, stabilized

Figures 4.4 and 4.5 demonstrate super-convergence to Δ_{lim} for the unstabilized and stabilized cases respectively. Continuous trend lines with slope -2 are closely followed by the experimental points. The error growth trend lines (dashed, slopes +1 and 0) are the same as in the non super-convergent cases, but the points of intersection with the downward sloping lines are different.

The construction of a super-convergent case follows from equation (4.9). Expressing the squared norms as dot products and carrying out the subtraction for $\beta_2 - \beta_1$, the difference of the dot products factorises to give

$$\beta_2 - \beta_1 = \tfrac{1}{2}(\frac{\boldsymbol{\rho}_2 - \boldsymbol{\rho}_1}{E} \times \hat{\mathbf{L}}) \bullet (\frac{\boldsymbol{\rho}_2 + \boldsymbol{\rho}_1}{E} \times \hat{\mathbf{L}}) \; . \tag{4.27}$$

Choosing $\hat{\mathbf{L}}$ to be parallel to either $(\boldsymbol{\rho}_2 - \boldsymbol{\rho}_1)$ or $(\boldsymbol{\rho}_2 + \boldsymbol{\rho}_1)$ will ensure that one of the factors is zero, resulting in $\beta_2 - \beta_1 = 0$. We chose the former case, with parameters given in Table 4.2.

4.8 Discussion and conclusions

We have investigated the formulas $\Delta = r_2 - r_1$ and $\Delta_s = \frac{(\boldsymbol{\rho}_2 - \boldsymbol{\rho}_1) \bullet (\mathbf{r}_2 + \mathbf{r}_1)}{r_2 + r_1}$ in the context of the receding edge geometry of Figure 4.1. Although Δ and Δ_s are mathematically identical (see equation (4.19)), their floating point evaluations are very different, as summarised by

$$\text{fl}(\Delta) = \Delta + O(L\varepsilon), \; \text{fl}(\Delta_s) = \Delta_s + O(E\varepsilon) \; , \tag{4.28}$$

where r_1, r_2 grow like L, and E refers to the constant edge length. Theoretically, both Δ and Δ_s approach Δ_{lim} of $O(E)$ as $L \to \infty$. As equation (4.28) shows, however, the approach of fl(Δ) to Δ_{lim} is halted and reversed at sufficiently large L, whereas fl(Δ_s) can approach Δ_{lim} to within $O(E\varepsilon)$, i.e. to within the floating point truncation error in Δ_s, a result that cannot be bettered. This improvement for fl(Δ_s) is obtained by identifying dominant terms in Δ, and canceling them analytically *before* floating point evaluation.

The approach of Δ to Δ_{lim} is conveniently displayed graphically on log-log scales. The observed slope of -κ ($\kappa = 1, 2$ for normal/super convergence) for the envelope of calculated points indicates that, initially, $(\Delta - \Delta_{lim})/E = O(\gamma^\kappa)$, where $\gamma = E/L$. The divergent error envelope of slope +1 indicates error growth from finite precision proportional to $O(\gamma^{-1})$.

The simple straight-line theoretical trend relationships allows *a prioi* performance predictions to be made about the algorithms. Thus, in the super-convergent unstabilized case, the lines are $y = -2x$ and $y = x + \log_{10}\varepsilon$, with intersection point $(x, y) = (-\frac{1}{3}\log_{10}\varepsilon, \frac{2}{3}\log_{10}\varepsilon)$. This allows $(\Delta - \Delta_{lim})/E$ to have a closest approach at $\gamma^{-1} \approx \varepsilon^{-1/3}$, with a minimum difference of $\varepsilon^{2/3}$. Figure 4.4 confirms this for actual calculations.

These techniques are to be used in formulating stable gravi-magnetic anomaly algorithms.

Chapter 5

Finite expansions for receding edge

5.1 Introduction

The purpose of this chapter is to demonstrate the concept of numerical instability, arising from a formula evaluated in floating point arithmetic. For a fixed polygonal edge, the formula calculates the difference of vertex distances from an increasingly remote observer. We develop a theory that is able to describe the observed experimental instability. sdaf

Identification of the cause of numerical instability also gives the theoretical means of designing a form of the calculation to be free from numerical instability. We verify this experimentally.

Although the discussion concerns a very special idealised case, the approach is generic and relevant to the much more complicated situations encountered in gravi-magnetic anomaly calculation of polyhedral targets, to be discussed in future chapters.

We note that for a number n expressible within the floating point range, the truncation error is $O(|n|\varepsilon)$, where ε is the floating point precision constant that expresses the finite information (approximately $log_{10}\varepsilon$ decimal digits) that can be represented. It may be regarded as a rounding error. This error will feed into all the arithmetic operations, and in unfavourable circumstances can accumulate and significantly corrupt the calculated result. The robustness of an algorithm to accumulation of rounding error is a measure of its numerical stability. The polyhedral anomaly $a(\gamma)$ as a function of the reciprocal dimensionless distance γ from an observer would be expected to be increasingly similar to the equivalent point source anomaly $a_p(\gamma)$, say, at increasingly large observer distances, that is, as $\gamma \to 0$. We can write

$$a(\gamma) = a_p(\gamma) + \delta(\gamma) \ , \tag{5.1}$$

where

$$\delta(\gamma) = a(\gamma) - a_p(\gamma) \ . \tag{5.2}$$

Although the ”short fall” $\delta(\gamma)$ would be expected to reach zerot faster than $a(\gamma)$ or $a_p(\gamma)$ separately as $\gamma \to 0$, it cannot reasonably be computed in floating point arithmetic as the difference expression 5.2, because of destructive cancellation. To make equation 5.2 meaningful, analytical cancellation of dominant terms would have to be achieved. The resultant formula for $\delta(\gamma)$ can then be used to compute $a(\gamma)$ as a perturbation of $a_p(\gamma)$, in equation 5.1.

Equation 5.1 expresses $a_p(\gamma)$ as the first term in an expansion of $a(\gamma)$, with $\delta(\gamma)$ an exact remainder term of higher order. We shall pursue this analogy in this chapter, applied to some very simple cases. The approach is to be used in later chapters for developing anomaly formulae with enhanced numerical stability.

5.2 A very simple example

For the purpose of illustration, define $a(\gamma)$ and $a_p(\gamma)$ according to

$$a(\gamma) = 1/(1-\gamma)\ ,\ a_p(\gamma) = 1 \text{ (constant)}\ , \tag{5.3}$$

Clearly, $a(\gamma) \to a_p$ as $\gamma \to 0$, and so we have in analogy with equations 5.1 and 5.2,

$$a(\gamma) \;=\; 1 + \delta(\gamma)\ , \tag{5.4}$$

$$\delta(\gamma) \;=\; \frac{1}{1-\gamma} - 1\ . \tag{5.5}$$

Simplification of equation 5.5 gives

$$\delta(\gamma) = \frac{1-(1-\gamma)}{1-\gamma} = \frac{\gamma}{1-\gamma}\ . \tag{5.6}$$

Crucially, the intermediate expression saw the analytical cancellation of $O(1)$ terms in the numerator, leaving the higher order $O(\gamma)$ remainder term. The start of the expansion 5.4 can therefore be given as

$$a(\gamma) = 1 + \frac{\gamma}{1-\gamma}\ . \tag{5.7}$$

This gives the required decomposition of $a(\gamma)$ into the first term of $O(1)$ of a series, and its $O(\gamma)$ exact remainder term.

In the present case the remainder term contains the same factor $1/(1-\gamma)$ as the source term, and n-fold reapplication of its decomposition yields the expansion formula

$$a(\gamma) = 1 + \gamma + \gamma^2 + \ldots + \gamma^{n-1} + \frac{\gamma^n}{1-\gamma}\ . \tag{5.8}$$

In general, the decomposition of a remainder into a base term and an additional higher order exact remainder term can be used for formulating an exact finite expansion.

5.3 Application to the receding edge

In the previous chapter, analysis of the vertex distance difference as measured by an observer with increasing dimensionless distance $1/\gamma$ yielded an expression $\Delta_s(\gamma)$ with limiting value $\lim_{\gamma\to 0}\Delta_s(\gamma) = \Delta_{lim}$, as given by equations (4.20) and (4.4). We plotted the relative difference $(\Delta_s(\gamma) - \Delta_{lim})/E$ for decreasing γ (increasing $\gamma^{-1} = L/E$), and found that the finite nature of floating point precision prevented Δ_s approaching Δ_{lim} at sufficiently small γ.

The aim in this section is to derive an appropriate perturbation term $\delta(\gamma)$ where

$$\Delta_s(\gamma) = \Delta_{lim} + \delta(\gamma) \,, \tag{5.9}$$

and $\delta(\gamma)$ is computed from terms of a higher order of smallness than either of $\Delta_s(\gamma)$ or Δ_{lim}. Under these circumstances the unstable computation $(\Delta_s(\gamma) - \Delta_{lim})/E$ can be replaced by the stable computation of $\delta(\gamma)/E$ that will not be corrupted by rounding error at decreasing values of γ as $\gamma \to 0$.

5.4 Determination of $\delta(\gamma)$

Formally, we define function $\delta(\gamma)$ from equation 5.9, in analogy with equation 5.2, by

$$\delta(\gamma) = \Delta_s(\gamma) - \Delta_{lim} \,, \tag{5.10}$$

and then systematically attempt to perform analytical cancellation of dominant terms. The necessary elmentary algebraic steps are now carried out.

Substituting for equations (4.20) and (4.4) into equation 5.10, we obtain

$$\delta(\gamma) = \frac{(\boldsymbol{\rho}_2 - \boldsymbol{\rho}_1) \bullet (\mathbf{r}_2 + \mathbf{r}_1)}{r_2 + r_1} - (\boldsymbol{\rho}_1 - \boldsymbol{\rho}_2) \bullet \hat{\mathbf{L}}. \tag{5.11}$$

Regrouping equation (4.11) gives

$$\delta(\gamma) = (\boldsymbol{\rho}_2 - \boldsymbol{\rho}_1) \bullet \left\{ \frac{\mathbf{r}_2 + \mathbf{r}_1}{r_2 + r_1} + \hat{\mathbf{L}} \right\} = (\boldsymbol{\rho}_2 - \boldsymbol{\rho}_1) \bullet \left\{ \frac{\mathbf{r}_2/L + \mathbf{r}_1/L}{r_2/L + r_1/L} + \hat{\mathbf{L}} \right\} \,. \tag{5.12}$$

The vectors $\mathbf{r}_1/L, \mathbf{r}_2/L$ and their magnitudes $r_1/L, r_2/L$ are functions of the parameter γ via definitions (4.1) and the relation $L = E/\gamma$. These allow us to introduce scaled variables $\tilde{\mathbf{r}}_i, \tilde{r}_i$

$$\tilde{\mathbf{r}}_i = \mathbf{r}_i/L = (\boldsymbol{\rho}_i/E)\gamma - \hat{\mathbf{L}}, \;\; \tilde{r}_i = r_i/L = ||\tilde{\mathbf{r}}_i||, \; i = 1, 2 \,, \tag{5.13}$$

that can be computed even in the limit $\gamma \to 0$,

$$\lim_{\gamma \to 0} \tilde{\mathbf{r}}_i = -\hat{\mathbf{L}}, \quad \lim_{\gamma \to 0} \tilde{r}_i = 1, \; i = 1, 2 \,. \tag{5.14}$$

Substituting for $\mathbf{r}_i/L$ into the right hand braces in equation 5.12, we obtain

$$\delta(\gamma) = \left(\frac{\boldsymbol{\rho}_2 - \boldsymbol{\rho}_1}{\tilde{r}_2 + \tilde{r}_1} \right) \bullet \left\{ (\boldsymbol{\rho}_2/E + \boldsymbol{\rho}_1/E)\, \gamma + \hat{\mathbf{L}} \left[(\tilde{r}_2 - 1) + (\tilde{r}_1 - 1) \right] \right\} \,. \tag{5.15}$$

Since $\tilde{r}_i \approx 1$ as $\gamma \to 0$, the terms in square brackets will lead to numerical cancellation errors. These term must be subjected to analytical cancellation of dominant terms, to match the previous $O(\gamma)$ term. We use

$$(\tilde{r}_i - 1)(\tilde{r}_i + 1) = ||\tilde{\mathbf{r}}_i||^2 - ||\hat{\mathbf{L}}||^2 = (\tilde{\mathbf{r}}_i - \hat{\mathbf{L}}) \bullet (\tilde{\mathbf{r}}_i + \hat{\mathbf{L}}) \,, i = 1, 2 \,, \tag{5.16}$$

in which the last factor $(\tilde{\mathbf{r}}_i + \hat{\mathbf{L}})$ allows analytical cancellation of the $O(1)$ dominant terms $\hat{\mathbf{L}}$ on account of equation 5.13,

$$\tilde{\mathbf{r}}_i + \hat{\mathbf{L}} = (\boldsymbol{\rho}_i/E)\gamma + (-\hat{\mathbf{L}} + \hat{\mathbf{L}}) = (\boldsymbol{\rho}_i/E)\gamma \tag{5.17}$$

$$\tilde{r}_i - 1 = \left(\frac{\tilde{\mathbf{r}}_i - \hat{\mathbf{L}}}{\tilde{r}_i + 1} \bullet \frac{\boldsymbol{\rho}_i}{E} \right) \gamma \ , \ i = 1, 2 \ . \tag{5.18}$$

Thus the left hand difference of $O(1)$ quantities is reduced to an $O(\gamma)$ expression on the right. The right hand side can be stably computed even in the limit $\gamma \to 0$, when it reduces to $\left(-\hat{\mathbf{L}} \bullet \boldsymbol{\rho}_i/E\right)\gamma$. Substituting relations 5.18 into equation 5.15 gives the required stabilised result

$$\delta(\gamma) = \left(\frac{\boldsymbol{\rho}_2 - \boldsymbol{\rho}_1}{\tilde{r}_2 + \tilde{r}_1} \right) \bullet \left\{ (\boldsymbol{\rho}_2/E + \boldsymbol{\rho}_1/E) + \hat{\mathbf{L}} \left[\left(\frac{\tilde{\mathbf{r}}_2 - \hat{\mathbf{L}}}{\tilde{r}_2 + 1} \bullet \frac{\boldsymbol{\rho}_2}{E} \right) + \left(\frac{\tilde{\mathbf{r}}_1 - \hat{\mathbf{L}}}{\tilde{r}_1 + 1} \bullet \frac{\boldsymbol{\rho}_1}{E} \right) \right] \right\} \gamma \ . \tag{5.19}$$

The first factor is $O(E)$, while all the terms in the braces are of $O(1)$. The whole expression is therefore of $O(E\gamma)$. Since Δ_{lim} is of $O(E)$, we have achieved the aim of finding the exact higher order perturbation term $\delta(\gamma)$ from which $\Delta_s(\gamma)$ can be calculated, according to equation 5.9. Moreover, the rounding error in calculating $\delta(\gamma)$ from formula (4.19) is $O(E\gamma\varepsilon)$, so this error can never outgrow the value of $\delta(\gamma)$. This is in marked contrast to the calculations carried out in Chapter 4. We present some calculations for $\delta(\gamma)$, below.

5.5 Plots of the function $\delta(\gamma)$ for the the receding edge case

We have repeated the computational experiments of the previous chapter, but now use formula (4.19) for $\delta(\gamma)$ to express the difference $\Delta_s - \Delta_{lim}$. The graphs in Figures 5.1 and 5.2 track $\delta(\gamma)/E$ for increasing dimensionless observer-edge distances $L/E = \gamma^{-1}$, on logarithmic axes. We use the parameter data from Tables 4.1 (non super-convergent) and 4.02 (super-convergent).

The observed slope of -1 for the calculation points in Figure 5.1 shows that $\delta(\gamma)/E$ obeys a power law proportional to γ. This is as expected from the theory, equation 5.19. In contrast to the corresponding Figure 4.02, the downward slope is uninterrupted by growing rounding error. From the discussion above, the error in the calculation of $\delta(\gamma)/E$ is $O(\gamma\varepsilon)$. This leads to the indicated dotted line in Figure 5.1. It is parallel but always below the calculation trend line, and so the calculation of $\delta(\gamma)$ retains its significance to one part in $\varepsilon^{-1} \approx 10^{16}$ for all values of representable γ.

Figure 5.2 gives an interesting contrast. This case was constructed in Chapter 4 to give a super-convergence property $O(\gamma^2)$ for $\delta(\gamma)$. However, it is constructed in formula 5.19 as the $O(\gamma)$ remainder term to $\Delta - \Delta_{lim}$. To reconcile these apparently conflicting requirements, it is necessary for the expression factoring γ in equation 5.19 itself to be of $O(E\gamma)$, that is, the $O(E)$ terms must collapse to $O(E\gamma)$ through the application of floating point arithmetic, and not *a priori* analytical cancellation. This gives an effective $O(\gamma^2)$ functionality for $\delta(\gamma)/E$, corresponding to the initial slope of -2 in the figure. One

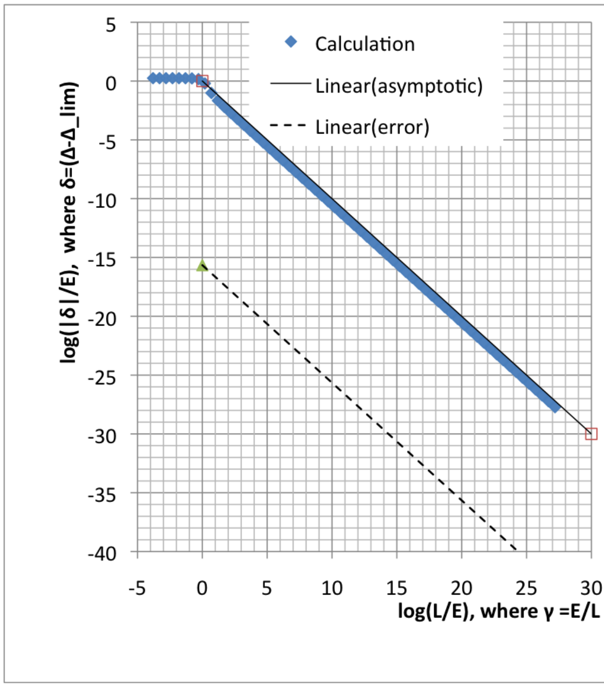

Figure 5.1: Stabilised δ, non super-convergent case

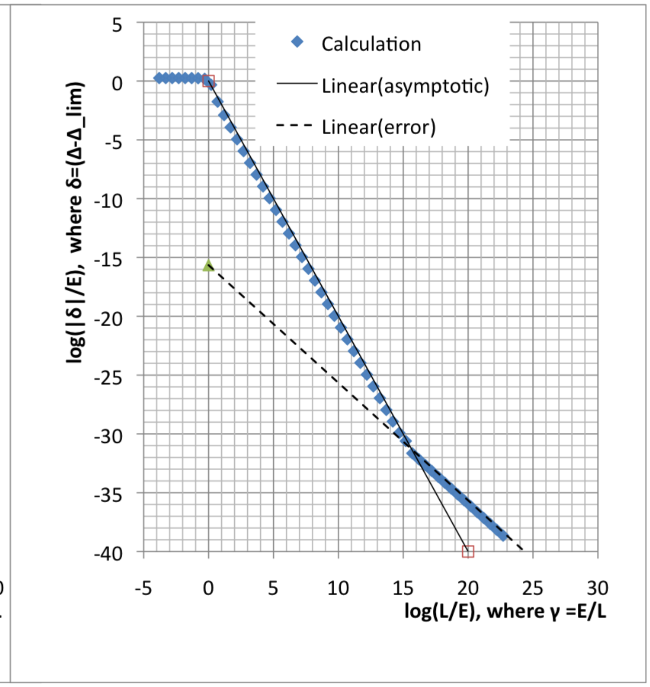

Figure 5.2: Stabilised δ, super-convergent case

order is derived from the factor γ in equation 5.19, the other through the cancellations in the coefficient of γ. The latter calculation will be subject to a relative rounding error $\gamma O(E\varepsilon)/E = O(\gamma\varepsilon)$, and this trendline of slope -1 is also shown in Figure 5.2 as the dashed line (the same line in Figure 5.1).

When the smallness in $\delta(\gamma)/E$ matches the rounding error, that is $\gamma^2 \approx \gamma\varepsilon$ or $\gamma \approx \varepsilon$, the calculation of $\delta(\gamma)$ cannot continue with an $O(\gamma^2)$ result, and defaults instead to an $O(\gamma)$ decrease, as shown in the plot. The calculated values of $\delta(\gamma)$, though continuing to decrease, are determined by rounding error.

In x-y space, the two trend lines are $y = -2x, y = \log\varepsilon - x$, and their point of intersection is $(x, y) = (\log\varepsilon^{-1}, 2\log\varepsilon) \approx (16, -32)$, as confirmed in Figure 5.2.

5.6 The asymptotic form of equation 5.19

The super-convergent case was constructed in Chapter 4 by taking $\hat{\mathbf{L}}$ parallel to $\boldsymbol{\rho}_2 - \boldsymbol{\rho}_1$. We can verify that $\delta(\gamma)$ in equation 5.19 is at least $O(\gamma^2)$ in this case by showing that the limiting form of the coefficient of γ, as $\gamma \to 0$, is zero.

Making use of the limiting forms in equation 5.14, we obtain for the coefficient of γ in equation 5.19,

$$(\boldsymbol{\rho}_2 - \boldsymbol{\rho}_1) \bullet \left\{ (\boldsymbol{\rho}_2 + \boldsymbol{\rho}_1) - \hat{\mathbf{L}} \left[\hat{\mathbf{L}} \bullet (\boldsymbol{\rho}_2 + \boldsymbol{\rho}_1) \right] \right\} / (2E) \tag{5.20}$$

$$= (\boldsymbol{\rho}_2 - \boldsymbol{\rho}_1) \bullet \left\{ \hat{\mathbf{L}} \times \left((\boldsymbol{\rho}_2 + \boldsymbol{\rho}_1) \times \hat{\mathbf{L}} \right) \right\} / (2E) . \tag{5.21}$$

The vector in the braces is perpendicular to $\hat{\mathbf{L}}$, by virtue of the cross product. Therefore, when the leading factor $(\boldsymbol{\rho}_2 - \boldsymbol{\rho}_1)$ is parallel to $\hat{\mathbf{L}}$, as in the construction for the super-convergent case, the resulting expression is zero on account of the dot product of orthogonal vectors. A γ-expansion of the full coefficient 5.19 therefore has a zero leading term followed (in general) by an $O(\gamma)$ term, and this leads to an overall $O(\gamma^2)$ functionality for $\delta(\gamma)$. We similarly comment that when $\hat{\mathbf{L}}$ is proportional to $(\boldsymbol{\rho}_2 + \boldsymbol{\rho}_1)$, then the inner cross product in equation 5.21 is zero, again leading to a super-convergent case. This possibility was already noted in Chapter 4.

5.7 Conclusion

We have shown how the difference $\delta(\gamma)$ of two expressions of increasing nearness with respect to a parameter γ, as $\gamma \to 0$, can be stabilised by prior analytical cancellation of dominant terms, and that this approach is equivalent to obtaining a decomposition of the differenced terms into a base term plus a higher order perturbation term (δ), as in the manner of an finite expansion with exact remainder term. This approach models the procedure we shall adopt when trying to express an anomaly formula for an extended target in terms of a perturbation of the equivalent source target. An anomaly formula of this nature for the extended target will inherit the numerical stability of the equivalent point source formula.

Chapter 6

Triangulated targets

6.1 Introduction

The aim of this chapter is to report on the application of the gravimagnetic anomaly formulas of error growth, published in the H.Holstein, B.Ketteridge, "Gravimetric Analysis of Uniform Polyhedra", 1996, [16] upon triangulated targets, with the expectation to gain improved efficiency.
Extensive Java code has being produced to closure the subject and validate all the issues involved under this research topic.
The results are outlining improved numerical stability and operation count, against polyhedral targets, over all implementations of error growth formulas, namely Vertex, Line and Surface [26]. From the existing literature with respect to graphics, I highlighted the fact that triangulated targets are used to approximate irregular targets extensively. The applicability of this issue in the case of gravity and magnetism will be discussed and commented separately.
Triangulated targets can be computationally cheaper and more attractive to be implemented over polyhedral targets considering that each facet has a fixed number of vertices.
This simplification is reflected in all data structures and the operations involved.
The reduced computational effort observed for calculating facet areas in coordination with the solid angle substitution of the 2nd arctangent term increased the overall performance of all the anomaly algorithms. This issue was proved by experiment and comparison.
It is a Geophysical practice that all target models are considered as abstractions or "good enough" approximations of the real irregular solids of unified density and magnetization residing inside earth. The difference in behaviour between regular and irregular targets is insignificant at the present stage.
A pre- validated as a solid shape tetrahedron is used, for testing all the algorithms included in the error growth classification as stated in Holstein et al. "Comparison of gravimetric formulas for uniform polyhedra",1999.

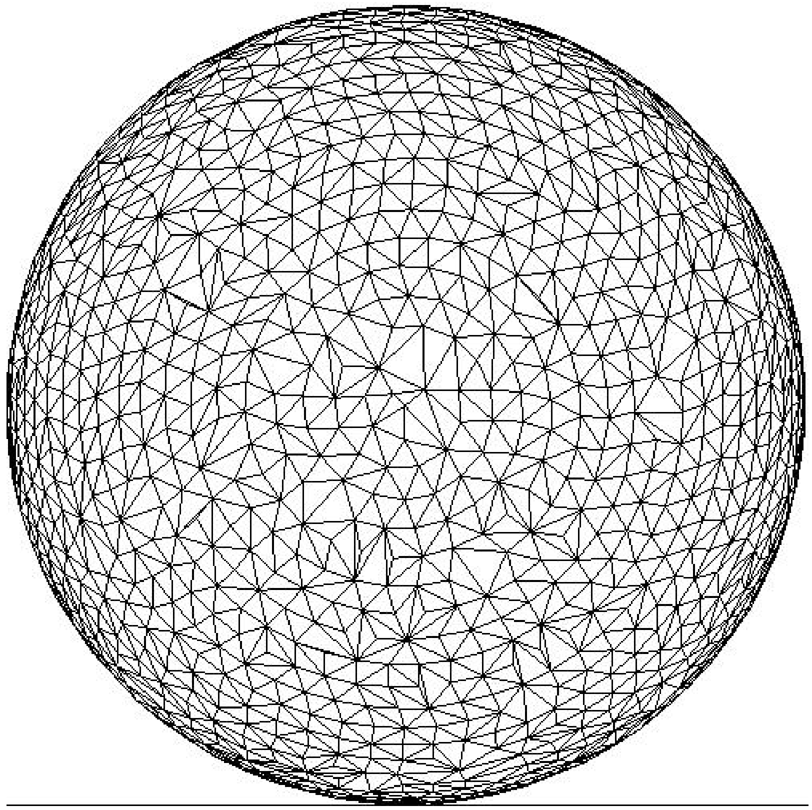

Figure 6.1: Triangulated-Sphere

6.2 Polyhedral targets

A polyhedral target is a regularly shaped body with an arbitrary number of facets. As noted in the paragraph above as many the facets the smoother the surface. Using an indefinite number of facets we end up with a sphere.
Each facet may have an arbitrary number of vertices.

6.3 Computational complexity

The closed form computation of the gravimagnetic anomaly on a polyhedral target is a function of the observation distance and the complexity of the calculations involved, constraining the distance to a critical value, depending to the error growth of the algorithm used. The complexity is also proportional to the total number of vertices of the target.

6.4 Reformulation

Every model we use is an approximated representation of a solid object with uniform density, much like integration is related to the actual volume. Density singularities however

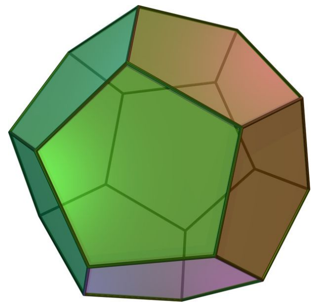

Figure 6.2: Dodekaedron

may be overcome by introducing new formulas with improved error control [12] .
The extreme abstraction of any solid object is a sphere, like the polyhedral earth viewed from a long distance as a sphere.
A very practical abstraction on any solid can be done by triangulation, decomposing the whole volume into a number of solid triangles well known as pyramids, alternatively called tetrahedra. Reformulation of a polyhedral target to a triangulated one, will involve a larger facet count, but the lower complexity on traversing each facet, will result in a lower overall complexity. Vertex, Line and Surface can be applied to this foundation with no significant changes and will create an advantage over efficiency and lower operation count.

Triangulation

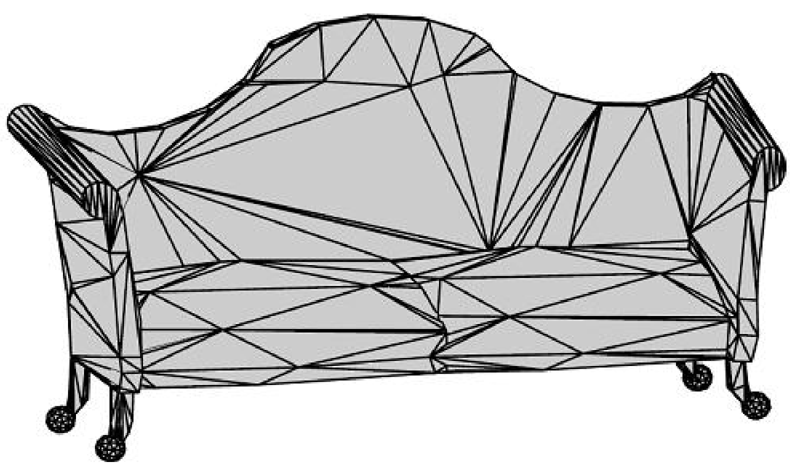

Figure 6.3: Triangulated coach

Triangles are very popular to mathematical and engineering society because they are widely used in many geometrical problems like distance measurement (Wikipedia, http://en.wikipedia.org/

) and the prerequisite knowledge lays in the sphere of elementary geometry.
The geometry of the facets of a polyhedron, can be changed without affecting the appearance of the original solid but this adds computing efficiency to the gravity algorithms.
Thus triangulation is the solid modeling technique of considering a target as a convex hull of solid triangles (tetrahedron). Due to the fact that a solid triangle can be well defined by Pythagoras, many efforts have being done to decompose objects to finite triangular elements suitable for analysis. A realistic example is the triangulated coach.

6.5 Target representation

Vectors provide a means for representing targets relatively, independent of any specific coordinate system. Usually we consider the origin to be located inside the target at an arbitrary vertex.

6.6 Solid Angle

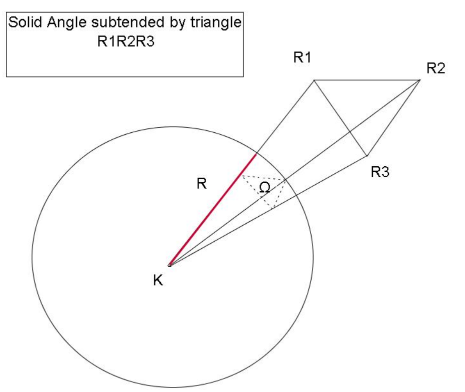

Figure 6.4: The Solid Angle approach

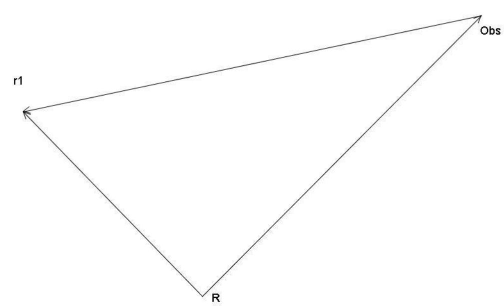

Figure 6.5: The position vector r1

$$\tan\left(\frac{1}{2}\Omega\right) = \frac{\vec{R1}.\vec{R2}.\vec{R3}}{R1R2R3 + (\vec{R1}.\vec{R2})R3 + (\vec{R1}.\vec{R3})R2 + (\vec{R2}.\vec{R3})R1} \tag{6.1}$$

Solid angle Ω is the projection on a sphere subtended by the triangle R1R2R3 expressed as part of the total sphere's surface as in figure 4. I selected the solid angle formula to be employed instead of the 2nd arctangent argument in all error growth methods (1). A triangulated model target was designed and tested for in and out conditions to successfully correspond to the solid angles subtended as expected (Ref). To validate the interior the solid angle must add for all facets at 4 and for the outside at 0. The results are found to be satisfactory with respect to efficiency and reduction in the operating loops gained from the calculation of each triangulated facet area.

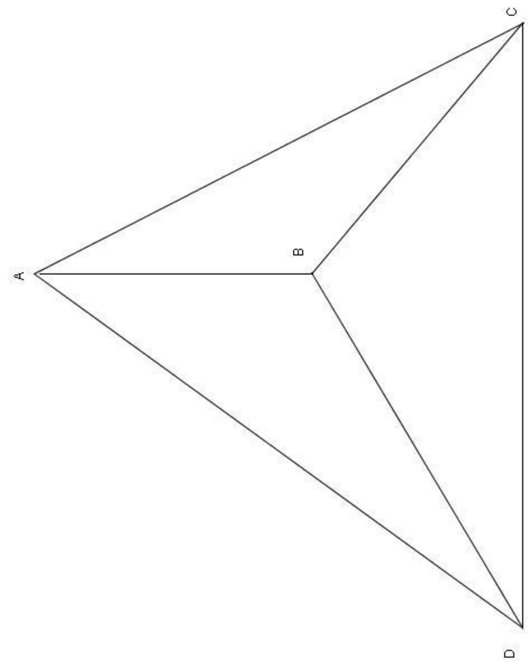

Figure 6.6: *Tetrahedron.*

6.7 Target Validation

Each target may be validated to satisfy the following assumptions: 1. Every convex hull that encloses a number of points has the sum of the area of the enclosing facets equal to zero. This condition can be applied to validate a target against the correctness of its closure. It has being tested on polyhedral, triangular and paralilepiped targets and the results were used to the rest of the process. 2. For triangular targets additional tests cover observation set ups for outside, inside, on the edge and on the surface conditions. For our experimental tetrahedral target these conditions have being validated for all set ups.

6.8 Tetrahedral targets

6.8.1 The target

A tetrahedral target is a special class of a polyhedral target with 4 facets and 4 subsequent vertices. All facets are triangles and therefore it is called a triangular target(figure 6.6. This type of target serves as the basic structure in decomposing complex structures like polyhedral targets.
A triangulated model target was designed and tested for in and out conditions to successfully correspond to the solid angles subtended as expected. It was used as a model for the implementation of all methods.

6.9 Physical problem derivation for calculating gravity anomaly

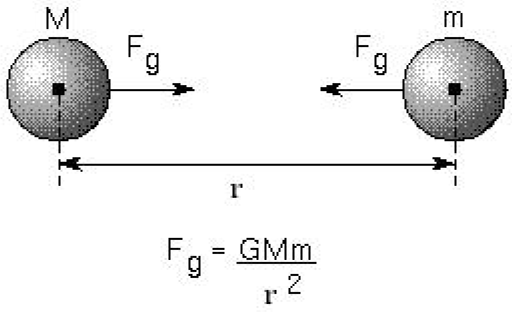

Figure 6.7: Newton's law of Gravity

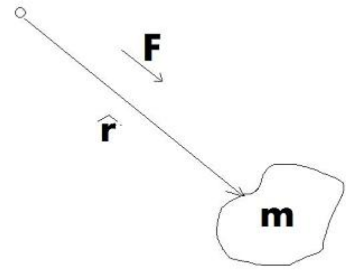

Figure 6.8: Gravity attraction of mass m from a point in space

From the Newtonian square law for one target, if we divide by M we get the gravitational field or equivalently the acceleration of mash M towards the observation point along $\vec{r}$

$$\frac{F_g}{M} = -G\frac{m}{r^2} \quad = \quad \delta\mathbf{F_g} = -G\frac{\rho\delta\upsilon\hat{\mathbf{r}}}{r^2} \tag{6.2}$$

where
F_g = gravitational force applied from a target to an observation point along direction $\hat{\mathbf{r}}$ = the unit vector or the direction of $\vec{r}$
δF_g = gravitational acceleration or vector field, along the direction $\hat{r}$
G = Universal gravitational constant $(6.672X10^-11Nm^2/kg^2)$
ρ = density of volume $\delta\upsilon$ of mass m
$\delta\upsilon$ or dv = volume integral of mass m
$\vec{r}$ = the vector distance from the observation point to an edge vertex of the target
r = the magnitude of the distance from the observation point to an edge vertex of the target
In vector form considering that ρ is constant we will get,

$$\delta\mathbf{F_g} = -G\frac{\delta\upsilon\hat{\mathbf{r}}}{r^2} \tag{6.3}$$

or

$$-\frac{\delta F_g}{G} = \int\limits_V \frac{\hat{\mathbf{r}}}{r^2}dv \tag{6.4}$$

Gauss Divergence theorem expressed by the formula:

$$\int\limits_V (div\mathbf{F})dv = \int\limits_S \mathbf{F}\cdot d\mathbf{s} \tag{6.5}$$

The right hand side of the above formula, expresses the net flux through surface S. (Gauss Divergence theorem proof: Appendices: B.2)
If we reverse engineer a function F for which ∇ F= $\frac{\hat{\mathbf{r}}}{r^2}$
we will be able to transform a volume integral to a surface integral:

$$\int\limits_V (\nabla \mathrm{F}) dv = \int\limits_S \mathrm{F} d\mathbf{S} \tag{6.6}$$

John Ketteridge in 1996 in his PhD thesis [16])describes the proof of: F=$\frac{1}{r}$
Therefore ,

$$\int\limits_V (\nabla(\frac{1}{r}) dv) = \int\limits_S \frac{d\mathbf{S}}{r} \tag{6.7}$$

the geometric gravity potential(Sheratt 2000:[33]).
On the other hand by substituting (equation B.40)div F with $\nabla \cdot \mathbf{a}$ and $\mathbf{F}$ with a general vector $\mathbf{a}$, we apply the divergence theorem. The gradient vector ∇ with x,y,z coordinates i,j,k , in cartesian form is :

$$\nabla = \mathbf{i}\frac{\partial}{\partial x} + \mathbf{j}\frac{\partial}{\partial y} + \mathbf{k}\frac{\partial}{\partial z} \tag{6.8}$$

with substitution we get:

$$\int\limits_V (\nabla \cdot \mathbf{a}) dv = \int\limits_S \mathbf{a} \cdot d\mathbf{S} \tag{6.9}$$

Lets write the vector surface element $d\mathbf{s}$ as $\mathbf{n} dS$ where $\mathbf{n}$ is the unit outward normal of the surface element and dS is its magnitude, we get:

$$\int\limits_V (\nabla \cdot \mathbf{a}) dv = \int\limits_S (\mathbf{a} \cdot \mathbf{n}) dS \tag{6.10}$$

Now if we put $\mathbf{a} = \hat{\mathbf{r}} = \frac{\mathbf{r}}{r}$ we obtain from equation 6.10:

$$\int\limits_V (\nabla \cdot \hat{\mathbf{r}}) dv = \int\limits_S ((\frac{\mathbf{r}}{r}) \cdot \mathbf{n}) dS \tag{6.11}$$

Reducing the brackets in the right hand side of equation 6.10

$$\int\limits_V (\nabla \cdot \hat{\mathbf{r}}) dv = \int\limits_S (\mathbf{r} \cdot \mathbf{n}) \frac{dS}{r} \tag{6.12}$$

From the manuscript of Holstein and Sherratt,2000 eq.14 we know that:

$$\frac{1}{2}(\nabla \cdot \hat{\mathbf{r}}) = \frac{1}{r} \tag{6.13}$$

If we substitute 6.13 into B.45 we get a volume integral transformed into a surface integral through Gauss Divergence([33]) or in other words the facet integrals can be expressed as the sum of contributions from the separate plane facets:S_i.([3])

$$V = \frac{1}{2}\int_V (\nabla \cdot \hat{\mathbf{r}}) dv = \frac{1}{2}\int_S (\mathbf{r} \cdot \mathbf{n})\frac{dS}{r} \tag{6.14}$$

Using Stokes curl theorem on the right hand of equation 6.14:

$$\int_S (curl\mathbf{F}) \cdot d\mathbf{S} = \oint_{\theta S} \mathbf{F} \cdot d\mathbf{r} \tag{6.15}$$

where dr is a boundary line element of the surface θS_i and in the polyhedral case , in which each facet is a polygonal area in which each vertex is joined by straight lines, a line segment.
Applying the same argument as before,
if a vector F where:

$$curl\mathbf{F} = \nabla \wedge \mathbf{F} = \frac{\mathbf{n_i}}{r} \tag{6.16}$$

can be found, then Stoke's theorem can be applied to the surface integral.
We know that (Okabe, 1979)[25] such a vector exists,

$$\mathbf{F} = \hat{\boldsymbol{\theta}}\frac{r - \upsilon}{R} \tag{6.17}$$

graphically expressed in a cylindrical polar coordinate space

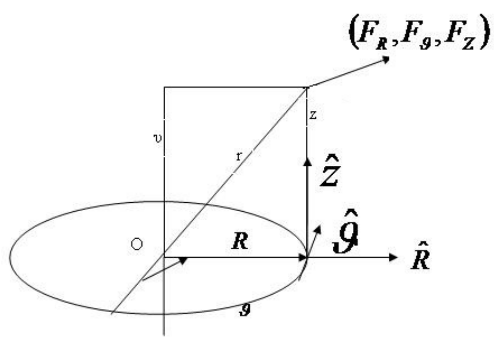

Figure 6.9: Stokes theorem: vector F in a surface θ-R,with υ constant

(Ketteridge:Ph.D thesis,1996 [16])
as in figure 6.9 and since:

$$\hat{\boldsymbol{\theta}} = \mathbf{n} \wedge \hat{\mathbf{R}} \tag{6.18}$$

$$\left(\mathbf{n} \wedge \hat{\mathbf{R}}\right) R = \mathbf{n} \wedge \mathbf{R} \tag{6.19}$$

$$\mathbf{n} \wedge \mathbf{R} = \mathbf{n} \wedge \mathbf{r} \tag{6.20}$$

leading to a closed form integration of cij contributions over each vertex j around a facet i, with respect to l:

$$c_{ij} = h_{ij} \int_{l_{1ij}}^{l_{2ij}} \frac{dl}{\sqrt{r_{0ij}^2 + l^2 + \upsilon_i^2}} \tag{6.21}$$

Considering that the arguments of the vertex formula are defined in terms of the unit edge tangent vector t_{ij}:

$$t_{ij} = (\mathbf{r}_{2ij} - \mathbf{r}_{1ij}) / |\mathbf{r}_{2ij} - \mathbf{r}_{1ij}| \tag{6.22}$$

$$\upsilon_i = \mathbf{r}_{ij} \cdot \mathbf{n}_i = \mathbf{r}_{2ij} \cdot \mathbf{n}_i \tag{6.23}$$

$$h_{ij} = \mathbf{r}_{1ij} \cdot (\mathbf{t}_{ij} \wedge \mathbf{n}_i) = \mathbf{r}_{2ij} \cdot (\mathbf{t}_{ij} \wedge \mathbf{n}_i) \tag{6.24}$$

$$l_{1ij} = \mathbf{r}_{1ij} \cdot \mathbf{t}_{ij}, l_{2ij} = \mathbf{r}_{2ij} \cdot \mathbf{t}_{ij} \tag{6.25}$$

$$r_{0ij} = \sqrt{\upsilon_i^2 + h_{ij}^2} \tag{6.26}$$

ommiting all subscripts we get:

$$c_{ij} = h \ln \left(\frac{r+l}{r_0} \right) + \upsilon \arctan \left(\frac{l}{h} \frac{\upsilon}{r} \right) - |\upsilon| \arctan \left(\frac{l}{h} \right) \tag{6.27}$$

If h=0 then $c_{ij} = 0$ Equation 6.21 expresses the Vertex method for evaluating a line integral over the target vertices and it is numerically computed through formula 6.27 Substituting term $\arctan\left(\frac{l}{h}\right)$ with the angle subtended by edge $\mathbf{r}_0, \mathbf{r}$ $2\pi\epsilon$ (Gotze and Lahmeyer[10])we get:

$$c_{ij} = h \ln \left(\frac{r+l}{r_0} \right) + \upsilon \arctan \left(\frac{l}{h} \frac{\upsilon}{r} \right) - |\upsilon| 2\pi\epsilon \tag{6.28}$$

Pohanka (1988,1990 [39])combined the two arctan terms

$$\arctan \left(\frac{l}{h} \frac{\upsilon}{r} \right) - \arctan \left(\frac{l}{h} \right) \tag{6.29}$$

to one as shown later in this chapter by arctan compaction, section 6.12.3:

$$\arctan \left(\frac{lh}{r_0^2 + r|\upsilon|} \right) \tag{6.30}$$

Then, equation 6.27 becomes

$$c_{ij} = h \ln \left(\frac{r+l}{r_0} \right) + \upsilon \arctan \left(\frac{lh}{r_0^2 + r\upsilon} \right) \tag{6.31}$$

6.10 Order of magnitude of anomaly formulae

Gravity field anomaly f_g from polyhedral target with outward normals $\mathbf{n}_i$ and gravitational density factor G_ρ is:

$$f_g = G_\rho \int\limits_V \nabla(1/r)dV = G_\rho \sum_i \mathbf{n}_i \int\limits_{S_i} dS/r \tag{6.32}$$

The left hand gives Newtonian complexity:
$O(\alpha^3/\delta^2)$
For each separate integration step the amplification factor is $\gamma^{-1} = \delta$. This amplification factor gives a total amplification of γ^{-3} of added complexity for the integration up to the vertex evaluation.If we now add the Newtonian complexity $O(\alpha^3/\delta^2) = O(\alpha\gamma^2)$
we get the total complexity of $O(\alpha\gamma^2\gamma^{-3})$
This is the Vertex method complexity. Therefore to retend any significance of the result we require that:
$\gamma^{-3} \ll \frac{1}{e}$ or $\gamma^{-3} \ll 1$ or $\gamma \gg e^{\frac{1}{3}}$ or $\delta^3 \ll \frac{1}{e}$
That means that for a double FP precision of 2^{-54} with machine constant $e \approx 2,22044604925031E-16$ a significant distance using the Vertex method, must be $\ll (\frac{1}{e})^{\frac{1}{3}}$ or
$1,65140371851821E+05$ times the target dimension α. In the sheet case the gravitational potential per unit thickness is given only by a surface integral found on the right of equation 7.2one integration step less. and a lower by δ stability horizon of $\gamma \gg e^{\frac{1}{2}}$ in numbers, 6,7108864E+07 times the target dimension α
For the Line method the stability is improved by 1 δ i.e $\gamma \gg \frac{1}{e}$ or significant distances of $\ll 4,5035996273705E+15$
For the thin sheet surface method we have γ^0 amplification factor or absolute stability at the Newtonian order of complexity, without any error growth. Therefore the anomaly calculation will not be distance bounded.

6.11 Methods for calculating gravity anomaly

Anomally algorithms exhibit the manner in which anomaly calculations in a given precision ϵ degrade with increasing dimensionless target distance $1/\gamma = \delta/\alpha$. All methods presented in the present work, are extensively discussed in the Holstein and Ketteridge 1996, "Gravimetric analysis for uniform Polyhedra". The methods are 3, namely Vertex, Line and Surface and form a classification standard for any new method with respect to error growth. They have being implemented from Holstein et al., in languages like C++, MAPLE and JAVA. Each method represents a different error growth class, after the precision break-down. The error growth analysis offers a precious tool for estimating the useful operating range for each method. All methods compute gravity anomaly by numerically evaluating volume integrals through transformations (the nature depends on the method) with respect to a specific observation point. A basic program flow is demonstrated in figure 6.11

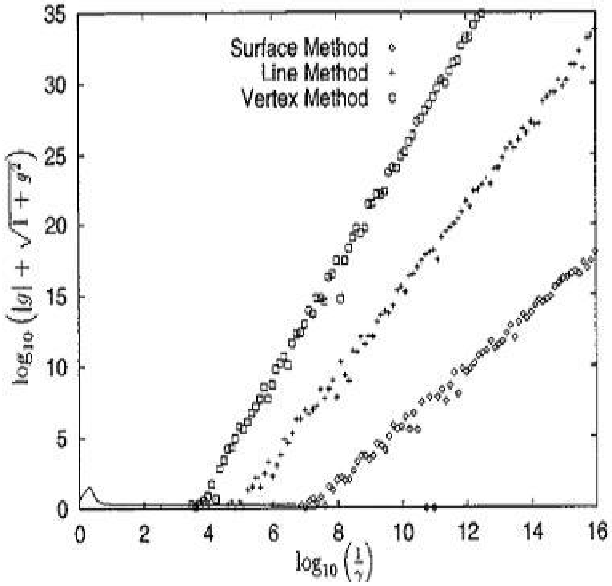

Figure 6.10: Error growth from the 3 anomally methods

6.11.1 Relative error estimation of anomaly formulae

The anomaly calculation is governed by a volume integral weighted by the inverse square law factor $\frac{1}{\delta^2}$ and thus has a magnitude of $O(\alpha\gamma^2)$. After the transformations to surface and line integrals order of dominant terms is amplified by γ^{-3}.
Where δ is a large quantity, representing a distance of the observation point from the target. If an anomaly of size α (i.e. the result) is computed by adding terms of $O(\alpha\gamma^{-3})$, then as the observation point becomes remote from the target (i.e. $\gamma \to 0$), the terms to be summed get larger and larger in relation to the anomaly itself, and destructive cancellation in the summation will make itself felt via rounding error that ultimately exceeds the size of the anomaly itself.

To express this in symbols: in a precision epsilon, the representation error in a number α is $O(\alpha\epsilon)$. When summing numbers of $O(\alpha\gamma^{-3})$, the representation error is $O(\alpha\gamma^{-3}\epsilon)$. The relative error (i.e. the error compared to the size of the correct answer) is then relative error $=$ $O(\alpha\gamma^{-3}\epsilon)/\alpha$, or relative error $= O(\gamma^{-3}\epsilon)$.

Note that the relative error expression is independent of the quantity that we are interested in, the anomaly α. The relative error depends on the growth factor γ^{-3} and the precision epsilon. This is a consequence of the way floating point arithmetic works. The relative representation error is epsilon no matter what the number is being represented. (This is an approximation, because of the saw-tooth effect: - the relative error can vary by almost a factor 2, as it concerns the least significant bit in the mantissa).

When the relative error is of order 1, the error is of the same size order as the anomaly. This means that all significance in the calculation is lost. So, to get meaningful results, the relative error has to be very much less than 1, hence the requirement relative error $<< 1$, or $O(\gamma^{-3}\epsilon) << 1$ (appendices:**??**) for valid calculations. This reasoning assumes there is no error in the calculation steps, i.e. you can imagine you have a machine of infinite precision to do each calculation for a particular summand, but then cut back to a precision epsilon to do the summation. In practice, of course, the calculation sub-steps are subject to rounding error as well, so the actual error could be (statistically) larger than indicated by the rel err formula. In practice, the above rel err formula gives a best estimate. Actual errors may be larger depending on the stability of the algorithm. Finally, note that actual errors CAN also be smaller than indicated by the formula, because rounding acts like a roulette wheel, and it is just possible that the errors cancel out. The statistical chance of this happening on a regular basis, however, are vanishingly small(this is not proved).

α is small like the target dimension in metrics: m^2,
γ is a ratio of a small quantity like α, over a large one like δ.
In terms of order of complexity each class of formulae appears to have its own error growth factor, depending in the order of the dominant terms involved in the evaluation. However, formulae for gravity and magnetic anomalies of uniform polyhedral targets exhibit a well-studied numerical instability (Strakhov et al. (1986)[27], Holstein and Ketteridge (1996)[16]). When computed in a finite floating point precision ", the results from such formulae steadily degrade to the point of succumbing totally to computational noise, as the target distance δ increases relative to the target size α. The formulas limiting floating point horizon is normally beyond the region of geophysical interest, but the loss of accuracy incurred on the way can be important when the target size to target distance ratio $\gamma = \alpha/\delta$ is much less than 1, as can happen for very finely tesselated targets or targets investigated in remote sensing. The instability arises from the analytical evaluation of the target source volume integral, which introduces a factor $1/\gamma$ at each integration stage from volume to surface, surface to line (edge), and edge to vertex end-points, resulting in summands magnified by a factor $1/\gamma^3$ over the anomaly size. An anomaly α therefore commits a truncation error of (α/γ^3), with a relative error ϵ/γ^3 This relative error becomes unbounded as $\gamma \to 0$. With a given precision symbolized by ϵ for a given platform(Appendices: E.1) we have exhibit the following anomaly formulae classes:
$\Rightarrow$ Vertex method has an error of $O(\alpha\gamma^-1\epsilon)$ and thus is proper for $\gamma \ggg \epsilon^{\frac{1}{4}}$
$\Rightarrow$ Line method $O(\alpha\epsilon)$ and thus is proper for $\gamma \ggg \epsilon^{\frac{1}{3}}$
$\Rightarrow$ Surface method $O(\alpha\gamma\epsilon)$ and thus is proper for $\gamma \ggg \epsilon^{\frac{1}{2}}$
$\Rightarrow$ Volume method expected to have $O(\alpha\gamma^2\epsilon)$ and thus will be proper for $\gamma \ggg \epsilon$

6.12 Formal solution

6.12.1 Defining the invariant quantity b_{ij}

We decompose the result of equation 6.27 in 2 terms abbreviated to log and arctan, respectively(equation 6.33).
As the distance from the target grows over a critical distance the error overcomes the real outcome, the truncation error being expressed as a function of the precision estimator(ϵ), in terms of a particular platform.

In that case the need for developing low order (O) algorithms is crucial and scientifically beneficiary. The difference in error growth between methods lies to the derivation from

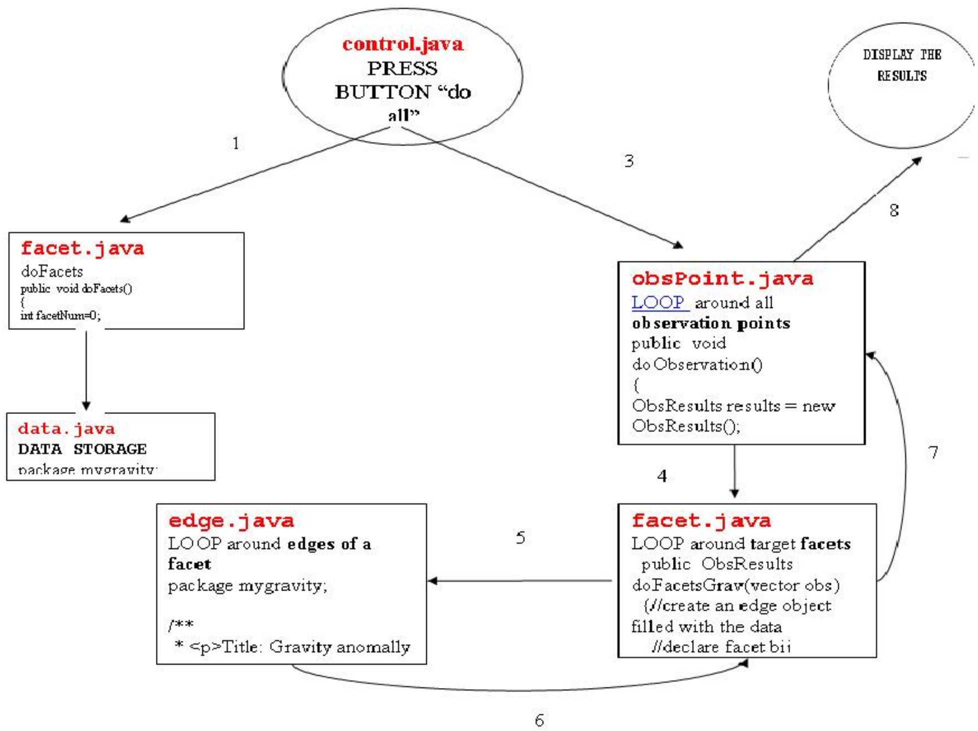

Figure 6.11: JAVA - implementating gravimagnetic anomaly, CLASS FLOW DIAGRAM

theory and affects their computational complexity. It is a stepwise refinement eliminating in each step redundancy with analytical cancellation. If the operation counts and algorithmic complexity are both optimal, the redundancy between large terms will be also optimal. This occurs because the computer decimal precision capabilities are constrained from a fixed number of bits. On the other hand theory states that the calculations may involve an infinite number of digits (see Fourier transforms).

Closed expressions for c_{ij} vertex contributions are given in terms of a unique vector quantity:

$$\mathbf{b}_{kij} = \left(b_{kij}^{(h)}, b_{kij}^{(n)} \right) \tag{6.33}$$

in the $(\hat{\mathbf{h_{ij}}}, \mathbf{n_i})$ plain the following relations are established:
k=1,2:

$$b_{kij}^{(h)} = ln \left(\frac{r_{kij} + l_{kij}}{r_{0ij}} \right) \tag{6.34}$$

$$b_{kij}^{(n)} = -\arctan \left(\frac{l_{kij}}{h_{ij}} \frac{\upsilon_i}{rkij} \right) + sign(\upsilon_i) \arctan \left(\frac{l_{kij}}{h_{ij}} \right) \tag{6.35}$$

$$\mathbf{b}_{kij} = \hat{\mathbf{h_{ij}}} b_{kij}^{(h)} - \mathbf{n}_i b_{kij}^{(n)} \tag{6.36}$$

In terms of differences at vertices k=1 and k=2 of edge ij and omiting k, terms c_{kij}, $\mathbf{b_{kij}}$ and c_{ij},$\mathbf{b_{ij}}$ are linked by,

$$c_{kij} = h_{ij} \int_0^{l_{kij}} \frac{dl}{\left(r_{0ij}^2 + l^2 \right)^{\frac{1}{2}}} = \mathbf{r_{kij}} \cdot \mathbf{b_{kij}} = h_{ij} b_{kij}^{(h)} + \upsilon_i b_{kij}^{(n)} \tag{6.37}$$

$$c_{ij} = c_{kij} ||_{k=1}^{k=2} = \mathbf{r_{1ij}} \cdot \mathbf{b_{ij}} = \mathbf{r_{2ij}} \cdot \mathbf{b_{ij}} = h_{ij} b_{kij}^{(h)} + \upsilon_i b_{kij}^{(n)} \tag{6.38}$$

Arctangent terms in equation 6.35 are evaluated in the range $[-\pi/2, \pi/2]$
From the above equations, ommiting subscript k, we link $\mathbf{c}_{ij}$ with $\mathbf{b}_{ij}$ to get:

$$c_{ij} = \mathbf{b}_{ij} \cdot \mathbf{r}_{ij} \tag{6.39}$$

6.12.2 Formulation of the numerical algorithms

To link theory with implementation we will drawback to the right hand side of equation 6.14 which we can transform from a surface integral to a numerically computable sum of contributions around the edges . The sum around edges

expression, can be computed around a loop structure apparently under the appropriate condition statement. Using the summation symbol $\sum$ over facets $\sum_i$ and edges respectively $\sum_j$ we can write:

$$V = \frac{1}{2}\int_S (\mathbf{r}\cdot\mathbf{n})\frac{dS}{r} = \frac{1}{2}\sum_i \mathbf{r}_i\cdot\mathbf{n}_i \sum_j c_{ij} = \frac{1}{2}\sum_i \mathbf{r}_i\cdot\mathbf{n}_i \sum_j \mathbf{b}_{ij}\cdot\mathbf{r}_{ij} \tag{6.40}$$

Let us now remember our two major constucts, the scalar quantity c_{ij} and the vector quantity $\mathbf{b}_{ij}$. Using the first we compute gravity potential V:

$$\sum_j c_{ij} = \sum_j \mathbf{b}_{ij}\cdot\mathbf{r}_{ij} = \sum_j h_{ij}b_{ij}^{(h)} + \sum_j \upsilon_i b_{ij}^{(n)} \tag{6.41}$$

$$\sum_i \mathbf{r}_i\cdot\mathbf{n}_i = \sum_i \upsilon_i \tag{6.42}$$

and therefore:

$$V = \frac{1}{2}\sum_i \upsilon_i \sum_j (h_{ij}b_{ij}^{(h)} + \upsilon_i b_{ij}^{(n)}) = \frac{1}{2}\sum_i \upsilon_i \sum_j c_{ij} \tag{6.43}$$

Using the second: $\mathbf{b}_{ij}$:

$$\sum_j \mathbf{b}_{ij} = \sum_j \hat{\mathbf{h}}_{ij}b_{ij}^{(h)} + \sum_i \mathbf{n}_i \sum_j b_{ij}^{(n)} \tag{6.44}$$

we compute gravity gradient $\mathbf{G}_g$:

$$\mathbf{G}_g = \sum_i \mathbf{n}_i \sum_j \mathbf{b}_{ij} \tag{6.45}$$

6.12.2.1 Substitution of the constructor quantity b_{ij}^n with Ω quantity

From the Holstein paper on gravimagnetic similarity ([15])the quantity Ω_i was introduced as:

$$\Omega_i = -\int_{S_i} \nabla\frac{1}{r}\cdot\mathbf{dS} = \int_{S_i} \hat{\mathbf{r}}\cdot\frac{\mathbf{dS}}{r^2} \tag{6.46}$$

in which Ω_i is the solid angle subtended by the facet i at the observation point. The sign of Ω_i is that of $\mathbf{r}\cdot\mathbf{n}_i$.In the same paper, after simplification of the surface and edge integrals, we get:

$$\int\limits_{S_i} dS/r = \sum_j h_{ij} C_{ij} - \upsilon_i \Omega_i \tag{6.47}$$

Considering that,

$$C_{ij} = \int\limits_{\partial S_{ij}} dl/r = b_{ij}^{(h)} \tag{6.48}$$

Equation 6.43 becomes:

$$V = \frac{1}{2} \sum_i \upsilon_i \left(\sum_j h_{ij} b_{ij}^{(h)} - \upsilon_i \Omega_i \right) \tag{6.49}$$

Also the constructor vector quantity $\mathbf{b}_{ij}$ can be defined as:

$$\mathbf{b}_{ij} = \hat{\mathbf{h}}_{ij} C_{ij} - \mathbf{n}_i \Omega_i \tag{6.50}$$

The above formulae 6.49,6.50 incorporate the solid angle subtended by facet i, to all gravi-magnetic computations and are candidates to improving computation efficiency of anomaly on tetrahedral targets, matter that we will extensively examine in the respective latter chapter.

6.12.3 Arctan compaction

The idea here is to reduce the computation complexity by combining the two arctan agruments to one. We start from the identity:

$$tan(A - B) = \frac{tanA - tanB}{1 - tanAtanB} \tag{6.51}$$

which leads to:

$$tan(\arctan a - \arctan b) = \frac{\tan(\arctan a) - \tan(\arctan b)}{1 + \tan(\arctan a)\tan(\arctan b)} = \frac{a - b}{1 + ab} \tag{6.52}$$

Hence:

$$\arctan a - \arctan b = \arctan \left(\frac{a - b}{1 + ab} \right) \tag{6.53}$$

Thus:

$$\arctan \frac{1}{h} - \arctan \frac{l\upsilon}{rh} = \frac{\frac{1}{h}\left(1 - \frac{\upsilon}{r}\right)}{1 + \frac{\upsilon}{r}\left(\frac{l}{h}\right)^2} = \tag{6.54}$$

$$\frac{\frac{1}{h}\left(1 - \frac{\upsilon}{r}\right) rh^2}{1 + (rh^2 + \upsilon l^2)} = \frac{lh\,(r - \upsilon)}{(r - \upsilon)\,h^2 + \upsilon\,(h^2 + l^2)} \tag{6.55}$$

$$= \frac{lh\,(r-\upsilon)}{(r-\upsilon)\,h^2+\upsilon\,(r_2-\upsilon_2)} = \frac{lh}{h^2+\upsilon\,(r+\upsilon)} \tag{6.56}$$

$$= \frac{lh}{(h^2+\upsilon^2)+r\upsilon} = \frac{lh}{r_0^2+r\upsilon} \tag{6.57}$$

The result matches with Pohanka 6.31 and Holstein Ketteridge (1996, [16]). Equation 6.57 will not work with h and υ both zero. If h=0 then the integral is zero. In all other cases, can be substituted in equation 6.27 above to give equation 6.31 and consequently equation 6.35 also becomes:

$$b_{kij}^{(n)} = -sign(\upsilon_i)arctan\left(\frac{l_{kij}h_{ij}}{r_{0ij}^2+r\upsilon_i}\right) \tag{6.58}$$

6.12.3.1 The solution of Strakhov-Line method

In two papers by Strakhov (1986,1988, [40, 27]) the following symbols were defined for a facet edge, using the notation as of paper Comparison of Gravimagnetic formulae by Holstein et al.([26]):

$$\Lambda = |L|/(r_2+r_1) \tag{6.59}$$

$$\Sigma = \frac{1}{2}(r_1+r_2-|L|\Lambda) \tag{6.60}$$

$$\lambda = h\Lambda/(|\upsilon|+\Sigma) \tag{6.61}$$

$$\mathbf{h}_{ij} = \mathbf{t}_{ij}\wedge\mathbf{n}_i \tag{6.62}$$

$$\mathbf{t}_{ij} = \frac{(\rho_{2ij}-\rho_{1ij})}{L_{ij}} \tag{6.63}$$

$$\mathbf{n}_i = \frac{\mathbf{A}_i}{|\mathbf{A}_i|} \tag{6.64}$$

$$h_{ij} = |\mathbf{h}_{ij}| = \mathbf{r}_{ij}\cdot\mathbf{h}_{ij} \tag{6.65}$$

$$\upsilon_i = \mathbf{r}\cdot\mathbf{n} \tag{6.66}$$

$$r_1 = |\mathbf{r}_1|, r_2 = |\mathbf{r}_2| = \left(\rho_i\cdot\rho_i - 2L\rho_i\cdot\hat{\mathbf{L}}L + L^2\right) \tag{6.67}$$

L_{ij} = edge length
ρ_{1ij},ρ_{2ij} = the position vectors from the local origin to the edge vertices $1_{ij}, 2_{ij}$
$\mathbf{r}_{1ij}, \mathbf{r}_{2ij}$ = the position vectors from the observation point to the edge vertices $1_{ij}, 2_{ij}$
$\hat{\mathbf{L}}L$=the position vector from the local origin to the observation point.

The effect of nearness of an observation point to an edge is expressed ([33])with the inequality:
$1 \geq \Lambda_{ij} \geq \frac{1}{2}$
In terms of the constructor vector quantity $\mathbf{b}_{ij}$ line method is defined ([22])as:

$$\sum_j \mathbf{b}_{ij} = 2\sum_j \mathbf{h}_{ij}b_{ij}^h - 2\sum_i \mathbf{n}_i\sum_j b_{ij}^n \tag{6.68}$$

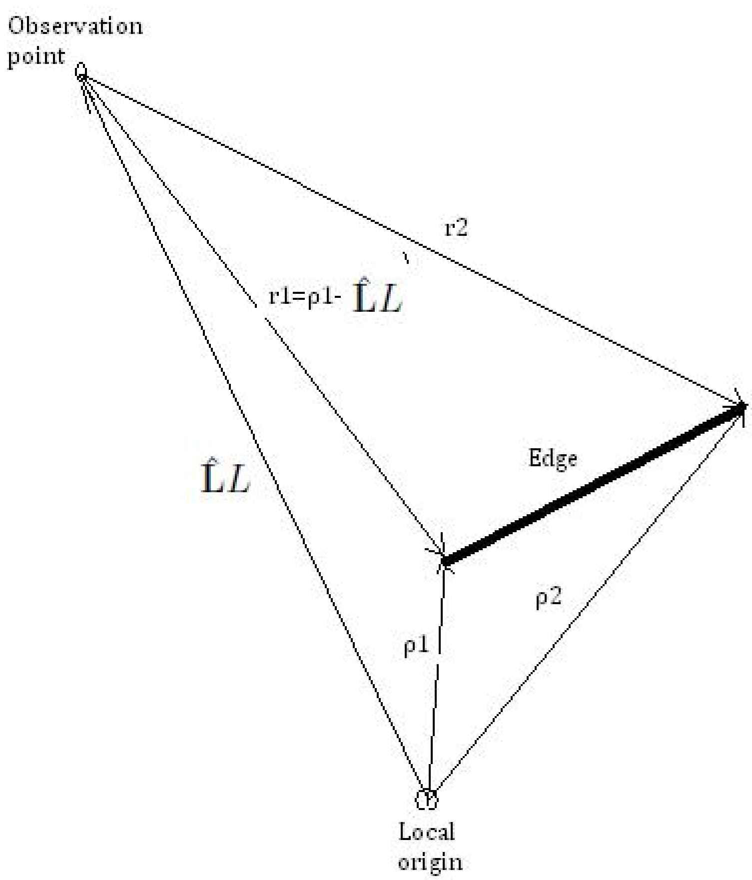

Figure 6.12: Edge vectors: r1,r2,ρ_1,ρ_2,$\hat{\mathbf{L}}L$

the constructor vector quantity being:

$$\mathbf{b}_{ij} = 2\mathbf{h}_{ij} b^h_{ij} - 2\mathbf{n}_i b^n_{ij} \tag{6.69}$$

with components:

$$b^h_{ij} = \arctan \Lambda_{ij} \tag{6.70}$$

$$b^n_{ij} = -\text{sign}(\upsilon_i) \arctan \lambda_{ij} \tag{6.71}$$

or:

$$\mathbf{b}_{ij} = 2\mathbf{h}_{ij} \text{arctanh}\Lambda_{ij} - 2\mathbf{n}_i \text{sign}(\upsilon_i) \arctan \lambda_{ij} \tag{6.72}$$

substituting in equation 6.68 with equations of components 6.70,6.71 and
$\Omega_i = 2sign(\upsilon_i) \sum_{j=1..3} \arctan \lambda_{ij}$
we get gravity field:

$$\sum_{j=1..3} \mathbf{b}_{ij} = \sum_{j=1..3} 2\mathbf{h}_{ij} \text{arctanh}\Lambda_{ij} - \mathbf{n}_i \Omega_i \tag{6.73}$$

and for gravity potential:

$$\sum_{j=1..3} \mathbf{r}_{ij} \cdot \mathbf{b}_{ij} = \sum_{j=1..3} 2h_{ij} \text{arctanh}\Lambda_{ij} - \upsilon_i \Omega_i \tag{6.74}$$

Where Ω is known to be the solid angle subtended by the facet at the observation point (Holstein 2002 [**?**]). It may be replaced by a single artangent as derived from Oosterom and Strackee(1983,[35])for the solid angle of a triangle,

$$\Omega_i = 2 \arctan \frac{2\upsilon_i \Lambda_i}{r_{i1} r_{i2} r_{i3} + r_{i1}(\mathbf{r}_{i2} \cdot \mathbf{r}_{i3}) + r_{i2}(\mathbf{r}_{i3} \cdot \mathbf{r}_{i1}) + r_{i3}(\mathbf{r}_{i1} \cdot \mathbf{r}_{i2})} \tag{6.75}$$

The above formula 6.74 is suitable for efficient computation as it will be examined in more detail in a later chapter.

6.12.3.2 The solution of Holstein et al - the Surface method

Surface method is implemented in stages.Through a stepwise analytical refinement starting from the Line method, pre-cancelling of large terms takes place before computation. This way less precision is required from complex operations in terms of magnitudes.
Step 1
Starting with Line method:

$$\frac{1}{2} \sum_j c_{ij} = \sum_j h_{ij} \text{arctanh}\Lambda_{ij} - |\upsilon_i| \arctan \lambda_{ij} \tag{6.76}$$

We define:
log term to be: $\sum_j h_{ij} \text{arctanh}\Lambda_{ij}$

Arctan term to be: $\sum_j |\upsilon_i| \arctan \lambda_{ij}$
Substituting we get:

$$\frac{1}{2}\sum_j c_{ij} = \text{log term - arctan term} \tag{6.77}$$

or:
if replacing with contructor term b_{ij}(6.38):
log term with $\sum_j h_{ij} b_{ij}^{(h)}$
arctan term with $\sum_j \upsilon_i b_{ij}^{(n)}$
we get:

$$\frac{1}{2}\sum_j c_{ij} = \sum_j h_{ij} b_{ij}^{(h)} - \sum_j \upsilon_i b_{ij}^{(n)} \tag{6.78}$$

Step 2
Differencing arctan terms

$$\text{arctanh}\Lambda_{ij} = \text{arctanh}(\Lambda_{ij} - \Lambda_{ij}), \arctan \lambda_{ij} = \arctan(\lambda_{ij} - \lambda_{ij}) \tag{6.79}$$

and then adding back-on the remaining offsets signed as appropriate,we get:
$h_{ij}\Lambda_{ij}, |\upsilon_i|\lambda_{ij}$

$$\frac{1}{2}\sum_j c_{ij} = \sum_j h_{ij}(\text{arctanh}\Lambda_{ij} - \Lambda_{ij}) - |\upsilon_i|(\arctan \lambda_{ij} - \lambda_{ij}) + \sum_j h_{ij}\Lambda_{ij} - |\upsilon_i|\lambda_{ij} \tag{6.80}$$

Step 3
We substitute the differences using the custom functions Atnh() and Atn()respectively for arctanhΛ_{ij} and $\arctan \lambda_{ij}$ defined by delayed arctanh and arctan series(Appendices:F)
Replace
arctanh$\Lambda_{ij} - \Lambda_{ij}$ with :
Λ_{ij}^3AtnhΛ_{ij}
where: Atnh$\Lambda_{ij} = \frac{1}{3} + \frac{\Lambda_{ij}^2}{5} + \frac{\Lambda_{ij}^4}{7}$
arctanh$\lambda_{ij} - \lambda_{ij}$ by λ_{ij}^3Atnλ_{ij}
where:
Atn$\lambda_{ij} = -\frac{1}{3} + \frac{\Lambda_{ij}^2}{5} - \frac{\Lambda_{ij}^4}{7}$
Hence:

$$\sum_j c_{ij} = 2\sum_j (h_{ij}\Lambda_{ij}^3 \text{Atnh}\Lambda_{ij} - |\upsilon_i|\lambda_{ij}^3 \text{Atn}\lambda_{ij}) + 2\sum_j h_{ij}\Lambda_{ij} - |u_i|\lambda_{ij} \tag{6.81}$$

If we want to substitute solid angle in the surface method the formula will become:

$$\text{logterm} - |\upsilon|\text{arctan(solid angle)} \tag{6.82}$$

Step 4 - Introduce quantities:

$\Lambda^*_{ij}, \lambda^*_{ij}$

to express the offset term $\Lambda_{ij}, \lambda_{ij}$ defined in the 1999 paper([26]), equations:(59),(60)

Hence:

$$\sum_j c_{ij} = 2\sum_j (h_{ij}\Lambda^3_{ij}\text{Atnh}\Lambda_{ij} - |\ \upsilon_i|\lambda^3_{ij}\text{Atn}\lambda_{ij}) + 2\sum_j \big(h_{ij}(\Lambda_{ij} - \Lambda^*_{ij}\big)$$
$$-|\upsilon_i|(\lambda_{ij} - \lambda^*_{ij})) + 2\sum_j (h_{ij}\Lambda^*_{ij} - |\upsilon_i|\lambda^*_{ij})$$

Step 5

Express the final sum by its analytical equivalent

$$\sum_j c_{ij} = 2\sum_j (h_{ij}\Lambda^3_{ij}\text{Atnh}\Lambda_{ij} - |\upsilon_i|\lambda^3_{ij}\text{Atn}\lambda_{ij}) + 2\sum_j (h_{ij}(\Lambda_{ij} - \Lambda^*_{ij}) - |\upsilon_i|(\lambda_{ij} - \lambda^*_{ij})) + \frac{2A_i}{r_c + |u_i|} \tag{6.83}$$

where A_i is the scalar area of facet i.

(Note that the cross-product formula for the (vector) area naturally calculates the facet area).

Step 6

We find expressions for differenced quantities $\Lambda_{ij} - \Lambda^*_{ij}$ and $\lambda_{ij} - \lambda^*_{ij}$ such that a vector $\vec{r}_c$ common to the whole target substitutes vectors $\vec{r}_1$, $\vec{r}_2$.

$$\Lambda_{ij} - \Lambda^*_{ij} = \Lambda_{ij}\Delta_{ij} \tag{6.84}$$

$$\lambda_{ij} - \lambda^*_{ij} = (\lambda_{ij} + \tilde{\lambda_{ij}})\Delta_{ij} + \tilde{\lambda_{ij}}\Lambda_{ij}\Lambda^*_{ij} \tag{6.85}$$

Step 7

Final step, substitution of differences

$$\begin{aligned}\sum_j c_{ij} &= 2\sum_j (h_{ij}\Lambda^3_{ij}\text{Atnh}\Lambda_{ij} - |\upsilon_i|\lambda^3_{ij}\text{Atn}\lambda_{ij}) \\ &+ 2\sum_j (h_{ij}\Lambda_{ij}\Delta_{ij} - |\upsilon_i|(\lambda_{ij} + \tilde{\lambda_{ij}})\Delta ij + \lambda_{ij}\tilde{\Lambda_{ij}}\Lambda^*_{ij}) \\ &+ \sum_i \frac{2A_i}{r_c + |u_i|}\end{aligned} \tag{6.86}$$

The last final expression gives the Surface method error growth and can be implemented without bugs, in a step by step refinement process, as indicated with the above sequence. Analytical cancellation gives results validating the theoretical error growth at the last step of the implementation. At this step let us create a friendly to computation formula, maping terms to variables as follows: log,arctan,offset1,offset2, to be evaluated at every edge(edge loop) and offset3 to be evaluated at every facet(facet loop). Writing in general form ommiting $\sum$ and subscripts we may have:

$$\text{Log} = h\Lambda^3 \text{Atnh}(\Lambda) \tag{6.87}$$

$$\text{Arctan} = -|\upsilon|\lambda^3 \text{Atn}(\lambda) \tag{6.88}$$

$$\text{offset1} = h\Lambda\Delta \tag{6.89}$$

$$\text{offset2} = -|\upsilon| \left(\lambda + \tilde{\lambda}\right) \Delta + \tilde{\lambda}\Lambda\Lambda^* \tag{6.90}$$

$$\text{offset3} = \frac{2A}{r_c + |\upsilon|} \tag{6.91}$$

thus including $\sum$s to indicate involved loop structures we could get :
$c_{ij} = 2\sum_j$(Log+Arctan+offset1+offset2) $+ 2\sum_i$offset3
(reference: 6.11)

If we want to substitute the solid angle formula into the surface method, we must substitute Arctan term and its offset2 term :

$$-|\upsilon_i|\lambda_{ij}^3 \text{Atn}(\lambda_{ij}) - |\upsilon_i|(\lambda_{ij} + \tilde{\lambda_{ij}})\Delta ij + \lambda_{ij}\tilde{\Lambda_{ij}}\Lambda_{ij}^*) \tag{6.92}$$

with:

$$(-|\upsilon_i|) * \text{Solid Angle formula} \tag{6.93}$$

and finally we get:

$$\begin{aligned}\sum_j c_{ij} &= 2\sum_j (h_{ij}\Lambda_{ij}^3 \text{Atnh}\Lambda_{ij}) \\ &+ 2\sum_j (h_{ij}\Lambda_{ij}\Delta_{ij}) - 2\sum_i |\upsilon_i| * [\text{Solid Angle}] + \frac{2A_i}{r_c + |u_i|}\end{aligned} \tag{6.94}$$

(where Solid Angle $= \frac{1}{2}\Omega$ as in equation: 6.75)

Explanation of the quantities used

r_c is a vector that represents a common for the whole target quantity, for example the position vector of the first vertex of the first facet, kept constant to replace all r_{ij} position vectors for all extrinsic computations of one target.

$$\Lambda_{ij} = \frac{L_{ij}}{(r_1 + r_2)_{ij}} \tag{6.95}$$

The error that Λ_{ij} a particular term could pay to the algorithm, is related with the order of that term. The order of Λ_{ij} is for example:

$$O\left(\Lambda_{ij}\right) = O\left(\frac{L_{ij}}{r_{1ij} + r_{2ij}}\right) = \left(\frac{\alpha}{\delta}\right) = O\left(\gamma\right) \tag{6.96}$$

This means that an error of $O(\gamma\epsilon)$ is paid for computing Λ_{ij}.

$$r_{mij} = \frac{1}{2}(r_{1ij} + r_{2ij}) \tag{6.97}$$

This is the average length of the $edge_{ij}$ position vectors .

$$\Lambda_{ij} = \frac{L_{ij}}{2r_{mij}} \tag{6.98}$$

Instead of the sum $r_{1ij} + r_{2ij}$ we use the average $2r_{mij}$ for the $edge_{ij}$ distance.

$$\Lambda^*_{ij} = \frac{L_{ij}}{2r_c} \tag{6.99}$$

We use the common to the target vector r_c instead of the $edge_{ij}$ common , $2r_{mij}$.

$$\Sigma_{ij} = \frac{1}{2}(r_{ij1} + r_{ij2} - Lij\Lambda_{ij}) \tag{6.100}$$

$$\lambda_{ij} = \frac{h_{ij}\Lambda_{ij}}{|u_i| + \Sigma_{ij}} \tag{6.101}$$

$$\Sigma^*_i = r_c \tag{6.102}$$

$$\Delta_{ij} = \frac{(\mathbf{r}_c - \mathbf{r}_1)\cdot(\mathbf{r}_c + \mathbf{r}_1)}{2r_c(r_c + r_1)} + \frac{(\mathbf{r}_c - \mathbf{r}_2)\cdot(\mathbf{r}_c + \mathbf{r}_2)}{2r_c(r_c + r_2)} \tag{6.103}$$

$$\lambda^*_{ij} = \frac{h_{ij}\Lambda^*_{ij}}{|u_i| + \Sigma^*_i} \tag{6.104}$$

$$\tilde{\lambda_{ij}} = \frac{\lambda^*_{ij} r_c}{|u_i| + \Sigma_{ij}} \tag{6.105}$$

Functions Atnh and Atn are defined by the delayed arctanh and arctan series:

Atnh=$\frac{1}{3} + \frac{x^2}{5} + \frac{x^4}{7} + ...$
Atn=$-\frac{1}{3} + \frac{x^2}{5} - \frac{x^4}{7} + ...$

The solid angle version

6.13 The gravi-magnetic computing package

Terms $\mathbf{b}_{ij}$ as in equation 6.38 establish the invariances and wrap up gravity and magnetic anomalies in one sole package.
As it is well described in Holstein-Sherratt manuscript since 2000 ([33]), gravity and magnetic anomalies can all be summarized in terms of one unique quantity the vector $\mathbf{b}_{kij}$ as shown above. Through an array of publications up to 2009([15, 22, 31, 2]), based to the 1st published in 2002 paper describing in full, the gravimagnetic similarity, a final set was produced.
The need for unification of gravity and magnetic calculations within one single package inspired Holstein et al to work towards a foundation of a set of governing equations. The goal was accomplished in 2002 with a relevant paper, improved thereafter to form a *protected environment* for all gravity and magnetic computations of geophysical and space interest(by substituting the constant of the universal gravitation G_e, to G_x,where x is an outer system) with components: gravity potential, gravity field, field gradient $\phi_g, \mathbf{f_g}, \mathbf{G_g}$ and magnetic potential, field and field gradient. $\phi_m, \mathbf{f_m}, \mathbf{G_m}$:
Every formula is evaluated at each edge ij of each facet i and has its own orthonormal vector triad($\mathbf{h}_{ij}, \mathbf{t}_{ij}, \mathbf{n}_i$) relative to which horizontal and vertical projections of the vertex position vectors are:

$$h_{ij} = \mathbf{r_{ij1}} \cdot \mathbf{h_{ij}} = \mathbf{r_{ij2}} \cdot \mathbf{h_{ij}}, v_i = \mathbf{r_{ij1}} \cdot \mathbf{n_i} = \mathbf{r_{ij2}} \cdot \mathbf{n_i} \tag{6.106}$$

$$\phi_g = \frac{1}{2} G\rho \sum_i v_i \sum_j \mathbf{b}_{ij} \cdot \mathbf{r}_{ij} \tag{6.107}$$

(gravitational potential with complexity tensor rank 0)

$$\mathbf{f}_g = \nabla \phi_g = -G\rho \sum_i \mathbf{n}_i \sum_j \mathbf{b}_{ij} \cdot \mathbf{r}_{ij} \tag{6.108}$$

(gravity field with complexity tensor of rank 1)

$$\mathbf{G}_g = \nabla \mathbf{f_g} = -G\rho \sum_i \mathbf{n}_i \sum_j \mathbf{b}_{ij} \tag{6.109}$$

(field gradient with complexity tensor of rank 2)

$$\phi_m = -\sum_i \mathbf{m} \cdot \mathbf{n}_i \sum_j \mathbf{b}_{ij} \cdot \mathbf{r}_{ij} \tag{6.110}$$

(magnetic potential with complexity tensor of rank 0)

$$\mathbf{f_m} = \nabla \phi_m = \sum_i \mathbf{m} \cdot \mathbf{n_i} \sum_j \mathbf{b_{ij}} \tag{6.111}$$

(magnetic field with complexity tensor of rank 1)

$$\mathbf{G_m} = \nabla \mathbf{f_m} = \sum_i \mathbf{m} \cdot \mathbf{n_i} \sum_j -\mathbf{B_{ij}} \tag{6.112}$$

(magnetic gradient with complexity tensor of rank 2, where $\mathbf{B_{ij}} = \nabla \mathbf{b_{ij}}$)

(Reference: HOLSTEIN: Gravimagnetic field tensor gradiometry formulas for uniform polyhedra,2006 [13])

$$\nabla^2 V = \sum_i \sum_j \mathbf{b}_{ij} \cdot \mathbf{n}_i = -\sum_i \sum_j \Omega_{ij} \tag{6.113}$$

(Laplacian of the gravity potential with complexity tensor of rank 0)

where the terms $\Omega_i j$ equal to the subtended solid angle by all the facets at the observation point. This is -4π for interior target points and zero for exterior points.

Chapter 7

Efficient Structures under Triangulation

7.1 Efficiency as a performance factor

The question is, if using an efficient implementation we could optimize the computing power of an anomaly algorithm. Anomaly algorithms align their accuracy with machine specific floating point precision. While this precision is fixed for any one machine, as we travel along large distances from the target, the significant digits get fewer and fewer. As this has being already investigated by Horst Holstein @ Edel Sherratt in their manuscript,"Performance metrics for computing gravi-magneto anomalies of uniform polyhedra" [33] and the outcome is that if:
$\gamma = \frac{\alpha}{\delta}$ where
α=dimensionless target volume, δ=distance from the observation point
γ crit=effective γ
η=relative accuracy
ϕ=1 with foreshortening
ϕ=0 no foreshortening
κ=-1 Vertex method, κ=0 Line method, κ=1 Surface method
ϵ=absolute error depending from the machine,
then the distances of an effective anomaly computation are bounded by the formulae:

$$\frac{1}{\gamma} < \frac{1}{{\gamma_{crit}}^{\eta,\phi,\kappa}} \tag{7.1}$$

$$\frac{1}{{\gamma_{crit}}^{\eta,\phi,\kappa}} = (\frac{\eta}{\epsilon})^{\frac{1}{\nu(\phi,\kappa)}} \tag{7.2}$$

$$\tag{7.3}$$

The above formulae indicate the limitations of the anomaly algorithms on foreshortened target distances. When the need to examine large number of observation distances and several targets per unit of time becomes apparent, the most efficient function of a particular algorithm could definitely improve machine's performance over time. To improve the efficiency of an algorithm, its structure must be analyzed and redundancy to be removed. Can we develop such a unique structure? Can we further improve this structure analytically? These questions arized the motivation for the chapter and divided the overall effort into 2 distinct parts, the structure optimization and the analytical improvement effort. Efficiency applied in a computation can reduce performance time, by removing redundancy of repeated operations. Under a naive scenario, redundancy is employed by copy-paste practice and this was apparent in my initial implementation. Copy - paste practice was a good idea at the beginning, for ease of implementation on understanding the background principles and the topic, but as the operations were repeated over and over again, in many different parts of the code, the program became heavy, wasting time on execution. Revising previous literature on the field by Hostein et al, I was found that I could save lots of repeated operations by storing them on their first execution, for future reference. The need to draw a clear separation line between intrinsic and extrinsic operations, became apparent. The part involving target calculations, the intrinsic part, should be disjoined from the part involving calculations depending on the observation point, the extrinsic part. The reason for this is that the operations regarding the target will be done once for each target, neglected as been not important to demonstrate efficiency improvements, while observation dependant operations computed times the observations points involved in a particular survey, will occupy most of the performance power. I also realized that many operations could now be moved from the extrinsic to the intrinsic part, saving intrinsic operations repeated in the extrinsic part which occupied a great deal of work load. As the creation of the most efficient implementation is not in the scope of this thesis, the decrease on the operation counts is considered as a genuine contribution on the field of algorithmic efficiency and therefore it should be investigated thoroughly. The trigger was the Horst Holstein @ Edel Sherratt manuscript([33]), where all efficiency issues were analytically presented. These issues were supported by the C++ computer program outcomes, acting as a proof. The contributions of that research towards a fast, reliable geophysical software, leaded to a uniform schema with quantification of both numerical error and computational efficiency create my manifest. On the other hand, Oosterom and Strackee ([35]) solid angle formula triggered another investigation leading to an analytical improvement of the anomaly algorithms. The formula to be placed under the microscope, computes the solid angle of a triangle projecting it on to a sphere(figure 6.4). To apply this formula on the anomaly algorithms, the target should be "triangulated", which means that each facet must be reformed into triangles with the new formulation having triangular facets referring to the original polyhedral target. The new concept was tested on the standard polyhedron by dividing each polygonal facet, into a number of triangles. The anomaly algorithms applied on the reformulated target produced the same gravity anomaly. The new formula was initially proved([15]) to be mathematically equal to the old and then was tested for any improvements on the error growth. The results were mapped on to a log-log plot, but the slopes being identical, showed that the performance gave no variations regarding the old Strakhov method for each of the error growth methods. As the error growth of the new formula did not give any improvement, the same formula was further tested searching for any efficiency improvements ([22]) With the background knowledge of the 2 major contributions ([22, 33]), my efforts were directed to a strategy towards the development of a revised implementation for every anomaly error growth class, separately implemented for Line and Surface error growth instances(anomaly algorithms classification, subsection 3.2.3 of this chapter), avoiding with this independent code building, an increase on computational complexity coming from a combined multi-method and multi-target, implementation. The strategy is described in details in the design part of the present chapter. This development was intended to include two separate implementations (old Strakhov and new Oosterom) for each anomaly case representing targets before and after triangulation in order to quantify any found arithmetic improvement.

7.2 Error analysis

7.2.1 Floating point limitations on accuracy

7.2.1.1 Truncation error

Floating point limited computer precision is a determining factor in the anomaly calculation. Floating point accuracy is defined to be the number of significant digits. Every computer language has its own data type. Floating point exceptions may cause memory licks and overflows. Generally every decimal number is represented internally as binary with a representation:
$x = + - m * 2E$
where mantissa m $1 <= m < 2$, E an integer.
According to the IEEE 754 standard every floating point number, is internally represented using a pattern of 3 parts: The Sign part, the Exponent part and the Fraction part. In C language single precision arithmetic has 23 digits of precision in mantissa while in double precision 51, 8 digits in the exponent while in double 11 and 1 digit for the sign. To perform a floating point operation such as a multiplication, many digits (if the number is irrational, an infinite number) are employed to produce the exact result. Because of the computer physical limited memories, only a certain number of digits can be processed. The remaining digits for an operation will be truncated and therefore an accuracy violation will be caused. To represent the rest of the digits rounding to the nearest digit strategy is used approximating the result of the operation with an almost exact result. The loss of digits quantifies the accuracy violation. If all the significant digits will be exhausted the result will not be meaningful. If not the operation produces an almost exact result. Since floating point calculations involve a bit of uncertainty, the distance between two floating point values bracketing a numerical value, is called epsilon. Epsilon typically represents the absolute error value for one particular computer system (for example, in Java for double precision arithmetic, epsilon is $2.2204460492503131e-016$) and is alternatively called ulp (units at the last place). The relative error now for a particular number, will be:
η =(result-expected result)/expected result
Summarizing, floating point approximation in computer systems with limited memories, involves a gap equal to $n * epsilon$ for a given number n, alternatively called truncation error or actual error. This gap represents a "break" on the continuation of the digital sequence representing a real number like π(3,14159 26535 89793 23846 26433 83279 50288 41971 69399 37510....). This gap would not exist if we could use an infinite number of digits for the real number, which is impossible. Therefore the larger the number the larger the truncation error will be. So η can be justified as:
$epsilon = gap/number$
The following algorithm computes epsilon (ϵ), in an IEEE-like format for any machine.

$epsilon = 1;$
$while((1 + epsilon) > 1)epsilon/ = 2;$
$Epsilon* = 2;$

Rounding to the nearest digit engages truncation error. Truncation error can never exceed rounding error and can be minimized using analytical cancellation of large operands. In our context, as the distance from the target is growing, operations involved engage larger numbers to compute smaller and smaller distances as the target is getting smaller. As these distances are getting significantly small the floating point precision of the specific machine is getting exhausted. Under this scenario, as the distance from the target γ is growing and γ is getting smaller and smaller the significant digits are getting less and less. The error of an anomaly method is estimated to be proportional to the order of the operations involved. We follow the anomaly error growth using different algorithms. Each of the algorithms appears to have its own error growth. Our purpose is to theoretically estimate the error growth class for every one and use this estimation as a measurement for the performance of every anomaly algorithm in the future. Previous work such as the manuscript of Edel Sheratt and Horst Holstein, 2000 ”Performance metrics for computing gravi-magneto anomalies of uniform polyhedra”, ”Comparison of Gravimagnetic Formulas for uniform polyhedra” by Horst Holstein et al, 1999, ”Gravimagnetic Analysis of uniform polyhedra” by Horst Holstein @ Ben Ketteridge, 1996, classify the anomaly methods according to their error growth into 3 distinct classes, namely Vertex, Line and Surface with descending error growth. Each method has a critical distance (figure 2.1) at which for a particular floating point arithmetic, all the significant digits are lost.

7.3 Arctan summation

$$tan(A - B) = \frac{tanA - tanB}{1 - tanAtanB} \tag{7.4}$$

to give only one arctangent argument equal to:

$$-uarctan(\frac{lh}{r_0^2 + ru}) \tag{7.5}$$

and consequently to:

$$c_{ij} = hl_n(\frac{r + l}{r_0}) - uarctan(\frac{lh}{r_0^2 + ru}) \tag{7.6}$$

7.3.1 Near the edge error

7.3.2 Error stabilization

7.4 Algorithmic efficiency using triangulation

7.4.1 Gravimagnetic equations using b_{ij}s

Approximation of a homogeneous target by a triangular target, has being exhaustively analysed in the paper by Horst Holstein et al, published in the EAGE London Conference in June 2007, [22]. This paper aimed to prove that triangular facets are particularly versatile allowing more efficient implementation and enhance numerical stability on anomaly formulae. The results were also verified with a Java program by the former. Following Holstein (2002a,b)[**?**],[15] the gravi-magnetic all anomaly formulae in one package can be expressed with the following equations:

$$\phi = G\rho \sum_i \upsilon_i \sum_j \mathbf{r}_{ij} \cdot \mathbf{b}_{ij} \tag{7.7}$$

Gravity potential

$$F = G\rho \sum_i \upsilon_i \sum_j \mathbf{b}_{ij} \tag{7.8}$$

Gravity field

$$\nabla F = -G\rho \sum_i \mathbf{n}_i \sum_j \mathbf{b}_{ij} \tag{7.9}$$

Gravity gradient

$$\Phi = G\rho \sum_i \upsilon_i \sum_j \mathbf{m} \cdot \mathbf{b}_{ij} \tag{7.10}$$

Magnetic potential

$$\Phi = -G\rho \sum_i \mathbf{n}_i \sum_j \mathbf{m} \cdot \mathbf{b}_{ij} \tag{7.11}$$

Magnetic field

7.4.2 Substitution of arctan terms using the Oesterom formula

7.4.3 Euler theorem for polyhedra

To estimate theoretically the operational counts using the arctan or the Oosterom method, Euler's theorem for polyhedra, is used. It states that every polyhedral topology maintains a linear relation between the number of facets, edges and vertices as demonstrated by the following data table

Table 7.1: Polyhedral topologies

Object	Facets	Edges	Vertices
Cube	6	12	8
Tetrahedron	4	6	4
Egyptian pyramid	5	8	5
Octahedron	8	12	6
Dodekahedron	12	30	20
Icosahedron	20	30	12

If you look at the above object data you can find the linear relation, true for all objects:

$$Vertices + Facets = Edges + 2 \tag{7.12}$$

Above formula generalizes all polyhedral topologies. For a *triangulated* polyhedron the following equities, will be also true:

$$E = 3F/2 \Rightarrow F = 2V - 4 and E = 3V - 6 \tag{7.13}$$

proof:

For any triangle it is true that each facet has 3 edges, so the number of edges must be 3 times as large the number of facets, therefore it is true that:

$$E = 3F$$

Due to commonality of the edge, each edge is shared by to faces. So if all edges are FX3=4X3=12, 1/2 of them are common, shared by 2 faces at most. Therefore half edge corresponds to one facet which means that the total number of edges which is 3F must be divided by 2 to exclude commonality. Therefore:

$$E = 3F/2, 2E = 3F \tag{7.14}$$

Now, from 7.14, substituting in 7.12 we get,

$$V+F = (3F/2)+2 => F-3F/2 = 2-V => -F/2 = 2-V => F = 2-V/-1/2 = -4+2V = 2V-4$$

also,from
7.12 and 7.14 solving for F we get

$$F = E + 2 - V(1) F = 2E/3(2)$$

the right parts of eq. 1,2 are equal and therefore

$$E + 2 - V = 2E/3 => E = 3V - 6$$

For quadrilateral surfaces where 1 edge is shared by 2 facets and a facet has 4 edges, it is true that

$$2E = 4F, E = 2F \tag{7.15}$$

Following same as above proving skepticism, substituting F,E in 7.12 from 7.15, we get

$$F = V - 2 \tag{7.16}$$

and

$$E = 2V - 4 \tag{7.17}$$

Using Euler's theorem, a unique formula for every topology, can be stated, if we estimate the work per vertex, per edge and per facet and then we can work out the overall work count for any (n vertices) topology. Assuming E to be the number of edges, F the number of facets, V the number of vertices, we compute:

$$W = cost(V) * n + cost(F) * (2n - 4) + cost(E) * (3n - 6)$$

or

$$W = n * (V) + 2 * (F) * (n - 2) + 3 * (E) * (n - 2)$$

Generalising above formula ,we may rewrite it as:

$$costV * n + costF * 2 * n + costE * 3 * n - (costF * 2 * 2 + costE * 3 * 2)$$

or

$$(costV + costF * 2 + costE * 3) * n \tag{7.18}$$

-

$$(costF * 4 + costE * 6) \tag{7.19}$$

which may be expressed as:

$$A * n - C \tag{7.20}$$

where A represents the contribution multiplier, n is the number of vertices and C is a fixed term(not depended on the number of vertices). If we substitute n with the number of vertices for any given polyhedron the overall operation count will be estimated, where cost V, cost F, cost E will be identified from the count analysis.

7.5 Implementation

Observing the above formula we can underline that the facet count has a 2 multiplier in front while the edge count a 3. From this we may state the following: if an optimized design can be found to transfer operations from edges to the facets, an effective decrease on the overall work count could be achieved. Assuming that we have already designed our efficient structure(as in Holstein-Sheratt [1]) to travel around a given target, V, F, E counts can be analytically estimated, by evaluating every necessary anomaly operation, times the number of facets, edges and vertices by applying Euler's theorem according to our a,b,c metric system(as in Chakraborty, [26]). The design of a theoretical operation counting layout, must account for both versions Strakhov and Oosterom and all possible gravi-magnetic cases and methods of error growth comprising the gravi-magnetic package, therefore the development of a strategy towards a Java program to report same number of counts, is the viable objective to validate theoretical outcomes. The anomaly algorithms will be implemented in 2 different versions for the old(the Strakhov version) and new(the Oosterom version), to quantify the results, later on. Also the implementation has to be developed in standalone modules for each of the anomaly cases and methods, to avoid overhead complexity from a parametrical implementation of the whole gravi-magnetic package in one multi-method and multi-target, programming unit. The outcome counts will be reported using inserted statements at the points where the a, b, c (a=multiplications/divisions, b=additions/subtractions, c=function calls) will be performed. If the actual results of the implementation effort will match their analytical ancestors, our implementation will be validated to be efficient.

7.5.1 Theoretical layout

The following gravity cases have being investigated, using methods Vertex, Line and Surface for both Strakhov and Oosterom versions representing the old and the new way of implementation before and after triangulation:

1. Gravity Potential,

2. gravity field,

3. gravity gradient,

4. magnetic potential,

5. magnetic field,

6. magnetic gradient.

Vertex method variations have not being included into the analysis, considered to be of minor importance regarding the research on efficiency improvements. Also cases regarding magnetic potential and magnetic field have not being included considered to be simple variants of the gravity field and gravity gradient cases, respectively. In my layout I classify my operations in the following order:

Start-up operations,
operations involving target properties (M.Chakraborty,ref), such as facet normals, edge vectors and lengths, performed once per target, pre-computed before the set of observation points to be scanned. These operations are not accounted to the overall operation counting.

Observation point operations,
the operations around one observation point repeated for all the observation points in range regarding vertices, facets and edges of the target.

Body counts
, operations performed just once for each observation point. Each category except body counts, may further classify operations into vertex, facet and edge operations been the computational attributes of a polyhedral target, upon which each operation is bounded to.

The counting strategy includes:
a=multiplications and divisions,
b=additions and subtractions,
c=function calls include:

logarithm, square root, arctangent (atan), hyperbolic arctangent(atanh) all other logical comparisons and assignments have been ignored.

The contributing factors towards efficient counting may be considered the:
Computational reuse
An edge was shared by at least two facets. Hence any edge calculation, such as ij common to two facets has been weighted 1 in the edge counts while any other not shared calculation, 2. Similarly each vertex is shared by at least 3 facets. Computational reuse will be switched on, if the vertex calculations and the shared edge calculations with the related results will be stored for reuse.
Branching
Arriving to an if statement, there is 50% probability that the running thread will follow a certain branch therefore all branching counts can be approximated as halves.
Common edge quantities AND branching
For edge shared quantities over branches they are further halved. The above 3 considerations may reduce if applied within an implementation, the operational counts of the gravity anomaly algorithms. The analysis has been presented using the following format: formula, count in a,b,c format and reference. References indicate the weighting factors according to the contributing factors of an Euler count.

7.5.2 Case study: gravity potential counting operations

Operations for the gravity potential will be analyzed for Line and Surface methods of error growth separately. Counting will be evaluated using a, b, c custom metrics. The overall work involved will be computed using Euler's theorem for polyhedra as in(7.12). The operations will be of floating point, or of an extended floating point, depending when scalars or vectors are involved. Tables used as indexes to the a, b, c counting system, of simple and extended types, will be appended to this chapter.

7.5.2.1 Line method - Strakhov variant

The working formula, giving the potential is:

$$2 * \sum_i \upsilon_i * \left(\left(\sum_j h_{ij} * arctanh(\Lambda_{ij}) \right) - \upsilon_i * \left(\sum_j arctan(\lambda_{ij}) \right) \right) \tag{7.21}$$

where:
i= facet index
j= edge index
υ_i = projection of the position vector on to the normal n_i
h_{ij}= projection of the position vector r on to the $\mathbf{h}_{ij}$
arctanh= arctan hyperborlic function
arctan=arctan function
Λ_{ij}= edge quantity (ref:chapter.section:3.3)
λ_{ij}= edge quantity (ref:chapter.section:3.3)
For the purposes of this study, we assume there is only one target model and many observation points.But in more complex cases like data survey for stochastic inversion, we may need to compute thousands of target models in probably many different orientations, searching for best fitting model. In the table 7.3 operations have being distinguished and classified according to their repeatability per target, or observation point. So, classification to intrinsic for once per target computed quantities and extrinsic for repeatably computed quantities for each observation point. The once per observation point computed quantities are called body counts. The use of bracketing for the restored quantities save us variable names ($\{\}$)and the bracketed quantities is assumed not to increase counts.

Table 7.2: Counting vector operations in terms of a,b,c

Operation	a	b	c
vector division by a scalar(vector,double)	3	0	0
vector cross product(vector,vector)	3	3	0
vector multiplication by scalar(vector, double)	3	0	0
vector subtraction by vector(vector, vector)	0	3	0
vector addition to vector(vector, vector)	0	3	0
vector compute unit vector (vector)	6	2	1
double dot product of vectors(vector, vector)	3	2	0
double magnitude(vector v)	3	2	1

Formula	a	b	c	weights
Intrinsic	37	29	35	
Facet	19	13	3	
$\mathbf{n}_i = (\mathbf{R}_{ij2} - \mathbf{R}_{ij1}) \bigwedge (\mathbf{R}_{ij3} - \mathbf{R}_{ij1})$	5	8	5	
$\hat{\mathbf{n}} = \frac{\mathbf{n}}{\lvert\mathbf{n}\rvert}$	6	2	1	
$\mathbf{A}_i = \frac{\lvert\{\mathbf{n}_i\}\rvert}{2}$	4	2	1	
$\sum_i A = \sum_i A + \lvert A\rvert_i$	3	3	1	
$\sum_i \mathbf{A} = \sum_i \mathbf{A} + \mathbf{A}_i$	0	3	0	
Edge	18	16	2	
$L = \sqrt{\mathbf{t} \cdot x^2 + \mathbf{t} \cdot y^2 + \mathbf{t} \cdot z^2}$	3	2	1	
$\mathbf{t}_{ij} = \mathbf{R}_{ij2} - \mathbf{R}_{ij1}$	0	3	0	
$\mathbf{t}_{ijsuc} = \mathbf{R}_{ij3} - \mathbf{R}_{ij1}$	0	3	0	
$\hat{\mathbf{t}}_{\mathbf{ij}} = \frac{\{\mathbf{R}_{ij2} - \mathbf{R}_{ij1}\}}{\{L\}}$	3	0	0	
$\mathbf{h}_{\mathbf{ij}} = \hat{\mathbf{t}}_{\mathbf{ij}} \bigwedge \hat{\mathbf{n}}_{\mathbf{i}}$	6	3	0	2
$\hat{\mathbf{h}}_{\mathbf{ij}} = \frac{\{\mathbf{h}_{\mathbf{ij}}\}}{\lvert\{\mathbf{h}_{\mathbf{ij}}\}\rvert}$	6	2	1	
$\mathbf{T}_{\mathbf{area}} = \mathbf{T}_{\mathbf{area}} + \mathbf{T}_{\mathbf{trianglearea}}$	0	3	0	
Extrinsic	24	20	4	
Vertex	3	5	1	
$\mathbf{r} = \mathbf{R}_{ij} - \mathbf{R}_{ijobs}$	0	3	0	
$r = \lvert\mathbf{r}\rvert$	3	2	1	
Edge	17	12	3	

$h = \mathbf{r} \cdot \{(\mathbf{t} \bigwedge \mathbf{n})\}$	3	2	0	2
$\{r_1\} + \{r_2\}$	0	1	0	
$\Lambda_{ij} = \frac{\{L\}}{\{r_1+r_2\}}$	1	0	0	
$arctanh\{\Lambda_{ij}\}$	0	0	1	
$h_{ij} * \{arctanh\{\Lambda_{ij}\}\}$	1	0	0	2
$arctan\{\lambda_{ij}\}$	0	0	1	2
$\{\lvert\upsilon\rvert\} * \{arctan\{\lambda_{ij}\}\}$	1	0	0	2
$\{\Sigma_j\} + \{h_{ij} * \{arctanh\{\Lambda_{ij}\}\}\} + \{\{\lvert\upsilon\rvert\} * \{arctan\{\lambda_{ij}\}\}\}$	0	2	0	2
$lambda' = \frac{\{(r_{1ij}+r_{2ij})\}-\{L_{ij}\}*\{\Lambda_{ij}\}}{2}$	2	1	0	
$\lambda_{ij} = \frac{h_{ij}*\Lambda_{ij}}{lambda'+\lvert\upsilon_i\rvert}$	2	1	0	2
Facet pre-edge	3	2	0	
$\upsilon = \mathbf{r} \cdot \mathbf{n}$	3	2	1	
Facet post-edge	1	1	0	
$\Sigma_{previousfacets} + \upsilon_i * (\{\Sigma_{edgeslogterms}\})$	1	1	0	
Facet	4	3	0	
Summarized Extrinsic operations	a	b	c	
Vertex	3	5	1	
Edge	17	12	3	
Facet	4	3	0	

Table 7.3: Metrics on operations of Line - Strakhov variant

Evaluating the expression An-C(7.20)
A =costV+costF*2+costE*3 (7.18)
C =costF*4+costE*6(7.19)
we will get for a , b , c:
119n-220
Keeping operations(a,b) apart from function calls(c) we get:

a , b	109n-202
c	10n-18

An example:evaluating specific target
Evaluating for standard tetrahedron where n=4 we will be counting:
119*4-220=476-220=**256**
The result will be the overall total operations for a target at an observation point.
Keeping arithmetic operations (a, b) apart from function calls(c) we will get:
a,b : 109*4-202=436-202=**234**
c : 10*4-18=40-18=**22**

7.5.2.2 Line method-Oosterom variant

The working formula is:

$$2\sum_i \upsilon_i * \left(\left(\sum_j \left(h_{ij} * \text{arctanh}\left(\Lambda_{ij}\right)\right)\right) - |\upsilon_i| * (\Omega_i/2)\right) \tag{7.22}$$

where:
i= facet index
j= edge index
υ_i = projection of the position vector on to the normal n_i
h_{ij}= projection of the position vector r on to the $\mathbf{h}_{ij}$
arctanh= arctan hyperborlic function
Ω=Solid angle formula 6.75
Λ_{ij}= edge quantity (ref:chapter.section:3.3)

Formula	a	b	c	weights
Intrinsic	34	26	4	
Facet	16	11	2	
$\sum_i A = \sum_i A + \lvert A_i \rvert$	3	3	1	
$\sum_i \mathbf{A} = \sum_i \mathbf{A} + \lvert \mathbf{A}_i \rvert$	0	3	0	

$\mathbf{n}_i = \{(\mathbf{R}_{ij2} - \mathbf{R}_{ij1})\} \bigwedge \{(\mathbf{R}_{ij3} - \mathbf{R}_{ij1})\}$	6	3	0	
$\hat{\mathbf{n}}_i = \frac{\{\mathbf{n}_i\}}{\{\|\mathbf{n}_i\|\}}$	6	2	1	
$\|\mathbf{A}_i\| = \frac{\{\|\mathbf{n}_i\|\}}{2}\|$	1	0	0	
Edge	18	13	2	
$L = \sqrt{\mathbf{t} \cdot x^2 + \mathbf{t} \cdot y^2 + \mathbf{t} \cdot z^2}$	3	2	1	
$\mathbf{t}_{ij} = \mathbf{R}_{ij2} - \mathbf{R}_{ij1}$	0	3	0	
$\mathbf{t}_{ijsuc} = \mathbf{R}_{ij3} - \mathbf{R}_{ij1}$	0	3	0	
$\hat{\mathbf{t}}_{\mathbf{ij}} = \frac{\{\mathbf{R}_{ij2} - \mathbf{R}_{ij1}\}}{\{L\}}$	3	0	0	
$\mathbf{h}_{\mathbf{ij}} = \hat{\mathbf{t}}_{\mathbf{ij}} \bigwedge \hat{\mathbf{n}}_{\mathbf{i}}$	6	3	0	
$\hat{\mathbf{h}}_{\mathbf{ij}} = \frac{\{\mathbf{h}_{\mathbf{ij}}\}}{\|\{\mathbf{h}_{\mathbf{ij}}\}\|}$	6	2	1	
Extrinsic	26	21	3	
Vertex	3	5	1	
$\mathbf{r} = \mathbf{R}_{ij} - \mathbf{R}_{ijobs}$	0	3	0	
$r = \|\mathbf{r}\|$	3	2	1	
Facet pre-edge	3	2	0	
$\upsilon = \mathbf{r} \cdot \mathbf{n}$	3	2	0	
Edge	12	9	1	
$h = \mathbf{r} \cdot \{(\hat{\mathbf{t}} \bigwedge \mathbf{n})\}$	1	0	0	
$\{r_1\} + \{r_2\}$	0	1	0	2
$\Lambda_{ij} = \frac{\{L\}}{\{r_1 + r_2\}}$	1	0	0	
$arctanh\{\Lambda_{ij}\}$	0	0	1	

$h_{ij} * \{arctanh\{\Lambda_{ij}\}\}$	1	0	0	2
$c_{ij} = \{h_{ij} * \{arctanh\{\Lambda_{ij}\}\}\}$	0	1	0	2
$R_{1obs} \cdot R_{2obs}$	3	2	0	
Facet post-edge $Oesterom_{formula} = \frac{nominator_{quantity}}{denominator_1 + denominator_2}$	8	5	1	
$nominator_{quantity} = \upsilon_i * \lvert\mathbf{A}_i\rvert$	1	0	0	
$denominator_1 = \lvert r_1\rvert * \lvert r_2\rvert * \lvert r_3\rvert$	2	0	0	
$denominator_2 = \mathbf{r_1} \cdot \mathbf{r_2} * r_3 + \mathbf{r_2} \cdot \mathbf{r_3} * r_1 + \mathbf{r_1} \cdot \mathbf{r_3} * r_2$	3	2	0	
$SA = (-\upsilon) * atan2 \frac{\{nominator\}}{denominator_1 + denominator_2}$	1	1	1	
$\sum_i c_i = \sum_i c_i + \upsilon_i * \left(\sum_j c_{ij} + \{SA\}\right)$	1	2	0	
Facet Summarized Extrinsic operations	11 a	7 b	1 c	
Vertex	3	5	1	
Edge	12	9	1	
Facet	11	7	1	

Table 7.4: Metrics on operations of Line - Oesterom variant

Evaluating formula An-C(7.20)
A =costV+costF*2+costE*3 (7.18)
C =costF*4+costE*6(7.19)
we will get for a , b , c:
113n-208
Keeping operations(a,b) apart from function calls(c) we get:

a , b	107n-198
c	6n-10

An example:evaluating for standard tetrahedron
For number of vertices n=4:
113*4-208=452-208=**244**

The result will be the overall total operations for a target at an observation point.
Keeping arithmetic operations (a, b) apart from function calls(c) we will get:
a,b : **230**
c : **14**

Summary for the Line method

Table 7.5: In terms of vertices, in form:An+C

method	abc	ab	c
strakhov	119n-220	109n-202	10n-18
Oosterom	113n-208	107n-198	6n-10
Improvement	**6n-12**	**2n-4**	**4n-8**

Table 7.6: Example: tetrahedron, n=4

method	abc	ab	c
Strakhov	256	234	22
Oosterom	244	230	14
Improvement	**12**	**4**	**8**

Results

Looking at the summary of the results for the 2 variants of the Line method, a slight superiority is emerging in the Oosterom's variant, decreasing counts for the gravity potential passing Solid angle operations to the facet loop from the edge loop. This upgrades operation counter to decrease from operations for computing the arctan term times total number of edges to the less numberous operations for the computation of the solid angle formula times the number of facets. Thus we get a decrease of,
Arctan term computations$_{Edges}$ - Solid angle computations$_{Facets}$

7.5.2.3 Surface method - Strakhov variant

The working formula:

$$C_{ij}/2 = \frac{A_i}{r_c + \upsilon} + \sum_j \left(h\Lambda^3 Atnh\Lambda - |\upsilon|\lambda^3 Atn\lambda\right) + \sum_j \left(h\Lambda\Delta - |\upsilon| \left(\left(\lambda + \widetilde{\lambda}\right)\Delta + \widetilde{\lambda}\Lambda\Lambda^*\right)\right)$$

where:
i= facet index
j= edge index
r_1, r_2= scalar mangitudes of the position vectors $\mathbf{r_1}$,$\mathbf{r_2}$, pointing from the observation point to the 2 vertices of an edge
A_i = scalar area of facet i
υ_i = scalar projection of the position vector r on to the normal n_i
h = scalar projection of the position vector $\mathbf{r}$ on to the vector $\mathbf{h}$
Atnh, Atn=custom functions(Appendix B) representing the taylor series:
Atnh= $\frac{1}{3} + \frac{x^2}{5} + \frac{x^4}{7} \dots$
Atn= $-\frac{1}{3} + \frac{x^2}{5} - \frac{x^4}{7} \dots$
$r_m = \frac{1}{2}(r_1 + r_2)$
$r_c =$ scalar magnitude of the position vector $\mathbf{r_c}$ from the observation point to the centroid of the target, common to all target calculations.
$\Sigma = \frac{1}{2}(r_1 + r_2 - |L|\Lambda)$
$\Sigma^* = r_c$
$\Lambda = \frac{L}{2r_m}$
$\Lambda^* = \frac{L}{2r_c}$
$\lambda = \frac{h\Lambda}{(|\upsilon|+\Sigma)}$
$\lambda^* = \frac{h\Lambda}{(|\upsilon|+\Sigma^*)}$
$\widetilde{\lambda} = \frac{\lambda^* r_c}{(|\upsilon+\Sigma|)}$
$\Delta = \frac{(\mathbf{r_c}-\mathbf{r_1})\cdot(\mathbf{r_c}+\mathbf{r_1})}{2r_c(r_c+r_1)} + \frac{(\mathbf{r_c}-\mathbf{r_2})(\mathbf{r_c}+\mathbf{r_2})}{2r_c(r_c+r_2)}$ (scalar quantity)

All subscripts i, j in the variables, are omitted for clarity. In the implementation for simplicity, it is sometimes convenient to represent parts of the surface method using variables, for example surface formula could look something like: A+B+C1-C2+C3, were:
$A = \frac{A_i}{r_c+\upsilon}$
$B = \sum_j (h\Lambda^3 Atnh\Lambda - |\upsilon|\lambda^3 Atn\lambda)$
$C1 = \sum_j (h\Lambda\Delta)$
$C2 = \sum_j |\upsilon| \left(\lambda + \widetilde{\lambda}\right)\Delta$
$C3 = \sum_j \widetilde{\lambda}\Lambda\Lambda^*$

Formula	a	b	c	weights
Intrinsic	34	27	4	
Facet	16	9	2	
$\sum_i A = \sum_i A + \lvert A_i \rvert$	3	3	1	
$\sum_i \mathbf{A} = \sum_i \mathbf{A} + \lvert \mathbf{A}_i \rvert$	0	3	0	
$\mathbf{n}_i = \{(\mathbf{R}_{ij2} - \mathbf{R}_{ij1})\} \bigwedge \{(\mathbf{R}_{ij3} - \mathbf{R}_{ij1})\}$	6	3	0	
$\hat{\mathbf{n}}_i = \frac{\{\mathbf{n}_i\}}{\{\lvert \mathbf{n}_i \rvert\}}$	6	2	1	
$\lvert \mathbf{A}_i \rvert = \frac{\{\lvert \mathbf{n}_i \rvert\}}{2} \rvert$	1	0	0	
Edge	18	18	2	
$L = \sqrt{\mathbf{t} \cdot x^2 + \mathbf{t} \cdot y^2 + \mathbf{t} \cdot z^2}$	3	2	1	
$\mathbf{t}_{ij} = \mathbf{R}_{ij2} - \mathbf{R}_{ij1}$	0	3	0	
$\mathbf{t}_{ijsuc} = \mathbf{R}_{ij3} - \mathbf{R}_{ij1}$	0	3	0	
$\hat{\mathbf{t}}_{\mathbf{ij}} = \frac{\{\mathbf{R}_{ij2} - \mathbf{R}_{ij1}\}}{\{L\}}$	3	0	0	
$\mathbf{h}_{\mathbf{ij}} = \hat{\mathbf{t}}_{\mathbf{ij}} \wedge \hat{\mathbf{n}}_{\mathbf{i}}$	6	3	0	
$\hat{\mathbf{h}}_{\mathbf{ij}} = \frac{\{\mathbf{h}_{\mathbf{ij}}\}}{\lvert \{\mathbf{h}_{\mathbf{ij}}\} \rvert}$	6	2	1	
$\mathbf{T}_{area} = \mathbf{T}_{area} + \mathbf{T}_{triangle}$	0	3	0	
Body counts	4	2	1	
$r_c = \lvert \mathbf{O} \rvert$	3	2	1	
$2 * r_c$	1	0	0	
Extrinsic	54	42	4	

Vertex	8	11	1	
$\mathbf{r} = \mathbf{R} - \mathbf{O}$	0	3	0	
$r = \lvert\{\mathbf{r}\}\rvert$	3	2	1	
$\{\mathbf{r}_c\} + \{\mathbf{r}\}$	0	3	0	
$R'_\Delta = (\{\mathbf{r}_c - \mathbf{r}\}) \cdot (\{\mathbf{r}_c + \mathbf{r}\})$	3	2	0	
$R_\Delta = \frac{\{R'_\Delta\}}{\{2*r_c\}*\{\lvert\mathbf{r}_c\rvert+r\}}$	2	1	0	
Facet pre-edge	3	2	0	
$\upsilon = \mathbf{r} \cdot \mathbf{h}$	3	2	0	
Edge	41	26	3	
$h = \{\mathbf{r}\} \cdot \{\left(\hat{\mathbf{t}} \wedge \hat{\mathbf{n}}\right)\}$	3	2	0	2
$\{\lvert\mathbf{r}_1\rvert\} + \{\lvert\mathbf{r}_2\rvert\}$	0	1	0	
$\Lambda = \frac{\{L\}}{\{\lvert\mathbf{r}_1\rvert\}+\{\lvert\mathbf{r}_2\rvert\}}$	1	0	0	
$\Sigma = \frac{(\{\lvert\mathbf{r}_1\rvert\}+\{\lvert\mathbf{r}_2\rvert\}-\{L\}*\{\Lambda\})}{2}$	2	1	0	
$\Lambda_* = \frac{\{L\}}{\{2r_c\}}$	1	0	0	
$\Sigma^* = r_c$	0	0	0	
$\lambda = \frac{\{h\}*\{\Lambda\}}{\{\upsilon\}+\{\Sigma\}}$	2	1	0	2
$\lambda^* = \frac{\{h\}*\{\Lambda_*\}}{\{\upsilon\}+\{\Sigma^*\}}$	2	1	0	2
$\widetilde{\lambda} = \frac{\{\lambda\}*\{r_c\}}{\{\upsilon\}+\{\Sigma\}}$	2	1	0	2
$\Sigma = \frac{(\{\lVert\mathbf{r}_1\rvert\}+\{\lVert\mathbf{r}_2\rvert\})-L*\Lambda}{2}$	2	1	0	
$\{\Lambda\} * \{\Lambda\}$	1	0	0	
$\{\lambda^*\} * \{\lambda^*\} * \{\lambda^*\} = \lambda^{*3}$	2	0	0	2

$\{\Lambda^{*}\} * \{\Lambda^{*}\} * \{\Lambda^{*}\} = \Lambda^{*3}$	2	0	0	
$\Delta = \{R_{\Delta 1}\} + \{R_{\Delta 2}\}$	0	1	0	
$\Delta * \Lambda$	1	0	0	
$Atnh\,(\Lambda)$	0	0	1	
$Atn\,(\lambda)$	0	0	1	2
$\{\Lambda^{3}\} * \{Atnh\,(\Lambda)\}$	1	0	0	
$b^{h} = h * \{\Lambda^{3} * Atnh\,(\Lambda)\}$	2	0	0	2
$b^{n} = -\lvert\upsilon\rvert * \{\lambda^{3} * Atn\,(\lambda)\}$	2	0	0	2
$offset = h * \{\Delta * \Lambda\} - \left(\lambda + \widetilde{\lambda} * \Delta + \widetilde{\lambda} * \{\Lambda * \Lambda\}\right)$	0	3	0	2
$c_i = \sum_{c_i} + b^{h} + b^{n} + \{offset\}$	0	3	0	2
Facet post-edge	2	3	0	
$facet_{o}ffset = \frac{\{\frac{A_i}{2}\}}{\{\lvert\upsilon\rvert\} + \{r_c\}}$	1	1	0	
$\sum_j c_{ij} = c_i + facet_{o}ffset$	0	1	0	
$c_{ij} = c_{ij} + \sum_i \upsilon * \sum_i c_{ij}$	1	1	0	
Facet totals	5	5	0	

Summarized Extrinsic operations	a	b	c	totals
Vertex	8	11	1	20
Edge	41	26	3	70
Facet	5	5	0	10
Per target(body counts)	4	2	1	7

Evaluating formula An-C(7.20)
A =costV+costF*2+costE*3 (7.18)
C =costF*4+costE*6(7.19)
we will get for a , b , c:
250n-453
Keeping operations(a,b) apart from function calls(c) we get:

a , b	240n-436
c	10n-17

An example:evaluating for standard tetrahedron
Applying for number of vertices n=4:
250*4-453=1000-453=**547**
The result is the overall count for one observation point.
Keeping arithmetic operations (a, b) apart from function calls(c):
a,b : **524**
c : **23**

7.5.2.4 Surface method - Oosterom variant

The working formula:

$$\sum_j c_{ij} = 2\sum_j \left(h_{ij}\Lambda_{ij}^3 \mathrm{Atnh}\Lambda_{ij}\right) + 2\sum_j \left(h_{ij}\Lambda_{ij}\Delta_{ij}\right) - 2\sum_i |\upsilon_i| * [\text{Solid Angle}] + \frac{2A_i}{r_c + |u_i|} \tag{7.23}$$

(ref: 7.23)

Formula	a	b	c	weights
Intrinsic	28	27	3	
Facet pre-edge	12	11	1	
$\mathbf{t}_{ij} = \mathbf{R}_{ij2} - \mathbf{R}_{ij1}$	0	3	0	
$\mathbf{t}_{ijsuc} = \mathbf{R}_{ij3} - \mathbf{R}_{ij1}$	0	3	0	
$\mathbf{n}_i = \{(\mathbf{R}_{ij2} - \mathbf{R}_{ij1})\} \bigwedge \{(\mathbf{R}_{ij3} - \mathbf{R}_{ij1})\}$	6	3	0	
$\hat{\mathbf{n}}_i = \frac{\{\mathbf{n}_i\}}{\{\lvert\mathbf{n}_i\rvert\}}$	6	2	1	
Edge $L = \sqrt{\mathbf{t}\cdot x^2 + \mathbf{t}\cdot y^2 + \mathbf{t}\cdot z^2}$	12 3	8 2	1 1	
$\hat{\mathbf{t}}_{\mathbf{ij}} = \frac{\{\mathbf{R}_{ij2} - \mathbf{R}_{ij1}\}}{\{L\}}$	3	0	0	
$\mathbf{h}_{\mathbf{ij}} = \hat{\mathbf{t}}_{\mathbf{ij}} \wedge \hat{\mathbf{n}}_{\mathbf{i}}$	6	3	0	
$\mathbf{T}_{area} = \mathbf{T}_{area} + \mathbf{T}_{triangle}$	0	3	0	
Facet post-edge $\mathbf{A}_i = \frac{\lvert\{\mathbf{n}_i\}\rvert}{2}$	4 4	2 2	1 1	
Facet total **Extrinsic**	16 40	13 33	2 4	
Target $\mathbf{r}_c = \mathbf{R}_c - \mathbf{O} = -\mathbf{O}$ If point c coincides with local origin then,	4 0	2 0	1 0	

$\mathbf{O}$ is the position vector from the target origin to the observation point and $\mathbf{r}_c$ is the position vector of the observation point to the point c.				
$r_c = \|\{\mathbf{O}\}\|$	3	2	1	
$2 * \{r_c\}$	1	0	0	
Vertex	13	14	1	
$r = \mathbf{R}_1 - \mathbf{O}$	0	3	0	
$\mathbf{r} = \|\{\mathbf{r}\}\|$	0	3	0	
$\{\mathbf{r}_c\} + \{\mathbf{r}\}$	0	3	0	
$R_{\Delta 1A} = (\{\mathbf{r}_c - \mathbf{r}_1\}) \cdot (\mathbf{r}_c + \mathbf{r}_1)$	3	2	0	
$R_{\Delta 2A} = (\{\mathbf{r}_c - \mathbf{r}_2\}) \cdot (\mathbf{r}_c + \mathbf{r}_2)$	3	2	0	
$R_{\Delta 1} = \frac{R_{\Delta 1A}}{2r_c(r_c+r_1)}$	2	1	0	
$R_{\Delta 2} = \frac{R_{\Delta 2A}}{2r_c(r_c+r_2)}$	2	1	0	
Facet pre-edge	3	2	0	
$\upsilon = \|\mathbf{r} \cdot \mathbf{n}\|$	2	1	0	
Edge	16	12	1	
$h = (\mathbf{r}) \cdot \left(\hat{\mathbf{t}} \wedge \hat{\mathbf{n}}\right)$	3	2	0	
$\|\mathbf{r}_1\| + \|\mathbf{r}_2\|$	0	1	0	
$(\mathbf{r}_1) \cdot (\mathbf{r}_2)$	3	2	0	
$\Lambda = \frac{\{L\}}{\|\mathbf{r}_1\|+\|\mathbf{r}_2\|}$	1	0	0	
$\Delta = \{R_{\Delta 1}\} + \{R_{\Delta 2}\}$	0	1	0	
$\Delta\Lambda$	1	0	0	
$Atnh\{\Lambda\}$	0	0	1	
$\{\Lambda^3\}\{\mathrm{Atnh}\Lambda\}$	1	0	0	
$b^h = h\{\Lambda^3 Atnh\Lambda\}$	1	0	0	
$\sum c_{ij} = \sum c_{ij} + b_h + h\,(\Delta\Lambda)$	1	2	0	
Facet post-edge	9	6	1	
υA_i	1	0	0	
$\mathbf{r}_1 \cdot \mathbf{r}_2 \|r_3\|$	1	0	0	
$\mathbf{r}_1 \cdot \mathbf{r}_3 \|r_2\|$	1	0	0	
$\mathbf{r}_2 \cdot \mathbf{r}_3 \|r_1\|$	1	0	0	
$\|r_1\|\|r_2\|\|r_3\|$	2	0	0	
$\{\|r_1\|\|r_2\|\|r_3\|\} + \{\mathbf{r}_1 \cdot \mathbf{r}_2 \|r_3\|\} + \{\mathbf{r}_2 \cdot \mathbf{r}_3 \|r_1\|\} + \{\mathbf{r}_1 \cdot \mathbf{r}_3 \|r_2\|\}$	0	3	0	
$Atn2\frac{\{\upsilon A_i\}}{\{\{\|r_1\|\|r_2\|\|r_3\|\}+\{\mathbf{r}_1\cdot\mathbf{r}_2\|r_3\|\}+\{\mathbf{r}_2\cdot\mathbf{r}_3\|r_1\|\}+\{\mathbf{r}_1\cdot\mathbf{r}_3\|r_2\|\}\}}$	0	1	1	Oesterom formula
Facet's solid angle = (-υ) $* Oesterom_F ormula$	2	0	0	
Facet offset =$A_i/2/\|\upsilon R_i\|$	1	0	0	
C_{ij}=Solid Angle+edge surface+offset	0	2	0	
Anomaly = Anomaly+υC_{ij}	1	0	0	

Facet total	12	8	1	
Summarized Extrinsic operations	a	b	c	totals
Vertex	8	11	1	20
Edge	16	12	1	29
Facet	12	8	1	21
Per target(body counts)	4	2	1	7

Evaluating formula An-C(7.20)
A =costV+costF*2+costE*3 (7.18)
C =costF*4+costE*6(7.19)
we will get for a , b , c:
149n-251
Keeping operations(a,b) apart from function calls(c) we get:

a , b	143n-242
c	6n-9

An example:evaluating for standard tetrahedron
Applying n=4:
149*4-251=596-251=**345**
The result is the overall count for one observation point.
Keeping arithmetic operations (a, b) apart from function calls(c) we will get:
a,b : **330**
c : **15**

Summary for the Surface method

Table 7.9: In terms of vertices, in form:An+C

method	abc	ab	c
strakhov	250n-453	240n-436	10n-17
Oosterom	149n-251	143n-242	6n-9
Improvement	**101n-202**	**97n-194**	**4n-8**

Results
Looking at the summary of the results for the 2 variant of the surface method, superiority is dramatically increased using the Oosterom's formula, as a big lot of operations (about 40) were transferred to the facet part of the implementation with an A contribution multiplier (equation:7.20) 2 instead of 3 when evaluated to the edge part.
The slight increase($< 5\%$)in the Oosterom version of the Line method was magnified using the Oosterom version of the Surface method ($> 40\%$)

7.6 Gravimagnetic Anomaly Formulae for Triangulated Homogeneous Polyhedra

Publication:*Gravimagnetic Anomaly Formulae for Triangulated Homogeneous Polyhedra*
H. Holstein(University of Wales, Aberystwyth),hoh@aber.ac.uk,
E. Sherratt (University of Wales, Aberystwyth),eds@aber.ac.uk,
C. Anastasiades (University of Wales, Aberystwyth), anastasiadescostas@yahoo.gr
EAGE 69th Conference and Exhibition - London, UK, 11 - 14 June 2007
(bibliography ref:[22])

Following Holstein (2002a, b)[**?**] and using that notation, the gravi-magnetic anomaly formulae for a homogenously constituted target can be written as

$$\begin{aligned}\phi &= G\rho \sum_i \upsilon_i \sum_j \mathbf{r}_{ij} \cdot \mathbf{b}_{ij},\\ \mathbf{F} &= G\rho \sum_i \upsilon_i \sum_j \mathbf{b}_{ij},\\ \nabla\mathbf{F} &= -G\rho \sum_i \mathbf{n}_i \sum_j \mathbf{b}_{ij}\end{aligned} \tag{7.24}$$

$$\begin{aligned}\Phi &= \sum_i \upsilon_i \sum_j \mathbf{m} \cdot \mathbf{b}_{ij},\\ H &= \sum_i \mathbf{n}_i \sum_j \mathbf{m} \cdot \mathbf{b}_{ij}\end{aligned} \tag{7.25}$$

for the gravity potential ϕ, the gravity field $\mathbf{F}$, the gravity field gradient $\nabla\mathbf{F}$, the magnetic

Table 7.10: Example: tetrahedron, n=4

method	abc	ab	c
Strakhov	547	524	23
Oosterom	345	330	14
Improvement	**202**	**194**	**9**

potential Φ and the magnetic field H, evaluated at a given observation point. In these formulae, G is the constant of universal gravitation, ρ is the density and **m** the magnetisation vector. The subscript i refers to enumeration of the polyhedral facets, with $\mathbf{n}_i$ being the unit outward facet normal. Vector $\mathbf{r}_{ij}$ is the position vector from the observation point to vertex j on facet i, and its successor in an anticlockwise order around the outward normal $\mathbf{n}_i$ is denoted by $\mathbf{r}_{ij}$, while υ_i is the projection of such a vectors on to the facet normal $\mathbf{n}_i$. The join from $\mathbf{r}_{ij}$ to $\mathbf{r}_{ij'}$ defines edge ij. The vector $\mathbf{b}_{ij}$ depends only on the target geometry of facet edge ij relative to the observation point, and is perpendicular to that edge. Formulae (7.24)-(7.25) share a common set of vector functions $\mathbf{b}_{ij}$. The history of anomaly formula derivation has seen many non-identical variants of these functions. Indeed, different formulations need only show inner sum equality rather than term by term equality. The formulations of $\mathbf{b}_{ij}$ may be classified according to two attributes: numerical stability and numerical efficiency (arithmetic complexity). The triangulated target algorithms that we propose possess enhanced qualities in both of these attributes, and are therefore candidates for improved computation. We demonstrate these properties in the sections below. We note that there is also some variation in the possible summed over terms in equations 7.24-7.25. We have chosen variants favouring the inner sums of $\mathbf{b}_{ij}$ (or $\mathbf{m} \cdot \mathbf{b}_{ij}$) over $\mathbf{r}_{ij} \cdot \mathbf{b}_{ij}$ whenever possible, as this leads to fewer operation counts in the new formulation.

7.6.1 Summary

Approximation of a homogeneous target by a polyhedron is useful in gravity and magnetics modelling, since shape approximation can be arbitrarily close while retaining a closed form solution for the anomaly. Shape approximation by triangular facets is particularly versatile, allowing individual vertices to be moved without compromising facet planarity. We show that triangular facets in fact allow a more efficient implementation and enhance the numerical stability of anomaly formulae, compared to their treatment as general polygonal facets. The basis for improvement lies in the use of a compact formula for the solid angle of a triangle. The claimed advantages are verified in example anomaly computations that exhibit reduced arithmetic complexity and enhanced numerical stability. The enhanced efficiency of the proposed formulae finds immediate application in the computationally intensive iterative forward modelling. Thus, both for ease of implementation and numeric computation, the use of triangulated targets is to be recommended.

7.6.2 Formulation of new equations

$$\begin{aligned} &2A_i\mathbf{n}_i = (\mathbf{r}_{i1} - \mathbf{r}_{i2}) \wedge (\mathbf{r}_{i2} - \mathbf{r}_{i3}), \\ &L_{ij}\mathbf{t}_{ij'} - \mathbf{r}_{ij}, \\ &\mathbf{h}_{ij} - \mathbf{t}_{ij} \wedge \mathbf{n}_i, j = 1..3. \end{aligned} \tag{7.26}$$

$$\begin{aligned} &l_{ij} = \mathbf{t}_{ij} \cdot \mathbf{r}_{ij}, \upsilon_i = \mathbf{n}_i \cdot \mathbf{r}_{ij}, h_{ij} = \mathbf{h}_{ij} \cdot \mathbf{r}_{ij}, \\ &r_{ij} = |\mathbf{r}_{ij}|, \overline{r}_{ij} = \frac{1}{2}\left(|\mathbf{r}_{ij}| + |\mathbf{r}_{ij'}|\right), j = 1..3 \end{aligned} \tag{7.27}$$

$$\mathbf{b}_{ij} = 2\mathbf{h}_{ij} arctanh \Lambda_{ij} - 2\mathbf{n}_i \text{sign}(\upsilon_i) \arctan \lambda_{ij} \tag{7.28}$$

where $\Lambda_{ij}, \lambda_{ij}$ are from Holstein et al.1999 [26]

$$\Lambda_{ij} = L_{ij}/2\overline{r}_{ij}, \lambda_{ij} = h_{ij} \left(\overline{r}_{ij} - L_{ij}\Lambda_{ij}/2 + |\upsilon_i|\right) \tag{7.29}$$

Using relations (7.27), equations (1) and (2) require the edge summations

$$\begin{aligned}\sum_{j=1..3} \mathbf{b}_{ij} &= \sum_{j=1..3} 2\mathbf{h}_{ij}\text{arctanh}\Lambda_{ij} - \mathbf{n}_i\Omega_i \\ \sum_{j=1..3} \mathbf{r}_{ij} \cdot \mathbf{b}_{ij} &= \sum_{j=1..3} 2h_{ij}\text{arctanh}\Lambda_{ij} - \upsilon_i\Omega_i\end{aligned} \tag{7.30}$$

where:

$$\Omega_i = 2\text{sign}\upsilon_i \sum_{j=1..3} \arctan \lambda_{ij} \tag{7.31}$$

is known to represent the solid angle subtended by the facet at the observation point (Holstein 2002)[15]. It may be replaced by a single arctangent term derived from Oosterom and Strackee (1983)[35] for the solid angle of a triangle,

$$\Omega_i = 2\arctan\{\frac{2\upsilon_i A_i}{r_{i1}r_{i2}r_{i3} + r_{i1}\left(\mathbf{r}_{i2}\cdot\mathbf{r}_{i3}\right) + r_{i2}\left(\mathbf{r}_{i3}\cdot\mathbf{r}_{i1}\right) + r_{i3}\left(\mathbf{r}_{i1}\cdot\mathbf{r}_{i2}\right)}\} \tag{7.32}$$

7.6.3 Numerical stability

A classification of published algorithms for $\mathbf{b}_{ij}$ has been made (Holstein and Ketteridge (1996)[32], Holstein et al. (1999)[26]) into surface, line or vertex types, according to whether the terms bij are of order $O(\gamma^2), O(\gamma)\text{or}O(1)$ respectively, where γ is the reciprocal dimensionless target distance α/δ, α being a typical linear target dimension and δ a typical distance between target and observation point. The resultant sums in the left hand sides of equations (7.30) are $O(\gamma^3)$ and $O(\delta\gamma^3)$ respectively. Thus, with increasing target distance ($\gamma \overset{tends}{\to} 0$), the summands become larger than the desired sums by unbounded factors $O(\gamma^{--1}), O(\gamma^{--2}), O(\gamma^{--3})$ respectively, leading to progressively more severe numerical instability with respect to surface, line and vertex types. Under conditions of finite length floating arithmetic, destructive cancellation will take place, leading to total information loss at a finite distance from the target, this being nearest for the vertex type and furthest for the surface type. In this classification, the contributions of Plouff (1976)[4], Okabe (1979)[25], Pohanka (1988)[39], Gotze and Lahmeyer (1988)[10], Ivan (1996), Guptasarma and Singh (1999)[8] are of the vertex type, while Strakov et al. (1986)[27] introduced a line type (equations (7.28),(7.29)), and Holstein et al (1999)[26] introduced a closed form surface type. Equation (7.29) indicates that $\Lambda_{ij}, \lambda_{ij}$ are both $O(\gamma)$, leading to $\Omega_i = O(\gamma)$ as $\gamma \overset{tends}{\to} 0$ in equation (8), this being characteristic of the line type. By comparison, the new arctangent argument in equation (9) is $O(\delta\alpha^2/\delta^3)$, leading to an improved

$\Omega_i = O(\gamma^2)$ as $\gamma \overset{tends}{\rightarrow} 0$. When used in combination with equation (7.30), the $O(\gamma)$ arctanh term dominates the new term as the source of numerical error, and the method defaults to the line type. When used in combination with formulas of the surface type, the overall size of the $\mathbf{b}_{ij}$ terms to $O(\gamma^2)$ is maintained.

7.6.4 Arithmetic complexity

A polyhedron shares each edge with two facets, and each vertex with at least three edges. A naive implementation of the anomaly formulae ignoring commonality will therefore suffer large arithmetic redundancy. We assess the effect of the new formulation in the absence of this redundancy. To this end, we created array-indexed vertex, facet and edge lists. The edge list links each edge to each of the two vertices forming it, and to each of the two facets sharing the edge. After choosing the observation point, we make a single pass through the lists, storing computed information for future reference as necessary. Finally, we traverse all edges of all facets, making use of the pre-computed information. Significant savings are achieved in this manner. For example, the expression ij arctanhΛ_{ij} in equation (7.30) is common to both facets sharing the same edge. We carry out the algorithmic arithmetic counts under this scenario of non-redundancy.
Eule's relation V+F=E +2 together with E=3F/2 for triangular facets gives F=2V-4 and E=3V-6. Counting the operations on each vertex, facet and edge therefore allows the total target work count to be usefully expressed in terms of the number of target vertices. The counts are given in Table 1. We have kept total counts of floating point arithmetic operations($\pm, *, /$) and of function invocations (sqrt, arctan, arctanh), as an ordered pair (.,.). We excluded all counts that arise from intrinsic polyhedral properties, such as the $(\mathbf{t}_{ij}, \mathbf{n}_i, \mathbf{h}_{ij})$vectors and the edge lengths L_{ij} calculations. Intrinsics are calculated once per target, with no further overhead at subsequent observation points.

7.6.5 Results

Table 1 gives the work counts for the gravi-magnetic anomaly formulae in equations (7.24) and (7.25). The work counts are given for the formula (7.25)-(7.26) using equation (7.32). The improvements over the counts based on expression (7.31) are also given. The new approach relegates computation from edges to the less numerous facets, making lower operation counts possible. The table also shows counts for formulae of the surface type. They employ a re-arrangement of formulae (77.30) and (7.31) to induce analytical cancellation of dominant terms in the summations (Holstein et al. 1999)[26], to gain numerical stability. Formula (7.32), having already the required numerical stability, makes such refinement unnecessary in the solid angle component, with consequent substantial saving in arithmetic overhead. Figure 1 demonstrates a numerical instability found in the anomaly formulae. The vertical component of gravity $g_z = \mathbf{F} \cdot \mathbf{z}$ was computed for a regular icosahedral target, having 20 triangular facets. The result was compared with an equivalent sphere, computed from the point source formula. With increasing distance from the target, the sphere and target become indistinguishable, hence the initial downward trend. With further increase of distance, however, the growth of numerical error in the polyhedral formulae makes the two solution become wider apart again. This trend is shown for vertex,

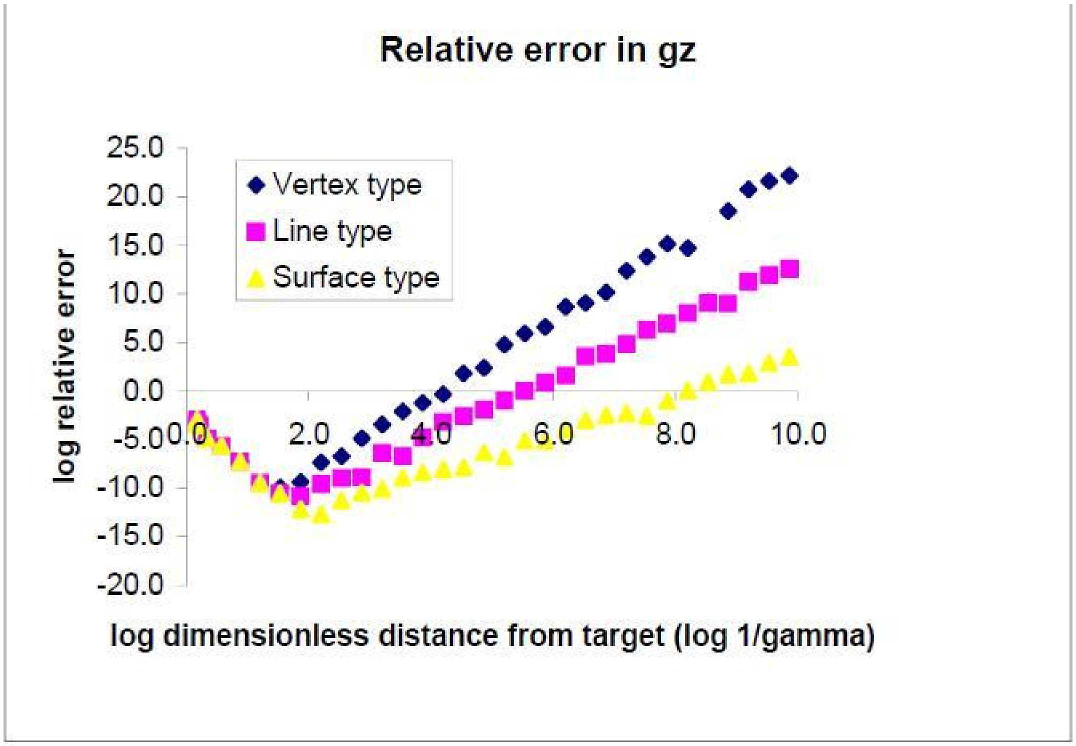

Figure 7.1: Stress-test of the new anomaly formulae. Relative errors between icosahedral and equivalent spherical targets are shown

line and surface type. The slopes of the scatter envelopes are 4, 3 and 2 respectively for the computations of g_z, consistent with theory (Holstein and Ketteridge(1996)). The solid angle formula (7.32) was used in all three algorithms, but the error growth is dominated by the logarithmic terms in the vertex and line methods. The surface method, however, retains the slope of 1, showing that the solid angle component is indeed $O(\gamma^2)$, characteristic of the surface method.

7.6.6 Conclusions

Table 1 – (Arithmetic, function) counts for a triangulated target with $n \geq 4$ vertices

	Line (new)	Improvement by	Surface (new)	Improvement by
φ	(110n-203, 6n-10)	(-3n+6, 4n-8)	(139n-223, 6n-9)	(60n-130, 4n-8)
F•z $= g_z$, Φ	(80n-143, 6n-10)	(27n-54, 4n-8)	(103n-161, 6n-9)	(98n-196, 4n-8)
F	(111n-203, 6n-10)	(30n-60, 4n-8)	(137n-227, 6n-9)	(94n-188, 4n-8)
∇**F**	(129n-235, 6n-10)	(26n-54, 4n-8)	(151n-253, 6n-9)	(88n-176, 4n-8)
H	(98n-177, 6n-10)	(11n-22, 4n-8)	(111n-175, 6n-9)	(92n-184, 4n-8)

Use of a solid angle algorithm in anomaly computation is not new. Thus, Guptasarma and Singh (1999) use such a component, which, however, always yields terms of O(1) no matter how far the target, and so can yield anomaly formulae only of the vertex (numerically least stable) type. Moreover, the arithmetic operation count is exceedingly high. We have demonstrated that the solid angle formula (7.31) maintains the expected error growth slope of the surface method (with the least slope 2), showing that this component does indeed have improved error characteristics when inserted into the vertex and line type formulae. Remarkably, in addition to enhanced stability, the new formula allowed anomaly formulae rearrangements to effect substantial reduction in arithmetic operation counts. The proposed formula has been analysed under the powerful methodology of gravimagnetic similarity to embrace all the standard gravi-magnetic anomalies for homogeneous triangulated polyhedral targets. In this context, variants of the anomaly formulae have been found that are both efficient and numerically stable. The new method should therefore be considered a strong contender in the development of reliable anomaly software.

Chapter 8

Gravity potential series expansion for homogeneous polyhedra

Publication:*Gravity potential series expansion for homogeneous polyhedra*
H. Holstein (Aberystwyth University), C. Willis (University of Bath) and C. Anastasiades (Aberystwyth University) EAGE - European Association of Geoscientists and Engineers - Rome, 2008 (bibliography ref:[2])

8.1 Point of expansion

Expansion methods have been used by other authors (e.g. Sigl (1985), Strykowski (2007)) introduced an expansion regime that involved series both at the observation point and a source point, and thereby could accommodate a variety of density models. Our approach is limited to polyhedral targets, and the formalism is developed only for the homogeneous(constant density) target case. This restriction has the benefit that the expansion coefficients at an arbitrary observation point are already available for the target in closed formulae without additional integration over the source distribution. Series expansion methods in gravity anomaly calculations provide a convenient representation of the local anomaly that do not require the complexity of a full anomaly computation at every evaluation point within a region of interest around an expansion point. We give one approach to obtaining such an expansion, appropriate when the causative body is a homogeneous polyhedral target. We make use of the known gravi-magnetic anomaly formulae for such targets, to obtain computationally stabilised coefficients of the series expansion around an interest point. We develop the formulae for the gravity potential as a the series expansion, and show that the method can have efficiency advantages over gridded interpolation as a means of expressing the local variation in potential. Expansion point $\mathbf{R}_*$ may be near or far from the target, or inside it so long as it does not intersect the target boundary. Formally, we develop the gravity potential function $\phi(\mathbf{R})$ as a three dimensional Taylor series around the expansion point $\mathbf{R}_*$

$$\phi(\mathbf{R}_* + \delta r) = \phi(\mathbf{R}_*) + \delta r : \nabla\phi + \frac{1}{2!}\delta r\delta r : \nabla\nabla\phi + \frac{1}{3!}\delta r\delta r\delta r : \nabla\nabla\nabla\phi + \mathbf{O}(\delta \mathbf{r^4}) \quad (8.1)$$

where all derivatives are evaluated at the expansion point R_* and the colon (:) denotes the operation of tensor contraction (Gumerov and Duraiswami (2005)[7]) The successive gradients of ϕ are seen immediately to relate to the gravity field, the gravity field gradient and to the gradient of the field gradient, or, by Poisson's relation, to the magnetic field gradient. As these quantities are available in closed form for an arbitrary homogeneous polyhedral target, the resulting series is immediately available. The terms will be given in the next section. The n_{th} order expansion term contains all 3^n in-line and cross derivatives of the potential ϕ. Some consideration to efficient evaluation must therefore be given. This is considered in the section on complexity, below. In the section on results and discussion, we compare our expansion method with gridded methods, and conclude that the expansion method is computationally more efficient.

8.1.1 Big O notation

Last term, means terms of the order of $\delta\mathbf{r}^4$ or above that approximate the accuracy of the result. In other words notation is used to represent higher order terms that are usually not so important compared to other terms in the series when you are taking some limit. But precisely, it tells you how quick such terms are approaching the limit.

8.1.2 Geometry and governing equations

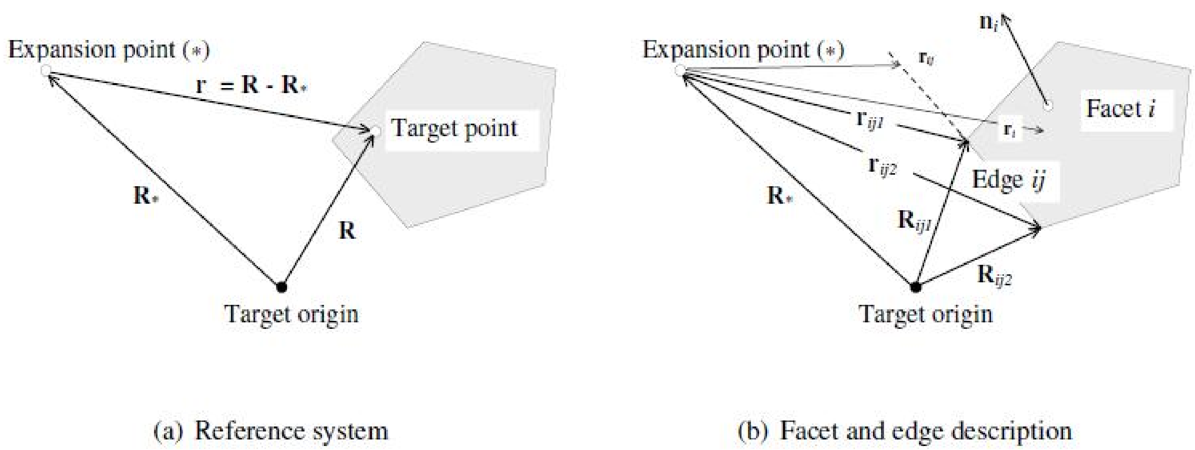

Figure 8.1: Geometric relationships

As shown in 8.1, we enumerate the polygonal facets of the polyhedral target by the index i, and denote by ij the jth edge of facet i . Relative to a target origin, the position vectors of the vertices of edge ij are taken as $\mathbf{R}_{ij1}$, $\mathbf{R}_{ij2}$, ordered so as to make a segment of an anticlockwise closed edge contour around the outward facet normal $\mathbf{n}_i$. The position vector of the expansion point is $\mathbf{R}_*$. Relative to the expansion point, the position vectors to the target vertices are

$$\mathbf{r}_{ij1} = \mathbf{R}_{ij1} - \mathbf{R}_*, \mathbf{r}_{ij2} = \mathbf{R}_{ij2} - \mathbf{R}_* \tag{8.2}$$

We further denote by $\mathbf{r}_{ij}$ any vector from the expansion point to a point on edge ij (natural choices being $\mathbf{r}_{ij1}$ or $\mathbf{r}_{ij2}$, and by $\mathbf{r}_i$ any vector from the expansion point to the surface of facet i, the ambiguity being removed on projection . The various gravi-magnetic anomalies are then given by

$$\phi(\mathbf{R}_*) = G\rho \sum_i \mathbf{r}_i \cdot \mathbf{n}_i \sum_j \mathbf{b}_{ij} \cdot \mathbf{r}_{ij} \qquad \in \Re^1 \tag{8.3}$$

$$\nabla\phi = -G\rho \sum_i \mathbf{n}_i \sum_j \mathbf{b}_{ij} \cdot \mathbf{r}_{ij} \qquad \in \Re^3 \tag{8.4}$$

$$\nabla\nabla\phi = G\rho \sum_i \mathbf{n}_i \sum_j \mathbf{b}_{ij} \qquad \in \Re^{3X3} \tag{8.5}$$

$$\nabla\nabla\nabla\phi = -G\rho \sum_i \mathbf{n}_i \sum_j \mathbf{B}_{ij} \qquad \in \Re^{3X3X3} \tag{8.6}$$

where

$$\mathbf{b}_{ij} = \mathbf{b}(\mathbf{R}_*, \mathbf{R}_{ij1}, \mathbf{R}_{ij2}, \mathbf{n}_i) \quad \in \Re^3, \quad \mathbf{B}_{ij} = \mathbf{B}(\mathbf{R}_*, \mathbf{R}_{ij1}, \mathbf{R}_{ij2}, \mathbf{n}_i) \quad \in \Re^{3X3} \tag{8.7}$$

are purely geometric vector and tensor functions respectively, defined on each edge of each facet of the polyhedron. Vector $\mathbf{b}_{ij}$ is physically dimensionless, while the rank 2 tensor $\mathbf{B}_{ij}$ has the dimension $(distance)^{-1}$. Explicit forms are given in Holstein (2002) and Holstein et al. (2007b)[13], and are not repeated here. The gradients on the left hand sides of equations 8.5 are taken with respect to variations of the expansion point $\mathbf{R}_*$, where they are also evaluated. The alternating signs on the right hand side of equation 8.5 are a consequence of the negative dependence of $\mathbf{R}_*$ in equation 8.4. The constant of universal gravitation G and the density contrast ρ of the target as well as the tensor dimensionalities are included in equations 8.5.

8.2 Terminology

8.2.1 Inner product space

In mathematics, an inner product space is a vector space with an additional structure called an inner product. This additional structure associates each pair of vectors in the space with a scalar quantity known as the inner product of the vectors.

8.2.2 Orthonormality

In linear algebra, two vectors in an inner product space are orthonormal if they are orthogonal and both of unit length. A set of vectors form an orthonormal set if all vectors in the set are mutually orthogonal and all of unit length. An orthonormal set which forms a basis is called an orthonormal basis.

8.2.3 Orthonormal basis

In mathematics, particularly linear algebra, an orthonormal basis for inner product space V with finite dimension is a basis for V whose vectors are orthonormal. For example, the standard basis for a Euclidean space R^n is an orthonormal basis, where the relevant inner product is the dot product of vectors. The image of the standard basis under a rotation or reflection (or any orthogonal transformation) is also orthonormal, and every orthonormal basis for R^n arises in this fashion. In our context the orthonormal basis of an edge as observed from an observation point, is comprised by the following unit vectors:
$(\hat{\mathbf{n}}_i, \hat{\mathbf{t}}_{ij}, \hat{\mathbf{h}}_{ij})$
where:
$\hat{\mathbf{n}}_i =$the unit facet normal,
$\hat{\mathbf{t}}_{ij} =$the unit tangent vector along edge ij
$\hat{\mathbf{h}}_{ij} =$the unit horizontal vector perpendicular to both $\hat{\mathbf{n}}_i$ and $\hat{\mathbf{t}}_{ij}$computed as: $\hat{\mathbf{t}} \wedge \hat{\mathbf{n}}$

8.2.4 Transpose of a Matrix

The transpose of a m by n matrix is defined to be a n by m matrix that results from interchanging the rows and columns of the matrix.

8.2.5 Symmetric Matrix

The elements located symetrically with respect to the principal diagonal are equal.

8.2.6 Tensor contraction

In multilinear algebra, a tensor contraction is an operation on one or more tensors that arises from the natural pairing of a finite-dimensional vector space and its dual. In components, it is expressed as a sum of products of scalar components of the tensor(s).

8.3 Series evaluation

Evaluation of the coefficients of the series will be carried out in a specified coordinate system, which we take to be defined at the expansion point by three mutually orthonormal unit vectors $(\hat{x}, \hat{y}, \hat{z})$. Projections of $\triangledown\triangledown\triangledown\phi$ on to these directions are then defined, from equation 8.6,by

$$\hat{\mathbf{q}} \cdot \triangledown\triangledown\triangledown\phi = -G\rho \sum_i \hat{\mathbf{q}} \cdot \mathbf{n}_i \sum_j \mathbf{B}_{ij} \quad \in \mathfrak{R}^{3X3}, \quad \hat{\mathbf{q}} \in (\hat{x}, \hat{y}, \hat{z}) \tag{8.8}$$

and will be stored as three $3X3$ matrices. The innermost contraction of the third order term in equation 8.1 can therefore be computed as the sum of three $3X3$ matrices.

$$\delta\rho : \triangledown\triangledown\triangledown\phi = \delta x(\hat{\mathbf{x}} \cdot \triangledown\triangledown\triangledown\phi) + \delta y(\hat{\mathbf{y}} \cdot \triangledown\triangledown\triangledown\phi) + \delta z(\hat{\mathbf{z}} \cdot \triangledown\triangledown\triangledown\phi) \quad \in \mathfrak{R}^{3X3} \tag{8.9}$$

where the probe vector $\delta\rho$ is represented by $(\delta x\hat{\mathbf{x}} + \delta y\hat{\mathbf{y}} + \delta z\hat{\mathbf{z}})$. The next levels of contraction can be achieved by combining the second and third order terms, and this in turn with the first and zero order terms, as a nested sequence

$$\phi_* + \delta\rho^T \left(\nabla\phi + \left(\nabla\nabla\phi + \left[\frac{\delta\rho}{3} : \nabla\nabla\nabla\phi \right] \right) \frac{\delta\rho}{2} \right) \tag{8.10}$$

similar to nested polynomial evaluation. During evaluation, the innermost round brackets combine as the sum of two 3X3 matrices. These are post multiplied by the column vector $\delta\rho/2$ to achieve the next level of contraction, yielding a vector, and this is added to the gradient vector $\nabla\phi$ as the sum to two 3X1 column matrices, which in turn is reduced to a scalar by premultiplying by the row matrix $\delta\rho$ and added to the scalar potential at the expansion point. The inner 3X3 matrices are symmetric, and for this reason the normally necessary internal transpose operations can be omitted.

8.4 Complexity

The arithmetic complexity of the right hand sides of equations 8.3-8.5 has been investigated by Holstein et al.(2007a)[22] for triangulated polyhedra. These serve as a useful upper bound for the cases of polyhedra with general polyhedral facets. A noteworthy feature of equations 8.3-8.5 is the high degree of algebraic re-use, since the same functions b_{ij} recur. The quantites B_{ij} in 8.6 are largely derived from expressions already calculated for the terms b_{ij} . Therefore, the complexity of computing all the expressions 8.3-8.6 is governed by the work to carry out one of the anomalies, augmented by the overheads of carrying out the different summation variants. On this basis, we estimate the number of floating point operations for the entire anomaly set to grow as 160n, where n is the number of vertices of the triangulated polyhedron. This includes function argument evaluation but ignores function invokations (sqrt, atan and atanh), as the latter do not dominate the calculations. To estimate the additional cost of evaluating the series (8.10) for each probe point around the expansion point, we note that the expression can be organised into 10 vector dot products, 4 vector additions, two vector scalings and 2 scalar additions. Taking account of matrix symmetry, the calculation has a complexity of 55 floating point operations. For p probe vectors and the one-time overhead of evaluating the gradients 8.3-8.6 at the expansion point, we estimate a (p,n) growth dependence of 160n + 69p floating point operations. For comparison, Lagrangian interpolation over a three-dimensional 3 x 3 x 3 grid, summarised by the formula:

$$\sum_{i,j,k=1..3} \phi(x_i, y_j, z_k) = \frac{(x - x_{i-1})(x - x_{i+1})(y - y_{i-1})(y - y_{i+1})(z - z_{i-1})(z - z_{i+1})}{(x_i - x_{i-1})(x_i - x_{i+1})(y_i - y_{i-1})(y_i - y_{i+1})(z_i - z_{i-1})(z_i - z_{i+1})} \tag{8.11}$$

with implied wrap round for out of range indices, requires 27 grid values for ϕ and for the denominators, evaluated once. Taking this into account, we arrive at a complexity of 27x (110n + 13p + 12) as the growth of the number of floating point operations with (n,p).

8.5 Results and discussion

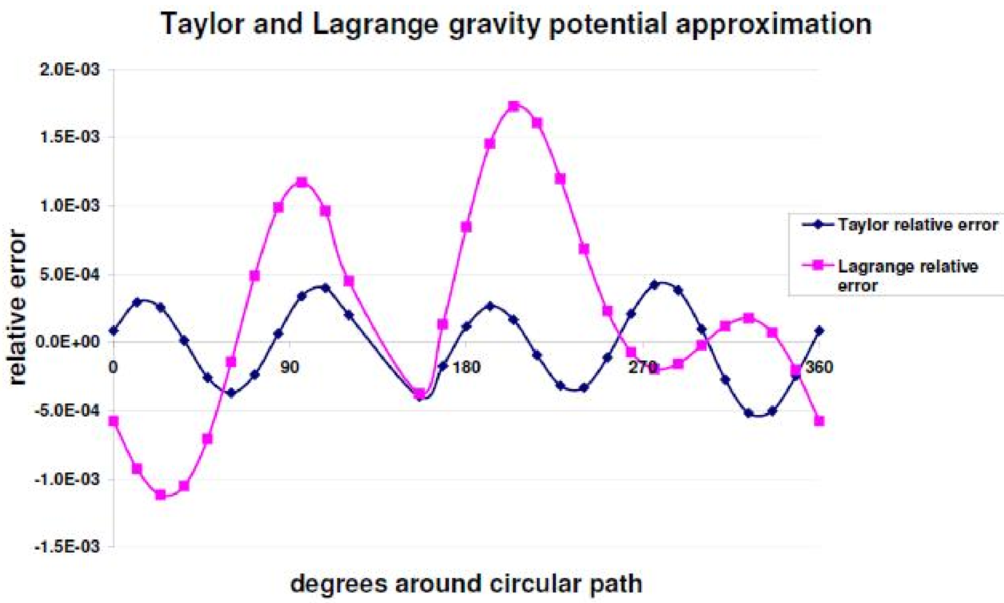

Figure 8.2: Comparison of Taylor and Lagrange methods for potential modelling

We have applied both Taylor and Lagrange methods to computations of the potential anomaly of the polyhedral target of Holstein et al. (1999)[26]. The model covers x- and y-extends of 50km, has a thickness of 10km and is at a depth of 12km. We placed the expansion point at [-10,-10,-2] and applied a probe radius of 5km. Within the probe volume there was a change of 43 per cent of the value of the potential. We also gridded the volume at $\pm 5km$ intervals into a three dimensional grid of 27 points. We evaluated the Taylor and Lagrange methods on a circular path of radius 5km, whose normal was directed along [1,1,1] to avoid alignment with coordinate axes. The result of the comparison is expressed in 8.2. Both methods show small errors relative to the correct result obtained from the anomaly formula at the probe point, although in this example, the Taylor method exhibits a better error distribution. The order of approximation of our Lagrange method is 2, while for the Taylor series it is 3. Generally, the Taylor error grows with distance from the expansion point, while the interpolation procedure has 27 centres in the region where exact results are to be had. Results from the complexity analysis above show that even though the Lagrange method has a lower order, it has both a higher start up cost (the coefficient of n) and a higher probing cost (the coefficient of p). On this basis, the Taylor method will always have a lower operational cost.

8.6 Conclusions

We have demonstrated that potential anomaly modelling by homogeneous polyhedra may usefully be augmented by Taylor series expansions that obtain the expansion coefficients from the anomaly formulae themselves, and thereafter allow rapid anomaly computation around the expansion point, in a manner that is competitive with other expansion methods. The approach extends to field and field gradient anomalies.

Chapter 9

Gravimagnetic anomaly formulae for extended homogeneous Prisms

Publication:

Horst Holstein[1],Costas Anastasiades[1], Ben Ketteridge[2](1)University of Aberystwyth, Wales, UK; (2) Hansard Global plc St.Petersburg, Russia, 2008
(bibilography ref:[2])

9.1 Finite forms of solids

Finite targets are 3D shapes enclosed by a n(finite number) number of facets. When the facets are polygons of a finite number, then the 3D shape is called polyhedron. Polyhedra is a top class of 3D shapes, including prisms and pyramides, case of which is a tetrahedron. When the base only is a polygon and the other n-sides is an extension(translation) of the base, the shape is called a prism. Therefore a prism is a shape created by the translation of a polygonal base having parallelograms as faces. A pyramid is a polyhedron or conic solid with a polygonal base and one top called apex. Each base edge and the apex are forming triangular faces. A tetrahedron is a convex polyhedron and exceptional case of a pyramid with 4 only triangular faces, a triangular base and 3 triangular facets created by the apex and the edges of the triangular base.

9.2 Elongated prisms

Elongated prisms are prisms created by an extended translation of the base, creating elongated sides relatively to their bases.

9.3 Thin sheets

Thin sheets are like very thin slices of elongated prisms with a limited (very small) thickness T near zero.

9.4 Anomaly algorithms for finite prismatic targets

All closed anomaly formulas studied so far, was for polyhedra and finite homogeneous prismatic targets, like the triangulated tetrahedral case. Triangulation of the homogeneous polyhedral case to a prismatic with finite number of triangulated facets, has being found to be of increased computational efficiency comparing to their polyhedral counterparts(chapter:7). All gravity and magnetic anomaly formulas are suffering from numerical illness when the observation point resides from the target. At this point of our research, in all error growth classes of algorithms although algorithmic stability was improved to an extend, using the Holstein method(surface) in its Oesterom version applied on prismatic targets, the numerical breakdown after finite precision is exceeded is delivering computational disaster for long δs(chapter 3,equation:3.1).

9.5 Anomaly algorithms for elongated prisms

Anomaly calculations normally contain two scale lengths. These are the typical target dimension, α, and the typical target distance from the observation point, δ. The targets considered here have an additional length scale,β, satisfying $\beta/\alpha << 1$ for a thin target, or $\beta/\alpha >> 1$ for an elongated target.

9.6 Reformulation of finite algorithms to their limiting extend

A limiting process, is the process with which we may approximate some quantity of a solid by computing the quantity first for a thin sheet of infinitecimal thickness and then considering the solid to be a stack of thin sheets of a specific thickness, integrating the stack with respect to the thickness parameter.
The target to distance ratio α/β for nearest target points remains unaffected by the limiting processes involving β. Either case of small or large β/α we describe as extended. We illustrate([**?**]) algorithm stabilization for two classes of extended targets:
the thin sheet and the elongated prism.
Historically, solutions for the infinitely thin sheet (Talwani, 1959, [36] Strakhov, 1984 [27]) and the infinite prism (Hubbert, 1949 [19]) have been obtained as isolated solutions. The purpose of our research is to reformulate the finite algorithms to allow targets to approximate limiting forms without numerical breakdown. The methods are generic and can apply to more general polyhedra.

9.7 Gravimagnetic similarity equations

In terms of gravimagnetic similarity (Holstein 2002, [15]) anomaly is determined by the following equations:

$$\begin{aligned} \mathbf{G} &= \sum_i \mathbf{n}_i \sum_j \mathbf{b}_{ij} \\ \mathbf{f} &= \sum_i \mathbf{n}_i \sum_j \mathbf{b}_{ij} \cdot \mathbf{r}_{ij} \\ \phi &= \frac{1}{2} \sum_i \mathbf{r}_i \cdot \mathbf{n}_i \sum_j \mathbf{b}_{ij} \cdot \mathbf{r}_{ij} \end{aligned} \tag{9.1}$$

With $\mathbf{G}\rho$ the gravitational constant times density, functions $\mathbf{G}\rho\mathbf{G}$, $\mathbf{G}\rho\mathbf{f}$, $\mathbf{G}\rho\phi$ express the gravity field gradient, vector field and potential, while $\mathbf{m} \cdot \mathbf{G}$, $\mathbf{m} \cdot \mathbf{f}$ give the magnetic field and potential for appropriate units of the magnetisation vector m, respectively.

9.7.1 The typical facet

We consider a typical facet with edges $[i, j]$,$[i, j']$,... and vertices $[(i, j), (i, j')]$,$[(i, j'), (i, j'')]$,... winded in an anticlockwise way, around the outward normal $\mathbf{n}_i$.

9.7.2 The b_{ij} terms

Considering orthonormal triad $(\mathbf{n}_i, \mathbf{t}_{ij}, \mathbf{h}_{ij})$, $\mathbf{b}_{ij}$ is by definition a function of the observation vectors and the orthonormal triad:
$(\mathbf{r}_{ij}, \mathbf{r}_{ij'}, \mathbf{n}_i, \mathbf{t}_{ij}, \mathbf{h}_{ij})$.
From Holstein (2002) ([15])$\mathbf{b}_{ij}$ is defined as:

$$\mathbf{b}_{ij} = \mathbf{h} b_{ij}^h + \tilde{\mathbf{n}} b_{ij}^n \tag{9.2}$$

where:

$\mathbf{h} = \mathbf{t} \wedge \mathbf{n}$
$\mathbf{t} = \frac{(\mathbf{r}_{ij'} - \mathbf{r}_{ij})}{L_{ij}}$
$\mathbf{n}$=normal of facet i
b_{ij}^h=2arctanhΛ_{ij}
$b_{ij}^n = 2 \arctan \lambda_{ij}$

$$\Lambda_{ij} = L_{ij}/(2\bar{r}), \bar{r}_{ij} = \frac{1}{2}(r_{ij} + r_{ij'}) \tag{9.3}$$

$$\tilde{\mathbf{n}} = \mathbf{n}_i sign(\mathbf{n}_i \cdot \mathbf{r}_i) \tag{9.4}$$

$\lambda_{ij} = \frac{\mathbf{h}_{ij} \cdot \mathbf{r}_{ij} \Lambda_{ij}}{(\bar{r}_{ij}(1 - \Lambda_{ij}^2) + |\mathbf{n}_i \cdot \mathbf{r}_{ij}|)}$

$\mathbf{r}_{ij}$ =position vector of vertex ij
L_{ij} =length of edge ij.
By rearranging terms, we can get the parity identities:

$$\mathbf{b}_{ij} = \mathbf{b}_{ij}\left(\mathbf{r}_{ij}, \mathbf{b}_{ij}\mathbf{h}_{ij}, \mathbf{t}_{ij}, \mathbf{n}_i\right) = \mathbf{b}_{ij}\left(\mathbf{r}_{ij}, \mathbf{b}_{ij}, \mathbf{h}_{ij}, -\mathbf{t}_{ij}, -\mathbf{n}_i\right) = -\mathbf{b}_{ij}\left(\mathbf{r}_{ij}, \mathbf{b}_{ij'}, -\mathbf{h}_{ij}, -\mathbf{t}_{ij}, \mathbf{n}_i\right) \tag{9.5}$$

9.8 The thin sheet

A thin sheet is comprised by 2 planar sheets, 1 top and one bottom. We consider a scalar distance between them, from bottom to the top L, alternatively called thin sheet thickness. We consider a mid-plane cutting the distance in the middle(1/2) between the bottom and top facets. If ρ_1, ρ_2, ρ_3 are the position vectors of the mid-plane, from the local co-planar origin, then the position vectors of the top ($\mathbf{r}_j^+$)and bottom ($\mathbf{r}_j^-$)faces relatively to the mid-plane's local position vectors, will be:

$$\mathbf{r}_j^+ = \mathbf{r}_0 + \rho_j + (L/2)\mathbf{n}, \mathbf{r}_j^- = \mathbf{r}_0 + \rho_j - (L/2)\mathbf{n}, j = 1, 2, 3 \tag{9.6}$$

9.8.1 Defining the edges

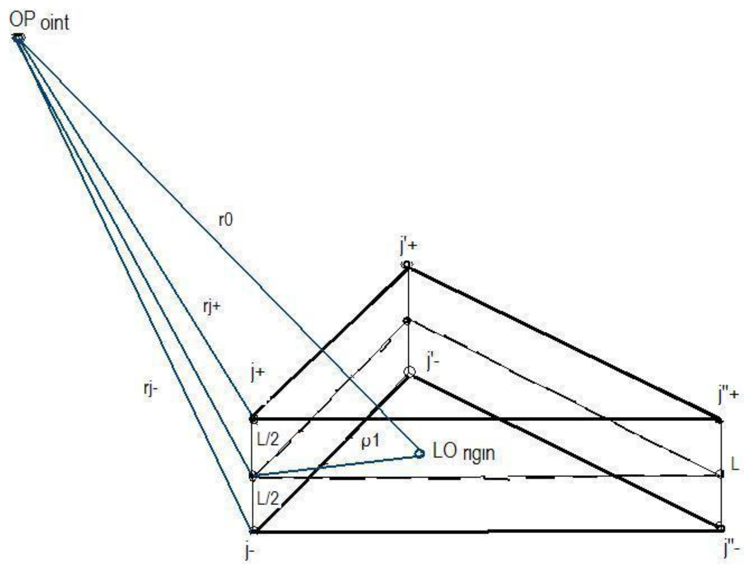

Figure 9.1: Magnification of an extended prismatic plate

In figure 9.1 a thin sheet is illustrated as observed from an observation point PO. The top face is (j^+, j'^+, j''^+) and the bottom (j^-, j'^-, j''^-), Mid face is illustrated with doted line. Local origin LO is co-planar with mid face, local and remote position vectors are colored in blue.

The edge j of the top facet, with its orthonormal triad $(\mathbf{h}_j, \mathbf{t}j, \mathbf{n})$ can now serve as a reference system for the other 5 edges of the adjacent thin facet and bottom facet. If we shrink the thickness of our target from the top plate to the bottom (that is the idea of a thin sheet)we can start with a reference edge j and add the associated edges to this edge as annotated in figure 9.2. If we take as a reference edge BC this serves as an edge of the top plate (ABCD) and the front (BB'C'C). From shrinking the target, reference edge BC of the top plate will meet edge B'C' of the bottom plate. In that sense edge B'C' will be associated to BC and will be edge of the front plate (BB'C'C) and of the bottom(A'B'C'D'). If we consider also edges BB' and CC' associated to BC which is obvious from figure 9.2 then

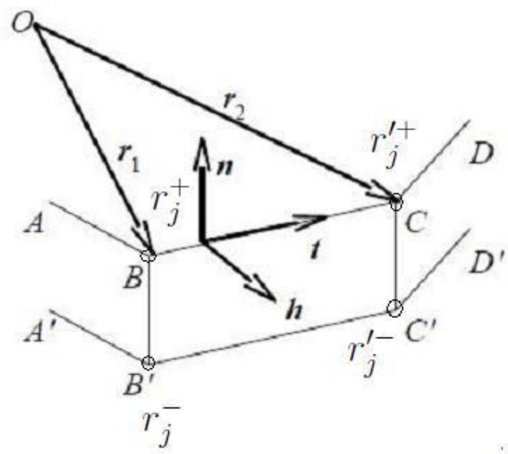

Figure 9.2: Part of a parallelepiped model, showing a top facet edge orthonormal vector triad (h,t,n). In the limiting thin-sheet case, short edges B'B, C'C, ... shrink to zero.Associated vertices (r_j^+,r_j^-,$r_j'^+$,$r_j'^-$)to the reference edge BC are also illustrated

the total associated edges to our reference edge BC are 5, namely,
BC(top), CC'(front),B'B(front), C'B'(bottom),C'B'(front).
Assigning to each vertex the notation (j+,j-) for top and bottom vertices respectively and if j' is the successor to j vertex we have 4 vertices associated to the reference edge BC :
r_j^+,r_j^-,$r_j'^+$,$r_j'^-$.
So our 6 edges in terms of pairs of vertices become:

1. r_j^+, r_j^-
2. $r_{j'}^-, r_{j'}^+$
3. $r_{j'}^+, r_j^+$
4. $r_j^-, r_{j'}^-$
5. $r_j^+, r_{j'}^+$
6. $r_{j'}^-, r_j^-$

Now from (9.1) we get:

$$\begin{aligned}\mathbf{G} = \sum\nolimits_j \{ &\mathbf{h}_j \left[\mathbf{b}\left(\mathbf{r}_j^+, \mathbf{r}_j^-, -\mathbf{t}_j, \mathbf{n}, \mathbf{h}_i\right) + \mathbf{b}\left(\mathbf{r}_{j'}^-, \mathbf{r}_{j'}^+, \mathbf{t}_j, \mathbf{n}, \mathbf{h}_i\right)\right] + \\ &\mathbf{h_j}\left[\mathbf{b}\left(\mathbf{r}_{j'}^+, \mathbf{r}_j^+, -\mathbf{t}_j, \mathbf{n}, \mathbf{h}_i\right) + \mathbf{b}\left(\mathbf{r}_j^-, \mathbf{r}_{j'}^-, \mathbf{t}_j, -\mathbf{n}, \mathbf{h}_i\right)\right] + \\ &\mathbf{n}\left[\mathbf{b}\left(\mathbf{r}_j^+, \mathbf{r}_{j'}^+, \mathbf{t}_j, \mathbf{n}, \mathbf{h}_i\right) - \mathbf{b}\left(\mathbf{r}_{j'}^-, \mathbf{r}_j^-, -\mathbf{t}_j, -\mathbf{n}, \mathbf{h}_j\right)\right]\}\end{aligned} \tag{9.7}$$

As you see in equation 9.7 gravity anomaly is expressed as a sum of edge gravities.

9.8.2 The exact finite ratio

As L $\stackrel{tends}{\rightarrow}$0 , top and bottom plates will approach each other, leading to a zero anomaly. We therefore seek an expression for G/L , such that its computation as L $\stackrel{tends}{\rightarrow}$0 is not invalidated by numerical cancellation error.

$$\begin{aligned}\mathbf{G}/L = \sum\nolimits_j \{ \mathbf{h}_j \left[-\mathbf{b}\left(\mathbf{r}_j^-, \mathbf{r}_j^+, \mathbf{t}_j, \mathbf{n}, \mathbf{h}_j\right)/L + \mathbf{b}\left(\mathbf{r}_j^-, \mathbf{r}_{j'}^+, \mathbf{t}_j, \mathbf{n}, \mathbf{h}_i\right)/L\right] \\ - \mathbf{h}_j \left[\mathbf{\Delta b}\left(\mathbf{r}_j, \mathbf{r}_{j'}, \mathbf{t}_j, -\mathbf{n}, \mathbf{h}_i\right) + \mathbf{n}\mathbf{\Delta b}\left(\mathbf{r}_j, \mathbf{r}_{j'}, \mathbf{t}_j, \mathbf{n}, \mathbf{h}_i\right)\right]\}\end{aligned} \tag{9.8}$$

Using relations 9.5, we can express G into meaningful ratios where limits as $L \stackrel{tends}{\rightarrow} 0$ exist in which $\Delta f(\mathbf{r}) = (f(\mathbf{r}^+) - f(\mathbf{r}^-))/L$ represents an exact finite difference ratio of a quantity $f(\mathbf{r})$ defined on the top(+) and bottom(-) plates. The first line in equation (9.8) contains b functions of nearby arguments r- , r+ . The parameter L in these functions is factored by L.

9.8.3 Stabilizing arctan, arctanh expressions

Consequently, we need stable expressions for arctanh and arctan functions at small arguments, divided by L. We use

$$\begin{aligned}arctan\left(L\xi\right)/L = \xi\left(1 + \left(L\xi\right)^2 Atn\left(L\xi\right)\right); Atn(x) = -\frac{1}{3} + \frac{1}{5}x^2 - \frac{1}{7}x^4 + \dots \\ arctanh\left(L\xi\right)/L = \xi\left(1 + \left(L\xi\right)^2 Atnh\left(L\xi\right)\right); Atnh(x) = \frac{1}{3} + \frac{1}{5}x^2 + \frac{1}{7}x^4 + \dots\end{aligned} \tag{9.9}$$

for ξs as defined in 9.13

9.8.4 Δ operator

$$\begin{aligned}\Delta b_j^{(n)} = 2\left[arctan\lambda_j\right]^+/L = 2arctan\left(L\Delta\lambda_j\left(1 + \lambda_j^-\lambda_j^+\right)\right)/L \\ \Delta b_j^{(h)} = 2\left[\arctan\Lambda_j\right]^+/L = 2\arctan\left(L\Delta\Lambda_j\left(1 + \Lambda_j^-\Lambda_j^+\right)\right)/L\end{aligned} \tag{9.10}$$

Requirement of Δ operator in the second line of equation 9.8 from 9.2 with evaluation as in equation 9.9

9.8.5 Differential calculus analogues

The Δ operator applied to compound 9.13expressions such as l,L obeys differential calculus analogues, using overbar notation $\overline{a} = \frac{1}{2}(a^- + a^+)$:

$$
\begin{aligned}
&\Delta(\alpha \pm b) = \Delta\alpha \pm \Delta b; \Delta(\alpha b) = \Delta\alpha\overline{b} + \overline{\alpha}\Delta b; \Delta(\alpha/b) = (\Delta(\alpha\overline{b} - \overline{a}\Delta b)/(b^+b^-);\\
&\Delta(1/b) = -\Delta b/b^+b^-;\\
&\Delta\left(\sqrt{\alpha}\right) = \Delta\alpha/\left(\sqrt{\alpha^-} + \sqrt{\alpha^+}\right);\\
&\Delta(|\alpha|) = \Delta\alpha\left(\alpha^- + \alpha^+\right)/\left(|\alpha^-| + |\alpha^+|\right)
\end{aligned}
\tag{9.11}
$$

As you can see in equation 9.14 we use differential calculus analogues, using overbar notation $\overline{a} = \frac{1}{2}(a^- + a^+)$ In this way, all operations Δ will ultimately be stably applied to basic terms $\mathbf{r}$ and r,

$\Delta\mathbf{r}_j = \Delta\mathbf{r}_{j'} = (\mathbf{r}_j^+ - \mathbf{r}_j^-)/L = \mathbf{n}$ (equation:9.6)

$$
\begin{aligned}
&\Delta r_j = (r_j^+ - r_j^-)/L = (\mathbf{r}_j^+ - \mathbf{r}_j^-)\cdot(\mathbf{r}_j^+ + \mathbf{r}_j^-)/L(r_j^+ + r_j^-) =\\
&\Delta\mathbf{r}_j \cdot \overline{\mathbf{r}}_j/\overline{r}_j = \mathbf{n}\cdot\overline{\mathbf{r}}_j/\overline{r}_j
\end{aligned}
\tag{9.12}
$$

$$
\begin{aligned}
\Delta b_j^{(n)} &= 2\left[\arctan\lambda_j\right]^+/L = 2\arctan\left(L\Delta\lambda_j\left(1 + \lambda_j^-\lambda_j^+\right)\right)/L\\
\Delta b_j^{(h)} &= 2\left[\arctan\Lambda_j\right]^+/L = 2\arctan\left(L\Delta\Lambda_j\left(1 + \Lambda_j^-\Lambda_j^+\right)\right)/L
\end{aligned}
\tag{9.13}
$$

Requirement of Δ operator in the second line of equation 9.8 from 9.2 with evaluation as in equation 9.9

9.8.6 Differential calculus analogues

The Δ operator applied to compound 9.13expressions such as l,L obeys differential calculus analogues, using overbar notation $\overline{a} = \frac{1}{2}(a^- + a^+)$:

$$
\begin{aligned}
&\Delta(\alpha \pm b) = \Delta\alpha \pm \Delta b; \Delta(\alpha b) = \Delta\alpha\overline{b} + \overline{\alpha}\Delta b; \Delta(\alpha/b) = (\Delta(\alpha\overline{b} - \overline{a}\Delta b)/(b^+b^-);\\
&\Delta(1/b) = -\Delta b/b^+b^-;\\
&\Delta\left(\sqrt{\alpha}\right) = \Delta\alpha/\left(\sqrt{\alpha^-} + \sqrt{\alpha^+}\right);\\
&\Delta(|\alpha|) = \Delta\alpha\left(\alpha^- + \alpha^+\right)/\left(|\alpha^-| + |\alpha^+|\right)
\end{aligned}
\tag{9.14}
$$

As you can see in equation 9.14 we use differential calculus analogues, using overbar notation $\overline{a} = \frac{1}{2}(a^- + a^+)$ In this way, all operations Δ will ultimately be stably applied to basic terms $\mathbf{r}$ and r,

$\Delta\mathbf{r}_j = \Delta\mathbf{r}_{j'} = (\mathbf{r}_j^+ - \mathbf{r}_j^-)/L = \mathbf{n}$ (equation:9.6)

$$\begin{aligned}&\Delta r_j = (r_j^+ - r_j^-)/L = (\mathbf{r}_j^+ - \mathbf{r}_j^-)\cdot(\mathbf{r}_j^+ + \mathbf{r}_j^-)/L(r_j^+ + r_j^-) = \\ &\Delta\mathbf{r}_j \cdot \overline{\mathbf{r}}_j/\overline{r}_j = \mathbf{n}\cdot\overline{\mathbf{r}}_j/\overline{r}_j\end{aligned} \tag{9.15}$$

Formulae for $\mathbf{f}/L, \phi/L$ are treated similarly, but require extra vector dot products, according to equation (9.1). These must be included under the Δ operation. Thus

$$\begin{aligned}&\Delta(\mathbf{b}_j\cdot\mathbf{r}_j) = \Delta(\mathbf{b}_j)\cdot\overline{\mathbf{r}}_j + \overline{\mathbf{b}}_j\cdot\Delta(\mathbf{r}_j)\\ &\Delta(\mathbf{r}_j\cdot\mathbf{n}\mathbf{b}_j\cdot\mathbf{r}_j) = \Delta(\mathbf{r}_j\cdot\mathbf{n})\overline{(\mathbf{b}_j\cdot\mathbf{r}_j)} + \overline{(\mathbf{n}\cdot\mathbf{r}_j)}\Delta(\mathbf{b}_j\cdot\mathbf{r}_j)\end{aligned} \tag{9.16}$$

The thin sheet algorithm may therefore be expressed in simple sequential steps, that pass previously calculated results into subsequent steps. The algorithm is stable as $L \overset{tends}{\rightarrow} 0$.

9.9 The elongated prism

9.9.1 The cross section

As in the thin sheet, let vertices 1,2,3 of the polygonal cross-section of a right elongated prism be given by position vectors ρ_1, ρ_2, ρ_3 relative to a local target origin, whose position vector is ρ_0 relative to the observation point. Front(+) and back(-) facets are separated by sides of length L, at vertices $\mathbf{r^+}_j, \mathbf{r^-}_j$ $\mathbf{r}_j, mathbfr_j$relative to the observation point, given by:

$$\mathbf{r^+}_j = \mathbf{r}_0 + \mathbf{r^-}_j, \mathbf{r^-}_j = \mathbf{r^+}_j - L\mathbf{n}, j = 1, 2, 3... \tag{9.17}$$

where $\mathbf{n}$ is the outward normal of the front facet. Without loss of generality, we take vectors $\mathbf{r}_0, \rho_1, \rho_2, \rho_3$ to be coplanar. Superposition of two such prisms of different lengths recovers the general case of an observation point that is not in the front facet plane. Equation (9.7) applies to the current geometry as well. However, in this geometry, unbounded logarithmic terms arise in $\mathbf{b}(\mathbf{r^+}_j, \mathbf{r^-}_j), \mathbf{b}(\mathbf{r^-}_{j'}, \mathbf{r^+}_{j'})$ representing contributions from edges of length L as $L \overset{tends}{\rightarrow} 0$. The summation implied by equation (9.1), however, can lead to finite results because of cancellation. The goal of this section is to present numerically stable formulae that allow the limit $L \overset{tends}{\rightarrow} 0$ to be approached without overflow. We express scaling by 1/L via the notation $(.)L =^{\sim}$ .Scaled lengths harmlessly enter computations with $\widetilde{\mathbf{r}}_j^+ \overset{tends}{\rightarrow} 0, \widetilde{\mathbf{r}}_j^- \overset{tends}{\rightarrow} 0$ as $L \overset{tends}{\rightarrow} \infty$ where for vertex j (and similarly j')

$$\tilde{r}_j^+ = \frac{r_j^+}{L}, \tilde{r}_j^- = \frac{r_j^-}{L} = \sqrt{1 + \left(\tilde{r}_j^+\right)^2}, \tilde{\mathbf{r}}\cdot\mathbf{n} = -1, \tilde{\mathbf{r}}_j^+\cdot\mathbf{n} = 0 \tag{9.18}$$

9.9.2 logarithmic terms

Combining first line of equation 9.7 with 9.5 we get the following contributions:

$$\sum\nolimits_{j}\{\mathbf{h}_j\left[-\left(\mathbf{b}\left(\mathbf{r}_j^+,\mathbf{r}_j^-,\mathbf{t}_j,-\mathbf{n},\mathbf{h}_j\right)-\mathbf{t}_j\eta\right)+\left(\mathbf{b}\left(\mathbf{r}_{j'}^+,\mathbf{r}_{j'}^-,\mathbf{t}_j,-\mathbf{n},\mathbf{h}_j\right)-\mathbf{t}_j\eta\right)\right]\} \quad (9.19)$$

η is arbitrary but in for our case we choose suitably an η to cancel analytically the logarithmic growth in the $\mathbf{b}$ terms. This is found to be
$\eta = \ln 2L/r_0$
In terms of vertex contributions j, j' from equation 9.19 and equations 9.17,9.18,9.2, we get:

$$\begin{aligned}&-\mathbf{h}_j\mathbf{t}_j\left(b^{(h)}\left(\mathbf{r}_j^+,\mathbf{r}_j^-,\mathbf{t}_j,-\mathbf{n},-\mathbf{h}_j\right)-\mathbf{t}_j\eta\right)=-\mathbf{h}_j\mathbf{t}_j\left(\ln\frac{r_j^-+\mathbf{r}_j^-\cdot(-\mathbf{n})}{r_j^++\mathbf{r}_j^+\cdot(-\mathbf{n})}-\ln\frac{2L}{r_0}\right)\\&=-\mathbf{h}_j\mathbf{t}_j\left(\ln\frac{1+\tilde{r}_j^-}{2}-\ln\frac{r_j^+}{r_0}\right)=-\mathbf{h}_j\mathbf{t}_j\left(2arctanh\frac{\left(\tilde{r}_j^+\right)^2}{(1+\tilde{r}_j^-)(3+\tilde{r}_j^-)}-\ln\frac{r_j^+}{r_0}\right)\end{aligned} \quad (9.20)$$

Numerical evaluation is safe for $L \overset{tends}{\rightarrow} \infty$. Of course there are unbounded logarithmic terms. But this way, these are captured in expression (9.19), and stabilized. In the formulae (9.1) for f and j , the logarithmic offsets for h require compensatory sums.

$$\sum_{\mathbf{j}}\mathbf{h}_j\mathbf{t}_j\cdot\left(\mathbf{r}_j^+-\mathbf{r}_{j'}^+\right)\eta=0;\sum_{\mathbf{j}}\left(\mathbf{r}_j\cdot\mathbf{h}_j\right)\mathbf{t}_j\cdot\left(\mathbf{r}_j^+-\mathbf{r}_{j'}^+\right)=A\eta \quad (9.21)$$

where A is the cross-section area. Stabilizing offsets do not alter f, instead an extra term ($A\eta = A\ln 2L/r_0$) is required to evaluate ϕ , being an evidence of a logarithmic singularity for $L \overset{tends}{\rightarrow} \infty$ in gravity potential.

9.9.3 arctangent terms

Scaling as in equation (9.18) is recommended for the arctangent terms in equations (9.3) and (9.4) that involve the far edges. Hapilly, we will not suffer from an arctangent overflow, since function has a range $-\pi/2$ to $\pi/2$. Remarkably, if the right hand expression in

$$\overline{r}_j=\frac{1}{2}(r_j^++r_j^-),\Lambda=L/(2\overline{r}_j),\overline{r}_j(1-\Lambda^2) \quad (9.22)$$

arising as sub-expression in the arctangent argument (9.4) from the edges of length L , is independent of L, with value r_j^+ , so the latter value trivially stabilizes this term as $L \overset{tends}{\rightarrow} \infty$ Further consideration can be given to far edge terms in f and j that are of the form $Larctan(\xi/L)$ as $L \overset{tends}{\rightarrow} \infty$. Such terms were already discussed for the thin sheet case (equation (9.22)) in the context of 1/ $L \overset{tends}{\rightarrow} 0$. This completes the numerical algorithm stabilization for the anomaly of an arbitrarily elongated prism. The anomaly contribution of the far edges decays, in fact, more rapidly than indicated here, because of geometric constraints (9.22). While of interest for convergence to limiting forms, this is not relevant in numerical computations where larger terms dominate.

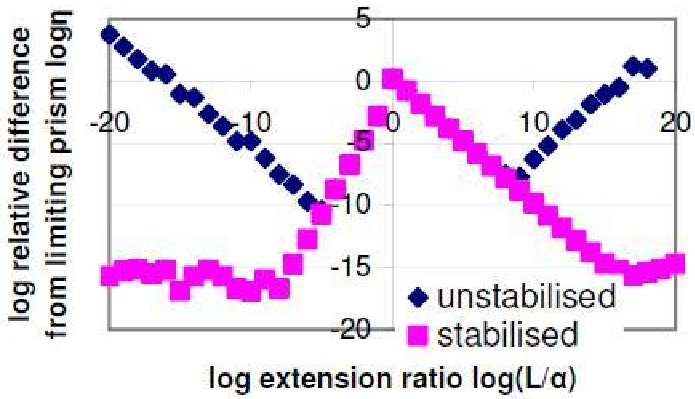

Figure 9.3: Comparison of extended and limiting prisms

9.10 Results and conclusions

With α being the length scale associated with the cross-section of a prismatic target, we placed an observation point at 5α from the target, and proceeded to calculate the gravity anomaly α for $L = \alpha 10^n$, where n is positive/negative for the elongated/thin prism respectively, using the unstabilized (u), stabilized (s) and limiting (l) algorithms in double float precision $\epsilon = 10^{-17}$. Difference ratios $\eta_{ul} = (\alpha_u - \alpha_l)/\alpha_l, \eta_{sl} = (\alpha_s - \alpha_l)/\alpha_l$ are then displayed as functions of L, as in the log-log plot of Figure 9.9.3. As the extension of the prism increases, both stabilized and unstabilised algorithms initially follow trends of approaching the limiting forms. At sufficiently high extension, however, the rising trend lines of the unstabilized algorithms show that they lose control of numerical error, and deviate more and more from the limiting forms, until all significance in the anomaly is lost. The stabilized algorithms,however, approach the limiting forms to the point where only the finite floating point precision prevents further approach, as indicated by a flattening of the trend lines. The graph shows that the unstabilized algorithms are able to achieve extension ratios up to 10^4 and down to 10^{-4} before adverse error growth sets in. This will be adequate in many practical circumstances, so that the additional stabilization complexity can be avoided.
Algorithms for targets of different lenght scales are numerically ill-conditioned. As it was shown, limiting forms offer an idealised approach for thin sheets and elongated prisms. The process involves cancellation of dominant terms, prior to computation and calculation of the exact finite differences, following differential calculus. In the case of the elongated prism the technique also includes the diverging logarithmic terms that have no global effect. In the potential case this was not achieved, indicating a singularity in the potential of

the elongated prismatic target.
Comparison of results of the limiting forms of the unstabilized and stabilized algorithms, gave a break down of the unstabilized forms at a certain point, while stabilized continued until they became indistinguishable from the limiting forms. In practice algorithmic break down occurs near limiting forms, therefore stabilized algoritms remain only of theoretical interst.

Chapter 10

Thin polygonal sheet anomaly

Publication:*Gravi-magnetic anomalies of uniform thin polygonal sheets*
Horst Holstein[1],Des Fitzgerald[2],Costas Anastasiades[3] (1)Aberystwyth University, UK, hoh@aber.ac.uk and Intrepid-Geophysics, Australia (2)Director, Intrepid-Geophysics, Australia, des@intrepid-geophysics.com (3)Aberystwyth University, UK, anastasiadescostas@yahoo.gr
11th SAGA Biennial Technical Meeting and Exhibition-2009
(bibliography ref:[2])

10.1 The thin planar sheet target model

Thin planar sheets are useful gravitational and magnetic models of dykes and veins, treated as two dimensional geophysical structures on the survey scale of a particular gravity or magnetic survey (Grant and West, 1965,[6]). As stacked laminae they can approximate three dimensional targets with varying material properties (Talwani and Ewing, 1959,[36]). Together with their reduced computational burden over a full polyhedral calculation they are a natural model choice in stochastic inversion (Wildman and Gazonas, 2009[41]). We show that the thin-sheet anomaly formulae are numerically more stable than the corresponding formulae for a finitely thick polyhedral target. We also demonstrate the possibility of finding versions of the thin-sheet formulae that are absolutely stable with respect to increasing target distance to target size ratio, though this stability is obtained at the expense of extra numerical complexity.

The thin-sheet derivations in the above studies are ad hoc, giving no indication of how the formulae are related to each other. Strakhov et al. (1986,[27]) were first to exploit the striking similarity among the polyhedral gravity and magnetic anomaly formulae, and indicate the same for the thin-sheet formulae, but did not give full details. Their derivation in terms of complex variable theory is somewhat unnatural for the problem. A simple vector/tensor derivation was given by Holstein (2002a)[**?**], and this is the form we shall use to extend the formulae to thin sheets. As well as expressing the gravi-magnetic thin-sheet anomalies in a single framework, this will include a new result for the magnetic field gradient tensor of a uniformly magnetized thin sheet. Our derivation considers the gravity potential anomaly a as a function of the parallelepiped thickness parameter T, and seeks an analytical expression for the limit of the anomaly per unit thickness, $\alpha(T)/T$, as T tends to zero. This is equivalent to differentiation, but explicit differentiation does not have to be carried out, since the polyhedral anomaly formulae are known and form a derivative hierarchy. We simply take the appropriate terms from the next order of anomaly. Only for the magnetic field gradient thin-sheet formula do we need a new differentiated result, but by then all terms are algebraic and this explicit final differentiation is easy to perform. In summary, the entire set of gravi-magnetic thin-sheet formulae largely reuses the functions employed in the known polyhedral anomaly solutions, thus preserving similarity and aiding derivation. We verify the thin-sheet formulae by comparison with the finite thickness polyhedral parallelepiped for cases of decreasing thickness T, and with the numerically differentiated thin-sheet potential anomaly to approximate the field and field gradient with decreasing step length t. We find that the finite forms approach the limiting thin-sheet forms with second order accuracy $O(T^2), O(t^2)$ respectively, confirming the validity of our thin-sheet formulae. A synthetic survey over a 41 by 41 mesh showed that the thin-sheet formulae were computed more than twice as fast as the corresponding finite-thickness polyhedral parallelepiped formulae, supporting our conclusion that the thin-sheet formulae can be used to advantage in the modelling of 2D gravity and magnetic targets.

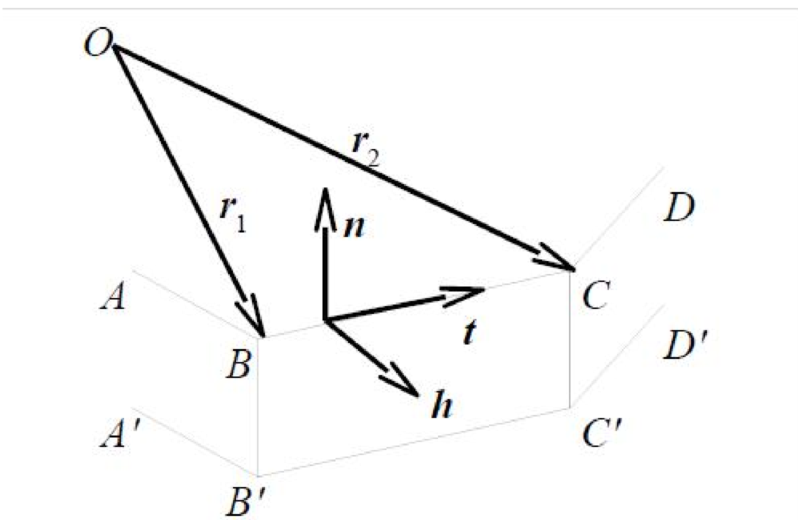

Figure 10.1: Part of a parallelepiped model, showing a top facet edge orthonormal vector triad (h,t,n). In the limiting thin-sheet case, short edges B'B, C'C, ... shrink to zero.

10.2 Gravimagnetic similarity([15]) polyhedral equations

$$h_{ij} = \mathbf{r}_{ij1} \cdot \mathbf{h}_{ij} = \mathbf{r}_{ij2} \cdot \mathbf{h}_{ij}, \upsilon_i = \mathbf{r}_{ij1} \cdot \mathbf{n}_i = \mathbf{r}_{ij2} \cdot \mathbf{n}_i \tag{10.1}$$

$$l_{ij1} = \mathbf{r}_{ij1} \cdot \mathbf{t}_{ij1}, l_{ij2} = \mathbf{r}_{ij2} \cdot \mathbf{t}_{ij1}, \bar{l}_{ij} = \left(l_{ij1} + \left(l_{ij2}\right) /2\right. \tag{10.2}$$

10.2.1 Gravity potential anomaly

$$\phi_g = \frac{1}{2} G\rho \sum_i \mathbf{r}_i \cdot \mathbf{n}_i \sum_j \mathbf{b}_{ij} \cdot \mathbf{r}_{ij} \tag{10.3}$$

10.2.2 Gravity field anomaly

$$f_g = \nabla \phi_g = -G\rho \sum_i \mathbf{n}_i \sum_j \mathbf{b}_{ij} \cdot \mathbf{r}_{ij} \tag{10.4}$$

10.2.3 Gravity gradient anomaly

$$G_g = \nabla f_g = G\rho \sum_i \mathbf{n}_i \sum_j \mathbf{b}_{ij} \tag{10.5}$$

10.2.4 Magnetic potential anomaly

$$\phi_m = -\sum_i \mu \cdot \mathbf{n}_i \sum_j \mathbf{b}_{ij} \cdot \mathbf{r}_{ij} \tag{10.6}$$

10.2.5 Magnetic field anomaly

$$f_m = \nabla \phi_m = \sum_i \mu \cdot \mathbf{n}_i \sum_j \mathbf{b}_{ij} \tag{10.7}$$

10.2.6 Magnetic Gradient anomaly

$$G_m = \nabla f_m = -\sum_i \mu \cdot \mathbf{n}_i \sum_j \mathbf{b}'_{ij} \tag{10.8}$$

Regarding the above 6 equations of the gravi-magnetic anomaly package,
$G\rho$ is the constant of universal gravitation times density,
μ the magnetization vector ,
$\mathbf{b}_{ij}$ is a vector function in the $\mathbf{n}_i, \mathbf{h}_{ij}$ plane (reference:9.7.2) encapsulating the Newtonian potential for edge ij.
The recurrence of the functions $\mathbf{b}_{ij}$ in equations (10.3)-(10.7) expresses the gravi-magnetic similarity for polyhedral targets. Only equation (10.8) requires a new term $\mathbf{b'}_{ij}$, equal to the tensor $-\nabla \mathbf{b}_{ij}$.
The formula for $\mathbf{b}_{ij}$ is

$$\mathbf{b}_{ij} = 2\mathbf{h}_{ij} arctanh \Lambda_{ij} - 2\mathbf{n}_i^s \arctan \lambda_{ij} \tag{10.9}$$

$$\Lambda = L/(2\overline{r}), \overline{r} = (|\mathbf{r}_1| + |\mathbf{r}_2|)/2$$
$$\mathbf{n}^s = \mathbf{n}\mathrm{sign}(\upsilon), \lambda = \frac{h\Lambda}{\overline{r}\,(1-\Lambda^2) + |\upsilon|} \tag{10.10}$$

$$\sum_j \mathbf{b}_{ij} \cdot \mathbf{r}_{ij} = \int_S dS/r \tag{10.11}$$

that is, the sum over the edge terms of a facet is equal to its area integral weighted by the reciprocal scalar distance from the observation point. Formulae (10.3)-(10.11) will now be adapted to the the thin-sheet case.

10.3 Thin sheet anomalies

10.3.1 Gravity potential thin sheet anomaly

The Newtonian gravity potential of a target of volume V is

$$\phi_g = G\rho \int_V dV/r \tag{10.12}$$

In the case of a thin sheet of constant thickness T, the volume element becomes dV = T dS , where dS is an element of surface. The limiting anomaly per unit thickness is then given by

$$\lim_T \to 0(\phi_g/T) = G\rho \int_S dS/r \tag{10.13}$$

where the integration is carried out over the surface S of the sheet. In practice, we shall retain a finite thickness parameter T in the formula so as to allow the target to have a finite volume and mass. Thus we express the thin-sheet gravity potential anomaly as

$$\phi_g = G\rho T \int_S dS/r \tag{10.14}$$

When the surface S is a planar polygon, equation (10.11) applies, and thus the thin-sheet potential is given by

$$\phi_g = G\rho T \sum_j \mathbf{b}_j \cdot \mathbf{r}_j \tag{10.15}$$

10.3.2 Gravity field thin sheet anomaly

Remarkably, expression (10.15) for the thin-sheet gravity potential ϕ_g is the top facet term in the polyhedral gravity field expression (10.4). As a consequence, its gradient, the gravity field of the thin-sheet anomaly, is by reference to equation (10.5) given by

$$\mathbf{f}_g = \nabla\phi_g = -G\rho T \sum_j \mathbf{b}_j \tag{10.16}$$

If only the component of gravity perpendicular to the plane of the thin-sheet target is required (for example, the vertical component of gravity in the case of a horizontal lamina), equations (10.9), (10.10) and (10.16)

$\mathbf{f}_g \cdot \mathbf{n} = \mathbf{n} \cdot (2\mathbf{h}_{ij} arctanh \Lambda_{ij} - 2\mathbf{n}\text{sign}(\upsilon)\arctan\lambda_{ij})$ because of orthonormality between $\mathbf{n}_i, \mathbf{h}_{ij}$

$\mathbf{n} \cdot \mathbf{h}_{ij} = 0$, and $\mathbf{n} \cdot \mathbf{n} = 1^2$ and the distributive property for scalar products, yields
$0 + (-1)^2 * 2\text{sign}(\upsilon)\arctan(\lambda_{ij})$
Summation upon edges and multiplying by the Gravitational density constant$G\rho T$ yields
$G\rho T 2\text{sign}(\upsilon)\sum_j \arctan(\lambda_{ij})$
and therefore:

$$\mathbf{f}_g \cdot \mathbf{n} = G\rho T\text{sign}(\upsilon)2\sum_j \arctan\lambda_j \tag{10.17}$$

Formally, this is the result of Talwani and Ewing (1959)[36], although our form uses half the number of trigonometric function evaluations. An early version of equation (10.16) was obtained by Ketteridge (1996)[16], using a limiting process on the polyhedral prism solution as the thickness T tends to zero.

10.3.3 The gravity gradient thin-sheet anomaly

Because $\mathbf{n} \cdot \mathbf{n} = 1$

$$\mathbf{G}_g = \nabla f_g = G\rho T\sum_j \mathbf{b}'_j \tag{10.18}$$

where tensor elements of $\mathbf{b}'_j = -\nabla\mathbf{b}_j$ are given in Holstein et al.(2007)[22]. Thus we find for the edges j of the top facet

$$\mathbf{b}'_j = (\mathbf{h}_j\mathbf{h}_j - \mathbf{n}\mathbf{n})\, d_j + (\mathbf{h}_j\mathbf{t}_j + \mathbf{t}_j\mathbf{h}_j)\, e_j/2 + (\mathbf{h}_j\mathbf{n} + \mathbf{n}\mathbf{h}_j)\, f_j \tag{10.19}$$

where:

$$\begin{aligned} d_j &= \frac{-2\Lambda_j}{(1-\Lambda_j^2)}\frac{h_j}{r_{j1}r_{j2}} \\ e_j &= \frac{-2\Lambda_j \bar{l}_j}{r_{j1}r_{j2}} \\ f_g &= \frac{-2\Lambda_j}{(1-\Lambda_j^2)}\frac{\upsilon}{r_{j1}r_{j2}} \end{aligned} \tag{10.20}$$

10.3.4 The magnetic thin-sheet potential anomaly

$$\phi_m = \mu \cdot \mathbf{f}_g / (G\rho) \tag{10.21}$$

10.3.5 The magnetic thin-sheet field anomaly

$$f_m = \mu \cdot \mathbf{G}_g / (G\rho) \tag{10.22}$$

10.3.6 The magnetic gradient thin-sheet anomaly

$$\mathbf{G}_m = \nabla \mathbf{f}_m \tag{10.23}$$

$$\mathbf{G}_m = -T\mu \cdot \sum_j \mathbf{b''}_j \tag{10.24}$$

where:

$$\mathbf{b''}_j = (\mathbf{h}_j\mathbf{h}_j - \mathbf{nn})\,\mathbf{d'}_j + (\mathbf{h}_j\mathbf{t}_j + \mathbf{t}_j\mathbf{h}_j)\,\mathbf{e'}_j/2 + (\mathbf{h}_j\mathbf{n} + \mathbf{n}\mathbf{h}_j)\,\mathbf{f'}_j \tag{10.25}$$

and

$$\mathbf{d'}_j = -\nabla d_j, \mathbf{e'}_j = -\nabla e_j, \mathbf{f'}_j = -\nabla f_j \tag{10.26}$$

The three vectors, expressed in the local $\mathbf{h}_j, \mathbf{t}_j, \mathbf{n}$ frame of the top-edge, can be assembled into the three columns of a 3 by 3 matrix A. This matrix is symmetric and has trace zero. Direct differentiation gives

$$A_{11} = h^2 Q - r_1 r_2 V \tag{10.27}$$

$$A_{22} = \left(\bar{l}^2 (R - \Lambda^2) - r_1 r_2\right) U \tag{10.28}$$

$$A_{33} = \left(\upsilon^2 Q - r_1 r_2\right) V \tag{10.29}$$

$$A_{12} = A_{21} = h\bar{l}PU \tag{10.30}$$

$$A_{13} = A_{31} = h\upsilon QV \tag{10.31}$$

$$A_{23} = A_{32} = \bar{l}\upsilon(R + \Lambda^2)V \tag{10.32}$$

where

$$P = 1 + r_1/r_2 + r_2/r_1 \tag{10.33}$$

$$Q = P + 2\Lambda^2/(1 - \Lambda^2) \tag{10.34}$$

$$R = P - \Lambda^2/(r_1 r_2) \tag{10.35}$$

$$U = 2\Lambda/(r1r2)^2 \tag{10.36}$$

$$V = U/(1 - \Lambda^2) \tag{10.37}$$

$$
\begin{aligned}
\mathbf{d}' &= -\nabla d = \mathbf{h}A_{11} + \mathbf{t}A_{21} + \mathbf{n}A_{31} \\
\mathbf{e}' &= -\nabla e = \mathbf{h}A_{12} + \mathbf{t}A_{22} + \mathbf{n}A_{32} \\
\mathbf{f}' &= -\nabla d = \mathbf{h}A_{13} + \mathbf{t}A_{23} + \mathbf{n}A_{33}
\end{aligned}
\tag{10.38}
$$

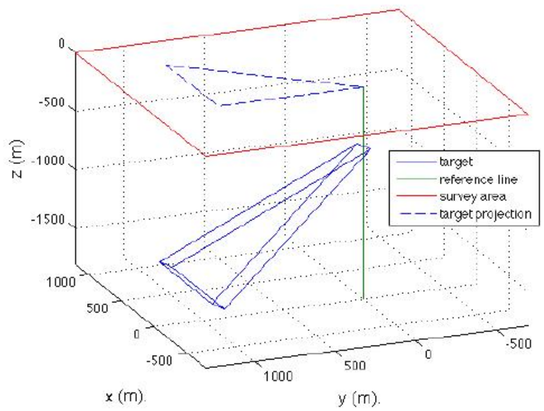

Figure 2. Thin target model used for synthetic modelling. Mid-plane vertices are at (0,0,-500), (0,900,-1700), (800,900,-1700). A vertical reference line is drawn to the surface point (0,0,0),. The projection of the target mid-plane on to the 2000m by 2000m survey area in the plane z=0 is also shown.

Figure 10.2:

10.4 Conclusions

Modelling of thin geological structures as limiting thinsheet bodies is appropriate in many survey situations, where the survey scale cannot adequately resolve such targets as three dimensional. We present a set of formulae giving the potential, field and field gradient in the gravity and magnetic cases when such targets have uniform density or magnetization. The formulae have a close affinity to the finite thickness polyhedral case, and this fact allowed a ready derivation of the limiting thinsheet formulae, in a common, uniform notation. Only in the magnetic gradient case were new relations required that were not already available from the full polyhedral case, and these were derived for this work. The resulting thin-sheet formulae exhibit the property of gravi-magnetic similarity, which allows them to be programmed efficiently in a single program with much reuse of the terms. Thus we offer a superior formulation that strongly emphasises commonality, and also provide a new result for the case of the magnetic gradient. The implicit differential relationships between the formulae was used to verify the correctness of the formulae, further confirmed by an asymptotic approach of the full polyhedral anomaly formulae to the limiting cases. In summary, this work provides a set of modelling formulae that will be useful in the interpretation of gravity and magnetic survey data. It will form part of the next version of the

target closure	ρ1ρ2ρ3ρ1'ρ2'ρ3'				
facets	5				
vertices	6				
edges	18	9 doubles			
thickness	t	1			
	x	y	z		
ρ1	0	0	-500		
ρ2	0	900	-1700		
ρ3	800	900	-1700		
ρ1'	0	0	-501		
ρ2'	0	900	-1701		
ρ3'	800	900	-1701		
facets					Area
1	ρ1	0	0	-500	
	ρ2	0	900	-1700	
	ρ3	800	900	-1700	
2	ρ3'	800	900	-1701	
	ρ1'	0	0	-501	
	ρ2'	0	900	-1701	
3	ρ2	0	900	-1700	
	ρ2'	0	900	-1701	
	ρ3'	800	900	-1701	
	ρ3	800	900	-1700	
4	ρ1	0	0	-500	
	ρ3	800	900	-1700	
	ρ3'	800	900	-1701	
	ρ1'	0	0	-501	
5	ρ2	0	900	-1700	
	ρ1	0	0	-500	
	ρ1'	0	0	-1401	
	ρ2'	0	900	-1701	

Figure 10.3: Thick sheet target data: Assuming figure 2,ρ_1, ρ_2, ρ_3 are the local position vectors of the top facet. Bottom facet is the reverse of the top, i.e has a negative y,z normal.

Geomodeller geophysics computation engine. The anticipated reduction in workload by a factor of between 3 and 6 in a section of the code more than doubled the speed over the full polyhedral case in the Matlab version, with even higher efficiencies found in the C++ version. The issue of validating the Full Tensor Magnetic Gradient code when remanence is involved has not yet been tackled, and remains a topic for further investigation

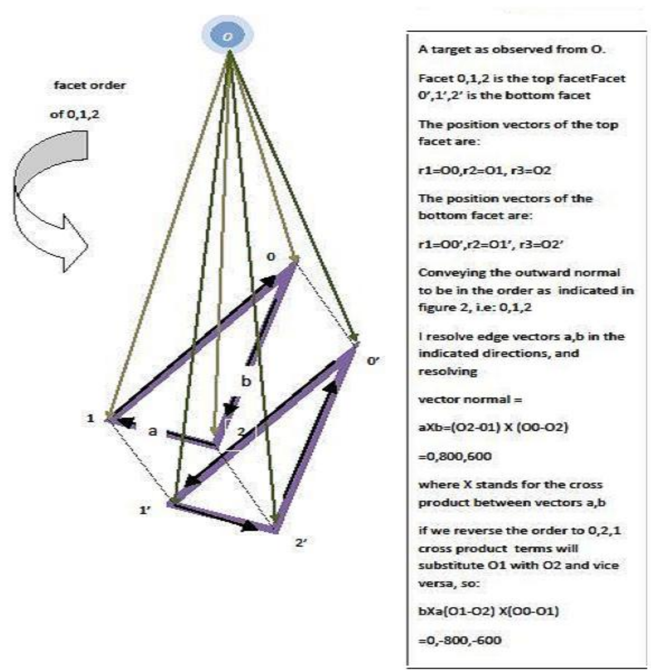

Figure 10.4: Visualization of a thin sheet in the anticlockwise order 0,1,2 with the observation point located at 0,0,0

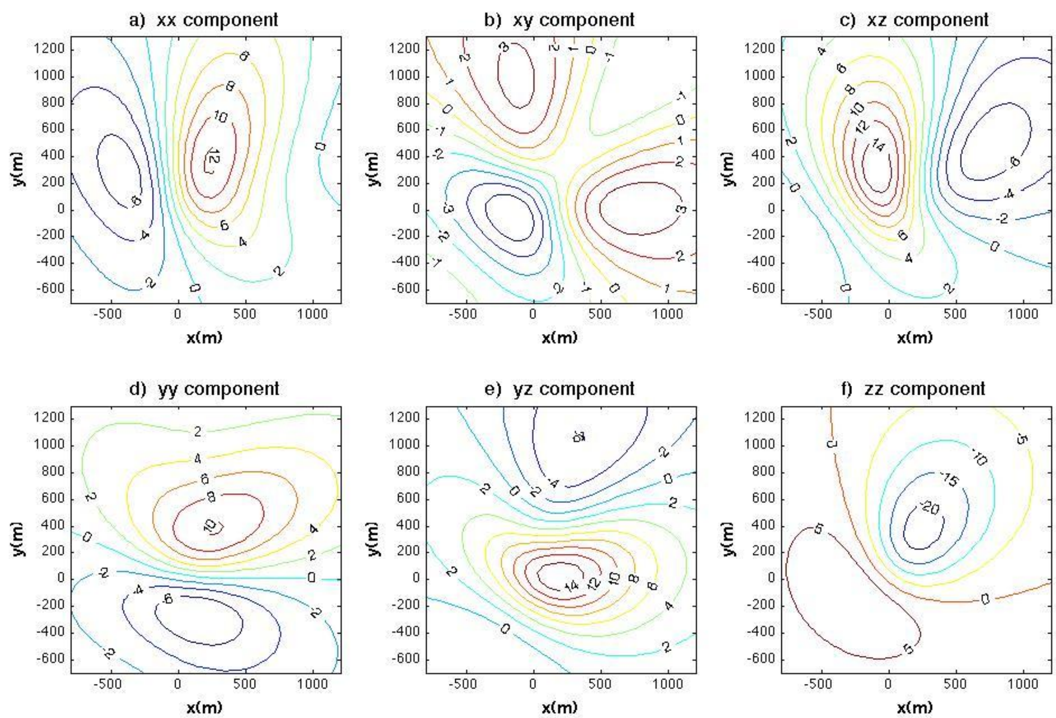

Figure 10.5: Limiting thin-sheet magnetic field gradient calculations, for the target shown in Figure 2, over the square survey area (-800m, -700m) to (1200m, 1300m). Contour values are in multiples of 0.01nT/m. The strength of the target magnetization vector was set to (1, 1, 1)1.0e05 nT/m and the target thickness parameter was set to T = 100m, giving a total magnetic anomaly of 61.028nT at the observation point (0,0,0)

Chapter 11

Asymptotic anomalies of Thin Polygonal Sheets

Publication:*Asymptotic anomalies of thin polygonal sheets*

Horst Holstein[1],Costas Anastasiades[2] (1)Aberystwyth University, UK, hoh@aber.ac.uk and Intrepid-Geophysics, Australia (2)Aberystwyth University, UK, anastasiadescostas@yahoo.gr

EAGE conference,Saint Petersburg, Russia,April 2010
(bibliography ref:[17])

11.1 Introduction

Regarding the stability of the polyhedral targets(Holstein and Ketteridge 1996 [16]), here we adapt the analysis of previous workers (Holstein et al.,Strakhov et al.)to the thin sheet case. We find that the new formulae suffer a lower degree of instability than those in the polyhedral case. In particular we demonstrate a stable version of the thin sheet formulae that suffers no error growth with increasing target distance.

11.1.1 Why we reside from the target

Airborne gravimetry is a tool for mapping the geophysical infrastructure. To improve speed and accuracy of airborne gravimetric surveys measuring equipment need to be elevated to high altitudes, in order to capture a wider range of the earth's gravity field. These surveys can be done by airplanes with special onboard equipment for geophysical exploration, or even satelites orbiting earth in a continuous basis, so that collected data are updated at every orbit.

11.1.2 Instruments measuring gravity

Measuring instruments are basically 2 types: Gravimeters and Gradiometers. Gravimeters measure gravity in terms of scalars and need corrections not only for shape and topography of earth but also for altitudal linear or angular accelerations. In contrast gradiometers measure gravity gradients in terms of tensor quantities which is a more sophisticated approach as more information is included in the gravity gradients. Corrections for altitudal linear and angular velocities are anticipated by smoothing.

Figure 11.1: Free fall gravimeter

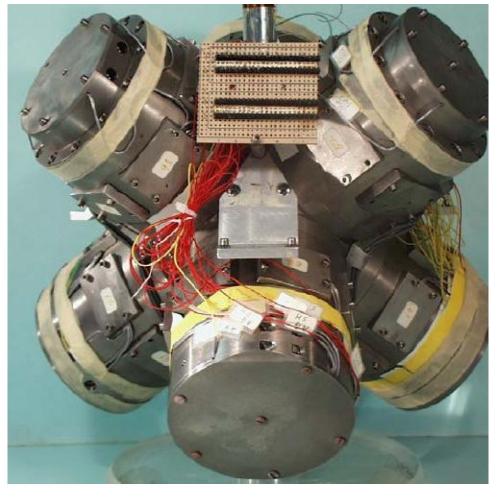

Figure 11.2: A 3 axis gradiometer (conducted by NASA)

11.2 Source of instability of anomaly algorithms

Anomaly formula suffer from numerical instability as the observation point resides from target. Closed formulae for the polyhedral target anomaly are obtainable from the volume integral of the known point source anomaly. For example, the gravity field anomaly $\mathbf{f}_g$ from a polyhedral target with outward facet normals $\mathbf{n}_i$ and gravitational density factor $G\rho$ is given by

$$\mathbf{f}_g = G\rho \int\limits_V \nabla(1/r)dV = G\rho \sum_i \mathbf{n}_i \int\limits_{S_i} dS/r \qquad (11.1)$$

Given a target of linear dimension α and distance δ from the observation point, the left integral is seen to be $O(\alpha^3/\delta^2)$, whereas the right hand expression has sums of $O(\alpha^2/\delta)$ integrals. It is amplified by $\gamma^{-1} = \delta/\alpha$, where γ is the reciprocal dimensionless target distance. Two further integrations, converting each surface integral into a sum of line integrals over the edges of the polygonal facets, and each line integral into expression differences evaluated at the edge vertex end-points, account for a combined amplification factor of γ^{-3} in the summed closed form terms. Sufficiently far from the target as $\gamma \to 0$, the target anomaly $O(\alpha\gamma^2)$ will be overtaken by the rounding error$O(\alpha\gamma^2\gamma^{-3})$ committed in floating point evaluation under a precision precision ϵ. Cancellation causes the closed formula to suffer progressive error to the point of destruction. Retention of significance requires $\gamma^{-3}\epsilon \ll 1$, that is, $\gamma \gg \epsilon^{1/3}$ We note that the gravitational potential per unit sheet thickness is given by a single surface integral of the type found on the right of equation (11.1). Two integration stages only are needed for a closed solution, with amplification γ^{-2}. Thus thin sheet formulae are inherently more stable than their polyhedral counterparts, with superior stability horizon of $\gamma \gg \epsilon^{1/2}$. The commonality of integrals to both polyhedral and thin sheet targets will be exploited to advantage in the thin-sheet analysis below.

$$
\begin{aligned}
\phi g &= G\rho T \sum_j \mathbf{b}_j \cdot \mathbf{r}_j \\
\mathbf{f}_g &= -G\rho T \sum_j \mathbf{b}_j, \\
\mathbf{G}_g &= G\rho T \sum_j \mathbf{b'}_j, \\
\phi_m &= -\mathbf{m} \cdot T \sum_j \mathbf{b}_j, \\
\mathbf{f}_g &= \mathbf{m} \cdot T \sum_j \mathbf{b'}_j, \\
\mathbf{G}_m &= -\mathbf{m} \cdot T \sum_j \mathbf{b''}_j
\end{aligned}
\tag{11.2}
$$

Vector m parameterises the magnetic dipole moment per unit volume, including the factor $\mu_0/4\pi$. The sign convention follows relationships $\triangledown\phi = \mathbf{f}, \triangledown\mathbf{f} = \mathbf{G}$ both for gravity and magnetics, and Poisson's relation $\mathbf{m} \cdot \mathbf{f}_g = G\rho\phi_m$. Summation is carried out over the j-enumerated edges of the polygonal sheet, $\mathbf{r}j$ being a position vector to edge j. Formulae for the vector $\mathbf{b}_j$ and its rank-2 tensor gradient $\mathbf{b'}_j$ are available from the literature on polyhedral targets (Holstein (2002)[15]; Holstein et al. (2007)[22]), while the double gradient rank-3 tensor $\mathbf{b''}_j$ appears in Holstein et al (2009)[2] in the thin-sheet context.

11.3 Stability variants of the vectors b_j

Walking through unstable : $O(\alpha\gamma^2/\gamma^{-3})$ to stable form:$O(\alpha\gamma^2)$

11.3.1 The Strakhov variant of vectors b_j

Contribution:simplification of anomaly algorithms by 1 order of magnitude

$$
\begin{aligned}
&O(\delta) \rightarrow O(\alpha) \\
&\gamma^{-3} \rightarrow \gamma^{-2}
\end{aligned}
\tag{11.3}
$$

Strakhov et al. (1986)[27] recognised the non-uniqueness of vectors $\mathbf{b}_j$, as only their sums matter. He devised a variant in which differenced edge vertex expressions, from the third integration step above, replaced $O(\delta)$ vertex distances by $O(\alpha)$ inter vertex separations, thereby eliminating one order γ^{-1}growth error. This transforms a polyhedral vertex algorithm with γ^{-3} growth terms, to a stabilised line variant with $O(\gamma^{-2})$ growth terms.

11.3.2 The Holstein variant of vectors b_j

Contribution:simplification of anomaly algorithms by 2 orders of magnitude, in 2 steps

- Polyhedral case:

$$\begin{aligned}&O(\alpha) \to O(\alpha\gamma)\\&\gamma^{-2} \to \gamma{-1}\end{aligned} \tag{11.4}$$

- Thin sheet case

$$\begin{aligned}&O(\alpha\gamma) \to O\left(\alpha\gamma^2\right)\\&\gamma{-1} \to \gamma^0\text{(totally stable)}\end{aligned} \tag{11.5}$$

Holstein (2002)[15] expressed this conversion in terms of analytical cancellation of dominant terms before computation. He achieved further cancellation of the next dominant terms, to recover a polyhedral surface variant, with growth factor of only γ^{-1}. Since thin-sheet anomaly formulae are derived with one fewer integration step than the polyhedral formulae, they will exhibit one order lower error growth than their polyhedral counter parts. Thus, thinsheet line and surface variants have error growths of γ^{-1} and γ^0 (totally stable) respectively. These claims are verified below. We omit discussion of the least stable variant, the γ^{-2} vertex algorithm.

11.4 Thin-sheet line variant

Consider a thin-sheet target with unit surface normal $\mathbf{n}$, whose j^{th} edge has a counter clockwise unit tangent vector $\mathbf{t}_j$, and an in-plane horizontally outward unit vector $\mathbf{h}_j$ perpendicular to edge and normal, as shown in Figure 1. Relative to a target origin, the position vectors of edge j vertices are $\mathbf{R}_{j1}$, $\mathbf{R}_{j2}$, ordered anticlockwise around facet normal $\mathbf{n}$. The position vector of the observation point is $\mathbf{R}_*$. Relative to the observation point, position vectors to the target vertices are

$$\mathbf{r}_{j1} = \mathbf{R}_{ij} - \mathbf{R}_*, \mathbf{r}_{j2} = \mathbf{R}_{j2} - \mathbf{R}_* \tag{11.6}$$

In equation 11.6 we must clarify that accroding to geometry, the direction of vector R_* is according to the context pointing from the local origin to the observation point, while in contrast, we my have an opposite case with vector R_* pointing the other way round, i.e from the observation point to the local origin if that is stated in the context and forms an apriori assumption.

11.4.1 Mid-points

A mid point of 2 quantities, is defined to be half way the sum of the 2 quantities. The quantities could be either vectors or magnitudes of vectors. We use the overline bar. Observation point related position vectors mid-points are defined by:

$$\overline{\mathbf{r}}_j = \frac{\mathbf{r}_{j1} + \mathbf{r}_{j2}}{2} \tag{11.7}$$

Local position vectors mid-points are defined by:

$$\overline{\mathbf{R}}_j = \frac{\mathbf{R}_{j1} + \mathbf{R}_{j2}}{2} \tag{11.8}$$

$$\overline{r}_j = \frac{r_{j1} + r_{j2}}{2} \tag{11.9}$$

11.4.2 Vector projections and magnitudes

Vertex vector projections and magnitudes are defined by

$$\begin{aligned} h_j &= \mathbf{h}_j \cdot \mathbf{r}_{ij} = \mathbf{h}_j \cdot \mathbf{r}_{j2}, \\ \bar{l}_j &= \overline{\mathbf{r}}_j \cdot \mathbf{t}_j, \forall j : \upsilon = \overline{\mathbf{r}}_j \cdot \mathbf{n} \end{aligned} \tag{11.10}$$

$$\begin{aligned} \overline{\mathbf{R}}_j &= \frac{1}{2}\left(\mathbf{R}_{j1} + \mathbf{R}_{j2}\right), \\ L_i &= |\mathbf{R}_{j2} - \mathbf{R}_{j1}|, r_{j1} = |\mathbf{r}_{j1}|, \\ r_{j2} &= |\mathbf{r}_{j2}|, \overline{r}_j = \frac{1}{2}(r_{j1} + r_{j2}) \end{aligned} \tag{11.11}$$

11.4.3 Tensors b'_j and b''_j

We assume that the local target origin is $O(\alpha)$ from any vertex. Crucially, the difference of $O()\delta$ terms $\mathbf{r}_{j2} - \mathbf{r}_{j1}$ can now be computed as the $O(\alpha)$ edge length L_j , as above. Line method variants of vector $\mathbf{b}_j$ and its gradient $\mathbf{b'}_j = -\nabla \mathbf{b}_j$ can then be stated as

$$\mathbf{b}_j = 2\mathbf{h}_j arctanh \Lambda_i - 2\mathbf{n}\mathbf{sign}(\upsilon) \arctan \lambda_j \tag{11.12}$$

$$\mathbf{b'}_j = \left(\mathbf{h}_j\mathbf{h}_j - \mathbf{n}\mathbf{n}\right) d_j + \left(\mathbf{h}_j\mathbf{t}_j + \mathbf{t}_j\mathbf{h}_j\right) e_j/2 + \left(\mathbf{h}_j\mathbf{n} + \mathbf{n}\mathbf{h}_j\right) f_j \tag{11.13}$$

where

$$\begin{aligned} \Lambda_j &= \frac{2L_j}{\overline{r}}, \\ \lambda_j &= \frac{h_j \Lambda_j}{\overline{r}(1 - L_j^2) + |\upsilon|}, \\ d_j &= \frac{-2\Lambda_j}{(1 - \Lambda_j^2)} \frac{h_j}{r_{j1} r_{j2}} \\ e_j &= \frac{-2\Lambda_j \bar{l}_j}{r_{j1} r_{j2}} \\ f_g &= \frac{-2\Lambda_j}{(1 - \Lambda_j^2)} \frac{\upsilon}{r_{j1} r_{j2}} \end{aligned} \tag{11.14}$$

Equations 11.12 and 11.13, together with a formula for b''_j from Holstein et al. (2009)[2], allow the thin-sheet anomaly equations 11.2 to be computed by the line variant. The results section shows the computational error growth for this method. Next, we discuss the surface variant for improved numerical stability.

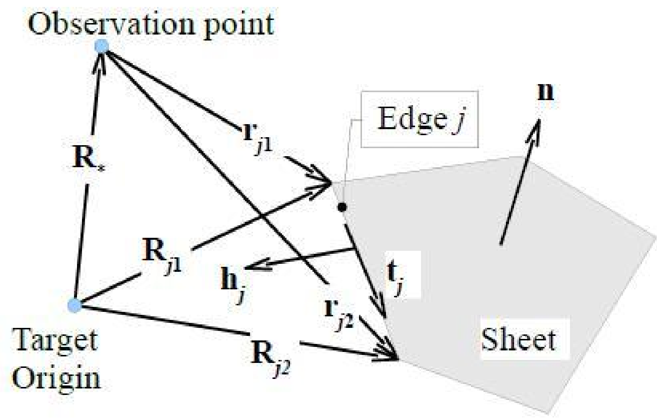

Figure 11.3: Reference systems for a thin-sheet target.

11.5 Thin-sheet surface variant

11.5.1 Tensors b'_j, b''_j

The thin-sheet surface variant of vectors $\mathbf{b}_j$ may be taken unchanged from the polyhedral literature(Holstein (2002)[**?**]). Surface variants for tensors $\mathbf{b}'_j$and$\mathbf{b}''_j$ are not available in the literature. An outline derivation for the first is now given, while the second is not considered here.

11.5.2 The centroid concept

The centroid of a body is the center of gravity, the point where the gravity is acting. Gravity forces acting on the centroid, completely cancel each other. That is why a body can balance horizontally lying on its vertical axis of symmetry.
(http://en.wikipedia.org/wiki/Centroid,
http://pages.uoregon.edu/struct/courseware/461/461_lectures/461_lecture28/461_lecture28.html)
Symmetry can help us to find the center of gravity. In a very thin slice, such as a cross-section, or a floor, using symmetry we can draw lines of symmetry. As an example in the figure 11.5.2the centroid of a triangle ABC is illustrated. Lines of symmetry could be one or many. These lines meet at the center of gravity. The same method can be performed to a 3D body. The point of gravity can be computed for every 3D or 2D exactly.
For our purposes assuming that our vertex position vectors meet at an observation point considering our vertices to be a set of n points for a n-vertex shape, we define our centroid c to be:

$$c = \frac{r_1 + r_2 + r_3 + ...r_n}{n} \tag{11.15}$$

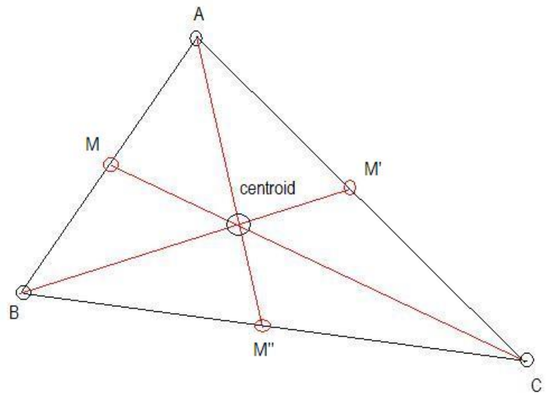

Figure 11.4: The centroid of a triangle.Points M,M',M" are the mid points of the sides AB,AC,BC

11.5.3 Linear superposition

In physics and systems theory, the superposition principle, also known as superposition property, states that, for all linear systems, the net response at a given place and time caused by two or more stimuli is the sum of the responses which would have been caused by each stimulus individually. Mathematically, for a linear system, F, defined by F(x) = y, where x is some sort of stimulus (input) and y is some sort of response (output), the superposition (i.e., sum) of stimuli yields a superposition of the respective responses: $F(x_1 + x_2) = F(x_1) + F(x_2)$
(Reference:http://en.wikipedia.org/wiki/Superposition_principle)
As an analogy in a geometrical illustration , as in figure 11.5.3 we can substitute a vector quantity by its components. If V_c is pointing at the center of gravity where all gravities add to zero,then vector V_j can be superimposed by its component vectors δ, V_c without any change in the gravitational effect of our system.

11.5.4 Reformulation using the centroid concept and linear superposition

Analytical pre-cancellation of dominant terms forms the basis of the surface method. To this end, define a point in or near the sheet, which we take as the centroid of its N vertices. Position vectors $\mathbf{R}_c, \mathbf{r}_c$ of the centroid, relative to the local target origin and to the observation point, and their magnitudes R_c, r_c, are

$$\begin{aligned} \mathbf{R}_c &= \frac{1}{N}\sum_j \mathbf{R}, \\ \mathbf{r}_c &= \frac{1}{N}\sum_j \mathbf{r}_j, \\ R_c &= |\mathbf{R}_c|, r_c = |\mathbf{r}_c| \end{aligned} \tag{11.16}$$

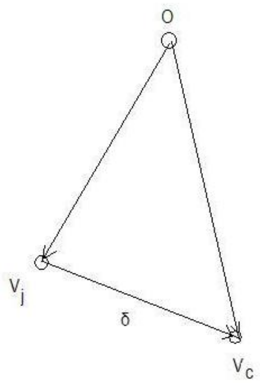

Figure 11.5: Superposition allows substituting OV_j by $\delta - OV_c$

For a distant target, we identify dominant $O(\alpha/\delta^2) = O(\gamma^2/\alpha)$ terms in relations (11.14) as

$$\begin{aligned} \Lambda_j^* &= \frac{2L_j}{r_c}, \\ d_j^* &= -h_{cj}\frac{2\Lambda_j^*}{r_c^2}, \\ e_j^* &= -l_{cj}\frac{2\Lambda_j^*}{r_c^2}, \\ f_j^* &= -\upsilon\frac{2\Lambda_j^*}{r_c^2} \end{aligned} \tag{11.17}$$

where $h_{cj} = \mathbf{h}_j \cdot \mathbf{r}_c, l_{cj} = \mathbf{t}_j \cdot \mathbf{r}_c$ for edge j. When terms d_j^*, e_j^*, f_j^* substitute their unstarred counterparts in equation (11.14),summation over the sheet edges in the formulae (11.14) involving $\mathbf{b}'_j$ results in cancellation to zero. Linear superposition then allows use of the $O(\gamma)$ reduced differences

$$\begin{aligned} &\delta d_j = d_j - d_j^*, \\ &\delta e_j = e_j - e_j^*, \delta f_j = f_j - f_j^* \end{aligned} \tag{11.18}$$

11.5.5 Analytical cancellation of dominant terms-stabilization

11.5.5.1 Quantities $\delta\mathbf{r}_{jc}, \delta r_{jc}, \Delta_{jc}$

Numerical stabilisation, requires prior analytical cancellation of dominant terms. Thus, $\delta\mathbf{r}_{jc} = \overline{\mathbf{r}}_j - \mathbf{r}_c, \delta r_{jc} = \overline{r}_j - r_c$ and $\Delta_{jc} = \overline{\mathbf{r}}_j/\overline{r}^2 - \mathbf{r}_c(\overline{r}_j/r_c^3)$ are stabilised as

$$\begin{aligned} \delta\mathbf{r}_{jc} &= \overline{\mathbf{R}}_j - \mathbf{R}_c, \\ \delta r_{jc} &= \frac{1}{2}\sum_{k=1,2}\left(\mathbf{R}_{jk} - \mathbf{R}_c\right)\cdot\left(\left(\mathbf{r}_{jk} + \mathbf{r}_c\right)/\left(r_{jk} + r_c\right)\right) \end{aligned} \tag{11.19}$$

$$\mathbf{\Delta}_{jc} = \delta\mathbf{r}_{jc}/\overline{r}^2 - \delta\mathbf{r}_{jc}\left(\mathbf{r}_c/r_c\right)\left(1/\overline{r}^2 + 1/\left(\overline{r}_j r_c\right) + 1/r_c^2\right) \tag{11.20}$$

11.5.5.2 Quantities $\delta d_j, \delta e_j, \delta f_j$

The stabillised differences for $\delta d_j, \delta e_j, \delta f_j$ are then given by

$$\begin{aligned}&\delta d_j = -\mathbf{h}_j \cdot \mathbf{\Delta}_{jc} - h_j\xi_j, \delta e_j = -\mathbf{t}_j \cdot \mathbf{\Delta}_{jc} - \bar{l}_j\eta_j,\\&\delta f_j = -\mathbf{n} \cdot \mathbf{\Delta}_{jc} - \upsilon\xi_j\end{aligned} \tag{11.21}$$

where

$$\begin{aligned}\xi_j &= \left(1/\left(1-\Lambda^2\right) + \bar{l}_j^2/\overline{r}_j^2\right) 2\Lambda_j/\left(r_{j1}r_{j2}\right),\\ \eta_j &= \left(\bar{l}_j^2/\overline{r}_j^2\right) 2\Lambda_j/\left(r_{j1}r_{j2}\right)\end{aligned} \tag{11.22}$$

11.5.6 Stabilized b'_j term

Equations 11.21,11.22 together with equation 11.13 give the stabilized version of $\mathbf{b}'_j$

11.6 Results

Using a point source (Pedersen and Rasmussen (1990)[24]) located at the sheet centroid, relative differences in an anomaly a between the thin-sheet target and the equivalent point source were computed from

$$\text{relative difference} = \max\left(|\alpha_{sheet} - \alpha_{point}|/|\alpha_{point}|, \epsilon\right) \tag{11.23}$$

The max function avoids fortuitous zero relative differences, and reflects the reality of a lower bound on the floating point precision. When the anomaly is a vector or tensor, the maximum norm was used. The geometry of the sheet target used is described in Holstein et al. (2009)[2], but the log-log scatter plots in Figure 11.6 are generic and indicate trends common to all target models, provided the target can be reasonably ascribed some characteristic length α. The point source anomaly formula does not suffer from rounding error instability, and so is a reliable reference, particularly at large target distances. Both line (Figure 11.6(a)) and surface (Figure 11.6(b)) variants show scatter plots with initial quadratic approach between sheet model and point source for increasing target distance. However, the slope 1 trend-line representing error growth in the line variant overtakes the downward trend at $1/\gamma = \epsilon^{-1/3} \approx 10^{5.2}$, and prevents further approach to the point source. The trend slope of 1 corresponds to the predicted error growth of γ^{-1} for the line variant. The relative error becomes 1 when $\gamma^{-1} = \epsilon^{-1}$, again as predicted. By contrast, the surface variant Figure 11.6(b) does not show the progressive error growth. It continues its quadratic approach to the point source until $\gamma^{-1} = \epsilon^{-1}$, where relative difference is ϵ. This is the floating point limit, further approach being impossible in that precision. The error trend is then horizontal, corresponding to a constant relative error ϵ. The error growth that vanished was predicted for the surface variant. The case of the magnetic gradient anomaly is omitted from this plot, because the surface variant for the tensor $\mathbf{b}''_j$ has not yet been determined.

11.7 Conclusions

Our analysis for the thin-sheet anomaly error behaviour at large target distances has been confirmed by computational experiment for all the gravimagnetic anomalies, up to the magnetic field gradient. We successfully adapted the error theory for polyhedral anomalies to the thin-sheet case, and extended it to demonstrate stable zero error growth thin-sheet algorithms for all but the magnetic field gradient. The results are of interest to software designers, and give opportunities for the formulation of exact perturbations solutions.

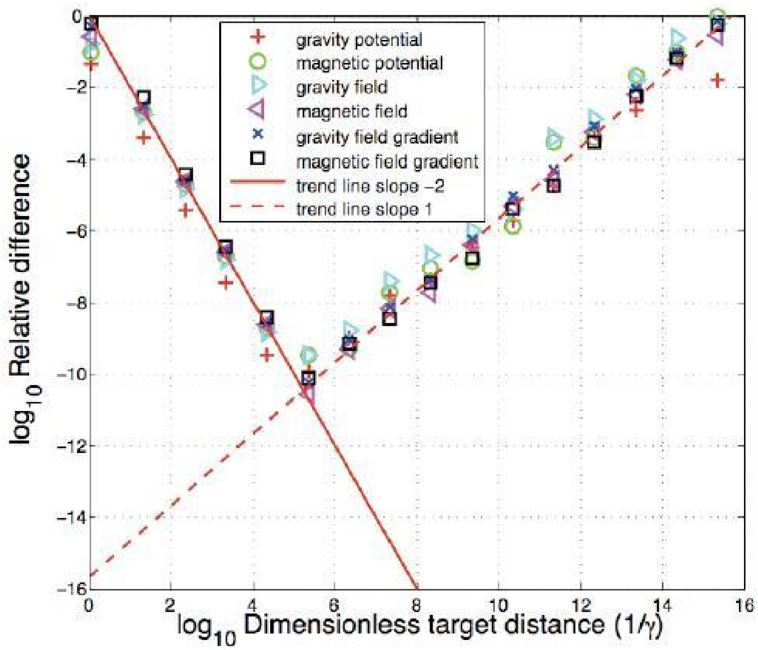

(a) Line variant

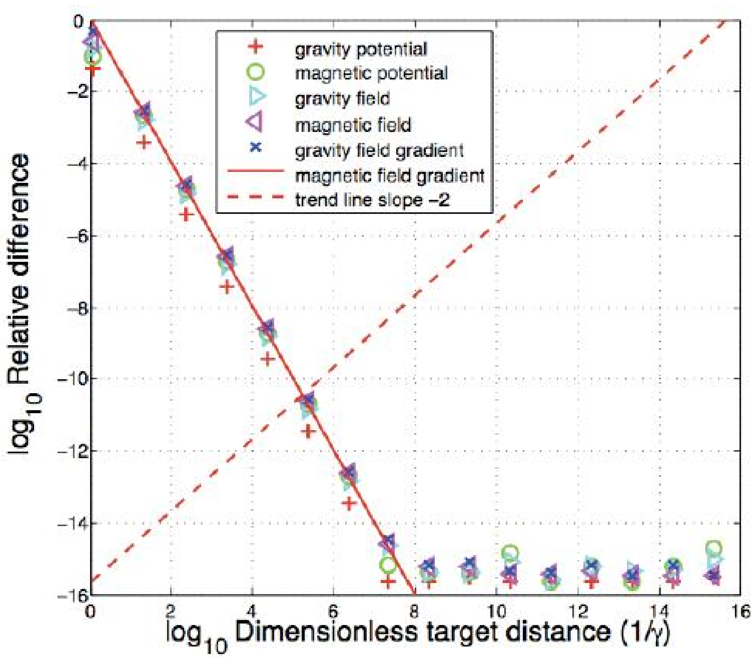

(b) Surface variant

Figure 11.6: Stability of thin-sheet anomaly algorithms, in precision $\epsilon (\log_{10} \epsilon \approx -15.7)$

Chapter 12

Exact Finite Expansion method for thin sheets

Publication:*Exact Finitely Expanded Gravity Anomaly of Uniform Thin Polygonal Sheets*
Horst Holstein[1],Des Fitzgerald[2],Costas Anastasiades[3] (1)Aberystwyth University, UK, hoh@aber.ac.uk and Intrepid-Geophysics, Australia (2)Director, Intrepid-Geophysics, Australia, des@intrepid-geophysics.com (3)Aberystwyth University, UK, anastasiadescostas@yahoo.gr
72TH EAGE Conference and Exhibition incorporating SPE EUROPEC 2010 Barcelona, Spain, 14 - 17 June 2010
(bibliography ref:[2])

12.1 Introduction

The instability of the relative error in gravi-magnetic anomaly formulae computed in given precision $epsilon$, arises from the analytical evaluation of the target source volume integral, which introduces a factor $1/\gamma$at each integration stage from volume to surface, surface to line (edge), and edge to vertex end-points, resulting in summands magnified by a factor $1/\gamma^3$over the anomaly size. An anomaly α therefore commits a truncation error of (α/γ^3), with a relative error ϵ/γ^3. This relative error becomes unbounded as $\gamma \to 0$.

12.2 Thin sheet geometry

A thin-sheet target has a unit surface normal $\mathbf{n}$, whose jth edge has a unit tangent vector $\mathbf{t}_j$oriented counter clockwise around $\mathbf{n}$, and an in-plane outward unit vector $\mathbf{h}_j$ perpendicular to edge and normal, as shown in figure 11.3. Relative to a local target origin, the position vectors of edge j vertices $\mathbf{R}_{j1}, \mathbf{R}_{j2}$ are ordered anticlockwise around facet normal $\mathbf{n}$. The position vector of the observation point is $\mathbf{R}_*$. Relative to the observation point, position vectors to the target vertices are

$$\mathbf{r}_{j1} = \mathbf{R}_{j1} - \mathbf{R}_*, \mathbf{r}_{j2} = \mathbf{R}_{j2} - \mathbf{R}_* \tag{12.1}$$

Vertex vector projections, edge lengths, mid-points and magnitudes are defined by

$$\begin{aligned} &h_j = \mathbf{h}_i \cdot \mathbf{r}_{jk}, l_{jk} = \mathbf{t} \cdot \mathbf{r}_{jk}, \\ &\forall j : \upsilon = \bar{\mathbf{r}}_j \cdot \mathbf{n}, r_{jk} = |\mathbf{r}_{jk}|, k = 1, 2, .. \end{aligned} \tag{12.2}$$

$$
\begin{aligned}
L_j &= |\mathbf{R}_{j2} - \mathbf{R}_{j1}|, \overline{\mathbf{R}}_j = \frac{1}{2}\left(\mathbf{R}_{j1} + \mathbf{R}_{j2}\right), \\
\overline{\mathbf{r}}_j &= \frac{1}{2}\left(\mathbf{r}_{j1} + \mathbf{r}_{j2}\right), \overline{r}_j = \frac{1}{2}\left(r_{j1} + r_{j2}\right)
\end{aligned}
\tag{12.3}
$$

The difference $\mathbf{r}_{j2} - \mathbf{r}_{j1}$ of $O(\delta)$ vectors can now be computed as the $O(\alpha)$ edge length L_j , as above.

12.3 Thin sheet gravity anomaly

Let $\mathbf{f}_g$ be the gravity field of the thin sheet of notional thickness T and density ρ. With G the constant of universal gravitation, the thin-sheet anomaly formula can then be written (Holstein et al. (2009)[2]) as

$$
\begin{aligned}
\mathbf{f}_g &= -G\rho T \sum_j \mathbf{b}_j, \\
\mathbf{b}_j &= 2\mathbf{h}_j arctanh \Lambda_j - 2\tilde{\mathbf{n}} \arctan \lambda_j
\end{aligned}
\tag{12.4}
$$

where

$$
\begin{aligned}
\Lambda_j &= \frac{L_j}{(2\overline{r}_j)} \\
\lambda_j &= \frac{h_j \Lambda_j}{\overline{r}_j} \\
\overline{r}_j &= \overline{r}_j \left(1 - \Lambda_j^2 + |v|\right) \\
\overline{\mathbf{n}} &= \mathbf{n}\text{sign}(v)
\end{aligned}
\tag{12.5}
$$

12.4 A review of error growth classes of the anomaly algorithms

12.4.1 Vertex type

By the taxonomy of Holstein and Ketteridge (1996)[16], an anomaly algorithm can be of Vertex, Line or Surface type (6.12.3.2), according to the floating point precision (single, double FP) the absolute error growth $\gamma^\kappa \epsilon$ of its summed over edges terms $\mathbf{b}_j$ with increasing the target distance $1/\gamma = \delta$. Pohanka's(1988)[39] vertex type with differences over vertices such as

$$
\frac{1}{2}\left[\ln\left(r_{jk} + l_{jk}\right)\right]_{\kappa=1}^{kappa=2}
\tag{12.6}
$$

has an error of O($\ln(1+\epsilon)/(1-\epsilon)$), giving $\kappa = 0$.

12.4.2 Line type

When the argument 12.6was substituted later by the mathematically equivalent expression arctan Λ_j in equation 12.4. Equations 12.4,12.5 (e.g Strakhov et al. 1986, [27]) representatives the Line type, evaluated O(γ) summands with κ=1.

12.4.3 Surface type

The Surface variant (Holstein et al. (1999)[26], Holstein (2002)[**?**]) achieves $O(\gamma^2)$ summands and κ = 2, by first expressing all $O(\delta)$ vertex position vectors as $O(\alpha)$ perturbations of some near-sheet vector $\mathbf{r}_c$ and then carrying out analytical cancellation of the dominant terms prior to numerical summation. Without loss of generality, we let $\mathbf{r}_c$($\mathbf{R}_c$ relative to the local target origin) coincide with the centroid. For A the area of the polygonal sheet, r_c the magnitude of vector $\mathbf{r}_c$ and $\tilde{r_c} = r_c|\upsilon|$, we obtain

$$\sum_j \mathbf{b}_j = -2\tilde{\mathbf{n}}A/(r_c\tilde{r}_c) + \sum_j \left(2\mathbf{h}_j(\Lambda_j^3\text{Athnh}\Lambda_j + \delta\Lambda_j) - 2\tilde{\mathbf{n}}(\lambda_j^3\text{Atn}\lambda_j + \delta\lambda_j)\right) \quad (12.7)$$

where quantities Atnh,Atn, $\delta\Lambda_j$,$\delta\lambda_j$,$\tilde{\lambda}$,Λ_j^*,λ_j^*,Δ_{jk}, $\overline{\Delta}_j = \frac{1}{2}(\Delta_{j1} + \Delta_{j2})\tilde{\lambda}_j = h_j\lambda_j^*/\tilde{r_c}\tilde{r_c} = r_c + |\upsilon|$

are computed stabilized into terms of O(γ^2) magnitude. The superscript $.^*$ star notation indicates that $O(\delta)$ j-subscripted quantities have been replaced by corresponding centroid-related quantities r_c or $\mathbf{r}_c$. Note that $|\upsilon| = \tilde{\mathbf{n}}\cdot\mathbf{r}_j = \tilde{\mathbf{n}}\cdot\mathbf{r}_c$ In favour of analytical manipulation we are going to split equation 12.7 into 'right' order terms RO($O(\gamma^2)$)and higher order terms HO. This yields:

$$\sum_j \mathbf{b}_j = \text{RO+HO} \quad (12.8)$$

12.4.4 Right order terms

$$\text{RO} = -2\tilde{\mathbf{n}}A/(r_c\tilde{r}_c) + 2\sum_j \left(\mathbf{h}_j\delta\Lambda_j^* - \tilde{n}\delta\lambda_j^*\right) \quad (12.9)$$

12.4.5 Higher order terms

$$\begin{aligned} \text{HO} = 2\sum_j \mathbf{h}_j \left(\Lambda_j^3\text{Atnh}\Lambda_j + \left[\delta\Lambda_j - \delta\Lambda_j^*\right]\right) \\ - \tilde{\mathbf{n}}\left(\lambda_j^3\text{Atn}\lambda_j + \left[\delta\lambda_j - \delta\lambda_j^*\right]\right) \end{aligned} \quad (12.10)$$

12.5 Exact finite expansion (EFE)

Differences in 12.10 are to be analytically manipulated to cancel second order terms in 12.9. We rename the resulting $O(\gamma^3)$differences as $\delta^2\Lambda_j$ and $\delta^2\lambda_j$ respectively. Recognizing the first as the $O(\gamma^2)$Newtonian equivalent point source term, we can express equation 12.8into the required EFE form:

$$\sum_j \mathbf{b}_j = -A\mathbf{r}_c/r_c^3 + 2\sum_j \mathbf{h}_j\left(\Lambda_j^3 \mathrm{Atnh}\Lambda_j + \delta^2\Lambda_j\right) - \tilde{\mathbf{n}}\left(\lambda_j^3 \mathrm{Atn}\lambda_j + \delta^2\lambda_j\right) \tag{12.11}$$

12.6 Results

In Figure 12.1.a the reference anomaly is the mass-equivalent point source placed at the target's centroid, whose formula is numerically stable at all target distances. Initially, the V,L,S,E algorithms all approach the point source anomaly in a manner proportional to γ^2, confirming they are correctly formulated. However, under the limited numerical precision characterized by the machine constant ϵ, the V and L algorithms beyond certain target distances diverge from the point source with unbounded numerical error growth $\gamma^{-\kappa}\epsilon$ for $\kappa = 2, 1$ respectively. The Surface algorithm remains stable with neutral error growth $\kappa = 0$. Only the new EFE algorithm continues to approach the point source. In Figure 12.1.b, the reference anomaly is the E algorithm. The plot shows that V and L algorithms have error growths of $\gamma^{-2}\epsilon$ and $\gamma^{-1}\epsilon$ respectively. When these exceed the departure from the point source, further approach to the point source is no longer possible, as shown in Figure 12.1.b. The neutral behaviour of the S algorithm compared to E is expected, since E and S both have $O(\gamma^2)$ dominant terms. Isolation and regrouping of second order terms into the Newtonian point source, achieved in the E algorithm, allowed analytical cancellation to be used in the difference $||\mathbf{a}_E - \mathbf{a}_r||_\infty$, to yield the purely third order $O(\gamma^3)$terms, used in Figure 12.1.a to produce the continuing downward deviation from the point source. The ratio of the deviation to the point source is then $O(\gamma^3/\gamma^2) = O(\gamma)$. An unanticipated feature in Figure 12.1.a is that this ratio is in fact $O(\gamma^2)$, as seen from the slope of -2. This indicates that third order terms in the E algorithm must also cancel, a step left for future verification.

12.7 Conclusions

We derived an exact finite expansion for the uniform thin polygonal sheet gravitational anomaly, by separating the dominant equivalent point source term and an exact higher order perturbation term expressing the finite target geometry. This formula is free from numerical instabilities seen in standard anomaly formulae. A theoretical analysis of numerical error growth is verified by actual computation, indicating correctness of the finite expansion. The results are of interest to software implementors, since a priori computational error estimates can be given. Gravimagnetic similarity suggests that the present methods may be extended to the magnetic case, and also to polyhedral targets. The methods developed

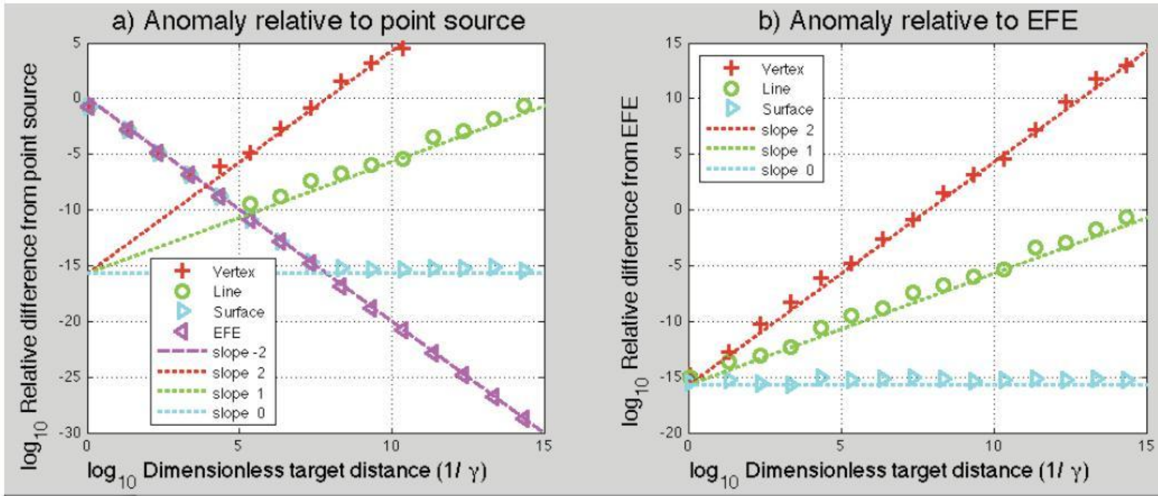

Figure 12.1: Numerical stability plots for gravity anomaly by Vertex, Line, Surface and EFE algorithms. Plot a) All four methods initially approach the point source with increasing target distance, followed by divergence of Vertex, Line and Surface algorithms. The new EFE algorithm remains stable. Plot b) Relative errors in the Vertex, Line and Surface algorithms compared to the EFE algorithm.

here show that the mild singularity inherent in the anomaly formulae cancels out in the low order terms, thereby permitting an order expansion. Since polyhedral anomaly formulae may be regarded as a weighted sum of sheet formulae, it is anticipated that the point source contributions from each facet will combine, allowing a stable separation into a volume point source and perturbations from the finite geometry. This is left for future research.

Chapter 13

A numerically stable magnetic anomaly formula for uniform polyhedra

Publication:*A numerically stable magnetic anomaly formula for uniform polyhedra*
Horst Holstein[1],Costas Anastasiades[2] (1)Aberystwyth University, UK, hoh@aber.ac.uk and Intrepid-Geophysics, Australia (2)Aberystwyth University, UK, anastasiadescostas@yahoo.gr (bibliography ref:[37])

13.1 Short review - anomaly algorithms on polyhedra

We have seing so far, that gravi-magnetic anomaly formulae for uniform polyhedral targets require summation of terms that can, with increasing target distance, far exceed their resultant sum. In the context of floating point arithmetic such formulae become numerically unstable on account of destructive cancellation during summation. This limits the usability of the formulae to a maximum target range. Recently we have shown how the instability may be overcome in the case of thin polygonal targets. The close formulation between polygonal sheet and polyhedral target anomaly formulae allows us to generalize stabilization to the polyhedral case. We derive a stabilized polyhedral magnetic anomaly formula, and demonstrate its zero error growth with increasing target distance. Stability is achieved at the cost of some extra numerical complexity. The approach can be extended to all the polyhedral gravi-magnetic anomaly formulae. Floating point arithmetic with finite precision e induces a well documented numerical instability in the standard anomaly formulae for uniform polyhedral targets (Strakhov et al. (1986)[27], Holstein et al. (1999)[26]). Beyond a certain target distance, numerical evaluation of the formulae fails to produce any correct significant digits, due to destructive cancellation in summing oppositely signed terms that are large compared to the final correct result. The large summands originate from the analytical point source integral over the target volume to obtain a closed form solution. The integration is performed in three stages: volume to surface, surface to line, and line to vertex (end-point). For example, with constant of universal gravitation G and density r, volume to surface integration leads to

$$G\rho \int_V \nabla \left(\frac{1}{r} \right) dV = G\rho \sum_i \mathbf{n}_i \int_{S_i} \frac{dS}{r} \tag{13.1}$$

where $\mathbf{n}_i$ is the unit outward normal to facet i of the polyhedron. Setting $\gamma = \alpha/\delta$, where α is a typical target dimension and δ is a typical distance of the target from the observation point, the left hand integral in equation (1) is seen to be of $O(\alpha^3/\delta^2) = O(\alpha\gamma^2)$, while the right hand side is a sum of terms of $O(\alpha^2/\delta) = O(\alpha\gamma)$. This represents a growth of γ^{-1}, becoming unbounded as the target distance increases. The remaining two integration stages each introduce a further factor γ, so that the final analytical anomaly expression is a sum of terms $O(\gamma^3)$ larger than the sum itself. This is the cause of the numerical instability during floating point evaluation.

13.2 Anomaly formulae for thin sheets

The right hand side of equation (13.1) may be interpreted as a vector sum of potentials from polygonal sheets represented by the polyhedral facets. This indicates that the anomaly formula for a thin polygonal sheet is related to the gradient of that anomaly for a polyhedral target. Significantly, the anomaly formula for a thin sheet requires only two integration stages (surface to line, line to vertex), and hence its summands suffer only two amplification steps, or γ^{-2}. Error growth is therefore less rapid in the sheet model. Stabilization will be achieved by cancellation of dominant terms prior to numerical evaluation. Successive reduction of two of the growth terms in polyhedral formulae was achieved by Holstein et al. (1999)[26]. Realization that this approach could eliminate the two growth factors in the sheet anomalies to achieve stabilized zero-error growth sheet formulae came in Holstein and Anastasiades (2010a,b)[17],[18]. It is the purpose of this article to extend the sheet results to also achieve stabilized polyhedral anomaly formulae. We demonstrate this for the magnetic field polyhedral anomaly formula.

13.3 Review: Thin sheet target geometry

Consider a polygonal sheet, or equivalently, a polygonal facet of a polyhedral target. Let its (outward) unit normal be $\mathbf{n}$, and its edges be enumerated by subscript j. Let edge j have a unit tangent vector $\mathbf{t}_j$ oriented counter clockwise around $\mathbf{n}$, and an in-plane outward unit vector $\mathbf{h}_j$ perpendicular to edge and normal, as shown in figure 11.3. Relative to a local target origin, the position vectors of edge j vertices $\mathbf{R}_{j1}$, $\mathbf{R}_{j2}$ are ordered anticlockwise around facet normal $\mathbf{n}$. The position vector of the observation point is $\mathbf{R}_*$. Relative to the observation point, position vectors to the target vertices are

$$\mathbf{r}_{j1} = \mathbf{R}_{j1} - \mathbf{R}_*, \mathbf{r}_{j2} = \mathbf{R}_{j2} - \mathbf{R}_* \qquad (13.2)$$

We assume that the local target origin is $O(\alpha)$ from any vertex. Crucially from 12.1,12.2, the difference of $|\mathbf{r}_{j2} - \mathbf{r}_{j1}|$of $O(\delta)$ vectors can now be computed as the $O\alpha$ edge length L_j, as in 12.3.

13.4 Achieved stability of anomaly algorithms for thin sheets and polyhedral targets

We noted above that sheet anomaly formulae suffer only two growth factors. Since the surface method removes two such factors, Holstein and Anastasiades (2010a)[17] argued that sheet surface method anomaly formulae should be stable with zero error growth, and verified this to be the case.
By contrast, polyhedral surface anomaly formulae retain one error growth factor, and so remain numerically moderately unstable.

13.5 A new stable polyhedral formula, the volume method of polyhedra

Holstein (2002)[15] induced a second $O(\gamma)$ reduction by constructing offsets $\mathbf{b}_j^*$ that allow dominant term removal in $\delta\mathbf{b}_j = (\mathbf{b}_j) - \mathbf{b}_j^*$, while accumulating offsets $\sum\limits_j \mathbf{b}_j^*$ as a pyramidal vector area, vertexed at the observation point, that collapses to the facet base area, smaller by a factor $O(\gamma)$, according to

$$\sum_j \mathbf{b}_j = \sum_j \delta\mathbf{b}_j + \sum_j \mathbf{b}_j^* \tag{13.3}$$

13.5.1 The facet centroid

The facet centroid located at position $\mathbf{R}_c$ relative to the local target origin, and position $\mathbf{r}_c$(magnitude r_c)relative to theovservation point (figure:11.3). Recasting equations 12.4,12.5 in terms of the centroid quantities,

$$\mathbf{b}_j^* = 2\mathbf{h}_j\Lambda_j^* - 2\tilde{\mathbf{n}}\lambda_j^* \tag{13.4}$$

$$\Lambda_j^* = \frac{L_j}{2r_c}, \lambda_j^* \frac{h_j\Lambda_j}{\tilde{r}_c}, \tilde{r}_c = r_c + |v| \tag{13.5}$$

As $\gamma \to 0$ with increasing target distance, the differences

$$\begin{aligned} \delta\Lambda_j &= \Lambda_j - \Lambda_j^* = O(\gamma^2) \\ \delta\lambda_j &= \lambda_j - \lambda_j^* = O(\gamma^2) \end{aligned} \tag{13.6}$$

$$\text{Atnh}(\Lambda_j) = (\text{arctanh}(\Lambda_j) - \Lambda_j)/\Lambda_j^3 = O(1), \text{Atn}(\lambda_j) = (\arctan(\lambda_j) - \lambda_j)/\lambda_j^3 = O(1) \tag{13.7}$$

must be computed from the formulae in Appendix A that have achieved dominant term removal, to avoid numerical destructive cancellation. The resulting surface method achieves a reduction of terms by a factor $O(\gamma^2)$ over the vertex method , and is summarized by equations (13.3) and

$$\delta\mathbf{b}_j = 2\mathbf{h}_j(\Lambda_j^3\text{Athnh}\Lambda_j + \delta\Lambda_j) - 2\tilde{\mathbf{n}}(\lambda_j^3\text{Atn}\lambda_j + \delta\lambda_j) \tag{13.8}$$

$$-2\tilde{\mathbf{n}}A/(r_c\tilde{r}_c) \tag{13.9}$$

where A is the facet area.

In this section we explore how insights from the sheet anomaly formulae can be used to remove the final growth factor in the polyhedra anomaly formula, to produce a stable zero error growth anomaly formula. We call such a formula a volume method, as cancellation of the last factor can only be brought about by considering all the polyhedral facets that enclose the target volume. The terms generated in the volume formula will be of the order of the integrand in the volume integral for the anomaly. Hence no destructive cancellation will take place on numerical evaluation. From equations (13.8) and (13.9), the dominant $O(\gamma^2)$ terms arising during of equation (13.3) are

$$\sum_j (2\mathbf{h}_j\delta\Lambda_j - 2\tilde{\mathbf{n}}A/(r_c\tilde{r}_c)) \tag{13.10}$$

Holstein and Anastasiades (2010b)[18] argued that this must contain the dominant equivalent point source term, namely $-A\mathbf{r}_c/r_c^3$. This fact is hidden, because $\delta\Lambda_j$ and $\delta\lambda_j$ still retain dependence on r_{j1} and r_{j2}. We therefore replace them by $\mathbf{r}_c$ in newly introduce terms $\delta\Lambda_j^*, \delta\lambda_j^*$, and define stabilized differences

$$\delta^2\Lambda_j = \delta\Lambda_j - \delta\Lambda_j^*, \delta^2\lambda_j = \delta\lambda_j - \delta\lambda_j^* \tag{13.11}$$

by cancelling the dominant $O(\gamma^2)$ terms to yield results of $O(\gamma^3)$, as in Appendix **??**. The second order terms in equation (13.10) now combine into the point source term

$$-A\mathbf{r}_c/r_c^3 = -2A\tilde{\mathbf{n}}/(r_c\tilde{r}_c) + \sum_j \left(2\mathbf{h}_j\delta\Lambda_j^* - 2\tilde{\mathbf{n}}\delta\lambda_j^*\right) \tag{13.12}$$

leading to a modified surface method 13.3

$$\sum_j \mathbf{b}_j = \sum_j \delta\mathbf{b}_j^* - A\mathbf{r}_c/r_c^3 \tag{13.13}$$

$$\delta\mathbf{b}_j^* = 2\mathbf{h}_j\left(\Lambda_j^3\mathrm{Atnh}\Lambda_j + \delta^2\Lambda_j\right) - 2\tilde{\mathbf{n}}\left(\lambda_j^3\mathrm{Atn}\lambda_j + \delta^2\lambda_j\right) \tag{13.14}$$

13.5.2 Target centroid - volume method

The significance of this form is that the dominant $O(\gamma^2)$ terms are captured entirely by the point source term, with higher terms of $O(\gamma^3)$ contained in the $\delta\mathbf{b}_j^*$ terms as a manifestation of the finite sheet geometry. Following (12.4), we now regard the polyhedral anomaly fm as a sum of sheet contributions. All terms in equations 13.13and 13.14 therefore bear an extra initial subscript i, enumerating the facets. The centroid of sheet i will now be at position vector $\mathbf{r}_{ic}$ relative to the observation point, with magnitude r_{ic}. Relative to the local target origin, the position vector is $\mathbf{R}_{ic}$. We take the centroid of the whole polyhedral target to be at $\mathbf{r}_p$ relative to the observation point, and $\mathbf{R}_p$ relative to the target origin. The displacement $(\mathbf{r}_{ic}-\mathbf{r}_{ip})$ from the target centroid to facet centroid is a difference of $O(\alpha)$ vectors, but equals the difference $(\mathbf{R}_{ic}-\mathbf{R}_{ip})$ of $O(\alpha)$ vectors, irrespective of the location of the observation point. This allows the Newtonian response $\mathbf{r}_{ic}/r_{ic}^3$ of facet i to be expressed as a response from the target centroid plus an $O(\gamma/\delta_2)$ offset $< \mathbf{r}_{ic}, \mathbf{r}_{ip} >$ that can be calculated (appendices:I.2.6) without destructive cancellation

$$\mathbf{r}_{ic}/r_{ic}^3 = \mathbf{r}_p/r_p^3 + < \mathbf{r}_{ic}, \mathbf{r}_{ip} > \tag{13.15}$$

Substitution of equation (13.12) into equation (12.4) to obtain $\mathbf{f}_m$ will require the summation

$$\sum_i \mathbf{n}_i \mathbf{A}_i \mathbf{r}_{ic}/r_{ic}^3 = \sum_i \mathbf{n}_i \mathbf{A}_i (\mathbf{r}_p/r_p^3 + < \mathbf{r}_{ic}, \mathbf{r}_{ip} >). \tag{13.16}$$

Closure of the polyhedral target ensures that the sum of its vector facet areas is zero, causing the remaining highest order $O(\gamma^2)$ terms to collapse to zero. This leads to the final result

$$\mathbf{f}_m = \mathbf{m} \cdot \sum_i \mathbf{n}_i \sum_j (\delta \mathbf{b}_{ij}^* + A_i < \mathbf{r}ic, \mathbf{r}_p >) \tag{13.17}$$

with $O(\gamma^3)$ summands. The three growth terms in the vertex method have been removed in the new volume method, and this will be reflected in the error plots.

13.6 Results

As reference anomaly solution, we used a point source of magnetization $\mathrm{V}\mathbf{m}$, where V is the volume of a polyhedral test target and $\mathbf{m}$ is its magnetization per unit volume. The point source formula has no destructive cancellation, and can be used at any target distance. With increasing target distance, we expect the polyhedral anomaly to approach that of the point source, until further closeness is prevented by the finite precision. As measure of the relative closeness of the polyhedral and points source magnetic anomalies $\mathbf{a}_{poly}$ and $\mathbf{a}_{point}$ respectively,we use a relative error measure Here $\epsilon \approx 10^{-15.7}$ is the machine floating point precision constant, and provides the correct lower bound for the relative difference of two nearly equal floating point numbers. The logarithm of the relative difference is then always defined. As test target, we took a triangular prismatic polyhedron shown in Figure 13.1. This test target was subjected to anomaly calculations for various target distances, for the vertex, line, surface methods and the new volume method. Figure 13.2 shows an initial downward trend, indicating the expected approach to the point source with increasing target distance. However, at about 10^3 target diameters, the vertex method errors have grown to equal the difference from the point source, and at greater target distances the effective deviation from the point source now increases. At about $10^{3.9}$ target diameters, a similar divergence from the point source anomaly occurs for the line method, and at about $10^{5.2}$, for the surface method. Finally, the new volume method approaches the point source until about 10^8 target diameters, after which the relative difference becomes the minimum possible, about ϵ, and remains so without growth throughout the remaining synthetic survey test to 10^16 target diameters. The observed integer error slopes from 3 down to 0 for the four methods is anticipated from the theory given above for the growth factors of γ^3 to γ^0

for the four methods. In particular, the aimed for stability of the new method has been demonstrated.

$$\text{relative difference} = \max\{\frac{||\mathbf{a}_{poly} - \mathbf{a}_{point}||}{||\mathbf{a}_{point}||}, \epsilon\} \tag{13.18}$$

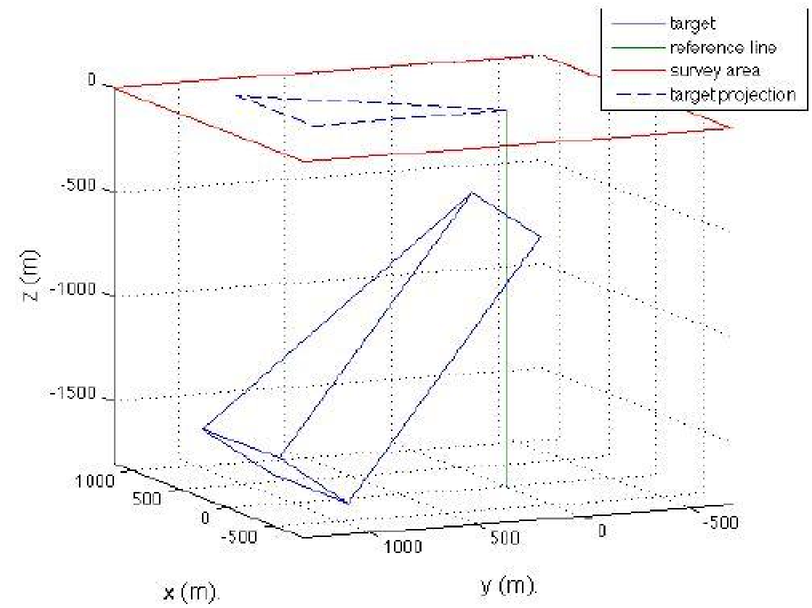

Figure 13.1: Triangular prismatic test target of thickness 400m.

13.7 Conclusions

Improved stability methods in the sequence of vertex, line and surface methods for polyhedral gravi-magnetic anomalies have been known for some years, but the formulation of a zero error growth method has not been achieved previously. A difficulty has been the appearance in the anomaly formulae of the absolute value of the normal projection jvij of the vertex position vectors on the i facets. Even though the target distance may be large, the value of vi may be small and of either sign, depending on whether the observation point is just above or below facet i. Differencing over terms jvij to devise offsets for cancelling dominant terms therefore could not be devised. The matter was resolved here by first constructing zero-growth anomaly formulae for the polygonal sheet anomaly. The dominant term there has to be the equivalent point source term, located at the sheet centroid. The centroid has the same vertical projection as any of the sheets vertex position vectors, and so the problem of differencing across near but unequal values of jvj does not arise. The key insight was to view the polyhedral anomaly as a sum of facet-sheet anomalies, and to exploit gravi-magnetic similarity for treating sheet and polyhedral anomalies in the same framework. The extra arithmetic complexity of the volume method means that it will not replace the simpler but less stable line method. However, the present work is likely to find application in the construction of reliable modelling software, forming a benchmark for testing algorithms that do not use the stabilized forms. This is particularly important when single precision has to be used, or where large target distance to target sizes occur, such as in whole earth modelling, or using models with very fine triangulations that have been generated by a visual renderer. The work presented here demonstrates the construction of a stable polyhedral magnetic anomaly formula. On account of gravi-magnetic similarity, stable algorithms can be found for all the standard gravi-magnetic anomalies of uniform polyhedral targets.

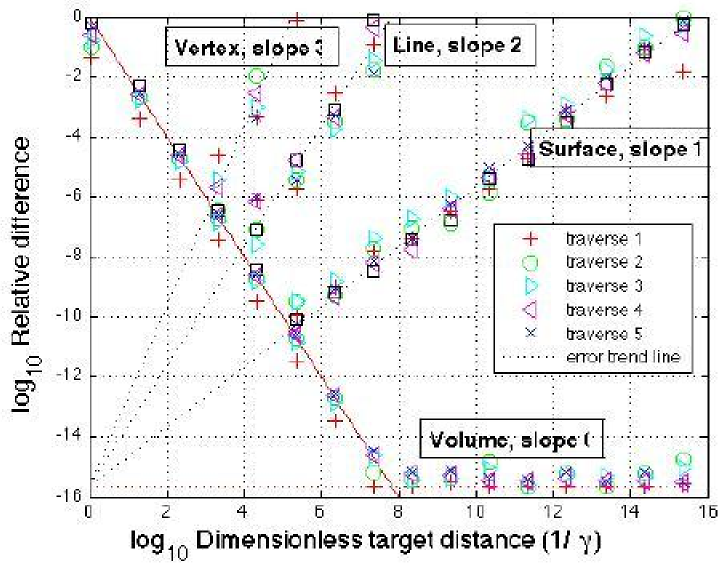

Figure 13.2: Error plots for Vertex, Line, Surface and Volume methods.

LIST OF FIGURES

Figure

Bibliography

[1] H.Holstein E.Sheratt (2000). The efficiency of algorithms for gravimagnetic anomalies of uniform polyhedra. Master's thesis, 2006.

[2] Horst Holstein Des Fitzgerald Konstantinos Anastasiades. Gravi-magnetic anomalies of uniform thin polygonal sheets. *11th SAGA Biennial Technical Meeting and Exhibition*, 2009.

[3] Konstantinos P. Anastasiades. Gravimagnetic modelling with polyhedra, 2006.

[4] Plouf D. Gravity and magnetic fields of polygonal prisms and applications to magnetic terrain corrections. *McGraw-Hill,New York.*, 41:727–741, 1976.

[5] E.W. (1976) Dijsktra. A discipline of programming. *Prentice-Hall Inc*, 1988.

[6] F.S Grant and G.F West. Interpretation theory in applied geophysics. *Geophysics*, 41:306–381, 1965.

[7] Gumerov and Duraiswami. 2005.

[8] D. Guptasarma and B. Singh. New scheme for computing the magnetic field resulting from a uniformly magnetized arbitrary polyhedron. *Geophysics*, 64:70–74, 1999.

[9] Haroon Al Rashid 2006 H. Error analysis of magnetic algorithms for uniformly magnetised polyhedra. Master's thesis, 2006.

[10] Gotze 1988 H.-J. and Lahmeyer B. Application of three-dimensional interactive modeling in gravity and magnetics. *Geophysics*, 53:1096–1108, 1988.

[11] Haaz. Relations between the potential of the attraction of the mass contained in a finite rectangular prism and its first and second derivatives. *Geofizikai Kozlemenek(In Hungarian)*, II(57-66), 1953.

[12] H.Holstein. Asymptotically improved gravimagnetic anomaly formulas for linear medium polyhedra. *SEG 2003 International Exposition and 73rd Annual Meeting Dallas Texas October 26-31*, 64, 2003.

[13] H Holstein. Gravimagnetic field tensor gradiometry formulas for uniform polyhedra, 2006.

[14] Horst Holstein. Gravimagnetic invariance for uniform polyhedra. *Geophysics*, 67:1126–1133, 2002.

[15] Horst Holstein. Gravimagnetic similarity for uniform polyhedra. *Geophysics*, 67:1134–1137, 2002.

[16] Horst Holstein and Ben Ketteridge. Gravimetry analysis of uniform polyhedra. 1996.

[17] Konstantinos Anastasiades Horst Holstein. Asymptotic anomalies of thin polygonal sheets. *EAGE conference,Saint Petersburg, Russia, 5 – 8 April 2010*, 2010.

[18] Konstantinos Anastasiades Horst Holstein, Des Fitzgerald. Exact finitely expanded gravity anomaly of uniform thin polygonal sheets. *72TH EAGE Conference & Exhibition incorporating SPE EUROPEC 2010 Barcelona, Spain, 14 – 17 June 2010*, 2010.

[19] M.K. Hubbert. A line-integral method of computing the gravimetric effects of twodimensional masses. *Geophysics*, 13:215–225, 1948.

[20] 1995 Blakely R. J. Potential theory in gravity and magnetic applications. *Cambridge Univ. Press*, 1995.

[21] Weiler K. Edge-based data structures for solid mdeling in curved-surface environments. *IEEE Computer Graphics and Aplications*, 5:21–40, 1985.

[22] H.Holstein E.Sherratt K.Anastasiades. Gravimagnetic anomaly formulae for triangulated homogeneous polyhedra. 2007.

[23] Guibas L. and Stolfi J. Primitives for the manipulation of genreal subdivisions and the computation of voronoi diagrams.a.c.m.trans. *Graphics*, 4:74–123, 2007.

[24] Pedersen L. and Rasmussen T. The gradient tensor of potential field anomalies: Some implications on data collection and data processing of maps. *Geophysics*, 55:1558–1566, 1990.

[25] Ocabe M. Analytical expressions for gravity anomalies due to homogeneous polyhedral bodies and translations into magnetic anomalies. *Geophysics*, 44:730–741, 1979.

[26] Horst Holstein H.Schurholz P.Starr A.J.and Chakraborty M.(1999). Comparison of gravimetric formulas for uniform polyhedra. *Geophysics*, 64:1438–1446, 1999.

[27] Strakhov V.N.Lapina M.I. and Yefimov A.B.(1986b). Solution of direct gravity and magnetic problems with new analytical expressions of the field of typical approximating bodies. 1986.

[28] Nagy. The gravitational attraction of a right rectangular prism. *Geophysics*, 31(362-371), 1966.

[29] X. Ni. *Free form solid modelling using hybrid CSG/BRep(constructive solid geometry/boundary representation) environment.* PhD thesis, University of Leeds, 1990.

[30] DHansen 1999 R. O. An analytical expression for the gravity field of a polyhedral body with linearly varying density. *Geophysics*, 64:75–77, 1999.

[31] H. Holstein* (Aberystwyth University) C. Willis (University of Bath) & K. Anastasiades (Aberystwyth University). Gravity potential series expansion for homogeneous polyhedra. *EAGE - exhibition and conference*, 2008.

[32] P.Ketteridge. *Gravimetric analysis for uniform polyhedra*. PhD thesis, University of Wales Aberystwyth, 1996.

[33] H.Holstein Edel Sheratt. Performance metrics for computing gravimagneto anaomalies of uniform polyhedra. 2000.

[34] Sorokin. Gravimetry and gravimetrical prospecting. *State Tech.Publ. Moscow*, 1951.

[35] Oosterom Strackee. Solid angle. *EAGE 69 Conference and exhibition*, E023, 1983.

[36] J.L. Worzel Talwani, M. and M. Landisman. Rapid gravity computations for twodimensional bodies with application to the mendocino submarine fracture zone. j. *Geophysical research*, 64:809–813, 1959.

[37] H. Holstein (Aberystwyth University) & K. Anastasiades (Aberystwyth University). A numerically stable magnetic anomaly formula for uniform polyhedra. *SEG - exhibition and conference-DENVER,COLORADO,October 2010*, 2010.

[38] USA University of Alberta, California. Lagrance identity proof via pythagorean identity, 2011.

[39] Pohanka V.(1988). Optimum expression for computation of the gravity field of a homogeneous polyhedral body. geophysical prospecting. 36:733–751, 1988.

[40] Strakhov V.N.(1982). The similarity of analytical expressions of gravitational and magnetic field elements of two and three-dimensional polygonal bodies and optimal computational processes of solution to forward problems for these bodies in teoriya i praktika intrpretatsii gravitatsionnykh anomaly. *Moscow IFZ AN SSSSR(in Russian)*, 1982.

[41] Raymond A. Wildman and George A. Gazonas. Gravitational and magnetic anomaly inversion using a tree-based geometry representation. *Geophysics*, 74(3):123–135, 2009.

APPENDICES

APPENDIX A

Lagrance proof

By Pythagoras we know that for a right angle triangle

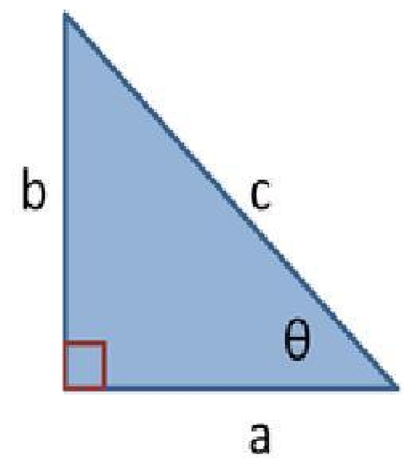

Figure A.1: a right angled triangle with sides a,b,c

with c=hypotenuse, a=adjacent to angle θ, b= opposite to angle θ:

$$\begin{gathered}\cos\theta = \frac{\text{a}}{\text{c}} \\ a = \cos\theta(c)\end{gathered} \tag{A.1}$$

and

$$\begin{gathered}\sin\theta = \frac{\text{b}}{\text{c}} \\ b = \sin\theta(c)\end{gathered} \tag{A.2}$$

and

$$\begin{gathered}c^2 = a^2 + b^2 + ab\cos\theta \\ \text{Law of cosines}\end{gathered} \tag{A.3}$$

Case $\angle\theta$ is a right angle$(\theta = 90^o), \cos\theta = 0$, the above formula A.3 reduces to the Pythagorian theorem

$$c^2 = a^2 + b^2 \tag{A.4}$$

Now since the dot-product of the vectors $\boldsymbol{\rho}, \hat{\mathbf{L}}$ is defined to be:

$$\boldsymbol{\rho} \cdot \hat{\mathbf{L}} = |\boldsymbol{\rho}||\hat{\mathbf{L}}| \cos\theta \tag{A.5}$$

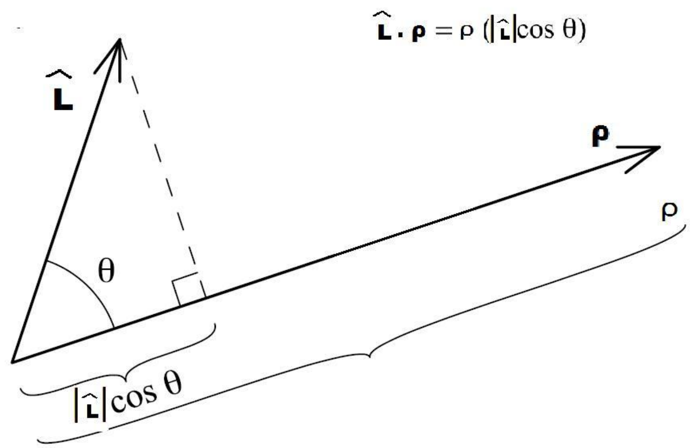

Figure A.2: Dot product geometrical definition, between vectors $\boldsymbol{\rho}$,$\hat{\mathbf{L}}$, where ρ= $|\boldsymbol{\rho}|$

and the cross-product of the vectors $\boldsymbol{\rho}, \hat{\mathbf{L}}$ is

$$\boldsymbol{\rho} \wedge \hat{\mathbf{L}} = |\boldsymbol{\rho}||\hat{\mathbf{L}}| \sin\theta \tag{A.6}$$

where θ= $\angle$ between vectors $\boldsymbol{\rho}$,$\hat{\mathbf{L}}$
By Lagrance identity, using the fundamental Pythagorean identity:

$$\sin^2\theta + \cos^2\theta = 1 \tag{A.7}$$

we get

$$\begin{aligned} |\boldsymbol{\rho} \wedge \hat{\mathbf{L}}|^2 &= |\boldsymbol{\rho}|^2|\hat{\mathbf{L}}|^2 - (\boldsymbol{\rho} \cdot \hat{\mathbf{L}})^2 \\ |\boldsymbol{\rho} \wedge \hat{\mathbf{L}}|^2 + (\boldsymbol{\rho} \cdot \hat{\mathbf{L}})^2 &= |\boldsymbol{\rho}|^2|\hat{\mathbf{L}}|^2 \end{aligned} \tag{A.8}$$

Because $\hat{\mathbf{L}}$ is normalized and it is a unit vector: $|\hat{\mathbf{L}}|^2 = 1$ equation A.8 becomes

$$|\boldsymbol{\rho} \wedge \hat{\mathbf{L}}|^2 + (\boldsymbol{\rho} \cdot \hat{\mathbf{L}})^2 = |\boldsymbol{\rho}|^2 \tag{A.9}$$

or

$$\begin{aligned} |\boldsymbol{\rho} \wedge \hat{\mathbf{L}}|^2 + (\boldsymbol{\rho} \cdot \hat{\mathbf{L}})^2 &= \boldsymbol{\rho} \cdot \boldsymbol{\rho} \\ |\boldsymbol{\rho} \wedge \hat{\mathbf{L}}|^2 &= \boldsymbol{\rho} \cdot \boldsymbol{\rho} - (\boldsymbol{\rho} \cdot \hat{\mathbf{L}})^2 \end{aligned} \tag{A.10}$$

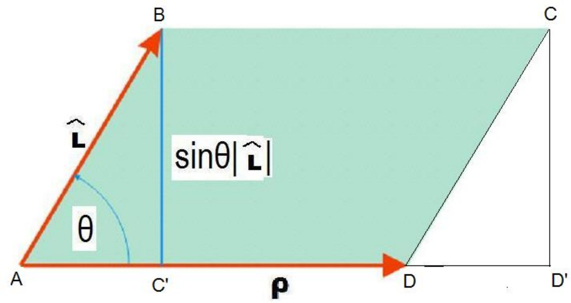

Figure A.3: Cross product geometrical justification,$\boldsymbol{\rho} \cdot \hat{\mathbf{L}} = |\boldsymbol{\rho}||\hat{\mathbf{L}}| \sin\theta$ between vectors $\boldsymbol{\rho}$,$\hat{\mathbf{L}}$. Parallelograms ABCD, BC'CD' are homeomorphic therefore they both have equal areas.

proof of equation A.8:

$$
\begin{aligned}
&|\boldsymbol{\rho} \wedge \hat{\mathbf{L}}|^2 = (|\boldsymbol{\rho}||\hat{\mathbf{L}}| \sin\theta)^2 \\
&= |\boldsymbol{\rho}|^2|\hat{\mathbf{L}}|^2(1 - \cos^2\theta) \\
&= |\boldsymbol{\rho}|^2|\hat{\mathbf{L}}|^2 - |\boldsymbol{\rho}|^2|\hat{\mathbf{L}}|^2(\cos^2\theta) \\
&= |\boldsymbol{\rho}|^2|\hat{\mathbf{L}}|^2 - (|\hat{\mathbf{L}}|(\cos\theta))^2 \\
&= |\boldsymbol{\rho}|^2|\hat{\mathbf{L}}|^2 - (\boldsymbol{\rho} \cdot \hat{\mathbf{L}})^2
\end{aligned}
\tag{A.11}
$$

(ref: [38])

Numerical test of the expression: $|\rho \wedge \hat{\mathrm{L}}|^2 + (\rho \cdot \hat{\mathrm{L}})^2 = \rho \cdot \rho$

We set			
vector ρ			
x	y	z	
5	3	2	
vector L_hat			
-1	-1	0	
norm(vector L_hat)			**vector L_hat . Vector L_hat**
-0,707106781	-0,7071	0	1,41421
Calculation of dot, cross products			
a=ρ.ρ			
38			
b=|ρ.L_hat|^2			
32			
c=||ρ X L_hat||^2			
x	**y**	**z**	**c**
1,414213562	-1,4142	-1,4142	6
Result			
c+b	**a**		
38	38		

APPENDIX B

The Gauss Divergence theorem

B.1 Abstract

The divergence theorem in vector calculus, also known variously as the theorem of Gauss, Ostrogradsky's or Gauss-Ostrogradsky, relates the effect of sources and sinks of a vector field inside a specified volume to the flux of the vector field across the boundary of the volume. The theorem expresses the balance between gains and losses of a vector field in and on the surface of a volume, and therefore finds frequent expression in the mathematical formulation of physical conservation laws. Formally, the theorem expresses equality between a volume integral of the divergence of the vector field (that is, the sum of sources and sinks throughout the volume), to a surface integral representing the net flux of the vector field out of the volume. Abstractly, the theorem indicates that if the volume integrand has a special form, namely the divergence of a vector field, then one level of integration can be performed to yield an integral of the flux of the vector field out of the the bounding surface of the volume.

It is instructive to devise an intuitive proof of the theorem by appealing to basic concepts of source, sink and flux, as typified by the motion of a fluid into and out of a region enclosed by a closed boundary.

B.2 Statement of the theorem

For illustrative purposes, we will identify the vector field **F** with a moving fluid, that is, at each point in space **F** has a magnitude (the fluid speed) and a direction (the direction of flow). Thus we identify**F** with the *velocity* of the fluid. The velocity may be changing in time, but our concern is with the velocity field at one instant of time, as in a snapshot. At that instant of time, the fluid flow will be (in general) different in different locations. In that sense, the vector field **F** is a function of position. We may express the position via a position vector **r** relative to some specified origin, in which case the functional form of the vector field is expressed by **F(r)**. Consider a region V in the fluid that has a closed surface S. The region occupies a three dimensional volume, and is conceptually placed there, without hindering the fluid flow. The region is regarded as fixed in space. In the absence of sources and sinks in the volume, and in the case of a constant density fluid, the amount of mass in the volume does not change over time, therefore the amount of fluid entering the volume is equal to the amount leaving at any instant. However, if there are sources and/or sinks, and/or if the density is variable, then there may be a net inflow or outflow of the volume at any instant. The balance between the net outflow over the boundary of the surface and the accumulation of fluid inside the volume is expressed by

$$\int_V (\mathrm{div}\boldsymbol{F})dV = \int_S \boldsymbol{F} \cdot \boldsymbol{dS}, \tag{B.1}$$

this being a statement of the theorem in mathematical notation. The terms in this equation will be explained below, and an outline proof will be given.

Introduction

The Gauss Divergence theorem is normally expressed by the equation:

$$\int_V (div\underline{\mathrm{F}})dV = \int_S \underline{\mathrm{F}} \cdot \mathrm{d}\underline{\mathrm{S}} \tag{B.2}$$

The right hand integral:

$$\int_S \underline{\mathrm{F}} \cdot \mathrm{d}\underline{\mathrm{S}} \tag{B.3}$$

represents the "flux" integral.
For a vector field $\underline{\mathrm{F}}$ integrated over the closed surface S of a volume,
an element $\underline{\mathrm{d}}$S represents the vector area element on the surface, directed
along the outward normal

If $\underline{\mathrm{n}}$ is the local unit outward normal, then $\mathrm{d}\underline{\mathrm{S}}=\underline{\mathrm{n}}\mathrm{dS}$, where dS is the scalar area of the element.

Illustration

Take $\underline{\mathrm{F}}$ to be the velocity vector field in a fluid.
Then $\underline{\mathrm{F}}$ (x,y,z) represents the vector velocity at the point (x,y,z).
The velocity can change at neighboring points.
So$\underline{\mathrm{F}}$ is a function of position at each point (x,y,z) in the moving fluid,
there is a velocity vector. The point (x,y,z) is fixed in space-does not move with the fluid.

Then consider a fixed volume immersed in the fluid - just a shape with no solid boundaries.

We can rise the question:
how much fluid is flowing into the volume? How much is flowing out?

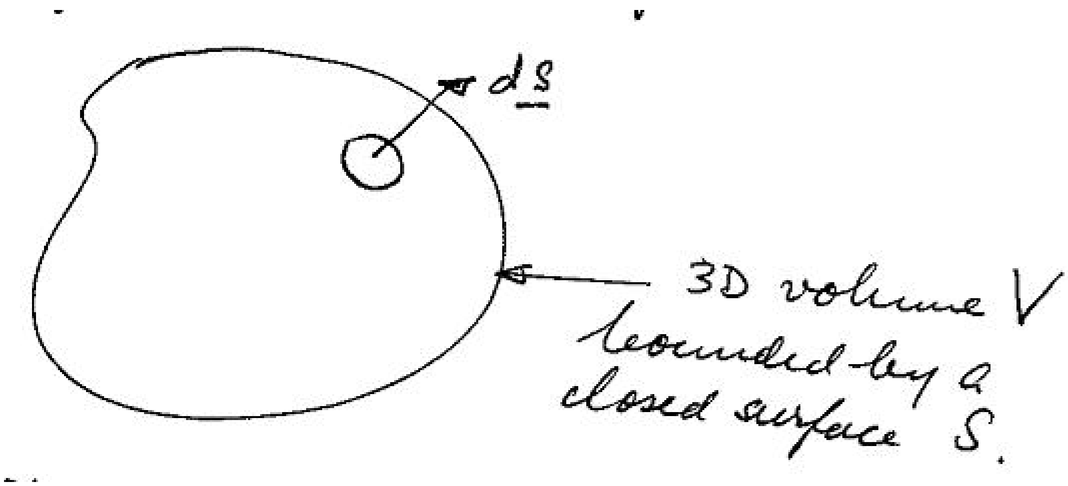

Figure B.1: Vector area element directed along the outward normal

When you consider a boundary point on the surface S of the volume,
you can resolve the velocity into direction along and perpendicular to the
surface at that point:
Only the normal component of velocity causes flow across the boundary.
The tangential part locally does not cross the boundary.
The normal part of the flow is $\underline{F} \cdot \underline{n}$, where $\underline{n}$ is the local normal.
Let the units of this velocity be measured in meters/second (or ms^{-1})
Then across a small area dS (units mxm=m^2)
the flow will be ($\underline{F} \cdot \underline{n}$)dS in units of (m$s^{-1}$)x$m^2$ or $m^3\ s^{-1}$.
This represents the volume of fluid crossing the boundary, per second,
at the element dS.
Note that if $\underline{n}$ and $\underline{F}$ point in opposite directions, then $\underline{F} \cdot \underline{n}$
is negative, representing the fluid volume per second flowing across dS into volume V.
The expression ($\underline{F} \cdot \underline{n})dS$ thus represents the <u>flux</u> of fluid (i.e volume /sec) flowing out of the boundary patch dS of volume V.
If this is a negative quantity then the fluid flows <u>into</u> the volume V at that patch.
A more compact expression for ($\underline{F} \cdot \underline{n})dS$ is $\underline{F} \cdot d\underline{S}$,
where $d\underline{S} = \underline{n}dS$ is the vector surface element patch (still an area, but directed along the outward normal.
The vector $\underline{n}$ is unit, so $|d\underline{S}| = |\underline{n}dS| = |\underline{n}|dS = dS$(eq.2)
If now we want an expression for the totality of fluid leaving the volume V, we have to sum the exit contribution over all surface patches that make up the entire surface S of the volume V. In that case, we write:

$$\text{flux(i.e vol/sec)} = \int_S \underline{F} \cdot d\underline{S} \tag{B.4}$$

where the integration is taken over the whole surface of the volume V.

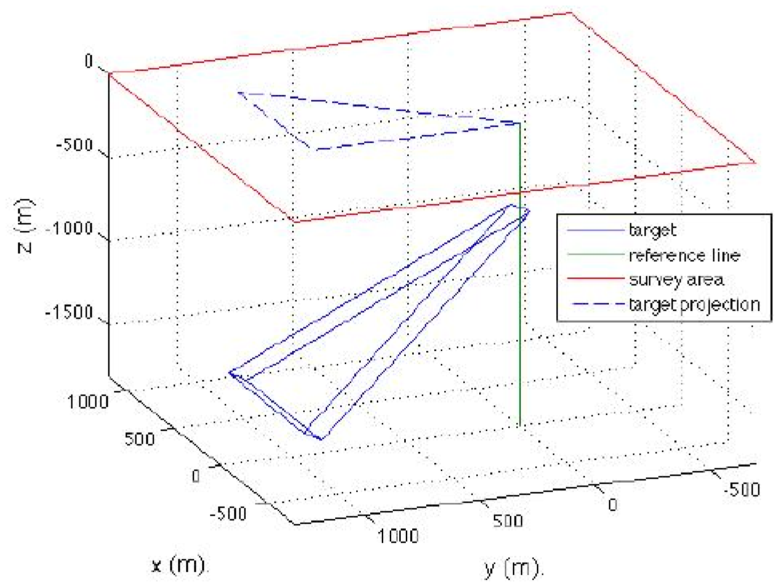

Figure 2. Thin target model used for synthetic modelling. Mid-plane vertices are at (0,0,-500), (0,900,-1700), (800,900,-1700). A vertical reference line is drawn to the surface point (0,0,0),. The projection of the target mid-plane on to the 2000m by 2000m survey area in the plane z=0 is also shown.

Figure B.2: Point (x,y,z)

If there are no fluid sources or sinks located in the volume V, then there can be no net outflow- as much entries V as leaves V.
In that case:

$$\int_S \underline{\mathrm{F}} \cdot \mathrm{d}\underline{\mathrm{S}} = 0 \tag{B.5}$$

On the otherhand,if these is a tap (or many taps) in the volume, and may be also some exit holes, then in general:

$$\int_S \underline{\mathrm{F}} \cdot \mathrm{d}\underline{\mathrm{S}} \neq 0 \tag{B.6}$$

+ve if there is a net outflow, -ve if there is a net inflow.
In some cases, the sources and sinks may be distributed continously throughout the volume.
The extend to which this happens is called the divergence of the vector field: div $\underline{\mathrm{F}}$(creation rate per unit volume)
If we sum up all the divergences throughout the volume V, we can write $\int_V (div\underline{\mathrm{F}})dV$ for the total, (div $\underline{\mathrm{F}}$)dV being the total production of fluid (+ve or -ve).
Note that div $\underline{\mathrm{F}}$ is a scalar function.

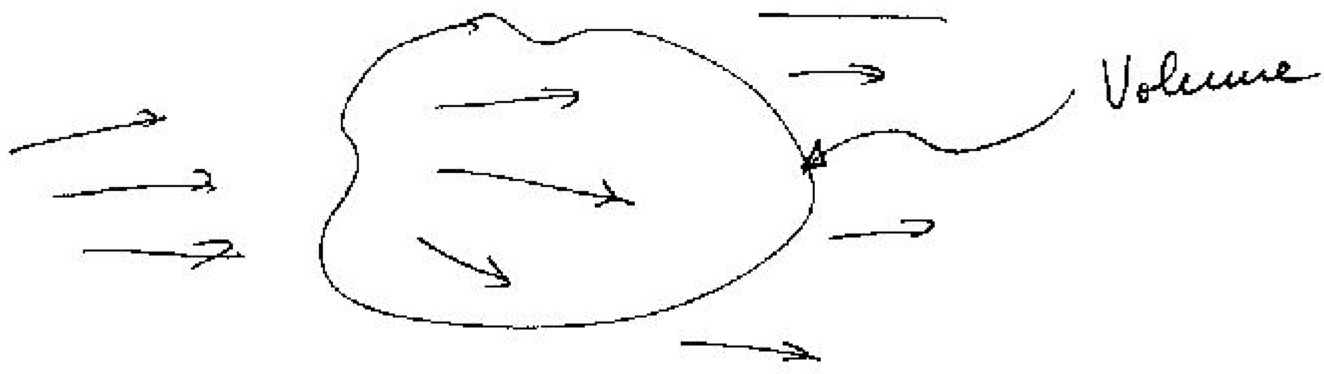

Figure B.3: Fixed volume immersed in the fluid

Equating the summed creation rates over the whole volume to the flux across the surface, we obtain:

$$\int_V (div\underline{F})dV = \int_S \underline{F}\cdot \underline{dS} \tag{B.7}$$

and this is the divergence theorem.
Suppose you consider two adjacent volumes V_1 and V_2 that share a common boundary

So the total exit flux is just the exit flux across the outer surface of the combined volumes.
i.e. Surface $S_1 \cup S_2$ minus the common bit $S_1 \cap S_2$.
$(\cup = union, \cap = intersection)$. If we have a whole array of sub-cubes making up a big cube,

then the sum of the fluxes from all the elementary cubes(inside and on its boundary) is just that of the big cube from its outer boundary(consisting of those parts of the elementary cubes that share an outer boundary).
If you take enough of these cubes (making them very small, then the contribution from an individual cube of volume ΔV and surface ΔS is:

$$\int_{\Delta V}(div\underline{F})dV = \int_{\Delta V} \underline{F}\cdot \underline{d}S$$

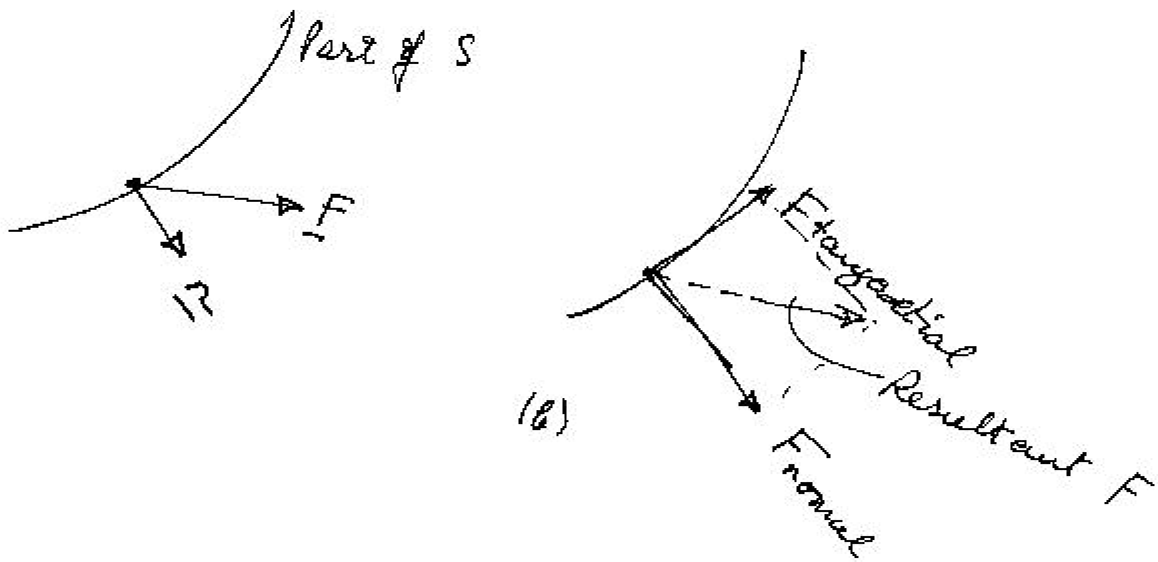

Figure B.4: Velocity vector of a boundary point on surface S

(eq.8)
where the elementary cube is inside or on the boundary of the big cube.
In this very small cube we can take div $\underline{\mathrm{F}}$ to be approximately constant, so,

$$(div\underline{\mathrm{F}})\Delta V = \int\limits_{\Delta S} \underline{\mathrm{F}} \cdot \mathrm{d}\underline{\mathrm{S}} \tag{B.8}$$

and so,

$$div\underline{\mathrm{F}} = \frac{1}{\Delta V}\int\limits_{\Delta S} \underline{\mathrm{F}} \cdot \mathrm{d}\underline{\mathrm{S}} \tag{B.9}$$

Strictly, this only holds in the limit, i.e.

$$(div\underline{\mathrm{F}}) = \lim_{\Delta V \to 0}\{\frac{1}{\Delta V}\int\limits_{\Delta S} \underline{\mathrm{F}} \cdot \mathrm{d}\underline{\mathrm{S}}\} \tag{B.10}$$

This leads to a practical way of finding an expression for div $\underline{\mathrm{F}}$ at a point (centre of a small volume).
The expression on the right hand side of eq.(11) can be evaluated from first principle for a small volume, e.g. a small cube.
In Cartesian coordinates, this yields:

$$div\underline{\mathrm{F}} = \frac{\partial F_x}{\partial x} + \frac{\partial F_y}{\partial y} + \frac{\partial F_z}{\partial z} \tag{B.11}$$

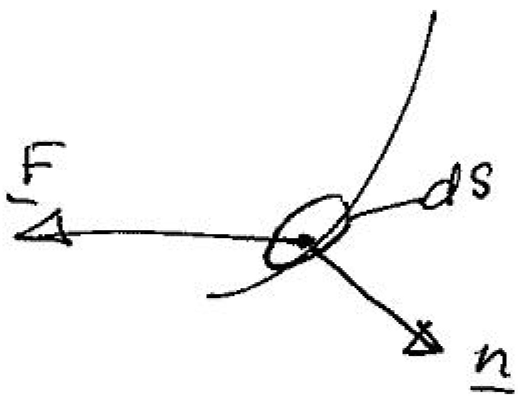

Figure B.5: Fluid volume per second across dS

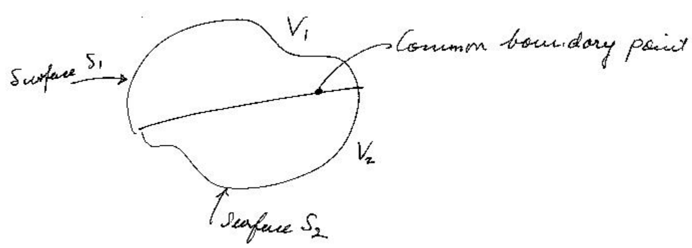

Figure B.6: Adjacent volumes

(sum of rates of changes of each component of $\underline{F}$ in that direction).
using the formula :

$$(div\underline{F}) = \lim_{\Delta V \to 0} \{ \frac{1}{\Delta V} \int_{\Delta S} \underline{F} \cdot d\underline{S} \} \tag{B.12}$$

to obtain the expression for div$\underline{F}$
We take a Cartesian coordinate system with orthogonal axes along unit vectors $\hat{x}, \hat{y}, \hat{z}$, defining the position of a general point (x,y,z).
Let $\underline{F}$ be a function of position. In terms of components, write

$$F(x, y, z) = F_x(x, y, z)\hat{x} + F_y(x, y, z)\hat{y} + F_z(x, y, z)\hat{z} \tag{B.13}$$

i.e each component is a function of (x,y,z).
Consider the elementary cube centered at (x,y,z), with sides of length δx, δy, δz .

Face BCGF has outward unit normal $\hat{x}$, face AEHD has outward unit normal $-\hat{x}$.
Their scalar areas are $\delta y \delta z$. An end -on view is :

An average of vector $\underline{F}$ on face BCGF is taken as:

$$\underline{F}(x + \frac{\delta x}{2}, y, z) = F_x(x + \frac{\delta x}{2}, y, z)\hat{x} + F_y(x + \frac{\delta x}{2}, y, z)\hat{y} + F_z(x + \frac{\delta x}{2}, y, z)\hat{z} \tag{B.14}$$

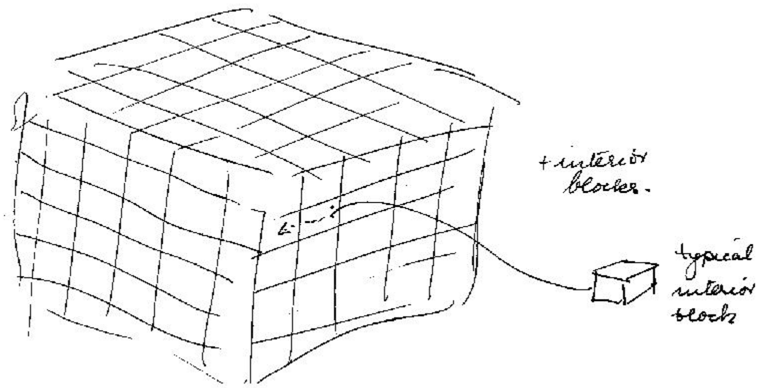

Figure B.7: Cuboid volume integral

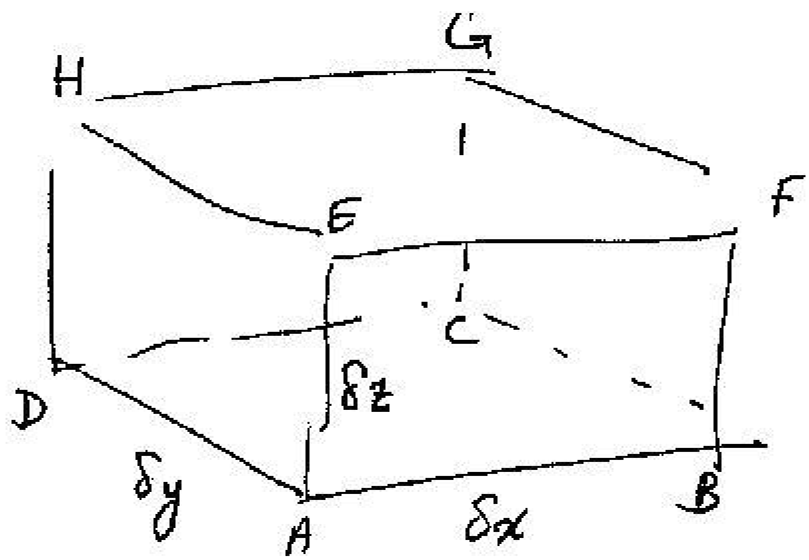

Figure B.8: Elementary cube centered at x,y,z

The vector area of face BCGF is $d\underline{S} = \hat{x}\delta y\delta z$ (eq.15).
Hence $\underline{F} \cdot d\underline{S}$ for this face is (from eq. 14 and 15):

$$\underline{F}(x + \frac{\delta x}{2}, y, z) \cdot (\hat{x}\delta y\delta z) = F_x(x + \frac{\delta x}{2}, y, z)\delta y\delta z \quad \text{(B.15)}$$

(since $\hat{x} \cdot \hat{x} = 1$ and $\hat{y} \cdot \hat{x} = \hat{z} \cdot \hat{x} = 0$) The vector area of face AEHD is

$$-\hat{x}\delta y\delta z \quad \text{(B.16)}$$

Hence $\underline{F} \cdot d\underline{S}$ for this face is:

$$(F_x(x - \frac{\delta x}{2}, y, z)\hat{x} + F_y(x - \frac{\delta x}{2}, y, z)\hat{y} + F_z(x - \frac{\delta x}{2}, y, z)\hat{z}) \cdot (-\hat{x}\delta y\delta z) \quad \text{(B.17)}$$

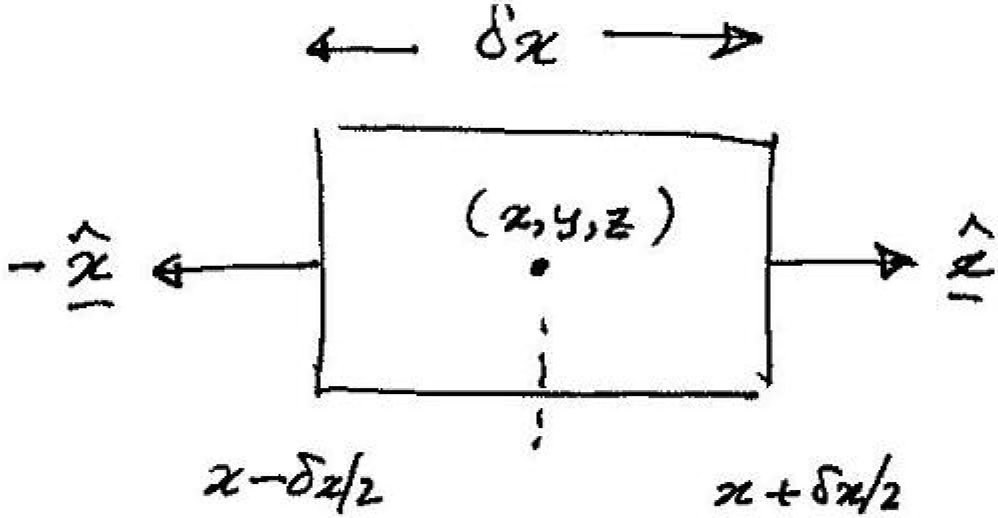

Figure B.9: Facet BCGF with outward normal $\hat{x}$

$$= -F_x(x - \frac{\delta x}{2}, y, z)\delta y \delta z \tag{B.18}$$

Hence from faces BCGF and AEHD,

$$(\underline{F} \cdot dS_{BCGF}) + (\underline{F} \cdot dS_{AEHD}) = (F_x(x + \frac{\delta x}{2}, y, z) - F_x(x - \frac{\delta x}{2}, y, z))\delta y \delta z \tag{B.19}$$

using results(16) and(19).

Now,

$$\frac{F_x(x + \frac{\delta x}{2} - F_x(x - \frac{\delta x}{2})}{(x + \frac{\delta x}{2}) - (x - \frac{\delta x}{2})} = \frac{F_x(x + \frac{\delta x}{2} - F_x(x - \frac{\delta x}{2})}{\delta x} \tag{B.20}$$

approximates the derivative of $F_x(x)$ at x:

$$\frac{F_x(x + \frac{\delta x}{2} - F_x(x - \frac{\delta x}{2})}{\delta x} \approx \frac{\partial F_x}{\partial x}\lfloor_x \tag{B.21}$$

hence :

$$F_x(x + \frac{\delta x}{2}) - F_x(x - \frac{\delta x}{2}) \approx \delta x \frac{\partial F_x}{\partial x}\lfloor_x \tag{B.22}$$

We can use this approximation in equation (20):

$$(\underline{F} \cdot d\underline{S}_{BCGF}) + (\underline{F} \cdot d\underline{S}_{AEHD}) \approx \frac{\partial F_x}{\partial x}\lfloor_{x,y,z} \delta x \delta y \delta z \tag{B.23}$$

$$\approx \frac{\partial F_x}{\partial x}\lfloor_{x,y,z} \Delta V \tag{B.24}$$

where we have put $\Delta V = \delta x \delta y \delta z$ - the volume of the elementary cuboidal element. Referring to Fig.9 we can likewise obtain results for

$$(\underline{\mathrm{F}} \cdot d\underline{\mathrm{S}}_{EFGH}) + (\underline{\mathrm{F}} \cdot d\underline{\mathrm{S}}_{ADCB}) \approx \frac{\partial F_z}{\partial z} \lfloor_{x,y,z} \Delta V \tag{B.25}$$

$$(\underline{\mathrm{F}} \cdot d\underline{\mathrm{S}}_{ABFE}) + (\underline{\mathrm{F}} \cdot d\underline{\mathrm{S}}_{DHGC}) \approx \frac{\partial F_y}{\partial y} \lfloor_{x,y,z} \Delta V \tag{B.26}$$

Adding (25)-(27), we get:

$$(\underline{\mathrm{F}} \cdot d\underline{\mathrm{S}}_{BCGF})+(\underline{\mathrm{F}} \cdot d\underline{\mathrm{S}}_{AEHD})+(\underline{\mathrm{F}} \cdot d\underline{\mathrm{S}}_{EFGH})+(\underline{\mathrm{F}} \cdot d\underline{\mathrm{S}}_{ADCB})+(\underline{\mathrm{F}} \cdot d\underline{\mathrm{S}}_{ABFE})+(\underline{\mathrm{F}} \cdot d\underline{\mathrm{S}}_{DHGC}) \approx \frac{\partial F_x}{\partial x}+\frac{\partial F_y}{\partial y}+\frac{\partial F_z}{\partial z}\lfloor \tag{B.27}$$

The left hand side of eq(28) is:

$$\int_S \underline{\mathrm{F}} \cdot \mathrm{d}\underline{\mathrm{S}} \tag{B.28}$$

where S is the entire surface of the elementary cube of Fig9.
Hence

$$\int_S \underline{\mathrm{F}} \cdot \mathrm{d}\underline{\mathrm{S}} \approx \left(\frac{\partial F_x}{\partial x} + \frac{\partial F_y}{\partial y} + \frac{\partial F_z}{\partial z}\right)_{x,y,z} \Delta V \tag{B.29}$$

The "$\approx$ " sign refers to equality + higher order of the differences $\delta x, \delta y, \delta z$. Thus

$$\frac{1}{\Delta V} \int_S \underline{\mathrm{F}} \cdot \mathrm{d}\underline{\mathrm{S}} \approx \left(\frac{\partial F_x}{\partial x} + \frac{\partial F_y}{\partial y} + \frac{\partial F_z}{\partial z}\right)_{x,y,z} + O(\delta x, \delta y, \delta z) \tag{B.30}$$

and in the limit of $\Delta V \to 0$ (with $\delta x \to 0, \delta y \to 0, \delta z \to 0$) the order correction term can be dropped:

$$\lim_{\Delta V \to 0} \left\{\frac{1}{\Delta V} \int_S \underline{\mathrm{F}} \cdot d\underline{\mathrm{S}}\right\} = \left(\frac{\partial F_x}{\partial x} + \frac{\partial F_y}{\partial y} + \frac{\partial F_z}{\partial z}\right)_{x,y,z} \tag{B.31}$$

Comparing with equation(11), the Cartesian form of div $\underline{\mathrm{F}}$ is given by:

$$div\underline{\mathrm{F}} = \left(\frac{\partial F_x}{\partial x} + \frac{\partial F_y}{\partial y} + \frac{\partial F_z}{\partial z}\right) \tag{B.32}$$

Case studies

The divergence theorem:

$$\int_S div\underline{\mathrm{F}} dV = \int_S \underline{\mathrm{F}} \cdot d\underline{\mathrm{F}} \tag{B.33}$$

holds for arbitrary volumes, not just for cuboidal ones used in the outlined proof sketch. The fundamental use of this relationship lies in the facet we have a volume integration on left of (34),and a surface integral on the right. This effectively expresses one level of integration. Eg. in Cartesian s, a volume integration requires 3 nested integrations,

$$\int_{x_1}^{x_2}\int_{y_1}^{y_2}\int_{z_1}^{z_2} \tag{B.34}$$

whereas the right hand side requires a sum of 2-nested integrals,

$$\int_{x_1}^{x_2}\int_{y_1}^{y_2} ...dxdy + \int_{y_1}^{y_2}\int_{z_1}^{z_2} ...dydz + \int_{z_1}^{z_2}\int_{z_1}^{z_2} ...dzdx \tag{B.35}$$

(assuming a cuboidal volume $(x_1, y_1, z_1)to(x_2, y_2, z_2)$) Consider the case when $\underline{F}$=$\underline{r}$, the position vector.
In that case ,

$$div\underline{F} = div\underline{r} = (\frac{\partial x}{\partial x} + \frac{\partial y}{\partial y} + \frac{\partial z}{\partial z}) = 3 \tag{B.36}$$

where $\underline{r} = (\hat{x}x + \hat{y}y + \hat{z}z)$.

Equation (34) gies, for this $\underline{F}$, div $\underline{F}$ =3, hence

$$3\int_V dV = \int_S \underline{r} \cdot d\underline{S} \tag{B.37}$$

or

$$\int_V dV = \frac{1}{3}\int_S \underline{r} \cdot d\underline{S} \tag{B.38}$$

The left hand integral is simply the geometric volume.
The right hand side is an expression for it.

<u>Case 1</u>

Take the volume to be a sphere, and let $\underline{r}$ be taken from the centre of the sphere. Then $\underline{r}$ and d$\underline{S}$ are parallel for all elementary area elements,

So ,

$$\boldsymbol{r} \cdot d\boldsymbol{S} = rdS \tag{B.39}$$

Hence,

$$\frac{1}{3}\int_S r \cdot d\, S = \frac{r}{3}\int_S dS \tag{B.40}$$

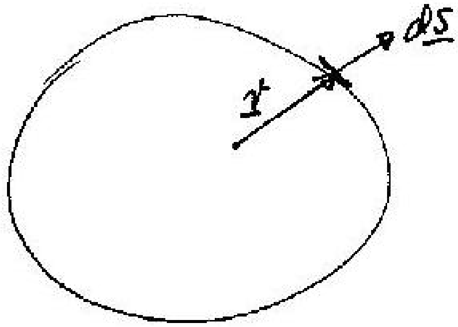

Figure B.10: Volume as a sphere

and $\int_S dS$ is just the area of the sphere.
We obtain , Volume of sphere =

$$\frac{r}{3}\text{X area of sphere} \tag{B.41}$$

The area of the sphere can be found to be

$$4\pi r^2 \tag{B.42}$$

hence the volume is :

$$\frac{r}{3}4\pi r^2 = \frac{4}{3}\pi r^3 \tag{B.43}$$

<u>Case 2</u>

Take the volume to be a pyramid, with base area A.

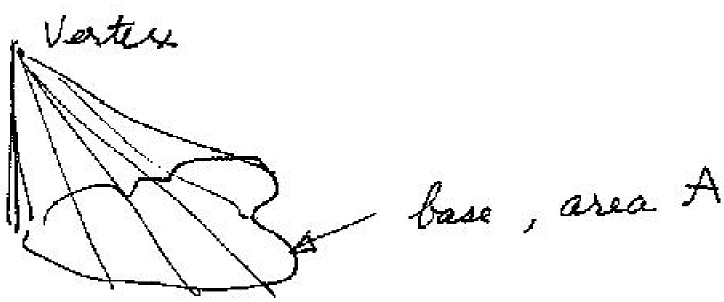

Figure B.11: Volume as a pyramid

Take r̲ to emanate from this vertex. Take n̲ to be
the outward normal of the plane base. Then **r** · **n** = constant (eq.44)
for all points on the base. We can write:

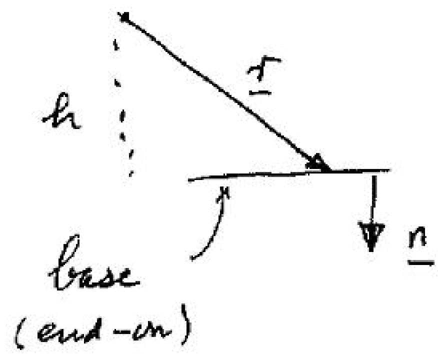

Figure B.12: In a pyramid: $\underline{n} \cdot \underline{n}$= constant

$$\underline{r} \cdot d\underline{S} = \underline{r} \cdot \underline{n} dS = hdS \tag{B.44}$$

where $\underline{r} \cdot \underline{n} = h$ is the '"height"' of the pyramid over the base.
From eq.(39) , ew then obtain

$$\int_V dV = \frac{1}{3} \int_S \underline{r} \cdot d\underline{S} = \frac{1}{3} \int_{Base} \underline{r} \cdot d\underline{S} + \frac{1}{3} \int_{Sides} \underline{r} \cdot d\underline{S} \tag{B.45}$$

$$\int_V dV = \frac{1}{3} \int_{base} \underline{r} \cdot d\underline{S} = \frac{h}{3} \int_{base} dS \tag{B.46}$$

using equation(45). $\int_{base} dS$ is simply the area of the base(=A,Fig12).Hence the volume of a pyramid is $\frac{h}{3}A$ (=$\frac{1}{3}$ height x area of base).
Note that in both cases 1,2 we have reduced the problem of finding the volume of a body to finding its surface area(or a part of it). So we have reduced the dimensionality of the problem.
In normal applications, div $\underline{F}$ is not constant. We may face a problem to evaluate

$$\int_V HdV \tag{B.47}$$

for some function H. If we can find a function $\underline{F}$ such that div $\underline{F}$ = H, then we can express the volume integral as:

$$\int_V HdV = \int_V (div\underline{F})dV = \int_S \underline{F} \cdot d\underline{S} \tag{B.48}$$

and so reduce the integral to a surface integration. It is this aspect that is used in the gravi-magnetic anomaly calculations of geometrical targets.

APPENDIX C

JAVA custom specification for functions: Atnh, Atn

For use by the Surface method(by H.Holstein), published in this thesis

AtnH()

```
public static double AtnH_D(double d)throws ArctanException
{
final double third=1.0D/3.0D;

int k = 0;
if(1.0D <= Math.abs(d))
                {
throw new ArctanException();
}
double dsqr = d*d;
if(dsqr > 0.0625D)
{
return (Math.log((1.0D + d) / (1.0D - d)) / 2.0D-d)/Math.pow(d,3);
}
if(d == 0.0D)
{
return 0.0D;
}
double test = third + dsqr / 5.0D;
k = 5;
double term=dsqr;
for(int i = 7; third < test; i += 2)
{
k = i;
term=term*dsqr;
test= third + term/ (double)i;
}
double res=0.0D;
```

```
for(int j = k; j >= 5; j -= 2)
{
res = 1.0D / (double)j + res* dsqr;
}
return third+res*dsqr;
// return (AtanH_D(d)-d)/Math.pow(d,3);
```

Atn()

```
public static double Atn_D(double d)throws ArctanException
{
final double third=-1.0D/3.0D;
int k = 0;
double dsqr = d*d;
if(dsqr > 0.0625D)
{
return (Math.atan(d)-d)/Math.pow(d,3);
}
if(d == 0.0D)
{
return 0.0D;
}
//case d <=  0.0625
double test = third + dsqr / 5.0D;
k = 5;
double term = dsqr;
for(int i = 7; third < test; i += 2)
{
k = i;
term=term*dsqr;
test= third + (term/ (double)k);
}
double res=0.0D;
int mod4_k=k%4;
int sign;
if (mod4_k==1)
sign=1;
else
sign=-1;
for(int j = k; j >= 5; j -= 2)
{
res =(sign* (1.0D /(double) j)) + res* dsqr;
sign=-sign;
}
return third+res*dsqr;
```

```
//return(Math.atan(d )-d)/Math.pow(d,3);
}
```

APPENDIX D

Edel Sherrat-eq14

Email to Costas regarding "Performance Article", 6^{th} February 2010

Horst Holstein (Aberystwyth University)

February 6, 2010

Equation (14), Performance article (HH and ES, 2000)

First we consider $\nabla \cdot \mathbf{r}$. In cartesians, the position vector $\mathbf{r}$ has components (x, y, z), so its divergence is

$$\frac{\partial x}{\partial x} + \frac{\partial y}{\partial y} + \frac{\partial z}{\partial z} = 3 \, . \tag{1}$$

We require $\nabla \cdot \hat{\mathbf{r}} = \nabla \cdot (\mathbf{r}/r)$. So we need

$$\nabla \cdot (\mathbf{r}/r) = \frac{\partial(x/r)}{\partial x} + \frac{\partial(y/r)}{\partial y} + \frac{\partial(z/r)}{\partial z} \tag{2}$$

where

r = sqrt(x^2+y^2+z^2)

Using the chain rule for each of the three terms in equation (2), we get

$$\begin{aligned}
\nabla \cdot (\mathbf{r}/r) &= \quad \frac{\partial x}{\partial x}(1/r) + x\frac{\partial(1/r)}{\partial x} \quad + \quad \frac{\partial y}{\partial y}(1/r) + y\frac{\partial(1/r)}{\partial y} \quad + \quad \frac{\partial z}{\partial z}(1/r) + z\frac{\partial(1/r)}{\partial z} \\
&= \quad (1/r) - \frac{x}{r^2}\frac{\partial r}{\partial x} + \quad (1/r) - \frac{y}{r^2}\frac{\partial r}{\partial y} \quad + \quad (1/r) - \frac{z}{r^2}\frac{\partial r}{\partial z} \\
&= \quad 3/r - \quad x\frac{\partial r}{\partial x} + y\frac{\partial r}{\partial y} + z\frac{\partial r}{\partial z} \quad /r^2
\end{aligned} \tag{4}$$

To get terms like ∂r, it's probably easiest to differentiate the square of equation (3) with respect to x, y and z. Thus

To get terms like $\frac{\partial r}{\partial x}$, it's probably easiest to differentiate the square of equation (3) with respect to x, y and z. Thus

$$2r\frac{\partial r}{\partial x} = \frac{\partial r^2}{\partial x} \tag{5}$$

$$= \frac{\partial (x^2 + y^2 + z^2)}{\partial x} \tag{6}$$

$$= 2x \tag{7}$$

so from equations (5) and (7),

$$\frac{\partial r}{\partial x} = x/r \ . \tag{8}$$

In a similar way, we find

$$\frac{\partial r}{\partial y} = y/r \ , \frac{\partial r}{\partial z} = z/r \ . \tag{9}$$

Now substitute results (8) and (9) into the last line of equation (4), to get

$$\nabla \cdot (\mathbf{r}/r) = 3/r - (x^2 + y^2 + z^2)/r^3 = 3/r - r^2/r^3 = 2/r \ . \tag{10}$$

Divide both sides by 2, and you get the required result

$$\tfrac{1}{2}\nabla \cdot \hat{\mathbf{r}} = \tfrac{1}{2}\nabla(\mathbf{r}/r) = 1/r \ . \tag{11}$$

This derivation is elementary but lengthy, and is typical of writing out terms in cartesians. The result does not depend on cartesians, and their use is totally artificial. There is a much shorter way, which does not require going into cartesian coordinates, and can be summarised as

$$\nabla \cdot (\mathbf{r}/r) = (\nabla \cdot \mathbf{r})/r - \mathbf{r} \cdot \nabla(1/r) = 3/r - \mathbf{r} \cdot \mathbf{r}/r^3 = 2/r \ . \tag{12}$$

2 Equation (15), HH & ES (2000), "Performance"

This equation is a straight application of the divergence theorem. For a general vector field **a**,

$$\int_V \nabla \cdot \mathrm{a}\, dv = \int_S \mathrm{a} \cdot d\mathrm{S} \ . \qquad (13)$$

Write the vector surface element dS as **n** dS, where **n** is the unit outward normal of the surface element, and dS is its magnitude. Regrouping gives

$$\int_V \nabla \cdot \mathrm{a}\, dv = \int_S (\mathrm{a} \cdot \mathbf{n})\, d\mathrm{S} \ . \qquad (14)$$

Now put $\mathrm{a} = \hat{\mathbf{r}} = \mathbf{r}/\mathbf{r}$, to obtain from equation (14)

$$\int_V \nabla \cdot \hat{\mathbf{r}}\, dv = \int_S ((\mathbf{r}/\mathbf{r}) \cdot \mathbf{n})\, d\mathrm{S} \ . \qquad (15)$$

The right hand term can be slightly reordered, requiring fewer brackets, as in

$$\int_V \nabla \cdot \hat{\mathbf{r}}\, dv = \int_S (\mathbf{r} \cdot \mathbf{n})\, d\mathrm{S}/\mathbf{r} \ , \qquad (16)$$

with the understanding that the final term $1/\mathbf{r}$ is still part of the integrand. This is equation (15) in HH & ES (2000).

APPENDIX E

Floating point precision

E.1 Floating point gap quantity ϵ

Every real number has its representable approximation which is different from system to system. EPSILON is the small bit that is lost when truncating to the last digit of the available precision. This bit is different for different computer systems. It can also be presented as the gap between 2 succesive floating point numbers (see Saw Tooth plot). Also we can say that it is the smallest real number x that a system can distinguish between number+x, number

http://www.akiti.ca/MachEps.html Machine epsilon, epsmch, is defined as the smallest positive number such that 1.0 + epsmch is not equal to 1.0.

http://lists.boost.org/Archives/boost/2001/12/21281.php measurable rounding error means the error is bounded by a predictable upper limit.

E.2 Floating point precision limitations

Floating point limited computer precision is a determining factor in the anomaly calculation. Floating point accuracy is defined to be the number of significant digits. Every computer language has its own data type. Floating point exceptions may cause memory licks and overflows. Generally every decimal number is represented internally as binary with a representation: $x = (+-)m * 2E$

where mantissa $m1 <= m < 2$, E an integer According to the IEEE 754 standard every floating point number, is internally represented using a pattern of 3 parts: The Sign part, the Exponent part and the Fraction part. In C language single precision arithmetic has 23 digits of precision in mantissa while in double precision 51, 8 digits in the exponent while in double 11 and 1 digit for the sign.

To perform a floating point operation such as a multiplication, many digits (if the number is irrational, an infinite number) are employed to produce the exact result. Because of the computer physical limited memories, only a certain number of digits can be processed. The remaining digits for an operation will be truncated and therefore an accuracy violation will be caused.

To represent the rest of the digits rounding to the nearest digit strategy is used approximating the result of the operation with an almost exact result. The loss of digits quantifies the accuracy violation. If all the significant digits will be exhausted the result will not be meaningful. If not the operation produces an almost exact result. Since floating point calculations involve a bit of uncertainty, the distance between two floating point values bracketing a numerical value, is called epsilon. Epsilon typically represents the absolute error value for one particular computer system (for example, in Java for double precision arithmetic, epsilon is 2.2204460492503131e-016) and is alternatively called ULP (units at the last place). The relative error now for a particular number, will be:

ϵ= (result-expected result)/expected result

Summarizing, floating point approximation in computer systems with limited memories, involves a gap equal to n*epsilon for a given number n, alternatively called truncation error or actual error. This gap represents a break on the continuation of the digital sequence representing a real number like p(3,14159 26535 89793 23846 26433 83279 50288 41971 69399 37510....). This gap would not exist if we could use an infinite number of digits for the real number, which is impossible. Therefore the larger the number the larger the truncation error will be. So e can be justified as: epsilon = gap/number

The following algorithm computes epsilon (e), in an IEEE-like format for any machine.

```
{
epsilon = 1;\\
while ((1 + epsilon) > 1) { \\
   epsilon /= 2; \\
}\\
Epsilon *= 2;\\
}
```

Rounding to the nearest digit engages truncation error. Truncation error can never exceed rounding error and can be minimized using analytical cancellation of large operands. In our context, as the distance from the target is growing, operations involved engage larger numbers to compute smaller and smaller distances as the target is getting smaller. As these distances are getting significantly small the floating point precision of the specific machine is getting exhausted. Under this scenario, as the distance from the target d is growing and γ is getting smaller and smaller the significant digits are getting less and less. The error of an anomaly method is estimated to be proportional to the order of the operations involved. We follow the anomaly error growth using different algorithms. Each of the algorithms appears to have its own error growth. Our purpose is to theoretically estimate the error growth class for every one and use this estimation as a measurement for the performance of every anomaly algorithm in the future. Previous work such as the unpublished paper of Edel Sheratt and Horst Holstein ”Performance metrics for computing gravi-magneto anomalies of uniform polyhedra, Comparison of Gravimagnetic Formulas for uniform polyhedra” by Horst Holstein et al, 1999, ”Gravimagnetic Analysis of uniform polyhedra by Horst Holstein @ Ben Ketteridge, 1996”, classify the anomaly methods according to their error growth into 3 distinct classes, namely Vertex, Line and Surface with descending error growth. Each method has a critical distance (figure 1a) at which for a particular floating point arithmetic, all the significant digits are lost.

E.3 truncation error

The truncation error in a floating point number α will mean that we represent a value between $\alpha(1+\epsilon)$ and $\alpha(1-\epsilon)$. So for the quotient a/b, we might actually be computing $\frac{\alpha(1+\epsilon)}{\alpha(1-\epsilon)} = ln\frac{a}{b} + ln\frac{1+\epsilon}{1-\epsilon}$
(by the product rule for logs) in which the second part represents the error. Now this term is:
$ln\frac{1+\epsilon}{1-\epsilon}$ =2arctanh$\epsilon = O(\epsilon)$ The change of sign in $(1 \pm \epsilon)$ is chosen so that the errors reinforce rather than cancel, to get a worst case.

E.4 ULP

From definition of ULP follows that ULP is a minimum value such that $1 + ULP! = 1$

As I explained above, 1 ULP is always 1 ULP regardless the exponent. In the particular case of exponent 1, the absolute value of 1 ULP is called the machine epsilon, and is equal to numeric limits<>:: $\epsilon()$ on conformant platforms. It follows from the ULP definition that ($1 + eps > 1$). For example, consider the average of two floating point numbers with identical exponents, but mantissas which differ by 1. The average should be a number midway between the original numbers, but the average cannot be represented without increasing the size of the mantissa. Although the mathematical operation is well-defined and the result is within the range of representable numbers, the average of two adjacent floating point values cannot be represented exactly. http://math.la.asu.edu/ eric/mat420/ulp.pdf

APPENDIX F

The ϵ pattern

Rounding relative error dx/x, when float x is increasing in a log2 scale

	Interval	log_2(x)	log_2(dx/x)	dx/x	log_2(dx)	dx	x	y=log_2(dx/x)	log10(dx/x)
						1,11022302462516000E-16			
0	**0,5-1**	-1,00000000	-52,000000	2,220446049250300000E-16	-5,300000000000000000E+01	1,11022302462515000E-16	0,5000000	-52,000000000000000000	-15,65355977
1		-0,95560588	-52,044394	2,153159805333620000E-16	-5,300000000000000000E+01	1,11022302462515000E-16	0,5156250	-52,044394119358500000	-15,66692374
2		-0,91253716	-52,087463	2,089831575764990000E-16	-5,300000000000000000E+01	1,11022302462515000E-16	0,5312500	-52,087462841250300000	-15,67988871
3		-0,87071698	-52,129283	2,030122102171700000E-16	-5,300000000000000000E+01	1,11022302462515000E-16	0,5468750	-52,129283016945000000	-15,69247784
4		-0,83007500	-52,169925	1,973729821555820000E-16	-5,300000000000000000E+01	1,11022302462515000E-16	0,5625000	-52,169925001442300000	-15,7047123
5		-0,79054663	-52,209453	1,920385772324580000E-16	-5,300000000000000000E+01	1,11022302462515000E-16	0,5781250	-52,209453365629000000	-15,71661152
6		-0,75207249	-52,247928	1,869849304631830000E-16	-5,300000000000000000E+01	1,11022302462515000E-16	0,5937500	-52,247927513443600000	-15,72819339
7		-0,71459778	-52,285402	1,821904450666910000E-16	-5,300000000000000000E+01	1,11022302462515000E-16	0,6093750	-52,285402218862300000	-15,7394744
8		-0,67807191	-52,321928	1,776356839400240000E-16	-5,300000000000000000E+01	1,11022302462515000E-16	0,6250000	-52,321928094887400000	-15,75046979
9		-0,64244800	-52,357552	1,733031062829500000E-16	-5,300000000000000000E+01	1,11022302462515000E-16	0,6406250	-52,357552004618100000	-15,76119365
10		-0,60768258	-52,392317	1,691768418476420000E-16	-5,300000000000000000E+01	1,11022302462515000E-16	0,6562500	-52,392317422778800000	-15,77165909
11		-0,57373525	-52,426265	1,652424966883940000E-16	-5,300000000000000000E+01	1,11022302462515000E-16	0,6718750	-52,426264754702100000	-15,78187825
12		-0,54056838	-52,459432	1,614869854000220000E-16	-5,300000000000000000E+01	1,11022302462515000E-16	0,6875000	-52,459431618637300000	-15,79186247
13		-0,50814690	-52,491853	1,578983857244660000E-16	-5,300000000000000000E+01	1,11022302462515000E-16	0,7031250	-52,000000000000000000	-15,80162231
14		-0,47643804	-52,523562	1,544658121217600000E-16	-5,300000000000000000E+01	1,11022302462515000E-16	0,7187500	-52,000000000000000000	-15,81116763
15		-0,44541115	-52,554589	1,511793054808710000E-16	-5,300000000000000000E+01	1,11022302462515000E-16	0,7343750	-52,000000000000000000	-15,82050765
16		-0,41503750	-52,584963	1,480297366166870000E-16	-5,300000000000000000E+01	1,11022302462515000E-16	0,7500000	-52,000000000000000000	-15,82965103
17		-0,38529016	-52,614710	1,450087215836930000E-16	-5,300000000000000000E+01	1,11022302462515000E-16	0,7656250	-52,000000000000000000	-15,83860588
18		-0,35614381	-52,643856	1,421085471520190000E-16	-5,300000000000000000E+01	1,11022302462515000E-16	0,7812500	-52,000000000000000000	-15,8473798
19		-0,32757466	-52,672425	1,393221050509990000E-16	-5,300000000000000000E+01	1,11022302462515000E-16	0,7968750	-52,000000000000000000	-15,85597997
20		-0,29956028	-52,700440	1,366428338000180000E-16	-5,300000000000000000E+01	1,11022302462515000E-16	0,8125000	-52,000000000000000000	-15,86441314
21		-0,27207955	-52,727920	1,340646671245460000E-16	-5,300000000000000000E+01	1,11022302462515000E-16	0,8281250	-52,000000000000000000	-15,87268567
22		-0,24511250	-52,754888	1,315819881037210000E-16	-5,300000000000000000E+01	1,11022302462515000E-16	0,8437500	-52,000000000000000000	-15,88080356
23		-0,21864029	-52,781360	1,291895883200170000E-16	-5,300000000000000000E+01	1,11022302462515000E-16	0,8593750	-52,000000000000000000	-15,88877249
24		-0,19264508	-52,807355	1,268826313857310000E-16	-5,300000000000000000E+01	1,11022302462515000E-16	0,8750000	-52,000000000000000000	-15,89659782
25		-0,16710999	-52,832890	1,246566203087890000E-16	-5,300000000000000000E+01	1,11022302462515000E-16	0,8906250	-52,000000000000000000	-15,90428465
26		-0,14201900	-52,857981	1,225073682344990000E-16	-5,300000000000000000E+01	1,11022302462515000E-16	0,9062500	-52,000000000000000000	-15,91183779
27		-0,11735695	-52,882643	1,204309721627280000E-16	-5,300000000000000000E+01	1,11022302462515000E-16	0,9218750	-52,000000000000000000	-15,91926181

	-0,09310940	-52,906891	1,184237892933490000E-16	-5,300000000000000000E+01	1,11022302462515000E-16	0,9375000	-52,000000000000000000	-15,92656105
	-0,06926266	-52,930737	1,164824156983760000E-16	-5,300000000000000000E+01	1,11022302462515000E-16	0,9531250	-52,000000000000000000	-15,93373963
	-0,04580369	-52,954196	1,146036670580800000E-16	-5,300000000000000000E+01	1,11022302462515000E-16	0,9687500	-52,000000000000000000	-15,94080149
	-0,02272008	-52,977280	1,127845612317610000E-16	-5,300000000000000000E+01	1,11022302462515000E-16	0,9843750	-52,000000000000000000	-15,94775035
1-2	0,00000000	-52,000000	2,220446049250310000E-16	-5,200000000000000000E+01	**2,22044604925031000E-16**	1,0000000	-52,000000000000000000	-15,65355977
	0,04439412	-52,044394	2,153159805333630000E-16	-5,200000000000000000E+01	2,22044604925031000E-16	1,0312500	-52,000000000000000000	-15,66692374
	0,08746284	-52,087463	2,089831575765000000E-16	-5,200000000000000000E+01	2,22044604925031000E-16	1,0625000	-52,000000000000000000	-15,67988871
	0,12928302	-52,129283	2,030122102171710000E-16	-5,200000000000000000E+01	2,22044604925031000E-16	1,0937500	-52,000000000000000000	-15,69247784
	0,16992500	-52,169925	1,973729821555830000E-16	-5,200000000000000000E+01	2,22044604925031000E-16	1,1250000	-52,000000000000000000	-15,7047123
	0,20945337	-52,209453	1,920385772324590000E-16	-5,200000000000000000E+01	2,22044604925031000E-16	1,1562500	-52,000000000000000000	-15,71661152
	0,24792751	-52,247928	1,869849304631840000E-16	-5,200000000000000000E+01	2,22044604925031000E-16	1,1875000	-52,000000000000000000	-15,72819339
	0,28540222	-52,285402	1,821904450666920000E-16	-5,200000000000000000E+01	2,22044604925031000E-16	1,2187500	-52,000000000000000000	-15,7394744
	0,32192809	-52,321928	1,776356839400250000E-16	-5,200000000000000000E+01	2,22044604925031000E-16	1,2500000	-53,321928094887400000	-15,75046979
	0,35755200	-52,357552	1,733031062829510000E-16	-5,200000000000000000E+01	2,22044604925031000E-16	1,2812500	-53,357552004618100000	-15,76119365
	0,39231742	-52,392317	1,691768418476430000E-16	-5,200000000000000000E+01	2,22044604925031000E-16	1,3125000	-53,392317422778800000	-15,77165909
	0,42626475	-52,426265	1,652424966883950000E-16	-5,200000000000000000E+01	2,22044604925031000E-16	1,3437500	-53,426264754702100000	-15,78187825
	0,45943162	-52,459432	1,614869854000230000E-16	-5,200000000000000000E+01	2,22044604925031000E-16	1,3750000	-53,459431618637300000	-15,79186247
	0,49185310	-52,491853	1,578983857244660000E-16	-5,200000000000000000E+01	2,22044604925031000E-16	1,4062500	-53,491853096329700000	-15,80162231
	0,52356196	-52,523562	1,544658121217610000E-16	-5,200000000000000000E+01	2,22044604925031000E-16	1,4375000	-53,523561956057000000	-15,81116763
	0,55458885	-52,554589	1,511793054808720000E-16	-5,200000000000000000E+01	2,22044604925031000E-16	1,4687500	-53,554588851677600000	-15,82050765
	0,58496250	-52,584963	1,480297366166870000E-16	-5,200000000000000000E+01	2,22044604925031000E-16	1,5000000	-53,584962500721200000	-15,82965103
	0,61470984	-52,614710	1,450087215836940000E-16	-5,200000000000000000E+01	2,22044604925031000E-16	1,5312500	-53,614709844115200000	-15,83860588
	0,64385619	-52,643856	1,421085471520200000E-16	-5,200000000000000000E+01	2,22044604925031000E-16	1,5625000	-53,643856189774700000	-15,8473798
	0,67242534	-52,672425	1,393221050510000000E-16	-5,200000000000000000E+01	2,22044604925031000E-16	1,5937500	-53,672425341971500000	-15,85597997
	0,70043972	-52,700440	1,366428338000190000E-16	-5,200000000000000000E+01	2,22044604925031000E-16	1,6250000	-53,700439718141100000	-15,86441314
	0,72792045	-52,727920	1,340646671245470000E-16	-5,200000000000000000E+01	2,22044604925031000E-16	1,6562500	-53,727920454563200000	-15,87268567
	0,75488750	-52,754888	1,315819881037220000E-16	-5,200000000000000000E+01	2,22044604925031000E-16	1,6875000	-53,754887502163500000	-15,88080356
	0,78135971	-52,781360	1,291895883200180000E-16	-5,200000000000000000E+01	2,22044604925031000E-16	1,7187500	-53,781359713524700000	-15,88877249
	0,80735492	-52,807355	1,268826313857320000E-16	-5,200000000000000000E+01	2,22044604925031000E-16	1,7500000	-53,807354922057600000	-15,89659782
	0,83289001	-52,832890	1,246566203087890000E-16	-5,200000000000000000E+01	2,22044604925031000E-16	1,7812500	-53,832890014164700000	-15,90428465
	0,85798100	-52,857981	1,225073682345000000E-16	-5,200000000000000000E+01	2,22044604925031000E-16	1,8125000	-53,857980995127600000	-15,91183779
	0,88264305	-52,882643	1,204309721627290000E-16	-5,200000000000000000E+01	2,22044604925031000E-16	1,8437500	-53,882643049361800000	-15,91926181
	0,90689060	-52,906891	1,184237892933500000E-16	-5,200000000000000000E+01	2,22044604925031000E-16	1,8750000	-53,906890595608500000	-15,92656105
	0,93073734	-52,930737	1,164824156983770000E-16	-5,200000000000000000E+01	2,22044604925031000E-16	1,9062500	-53,930737337562900000	-15,93373963
	0,95419631	-52,954196	1,146036670580810000E-16	-5,200000000000000000E+01	2,22044604925031000E-16	1,9375000	-53,954196310386900000	-15,94080149
	0,97727992	-52,977280	1,127845612317620000E-16	-5,200000000000000000E+01	2,22044604925031000E-16	1,9687500	-53,977279923499900000	-15,94775035

2-4	1,00000000	-52,000000	2,220446049250310000E-16	-5,100000000000000000E+01	4,440892098500620000E-16	2,0000000	-54,000000000000000000	-15,65355977
	1,04439412	-52,044394	2,153159805333630000E-16	-5,100000000000000000E+01	4,440892098500620000E-16	2,0625000	-54,044394119358500000	-15,66692374
	1,08746284	-52,087463	2,089831575765000000E-16	-5,100000000000000000E+01	4,440892098500620000E-16	2,1250000	-54,087462841250300000	-15,67988871
	1,12928302	-52,129283	2,030122102171710000E-16	-5,100000000000000000E+01	4,440892098500620000E-16	2,1875000	-54,129283016945000000	-15,69247784
	1,16992500	-52,169925	1,973729821555830000E-16	-5,100000000000000000E+01	4,440892098500620000E-16	2,2500000	-54,169925001442300000	-15,7047123
	1,20945337	-52,209453	1,920385772324590000E-16	-5,100000000000000000E+01	4,440892098500620000E-16	2,3125000	-54,209453365629000000	-15,71661152
	1,24792751	-52,247928	1,869849304631840000E-16	-5,100000000000000000E+01	4,440892098500620000E-16	2,3750000	-54,247927513443600000	-15,72819339
	1,28540222	-52,285402	1,821904450666920000E-16	-5,100000000000000000E+01	4,440892098500620000E-16	2,4375000	-54,285402218862200000	-15,7394744
	1,32192809	-52,321928	1,776356839400250000E-16	-5,100000000000000000E+01	4,440892098500620000E-16	2,5000000	-54,321928094887400000	-15,75046979
	1,35755200	-52,357552	1,733031062829510000E-16	-5,100000000000000000E+01	4,440892098500620000E-16	2,5625000	-54,357552004618100000	-15,76119365
	1,39231742	-52,392317	1,691768418476430000E-16	-5,100000000000000000E+01	4,440892098500620000E-16	2,6250000	-54,392317422778800000	-15,77165909
	1,42626475	-52,426265	1,652424966883950000E-16	-5,100000000000000000E+01	4,440892098500620000E-16	2,6875000	-54,426264754702100000	-15,78187825
	1,45943162	-52,459432	1,614869854000230000E-16	-5,100000000000000000E+01	4,440892098500620000E-16	2,7500000	-54,459431618637300000	-15,79186247
	1,49185310	-52,491853	1,578983857244660000E-16	-5,100000000000000000E+01	4,440892098500620000E-16	2,8125000	-54,491853096329700000	-15,80162231
	1,52356196	-52,523562	1,544658121217610000E-16	-5,100000000000000000E+01	4,440892098500620000E-16	2,8750000	-54,523561956057000000	-15,81116763
	1,55458885	-52,554589	1,511793054808720000E-16	-5,100000000000000000E+01	4,440892098500620000E-16	2,9375000	-54,554588851677600000	-15,82050765
	1,58496250	-52,584963	1,480297366166870000E-16	-5,100000000000000000E+01	4,440892098500620000E-16	3,0000000	-54,584962500721200000	-15,82965103
	1,61470984	-52,614710	1,450087215836940000E-16	-5,100000000000000000E+01	4,440892098500620000E-16	3,0625000	-54,614709844115200000	-15,83860588
	1,64385619	-52,643856	1,421085471520200000E-16	-5,100000000000000000E+01	4,440892098500620000E-16	3,1250000	-54,643856189774700000	-15,8473798
	1,67242534	-52,672425	1,393221050510000000E-16	-5,100000000000000000E+01	4,440892098500620000E-16	3,1875000	-54,672425341971500000	-15,85597997
	1,70043972	-52,700440	1,366428338000190000E-16	-5,100000000000000000E+01	4,440892098500620000E-16	3,2500000	-54,700439718141100000	-15,86441314
	1,72792045	-52,727920	1,340646671245470000E-16	-5,100000000000000000E+01	4,440892098500620000E-16	3,3125000	-54,727920454563200000	-15,87268567
	1,75488750	-52,754888	1,315819881037220000E-16	-5,100000000000000000E+01	4,440892098500620000E-16	3,3750000	-54,754887502163500000	-15,88080356
	1,78135971	-52,781360	1,291895883200180000E-16	-5,100000000000000000E+01	4,440892098500620000E-16	3,4375000	-54,781359713524700000	-15,88877249
	1,80735492	-52,807355	1,268826313857320000E-16	-5,100000000000000000E+01	4,440892098500620000E-16	3,5000000	-54,807354922057600000	-15,89659782
	1,83289001	-52,832890	1,246566203087890000E-16	-5,100000000000000000E+01	4,440892098500620000E-16	3,5625000	-54,832890014164700000	-15,90428465
	1,85798100	-52,857981	1,225073682345000000E-16	-5,100000000000000000E+01	4,440892098500620000E-16	3,6250000	-54,857980995127600000	-15,91183779
	1,88264305	-52,882643	1,204309721627290000E-16	-5,100000000000000000E+01	4,440892098500620000E-16	3,6875000	-54,882643049361800000	-15,91926181
	1,90689060	-52,906891	1,184237892933500000E-16	-5,100000000000000000E+01	4,440892098500620000E-16	3,7500000	-54,906890595608500000	-15,92656105
	1,93073734	-52,930737	1,164824156983770000E-16	-5,100000000000000000E+01	4,440892098500620000E-16	3,8125000	-54,930737337562900000	-15,93373963
	1,95419631	-52,954196	1,146036670580810000E-16	-5,100000000000000000E+01	4,440892098500620000E-16	3,8750000	-54,954196310386900000	-15,94080149
	1,97727992	-52,977280	1,127845612317620000E-16	-5,100000000000000000E+01	4,440892098500620000E-16	3,9375000	-54,977279923499900000	-15,94775035

4-8	2,00000000	-52,000000	2,220446049250310000E-16	-5,000000000000000000E+01	8,88178419700125000E-16	4,0000000	-55,000000000000000000	-15,65355977
	2,04439412	-52,044394	2,153159805333640000E-16	-5,000000000000000000E+01	8,88178419700125000E-16	4,1250000	-55,044394119358500000	-15,66692374
	2,08746284	-52,087463	2,089831575765000000E-16	-5,000000000000000000E+01	8,88178419700125000E-16	4,2500000	-55,087462841250300000	-15,67988871
	2,12928302	-52,129283	2,030122102171710000E-16	-5,000000000000000000E+01	8,88178419700125000E-16	4,3750000	-55,129283016945000000	-15,69247784
	2,16992500	-52,169925	1,973729821555830000E-16	-5,000000000000000000E+01	8,88178419700125000E-16	4,5000000	-55,169925001442300000	-15,7047123
	2,20945337	-52,209453	1,920385772324590000E-16	-5,000000000000000000E+01	8,88178419700125000E-16	4,6250000	-55,209453365629000000	-15,71661152
	2,24792751	-52,247928	1,869849304631840000E-16	-5,000000000000000000E+01	8,88178419700125000E-16	4,7500000	-55,247927513443600000	-15,72819339
	2,28540222	-52,285402	1,821904450666920000E-16	-5,000000000000000000E+01	8,88178419700125000E-16	4,8750000	-55,285402218862200000	-15,7394744
	2,32192809	-52,321928	1,776356839400250000E-16	-5,000000000000000000E+01	8,88178419700125000E-16	5,0000000	-55,321928094887400000	-15,75046979
	2,35755200	-52,357552	1,733031062829510000E-16	-5,000000000000000000E+01	8,88178419700125000E-16	5,1250000	-55,357552004618100000	-15,76119365
	2,39231742	-52,392317	1,691768418476430000E-16	-5,000000000000000000E+01	8,88178419700125000E-16	5,2500000	-55,392317422778800000	-15,77165909
	2,42626475	-52,426265	1,652424966883950000E-16	-5,000000000000000000E+01	8,88178419700125000E-16	5,3750000	-55,426264754702100000	-15,78187825
	2,45943162	-52,459432	1,614869854000230000E-16	-5,000000000000000000E+01	8,88178419700125000E-16	5,5000000	-55,459431618637300000	-15,79186247
	2,49185310	-52,491853	1,578983857244670000E-16	-5,000000000000000000E+01	8,88178419700125000E-16	5,6250000	-55,491853096329700000	-15,80162231
	2,52356196	-52,523562	1,544658121217610000E-16	-5,000000000000000000E+01	8,88178419700125000E-16	5,7500000	-55,523561956057000000	-15,81116763
	2,55458885	-52,554589	1,511793054808720000E-16	-5,000000000000000000E+01	8,88178419700125000E-16	5,8750000	-55,554588851677600000	-15,82050765
	2,58496250	-52,584963	1,480297366166880000E-16	-5,000000000000000000E+01	8,88178419700125000E-16	6,0000000	-55,584962500721200000	-15,82965103
	2,61470984	-52,614710	1,450087215836940000E-16	-5,000000000000000000E+01	8,88178419700125000E-16	6,1250000	-55,614709844115200000	-15,83860588
	2,64385619	-52,643856	1,421085471520200000E-16	-5,000000000000000000E+01	8,88178419700125000E-16	6,2500000	-55,643856189774700000	-15,8473798
	2,67242534	-52,672425	1,393221050510000000E-16	-5,000000000000000000E+01	8,88178419700125000E-16	6,3750000	-55,672425341971500000	-15,85597997
	2,70043972	-52,700440	1,366428338000190000E-16	-5,000000000000000000E+01	8,88178419700125000E-16	6,5000000	-55,700439718141100000	-15,86441314
	2,72792045	-52,727920	1,340646671245470000E-16	-5,000000000000000000E+01	8,88178419700125000E-16	6,6250000	-55,727920454563200000	-15,87268567
	2,75488750	-52,754888	1,315819881037220000E-16	-5,000000000000000000E+01	8,88178419700125000E-16	6,7500000	-55,754887502163500000	-15,88080356
	2,78135971	-52,781360	1,291895883200180000E-16	-5,000000000000000000E+01	8,88178419700125000E-16	6,8750000	-55,781359713524700000	-15,88877249
	2,80735492	-52,807355	1,268826313857320000E-16	-5,000000000000000000E+01	8,88178419700125000E-16	7,0000000	-55,807354922057600000	-15,89659782
	2,83289001	-52,832890	1,246566203087890000E-16	-5,000000000000000000E+01	8,88178419700125000E-16	7,1250000	-55,832890014164700000	-15,90428465
	2,85798100	-52,857981	1,225073682345000000E-16	-5,000000000000000000E+01	8,88178419700125000E-16	7,2500000	-55,857980995127600000	-15,91183779
	2,88264305	-52,882643	1,204309721627290000E-16	-5,000000000000000000E+01	8,88178419700125000E-16	7,3750000	-55,882643049361800000	-15,91926181
	2,90689060	-52,906891	1,184237892933500000E-16	-5,000000000000000000E+01	8,88178419700125000E-16	7,5000000	-55,906890595608500000	-15,92656105
	2,93073734	-52,930737	1,164824156983770000E-16	-5,000000000000000000E+01	8,88178419700125000E-16	7,6250000	-55,930737337562900000	-15,93373963
	2,95419631	-52,954196	1,146036670580810000E-16	-5,000000000000000000E+01	8,88178419700125000E-16	7,7500000	-55,954196310386900000	-15,94080149
	2,97727992	-52,977280	1,127845612317620000E-16	-5,000000000000000000E+01	8,88178419700125000E-16	7,8750000	-55,977279923499900000	-15,94775035
	3,00000000	-52,000000	2,220446049250310000E-16	-4,900000000000000000E+01	1,77635683940025000E-15	8,0000000	-56,000000000000000000	-15,65355977

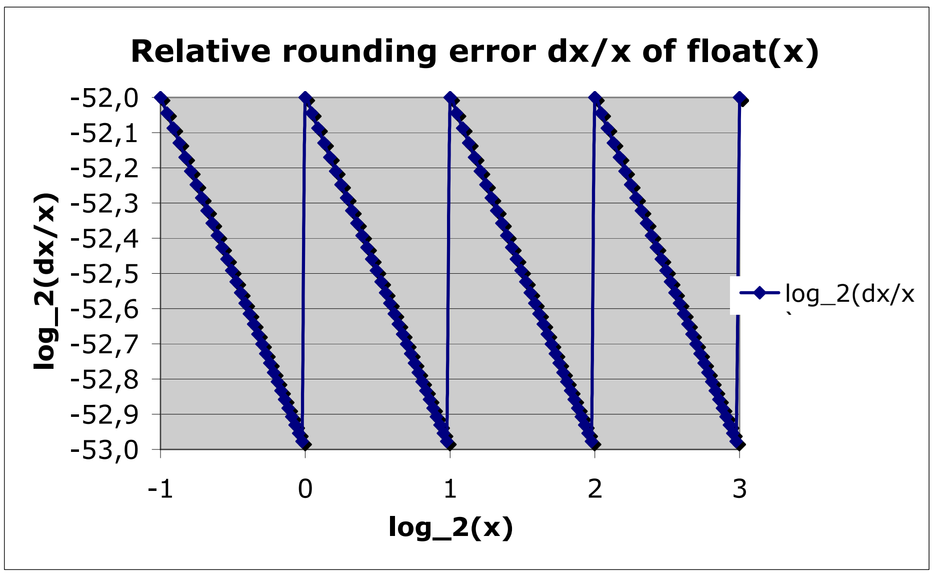

Saw tooth graph

illustrates that the relative rounding error decreases from a top value, for decimal increases of x, until log2(x) increases by 1. Then initializes again to the top value and decreases.
The pattern is repeated all the way, as x increases.

APPENDIX G

Vector Java class

This class is a package or methods for calculating vector quantities, which can be included in a Java implementation for gravity and magnetics.

```
import java.lang.Math;
import java.math.BigDecimal;
/**
 * <p>Title: Gravity anomally calculations</p>
 * <p>Description: Classes and operations for calculating gravity</p>
 * <p>Copyright: Copyright (c) 2006</p>
 * <p>Company: C.P.Anastasiades Ph.D</p>
 * @author Costas
 * @version 1.0
 */

/**
  * <p>Title: Polyhedron project</p>
  * <p>Description: Ph.D thesis project</p>
  * <p>Copyright: Copyright (c) 2005</p>
  * <p>Company: </p>
  * @author Costas P.Anastasiades
  * @version 1.1 extensively modified by H Holstein, 20th Feb 2006
  *

/** constructors for the class vector
  */

  public class vector {
    //count metrics ABC

    static int Counta=0,Countb=0,Countc=0;
     double x, y, z;
```

```
     double large = 1.0e+38;

    // totaly new vector
    public vector(double x, double y, double z) {
      this.x=x;
     this.y=y;
     this.z=z;

    }

    // totaly new vector
  public vector(double c) {
      this.set(c);
    }

    // new vector as clone of existing one
    public vector(vector v1) {
      this.x=v1.x;
      this.y=v1.y;
      this.z=v1.z;
    }

   // set all components to the same value c
    public void set(double c) {
      this.x=c;
      this.y=c;
      this.z=c;
    }

    public void set(double x, double y, double z) {
      this.x=x;
      this.y=y;
      this.z=z;
    }

    public void set(vector v1) {
      this.x=v1.x;
      this.y=v1.y;
      this.z=v1.z;
    }

/** dot calculates the dot product of two vectors v1 and v2
  * @param v1 is the first vector operand
  * @param v2 is the second vector operand
```

```
  * @returns the vector double result for v1 + v2
  */
    public static double dot(vector v1, vector v2)
    {
      return(v1.x*v2.x +v1.y*v2.y + v1.z*v2.z);
    }

/** magnitude calculates the magnitude of a vector
  * in the range -pi/2 to +pi/2
  * @param ()
  * @returns the double result for this magnitude of this
  */
   public static double magnitude(vector v)
   {
   return(Math.sqrt(v.x*v.x + v.y*v.y + v.z*v.z));
   }

/** maxComponent calculates the maximum absolute value of the
  * three components of this vector
  * @param ()
  * @returns the double result
  */
    public double maxComponent()
    {
        double max, tmp;
        max = Math.abs(this.x);
        tmp = Math.abs(this.y); if (max<tmp) max=tmp;
        tmp = Math.abs(this.z); if (max<tmp) max=tmp;
        return(max);
    }

/** angle calculates the radian angle between two vectors v1 and v2
  * in the range -pi/2 to +pi/2
  * @param v1 is the first vector operand
  * @param v2 is the second vector operand
  * @returns the double result
  */
  //  public static double angle(vector v1, vector v2)
    //{
      //  double result;
        //  result =
          //( dot(v1,v2) / (v1.magnitude() * v2.magnitude()) );
        // Note: |result| can exceed 1.0 on account of rounding
        //if (Math.abs(result)>1.0) result=Math.signum(result);
```

```
        //return(Math.acos(result));
    //}

/** multiply a vector (this) by a scalar s
  * @param s is the scaling factor argument
  * @return this - original vector multiplied by s
 */
  public void mulScalar(double s)
  {
     this.x *= s;
     this.y *= s;
     this.z *= s;
  }

/** multiply a vector v by a scalar s
  * @param v is vector to be scaled
  * @param s is the scaling factor argument
  * @return v*s as a new vector
 */
  public static vector mulScalar(vector v, double s)
  {
  vector newOne = new vector(v);
  newOne.mulScalar(s);
  return newOne;
  }

/** divide a vector(this) by a scalar s
  * Check for possible overflow - print warning if found
  * @param s is the scaling factor argument
  * @return this - original vector divided by s
 */
  public void divScalar(double s)
  {
        double tmp = Math.abs(s);
  // test for possible overflow
  if (tmp<1.0){
        if (s*large<this.maxComponent())
        System.err.println("*** Overflow from divScalar");
        }
     this.x /= s;
     this.y /= s;
     this.z /= s;
  }//abc(0,0,6)
```

```
//  public  vector divScalar(double n)
//  {
//  return new vector(this.x/n,this.y/n,this.z/n);
//
//  }


/** divide a vector v by a scalar s
  * @param v is vector argument
  * @param s is the scaling factor argument
  * @return v/s as a new vector
 */
  public static vector divScalar(vector v, double s)
  {
  vector newOne = new vector(v);
  newOne.divScalar(s);
  return newOne;//abc(0,0,8)
  }

/** cross product of two vectors v1 and v2
  * @param v1 is the first vector argument
  * @param v2 is the second vector argument
  * @return v1 cross v2 as a new vector
 */
  public static vector cross(vector v1,vector v2)
  {
  return new
  vector((v1.y*v2.z-v1.z*v2.y),
         (v1.z*v2.x-v1.x*v2.z),
         (v1.x*v2.y-v1.y*v2.x));
  }

/** vector adition of this and v
  * @param v is the vector argument
  * @return this + v, result in this
 */
  public void addVec(vector v)
  {
  this.x += v.x;
  this.y += v.y;
  this.z += v.z;
  }

/** vector addition of two vectors v1 and v2
```

```
  * @param v1 is the first vector argument
  * @param v2 is the second vector argument
  * @return v1 + v2 as a new vector
 */
  public static vector addVec(vector v1, vector v2)
  {
  vector newOne = new vector(v1);
  newOne.addVec(v2);
  return newOne;
  }

/** vector subtraction of this and v
  * @param v is the vector argument
  * @return this - v, result in this
 */
  public void subVec(vector v)
  {
  this.x -= v.x;
  this.y -= v.y;
  this.z -= v.z;
  }

/** vector subtraction of two vectors v1 and v2
  * @param v1 is the first vector argument
  * @param v2 is the second vector argument
  * @return v1 + v2 as a new vector
 */
  public static vector subVec(vector v1, vector v2)
  {
  vector newOne = new vector(v1);
  newOne.subVec(v2);
  return newOne;
  }

/** negation of this vector
  * @return -this, result in this
 */
  public void negVec()
  {
  this.x = -this.x;
  this.y = -this.y;
  this.z = -this.z;
  }
```

```
/** negation of a vector v
  * @param v
  * @return -v, result in a new vector
 */
  public static vector negVec(vector v)
  {
  vector newOne = new vector(v);Countc++;
  newOne.negVec();Countc++;
  return newOne;
  }

/** add a scaled version of another vector to this
  * @param v2 is the vector to be scaled
  * @param s is the scaling factor
  * @return this + v2*s as this
 */
    public void addScaled(vector v2, double s) {
        this.addVec(vector.mulScalar(v2,s));
    }

/** add a scaled version of a vector to another vector v1
  * @param v1 is the vector to be added to
  * @param v2 is the vector to be scaled
  * @param s is the scaling factor
  * @return v1 + v2*s as a new vector
 */
    public static vector addScaled(vector v1, vector v2, double s) {
        vector newOne = new vector(v1);Countc++;
        newOne.addVec(vector.mulScalar(v2,s));Countc++;
        return newOne;
    }

public static boolean equalVectors(vector a,vector b)
{
if (a.x==b.x&&a.y==b.y&&a.z==b.z)return true;
  return false;
}
public static boolean NotEqualVectors(vector a,vector b)
{
if (a.x==b.x&&a.y==b.y&&a.z==b.z)return false;
  return true;
}

  public String toString() {
```

```
  return "[" + this.x + ", " + this.y + ", " + this.z + "]";
  }

//implements the vector X vector operation and returns a matrix 3X3.
public static double[][] MulVec(vector a,vector b)
{double[][] ret=new double[3][3];
  ret[0][0]=a.x*b.x;
  ret[0][1]=a.y*b.x;
  ret[0][2]=a.z*b.x;
  ret[1][0]=a.x*b.y;
  ret[1][1]=a.y*b.y;
  ret[1][2]=a.z*b.y;
  ret[2][0]=a.x*b.z;
  ret[2][1]=a.y*b.z;
  ret[2][2]=a.z*b.z;
  return ret;

}
//implements addition between 2 matrices 3X3
public static double[][] addMatrix(double a[][],double b[][])
   {double c[][]=new double [3][3];
   for (int i=0;i<3;i++)
     for (int j=0;j<3;j++)
       c[i][j]=a[i][j]+b[i][j];
     return c;
}
}
}
```

APPENDIX H

Power series expansions

For $|x| < 1$

$$
\begin{aligned}
&1/(1-x) = 1 + x + x^2 + x^3 + x^4 + x^5 + ...\\
&= 1 + x + x^2 + x^3 + O(x^4)\\
&= 1 + x + x^2 + O(x^3)\\
&= 1 + x + O(x^2)\\
&= 1 + O(x)
\end{aligned}
\tag{H.1}
$$

How many terms will be included before the truncation takes over, depends from our needs and the application. We can see the limit of 1/(1-x) as $x \to 0$ is 1.
In terms of calculations if

$$1/(1-x) = 1/(0.9) = 1.1111111111111111 \tag{H.2}$$

the series development is

$$
\begin{aligned}
1/(0.9) &= 1 + (0.1) + (0.1)^2 + (0.1)^3 + (0.1)^4 + (0.1)5 + (0.1)^6\\
&= 1 + 0.1 + 0.01 + 0.001 + 0.0001 + 0.00001 + 0.000001 = 1.11111 + O(0.000001)
\end{aligned}
\tag{H.3}
$$

In the other cases, we get

$$
\begin{aligned}
&1/(0.9) = 1 + (0.1) + (0.1)^2 + (0.1)^3 + (0.1)^4 + O((0.1)^5) = 1.1111 + O(0.00001)\\
&1/(0.9) = 1 + (0.1) + (0.1)^2 + (0.1)^3 + O((0.1)^4) = 1.111 + O(0.0001)\\
&1/(0.9) = 1 + (0.1) + (0.1)^2 + O((0.1)^3) = 1.11 + O(0.001)\\
&1/(0.9) = 1 + (0.1) + O((0.1)^2) = 1.1 + O(0.01)\\
&1/(0.9) = 1 + O(0.1)
\end{aligned}
\tag{H.4}
$$

APPENDIX I

Computation quantities

I.1 Quantities of Vertex,Line,Surface method

I.1.1 ΛLambda

$$\Lambda_{ij} = \frac{\Lambda_{ij}}{(r_1 + r_2)_{ij}} \tag{I.1}$$

I.1.2 mid r_{ij}, position vector

$$r_{mij} = \frac{1}{2}(r_{1ij} + r_{2ij}) \tag{I.2}$$

I.1.3 λambda

$$\begin{aligned}
\lambda_{ij} &= \frac{h_{ij}\Lambda_{ij}}{|u_i| + \Sigma_{ij}} \\
\lambda^*_{ij} &= \frac{h_{ij}\Lambda^*_{ij}}{|u_i| + \Sigma^*_i} \\
\tilde{\lambda_{ij}} &= \frac{\lambda^*_{ij} r_c}{|u_i| + \Sigma_{ij}}
\end{aligned} \tag{I.3}$$

I.1.4 ΣSigma

$$\begin{aligned}
&\Sigma_{ij} = \frac{1}{2}(r_{ij1} + r_{ij2} - Lij\Lambda_{ij}) \\
&\Sigma^*_i = r_c
\end{aligned} \tag{I.4}$$

I.1.5 Functions Atnh and Atn are defined by the delayed arctanh and arctan series

$$\begin{aligned} \text{Atnh} &= \frac{1}{3} + \frac{x^2}{5} + \frac{x^4}{7} + ... \\ \text{Atn} &= -\frac{1}{3} + \frac{x^2}{5} - \frac{x^4}{7} + ... \end{aligned} \tag{I.5}$$

I.2 Stabilized quantities

I.2.1 Λambdas

$$\begin{aligned} \delta\Lambda_j &= \Lambda_j \overline{\Delta}_j \\ \Lambda_j^* &= L_j/(2r_c) \end{aligned} \tag{I.6}$$

I.2.2 λambdas

$$\begin{aligned} \delta\lambda_j &= (\lambda_j + \tilde{\lambda}_j)\overline{\Delta}_j + \tilde{\lambda}_j \Lambda_j \Lambda_j^* \\ \lambda_j^* &= h_j \Lambda_j^* / \tilde{r}_c \\ \tilde{\lambda}_j &= r_c \lambda_j^* / \tilde{r}_j \end{aligned} \tag{I.7}$$

I.2.3 Δeltas

$$\begin{aligned} \Delta_{ij} &= \frac{(\mathbf{r}_c - \mathbf{r}_1) \cdot (\mathbf{r}_c + \mathbf{r}_1)}{2r_c(r_c + r_1)} + \frac{(\mathbf{r}_c - \mathbf{r}_2) \cdot (\mathbf{r}_c + \mathbf{r}_2)}{2r_c(r_c + r_2)} \\ \overline{\Delta}_j &= \frac{1}{2}(\Delta_{j1} + \Delta_{j2}) \\ \Delta_{jk} &= \left(\frac{\mathbf{R}_c - \mathbf{R}_{jk}}{r_c} \right) \cdot \left(\frac{\mathbf{r}_c + \mathbf{r}_{jk}}{r_c + r_{jk}} \right), k = 1, 2 \end{aligned} \tag{I.8}$$

I.2.4 Centroid position vector r_c

$$\tilde{r}_c = r_c + |\upsilon| \tag{I.9}$$

I.2.5 Stabilized 2nd order differences ($O(\gamma^3)$)

$$
\begin{aligned}
&\delta^2\Lambda_j = \frac{1}{2}\left(\Lambda_j + \Lambda_j^*\right)\delta\overline{\Delta}_j + \frac{1}{2}\delta\Lambda_j\left(\overline{\Delta}_j + \overline{\Delta}_j^*\right) \text{ (B-1)}\\
&\delta^2\lambda_j = \frac{1}{2}\left(\delta\lambda_j + \delta\tilde{\lambda}_j\right)\\
&\left(\overline{\Delta}_j + \overline{\Delta}_j^*\right) + \frac{1}{2}\left(\lambda_j + \lambda_j^* + \tilde{\lambda}_j + \tilde{\lambda}_j^*\right)\delta\overline{\Delta}_j +\\
&\tilde{\lambda}_j\Lambda_j\Lambda_j^* \text{ (B-2))where}\\
&\delta\overline{\Delta}_j = \frac{1}{2}\left(\delta\Delta_{j1} + \delta\Delta_{j2}\right) \text{(B-3)}\\
&\delta\Delta_{jk} = -\frac{1}{2}\left(\left(\mathbf{r}_c - \mathbf{R}_{jk}\right)/r_c\right)^2 + \frac{1}{2}\Delta_{jk}^2 \text{(B-4)}\\
&\overline{\Delta}_j^* = \left(\mathbf{R}_c - \overline{\mathbf{R}}_j\right)\cdot\mathbf{r}_c/r_c^2 \text{(B-5)}\\
&\delta\Lambda_j^* = \Lambda_j^*\Delta_j^* \text{(B-6)}\\
&\tilde{\lambda}_j^* = \lambda_j^* r_c/\tilde{r}_c \text{(B-7)}\\
&\delta\lambda_j^* = \left(\lambda_j^* + \tilde{\lambda}_j^*\right) \text{(B-8)}\\
&\delta\tilde{\lambda}_j = \tilde{\lambda}_j^*\left(\overline{\Delta}_j r_c + \Lambda_j^2\tilde{r}_j\right) \text{(B-9)}
\end{aligned}
\tag{I.10}
$$

I.2.6 Sheet centroid offset

$$
\begin{aligned}
&\mathbf{r}_{ic}, \mathbf{r}_p >= \frac{\mathbf{r}_{ic}}{r_p^3} - \frac{\mathbf{r}_p}{r_p^3}\\
&= \frac{1}{2}\left(\mathbf{r}_{ic} - \mathbf{r}_p\right)\left(\frac{1}{r_{ic}^3} + \frac{1}{r_p^3}\right) +\\
&= \frac{1}{2}\left(\mathbf{R}_{ic} - \mathbf{R}_p\right)\left(\frac{1}{r_{ic}^3} + \frac{1}{r_p^3}\right) - \frac{1}{2}\left(\mathbf{r}_{ic} + \mathbf{r}_p\right)\frac{\delta r_{icp}}{r_{ic} r_p}\\
&X\left(\frac{1}{r_{ic}^2} + \frac{1}{r_{ic} r_p} + \frac{1}{r_p^2}\right) \text{(C-1)and}\\
&\frac{1}{2}\left(\mathbf{r}_{ic} + \mathbf{r}_p\right)\frac{1}{r_{ic}^3} - \frac{1}{r_p^3}\delta r_{icp} = r_{ic} - r_p\\
&= \left(\mathbf{R}_{ic} - \mathbf{R}_p\right)\cdot\left(\frac{\mathbf{r}_{ic} + \mathbf{r}_p}{r_p + r_{ic}}\right) \text{(C-2)}
\end{aligned}
\tag{I.11}
$$

I.3 Equations

I.3.1 Line method, gravity potential, Strakhov variant-$O(\gamma)$,chapter 6

$$\sum b_{ij} = 2 * \sum_i \upsilon_i * \left(\left(\sum_j h_{ij} * \text{arctanh}(\Lambda_{ij}) \right) - \upsilon_i * \left(\sum_j \text{arctan}(\lambda_{ij}) \right) \right) \tag{I.12}$$

I.3.2 Line method,gravity potential, Oesterom variant-$O(\gamma)$,chapter 6

$$\sum b_{ij} = 2 \sum_i \upsilon_i * \left(\left(\sum_j (h_{ij} * \text{arctanh}\,(\Lambda_{ij})) \right) - |\upsilon_i| * (\Omega_i/2) \right) \tag{I.13}$$

I.3.3 Line method,gravity field, Strakhov variant-$O(\gamma)$,chapter 6

$$\sum \mathbf{b}_{ij} = 2 \sum_j \mathbf{h}\text{arctanh}\Lambda - 2 \sum_j \tilde{\mathbf{n}}\text{arctan}\lambda \tag{I.14}$$

I.3.4 Surface method, gravity potential,Strakhov variant-$O(\gamma^2)$,chapter 6

$$\begin{aligned}\sum \mathbf{b}_{ij}/2 = \frac{A_i}{r_c + \upsilon} &+ \sum_j \left(h\Lambda^3 \text{Atnh}\Lambda - |\upsilon| \lambda^3 \text{Atn}\lambda \right) \\ &+ \sum_j \left(h\Lambda\Delta - |\upsilon| \left(\left(\lambda + \widetilde{\lambda} \right) \Delta + \widetilde{\lambda}\Lambda\Lambda^* \right) \right)\end{aligned}$$

I.3.5 Surface method,gravity potential, Oesterom variant-$O(\gamma^2)$,chapter 6

$$\begin{aligned}&\sum \mathbf{b}_{ij} = 2 \sum_j (h_{ij} \Lambda_{ij}^3 \text{Atnh}\Lambda_{ij}) \\ &+ 2 \sum_j (h_{ij} \Lambda_{ij} \Delta_{ij}) - 2 \sum_i |\upsilon_i| * [\text{Solid Angle}] + \frac{2A_i}{r_c + |u_i|}\end{aligned} \tag{I.15}$$

I.3.6 b_{ij}-volume method-chapter 12

$$
\begin{aligned}
&\sum_j \mathbf{b}_{ij} = \sum_j \delta\mathbf{b}_{ij} + \sum_j \mathbf{b}^*_{ij}\text{eq.8} \\
&\sum_j \mathbf{b}_j = \sum_j \delta\mathbf{b}^*_j - A\mathbf{r}_c/r_c^3\text{e.17} \\
&\mathbf{b}^*_{ij} = 2\mathbf{h}_j\Lambda^*_j - 2\tilde{\mathbf{n}}\lambda_j\text{eq.9} \\
&\delta\mathbf{b}_{ij} = \mathbf{b}_{ij} - \mathbf{b}^*_{ij} = 2\mathbf{h}\left(\Lambda^3\text{Atnh}\Lambda + \delta\Lambda\right) + \left(\lambda^3\text{Atn}\lambda + \delta\lambda\right)\text{eq.12} \\
&\sum_j \mathbf{b}_{ij}* = -2\tilde{\mathbf{n}}A/(r_c\tilde{r}_c)\text{eq.13} \\
&\delta\mathbf{b}^*_{ij} = 2\mathbf{h}\left(\Lambda^3\text{Atnh}\Lambda + \delta^2\Lambda\right) + \left(\lambda^3\text{Atn}\lambda + \delta^2\lambda\right)\text{eq.18}
\end{aligned}
\tag{I.16}
$$

I.3.7 Gravity field-volume method-chapter 12

$$
\sum \mathbf{b}_{ij} = \sum_i \mathbf{n}_i\mathbf{A}_i\mathbf{r}_{ic}/r_{ic}^3 = \sum_i \mathbf{n}_i\mathbf{A}_i(\mathbf{r}_p/r_p^3 + < \mathbf{r}_{ic}, \mathbf{r}_{ip} >). \tag{I.17}
$$

I.3.8 Measure of the relative closeness of the polyhedral and points source magnetic anomalies

$$
\text{relative difference} = max\frac{||\mathbf{a}_{poly} - \mathbf{a}_{point}||}{||\mathbf{a}_{point}||}, \epsilon \tag{I.18}
$$

APPENDIX J

Steps in the implementation of the surface method(H.Holstein)

To simplify the implementation of the surface method the process starting from the Line method is analysed in several steps. Through a stepwise refinement starting from the Line method, pre-cancelling of large terms, takes place before computation. This way less precision is required from complex operations in terms of magnitudes.

Step 1
Starting with Line method

$$\frac{1}{2}\sum_j c_{ij} = \sum_j h_{ij}\text{arctanh}\Lambda_{ij} - |u_i|\text{arctan }\lambda_{ij}$$

Step 2
Differencing log and arctan terms
and adding back-on the remaining offset

$$\frac{1}{2}\sum_j c_{ij} = \sum_j h_{ij}(\text{arctanh}\Lambda_{ij} - \Lambda_{ij}) - |u_i|(\text{arctan}\lambda_{ij} - \lambda_{ij}) + \sum_j h_{ij}\Lambda_{ij} - |u_i|\lambda_{ij}$$

Step 3
Substituting differences using custom functions Atnh() and Atn()defined by delayed arctanh and arctan series

arctanh$\Lambda_{ij} - \Lambda_{ij}$ by
Λ_{ij}^3AtnhΛ_{ij}

where $\text{Atnh}\Lambda_{ij} = \frac{1}{3} + \frac{\Lambda_{ij}^2}{5} + \frac{\Lambda_{ij}^4}{7}$
$\text{arctanh}\lambda_{ij} - \lambda_{ij}$ by
$\lambda_{ij}^3 \text{Atn}\lambda_{ij}$
where $\text{Atn}\lambda_{ij} = -\frac{1}{3} + \frac{\Lambda_{ij}^2}{5} - \frac{\Lambda_{ij}^4}{7}$Hence

$$\frac{1}{2}\sum_j c_{ij} = \sum_j (h_{ij}\Lambda_{ij}^3 Atnh\Lambda_{ij} - |u_i|\lambda_{ij}^3 Atn\lambda_{ij}) + \sum_j h_{ij}\Lambda_{ij} - |u_i|\lambda_{ij}$$

Step 4

Introduce quantities $\Lambda_{ij}^*, \lambda_{ij}^*$ to express offset $\Lambda_{ij}, \lambda_{ij}$as defined in the 1999 paper, equation(59),(60)

Hence

$$\frac{1}{2}\sum_j c_{ij} = \sum_j (h_{ij}\Lambda_{ij}^3 Atnh\Lambda_{ij} - |u_i|\lambda_{ij}^3 Atn\lambda_{ij}) + \sum_j h_{ij}(\Lambda_{ij} - \Lambda_{ij}^*) - |u_i|(\lambda_{ij} - \lambda_{ij}^*) + \sum_j (h_{ij}\Lambda_{ij}^* - |u_i|\lambda_{ij}^*)$$

Step 5

Express the final sum by its analytical equivalent

$$\frac{1}{2}\sum_j c_{ij} = \sum_j (h_{ij}\Lambda_{ij}^3 Atnh\Lambda_{ij} - |u_i|\lambda_{ij}^3 Atn\lambda_{ij}) + \sum_j h_{ij}(\Lambda_{ij} - \Lambda_{ij}^*) - |u_i|(\lambda_{ij} - \lambda_{ij}^*) + \frac{2A_i}{r_c+|u_i|}$$

where A_i is the scalar area of facet i. (Note that the cross-product formula for the (vector) area naturally calculates the facet area).

Step 6

We find expressions for differenced quantities $\Lambda_{ij} - \Lambda_{ij}^*$ and $\lambda_{ij} - \lambda_{ij}^*$ such that a vector $\vec{r}_c$ common to the whole target substitutes vectors $\vec{r}_1$, $\vec{r}_2$.

$$\Lambda_{ij} - \Lambda_{ij}^* = \Lambda_{ij}\Delta_{ij}$$

$$\lambda_{ij} - \lambda_{ij}^* = (\lambda_{ij} + \tilde{\lambda_{ij}})\Delta_{ij} + \tilde{\lambda_{ij}}\Lambda_{ij}\Lambda_{ij}^*$$

Step 7

Final step, substitution of differences

$$\sum_j c_{ij} = 2\sum_j (h_{ij}\Lambda_{ij}^3 Atnh\Lambda_{ij} - |u_i|\lambda_{ij}^3 Atn\lambda_{ij})$$
$$+ 2\sum_j (h_{ij}\Lambda_{ij}\Delta_{ij} - |\upsilon_i|(\lambda_{ij} + \tilde{\lambda}_{ij})\Delta ij + \tilde{\lambda}_{ij}\Lambda_{ij}\Lambda_{ij}^*)$$
$$+ \sum_i \frac{2A_i}{r_c|\upsilon_i|}$$

The last final expression gives the Surface method error growth and can be implemented without bugs, in a step by step refinement process, as indicated with the above sequence. Analytical cancellation gives results validating the theoretical error growth at the last step of the implementation.

Explanation of the quantities used

r_c is a vector that represents a common for the whole target quantity, for example the position vector of the first vertex of the first facet, kept constant to replace all r_{ij} position vectors for all extrinsic compuatations of one target.

$$\Lambda_{ij} = \frac{\Lambda_{ij}}{(r_1+r_2)_{ij}}$$
$$r_{mij} = \frac{1}{2}(r_{1ij} + r_{2ij})$$

$$\Lambda_{ij} = \frac{L_{ij}}{2r_{mij}}$$
$$\Lambda_{ij}^* = \frac{L_{ij}}{2r_c}$$

$$\Sigma_{ij} = \frac{1}{2}(r_{ij1} + r_{ij2} - Lij\Lambda_{ij})$$

$$\lambda_{ij} = \frac{h_{ij}\Lambda_{ij}}{|u_i|+\Sigma_{ij}}$$

$$\Sigma_i^* = r_c$$

$$\Delta_{ij} = \frac{(r_c-r_1)(r_c+r_1)}{2r_c(r_c+r_1)} + \frac{(r_c-r_2)(r_c+r_2)}{2r_c(r_c+r_2)}$$

$$\lambda_{ij}^* = \frac{h_{ij}\Lambda_{ij}^*}{|u_i|+\Sigma_i^*}$$

$$\tilde{\lambda}_{ij} = \frac{\lambda_{ij}^* r_c}{|u_i|+\Sigma_{ij}}$$

Functions Atnh and Atn are defined by the delayed arctanh and arctan series:

Atnh=$\frac{1}{3}+\frac{x^2}{5}+\frac{x^4}{7}+....$
Atn=$-\frac{1}{3}+\frac{x^2}{5}-\frac{x^4}{7}+....$

APPENDIX K

Test Data:Receding Edge case, plots:Du,Ds

RECEDING EDGE case, PLOTS :Du, Ds

D_u evaluation $D_u=||\mathbf{r}_2-\mathbf{r}_1||$

r_i formulae $\mathbf{r}_i=\mathrm{sqrt}(\boldsymbol{\rho}_i\ .\ \boldsymbol{\rho}_i\ -2\boldsymbol{\rho}_{i\ .}\ \mathrm{LLhat}+L^2)$

$\mathbf{r}_i/L=\mathrm{sqrt}(\boldsymbol{\rho}_i/L\ .\ \boldsymbol{\rho}_i/L\ -2\boldsymbol{\rho}_{i\ .}\ \mathrm{Lhat}/L+1)$

epsilon 2,22E-16

Local vectors	x	y	z	Dlim	-60,8112
ρ1	53,00	25,00	0,00	ρ1 dot ρ1	3434
ρ2	109,00	-5,00	0,00	ρ2 dot ρ2	11906
Lhat	0,7071	-0,70710678	0	edge	63,52952
ρ2-ρ1	56,00	-30,00	0,00	ρ1	58,60034

L	L/E	L^2	LLhat.x	LLhat.y	r1.x	r1.y	r2.x	r2.y
1	0,015740714	1	0,70710678	-0,707106781	52,29	25,71	108,29	-4,29
10	0,157407138	100	7,07106781	-7,071067812	45,93	32,07	101,93	2,07
100	1,574071375	10000	70,7106781	-70,71067812	-17,71	95,71	38,29	65,71
1000	15,74071375	1000000	707,106781	-707,1067812	-654,11	732,11	-598,11	702,11
10000	157,4071375	100000000	7071,06781	-7071,067812	-7018,07	7096,07	-6962,07	7066,07
100000	1574,071375	1E+10	70710,6781	-70710,67812	#######	70735,68	########	70705,68
1000000	15740,71375	1E+12	707106,781	-707106,7812	#######	########	########	########
10000000	157407,1375	1E+14	7071067,81	-7071067,812	#######	########	########	########
100000000	1574071,375	1E+16	70710678,1	-70710678,12	#######	########	########	########
1000000000	15740713,75	1E+18	707106781	-707106781,2	#######	########	########	########
1E+10	157407137,5	1E+20	7071067812	-7071067812	#######	########	########	########
1E+11	1574071375	1E+22	7,0711E+10	-70710678119	#######	########	########	########
1E+12	15740713751	1E+24	7,0711E+11	-7,07107E+11	#######	########	########	########
1E+13	1,57407E+11	1E+26	7,0711E+12	-7,07107E+12	#######	########	########	########
1E+14	1,57407E+12	1E+28	7,0711E+13	-7,07107E+13	#######	########	########	########
1E+15	1,57407E+13	1E+30	7,0711E+14	-7,07107E+14	#######	########	########	########
1E+16	1,57407E+14	1E+32	7,0711E+15	-7,07107E+15	#######	########	########	########
1E+17	1,57407E+15	1E+34	7,0711E+16	-7,07107E+16	#######	########	########	########
1E+18	1,57407E+16	1E+36	7,0711E+17	-7,07107E+17	#######	########	########	########
1E+19	1,57407E+17	1E+38	7,0711E+18	-7,07107E+18	#######	########	########	########
1E+20	1,57407E+18	1E+40	7,0711E+19	-7,07107E+19	#######	########	########	########
1E+21	1,57407E+19	1E+42	7,0711E+20	-7,07107E+20	#######	########	########	########

||r1||	||r2||	Du	log10(L/E)	log10(abs(Du-Dlim)/E)
58,27008	108,3779	50,108	-1,8029756	0,242030575
56,01803	101,95	45,932	-0,8029756	0,225364311
97,33551	76,05239	-21,28	0,19702442	-0,206070119
981,7515	922,3262	-59,43	1,19702442	-1,661245057
9980,353	9919,662	-60,69	2,19702442	-2,723096077
99980,22	99919,42	-60,8	3,19702442	-3,729301208
999980,2	999919,4	-60,81	4,19702442	-4,729921898
9999980	9999919	-60,81	5,19702442	-5,729984499
99999980	99999919	-60,81	6,19702442	-6,729656549
1E+09	1E+09	-60,81	7,19702442	-7,722647604
1E+10	1E+10	-60,81	8,19702442	-8,173549059
1E+11	1E+11	-60,81	9,19702442	-7,008116724
1E+12	1E+12	-60,81	10,1970244	-6,110341633
1E+13	1E+13	-60,81	11,1970244	-4,831025497
1E+14	1E+14	-60,81	12,1970244	-3,616291721
1E+15	1E+15	-60,75	13,1970244	-3,340000392
1E+16	1E+16	-62	14,1970244	-1,868911714
1E+17	1E+17	0	15,1970244	-1,039383012
1E+18	1E+18	0	16,1970244	-0,018992125
1E+19	1E+19	0	17,1970244	-0,018992125
1E+20	1E+20	0	18,1970244	-0,018992125
1E+21	1E+21	0	19,1970244	-0,018992125

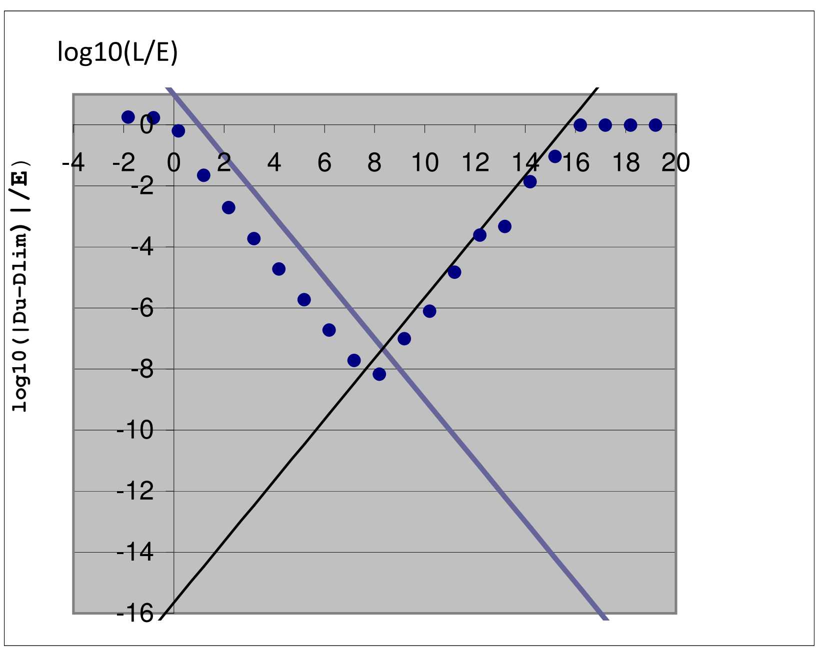

TREND LINES PLOTTING

DOWN		UP	
y	-x	y	log10(e)+x
-1,802975579	1,802976	-1,803	-17,456535
-0,802975579	0,802976	-0,803	-16,456535
0,197024421	-0,19702	0,197	-15,456535
1,197024421	-1,19702	1,197	-14,456535
2,197024421	-2,19702	2,197	-13,456535
3,197024421	-3,19702	3,197	-12,456535
4,197024421	-4,19702	4,197	-11,456535
5,197024421	-5,19702	5,197	-10,456535
6,197024421	-6,19702	6,197	-9,4565354
7,197024421	-7,19702	7,197	-8,4565354
8,197024421	-8,19702	8,197	-7,4565354
9,197024421	-9,19702	9,197	-6,4565354
10,19702442	-10,197	10,197	-5,4565354
11,19702442	-11,197	11,197	-4,4565354
12,19702442	-12,197	12,197	-3,4565354
13,19702442	-13,197	13,197	-2,4565354
14,19702442	-14,197	14,197	-1,4565354
15,19702442	-15,197	15,197	-0,4565354
16,19702442	-16,197	16,197	0,54346465
17,19702442	-17,197	17,197	1,54346465
18,19702442	-18,197	18,197	2,54346465
19,19702442	-19,197	19,197	3,54346465

Ds - stabilized variant = (Ds-Dlim)/E

evaluating expression

$$\boxed{(\rho_2 - \rho_1)\frac{\widetilde{\vec{r}_1} + \widetilde{\vec{r}_2}}{\widetilde{r}_1 + \widetilde{r}_2}}$$

l+vector_r1_curl)/(r2_curl+r1_curl)		Ds
x	y	
0,963622491	0,128499653	50,10786993
0,935998806	0,216133232	45,93193615
0,118685583	0,930983982	-21,28312684
-0,657648344	0,753232677	-59,42528756
-0,702518819	0,711664541	-60,69099009
-0,706651403	0,70756186	-60,79933438
-0,707061277	0,707152282	-60,80999999
-0,707102231	0,707111331	-60,81106488
-0,707106326	0,707107236	-60,81117135
-0,707106736	0,707106827	-60,811182
-0,707106777	0,707106786	-60,81118306
-0,707106781	0,707106782	-60,81118317
-0,707106781	0,707106781	-60,81118318
-0,707106781	0,707106781	-60,81118318
-0,707106781	0,707106781	-60,81118318
-0,707106781	0,707106781	-60,81118318
-0,707106781	0,707106781	-60,81118318
-0,707106781	0,707106781	-60,81118318
-0,707106781	0,707106781	-60,81118318
-0,707106781	0,707106781	-60,81118318
-0,707106781	0,707106781	-60,81118318
-0,707106781	0,707106781	-60,81118318

L/E	(Ds-Dlim)/E	log10(L/E)	log10(abs(Ds-Dlim)/E)
0,015740714	1,745945065	-1,802975579	0,242030575
0,157407138	1,680212886	-0,802975579	0,225364311
1,574071375	0,62219982	0,197024421	-0,206070119
15,74071375	0,021814986	1,197024421	-1,661245057
157,4071375	0,001891925	2,197024421	-2,723096077
1574,071375	0,000186509	3,197024421	-3,729301208
15740,71375	1,86242E-05	4,197024421	-4,72992187
157407,1375	1,86216E-06	5,197024421	-5,729983938
1574071,375	1,86213E-07	6,197024421	-6,729990145
15740713,75	1,86213E-08	7,197024421	-7,729990766
157407137,5	1,86213E-09	8,197024421	-8,729990831
1574071375	1,86213E-10	9,197024421	-9,7299907
15740713751	1,86213E-11	10,19702442	-10,7299894
1,57407E+11	1,86232E-12	11,19702442	-11,72994505
1,57407E+12	1,86221E-13	12,19702442	-12,72997114
1,57407E+13	1,8678E-14	13,19702442	-13,7286689
1,57407E+14	1,90136E-15	14,19702442	-14,72093645
1,57407E+15	1,11844E-16	15,19702442	-15,95138537
1,57407E+16	1,11844E-16	16,19702442	-15,95138537
1,57407E+17	1,11844E-16	17,19702442	-15,95138537
1,57407E+18	1,11844E-16	18,19702442	-15,95138537
1,57407E+19	1,11844E-16	19,19702442	-15,95138537

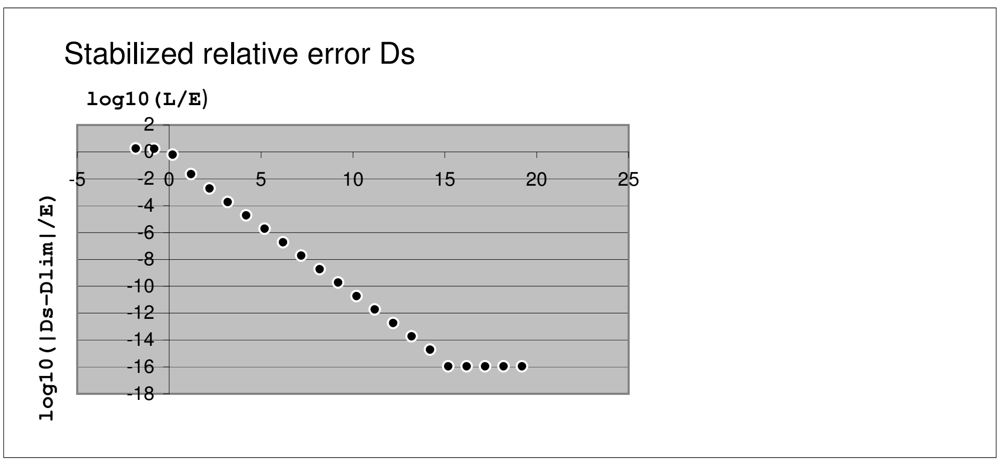

Testing the second order case : when 1. unit vector Lhat=$\rho_1+\rho_2/|\rho_1+\rho_2|$

2. unit vector Lhat=$\rho_1+\rho_2/|\rho_1+\rho_2|$

log10(L/E)	y
-1,8029756	0,20723911
-0,8029756	0,20550595
0,19702442	-0,4273147
1,19702442	-3,7889089
2,19702442	-5,8559565
3,19702442	-7,8623602
4,19702442	-9,8618816
5,19702442	-11,735272
6,19702442	-9,924026
7,19702442	-9,924026
8,19702442	-8,7551486
9,19702442	-6,7401781
10,1970244	-6,2686875
11,1970244	-5,8592354
12,1970244	-3,7373622
13,1970244	-2,812885
14,1970244	-1,5237066
15,1970244	-0,0877893
16,1970244	-0,0877893
17,1970244	-0,0877893
18,1970244	-0,0877893
19,1970244	-0,0877893

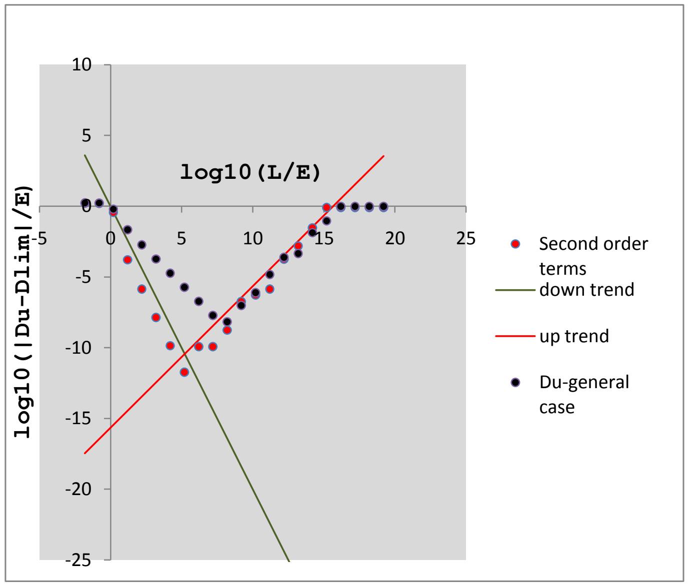

Trend line

x	y=-2x
-1,8029756	3,60595116
-0,8029756	1,60595116
0,19702442	-0,3940488
1,19702442	-2,3940488
2,19702442	-4,3940488
3,19702442	-6,3940488
4,19702442	-8,3940488
5,19702442	-10,394049
6,19702442	-12,394049
7,19702442	-14,394049
8,19702442	-16,394049
9,19702442	-18,394049
10,1970244	-20,394049
11,1970244	-22,394049
12,1970244	-24,394049
13,1970244	-26,394049
14,1970244	-28,394049
15,1970244	-30,394049
16,1970244	-32,394049
17,1970244	-34,394049
18,1970244	-36,394049
19,1970244	-38,394049

Evaluating term (ρ_i cross Lhat) in expression for β_i: when 1.Lhat=$\rho_1+\rho_2/|\rho_1+\rho_2|$			
unit vector Lhat			
0,99247	0,12253	0	
ρ_1 cross Lhat			|rho cross Lhat|
0	0	-18,318	0,04157
ρ_2 cross Lhat			
0	0	18,3177	0,04157

$\beta_2-\beta_1$ = 0

2.Lhat=$\rho_2-\rho_1/|\rho_2-\rho_1|$			
unit vector Lhat			
0,88148	-0,47222	0	
ρ_1 cross Lhat			|rho cross Lhat|
0	0	-47,0647	0,274416
ρ_2 cross Lhat			
0	0	-47,0647	0,274416
β_2-β_1		0	

(as in definition for β_i in chapter 4)

APPENDIX L

Derivation of α_i, β_i quantities for the receding edge case

L.1 Expressing r_i/L

Expressing equation **??** in terms of $\boldsymbol{\rho_i}$ and γ quantities, yields

$$r_i/L = \left(\frac{\gamma^2 \boldsymbol{\rho_i} \cdot \boldsymbol{\rho_i}}{E^2} - \frac{2\gamma \boldsymbol{\rho_i} \cdot \hat{\mathbf{L}}}{E} + 1 \right)^{1/2} \tag{L.1}$$

$$r_i/L = 1 + \frac{1}{2} \left(\frac{\gamma^2 \boldsymbol{\rho_i} \cdot \boldsymbol{\rho_i}}{E^2} - \frac{2\gamma \boldsymbol{\rho_i} \cdot \hat{\mathbf{L}}}{E} \right) - \frac{1}{8} \left(\frac{\gamma^2 \boldsymbol{\rho_i} \cdot \boldsymbol{\rho_i}}{E^2} - \frac{2\gamma \boldsymbol{\rho_i} \cdot \hat{\mathbf{L}}}{E} \right)^2 + O(\gamma^3) \tag{L.2}$$

Eliminating terms of order γ^3 and above from the squared expression, yields

$$r_i/L = 1 + \frac{1}{2} \left(\frac{\gamma^2 \boldsymbol{\rho_i} \cdot \boldsymbol{\rho_i}}{E^2} - \frac{2\gamma \boldsymbol{\rho_i} \cdot \hat{\mathbf{L}}}{E} \right) - \frac{1}{8} \left(\frac{4\gamma^2 (\boldsymbol{\rho_i} \cdot \boldsymbol{\rho_i})(\hat{\mathbf{L}} \cdot \hat{\mathbf{L}})}{E^2} \right) + O(\gamma^3) \tag{L.3}$$

and

$$r_i/L = 1 + \left(\frac{\gamma^2 \boldsymbol{\rho_i} \cdot \boldsymbol{\rho_i}}{2E^2} - \frac{2\gamma \boldsymbol{\rho_i} \cdot \hat{\mathbf{L}}}{2E} \right) - \left(\frac{\gamma^2 (\boldsymbol{\rho_i} \cdot \hat{\mathbf{L}})(\boldsymbol{\rho_i} \cdot \hat{\mathbf{L}})}{2E^2} \right) + O(\gamma^3) \tag{L.4}$$

ordering terms to decreasing powers of γ

$$r_i/L = 1 + \gamma^2 \left(\frac{\boldsymbol{\rho_i} \cdot \boldsymbol{\rho_i}}{2E^2} - \frac{(\boldsymbol{\rho_i} \cdot \hat{\mathbf{L}})(\boldsymbol{\rho_i} \cdot \hat{\mathbf{L}})}{2E^2} \right) - \gamma \frac{\boldsymbol{\rho_i} \cdot \hat{\mathbf{L}}}{E} + O(\gamma^3) \tag{L.5}$$

L.2 Defining α_i, β_i

To compromise with the form $(\alpha_i \gamma^2 + \beta_i \gamma + 1)$, we substitute γ^2 and γ constant multipliers from equation L.5 with α_i, β_is, which yields

$$\begin{aligned}
\alpha_i &= \frac{\boldsymbol{\rho_i} \cdot \boldsymbol{\rho_i} - (\boldsymbol{\rho_i} \cdot \hat{\mathbf{L}})(\boldsymbol{\rho_i} \cdot \hat{\mathbf{L}})}{2E^2} \\
&= \frac{||\boldsymbol{\rho_i} \wedge \hat{\mathbf{L}}||^2}{2E^2} \\
\beta_i &= -\frac{\boldsymbol{\rho_i} \cdot \hat{\mathbf{L}}}{E}
\end{aligned} \tag{L.6}$$

APPENDIX M

chapter 8 - Defining arctan at very small arguments ξs

arctan() re-defined as custom Atn()

$$arctan(L\xi) - L\xi = (L\xi)^3 \mathrm{Atn}(L\xi) \tag{M.1}$$

$$arctan(L\xi) = (L\xi)^3 \mathrm{Atn}(L\xi) + L\xi \tag{M.2}$$

$$arctan(L\xi) = L\xi((L\xi)^2 \mathrm{Atn}(L\xi) + 1) \tag{M.3}$$

Arctan at small arguments, divided by L

$$arctan(L\xi)/L = \xi((L\xi)^2 \mathrm{Atn}(L\xi) + 1) \tag{M.4}$$

where

$\mathrm{Atn}(x) = (-x^3/3 + x^5/5 - ....x^{2n+1}/(2n+1)/x^3 = (-1/3 + x^2/5 - x^4/7 + ... + x^{2n-2}/(2n+1))$, for n=1..$\infty$
$\arctan(x) = x - x^3/3 + x^5/5 - .... + x^{2n-1}/(2n-1)$

(M.5)

APPENDIX N

Testing of the expression $\beta_2 - \beta_1$ for special cases of $\hat{\mathrm{L}}$

<table>
<tr><td>Data</td><td>x</td><td>y</td><td>z</td></tr>
<tr><td>ρ1</td><td>53</td><td>25</td><td>0</td></tr>
<tr><td>ρ2</td><td>109</td><td>-5</td><td>0</td></tr>
<tr><td>Lhat</td><td>0,707106781</td><td>-0,707106781</td><td>0</td></tr>
<tr><td>|ρ1+ρ2|</td><td>$|\rho_1-\rho_2|$</td><td></td><td></td></tr>
<tr><td>163,2298992</td><td>63,5295207</td><td></td><td></td></tr>
<tr><td>Testing formula</td><td></td><td></td><td></td></tr>
</table>

$$\frac{1}{2}\left(\frac{||\boldsymbol{\rho_i} \wedge \hat{\mathbf{L}}||}{E}\right)^2$$

<table>
<tr><td>case1
ρ2
Lhat.x</td><td>Lhat.y</td><td>Lhat.z</td><td></td></tr>
<tr><td>(rho1.x+rho2.x)/|rho1+rho2|</td><td>(rho1.y+rho2.y)/|rho1+rho2|</td><td>(rho1.z+rho2.z)/|rho1+rho2|</td><td></td></tr>
<tr><td>ρ_2 cross Lhat.x</td><td colspan="2">(ρ2y*(ρ1z+ρ2z)/|ρ1+ρ2|-ρ2z*(ρ1y+ρ2y)/|ρ1+ρ2|)</td><td>0</td></tr>
<tr><td>ρ2 cross Lhat.y</td><td colspan="2">ρ2z*(ρ1x+ρ2x)/|ρ1+ρ2|-ρ2x*(ρ1z+ρ2z)/|ρ1+ρ2|</td><td>0</td></tr>
<tr><td>ρ2 cross Lhat.z</td><td colspan="2">ρ2x*(ρ1y+ρ2y)/|ρ1+ρ2|-ρ2y*(ρ1x+ρ2x)/|ρ1+ρ2|</td><td>18,31772</td></tr>
<tr><td>|ρ2 cross Lhat|^2</td><td colspan="2">sqrt(ρ2 cross Lhat.x^2+ρ2 cross Lhat.y^2+ρ2 cross Lhat.z^2)</td><td>18,318</td></tr>
<tr><td>ρ1</td><td></td><td></td><td></td></tr>
<tr><td>ρ_1 cross Lhat.x</td><td colspan="2">(ρ1y*(ρ1z+ρ2z)/|ρ1+ρ2|-ρ1z*(ρ1y+ρ2y)/|ρ1+ρ2|)</td><td>0</td></tr>
<tr><td>ρ_1 cross Lhat.y</td><td colspan="2">ρ1z*(ρ1x+ρ2x)/|ρ1+ρ2|-ρ1x*(ρ1z+ρ2z)/|ρ1+ρ2|</td><td>0</td></tr>
<tr><td>ρ_1 cross Lhat.z</td><td colspan="2">ρ1x*(ρ1y+ρ2y)/|ρ1+ρ2|-ρ1y*(ρ1x+ρ2x)/|ρ1+ρ2|</td><td>-18,3177</td></tr>
<tr><td>$|\rho_1$ cross Lhat|^2</td><td colspan="2">sqrt(ρ1 cross Lhat.x^2+ρ1 cross Lhat.y^2+ρ1 cross Lhat.z^2)</td><td>18,318</td></tr>
</table>

case2			
ρ2			
Lhat.x	Lhat.y	Lhat.z	
(rho1.x-rho2.x)/|rho1-rho2|	(rho1.y-rho2.y)/|rho1-rho2|	(rho1.z-rho2.z)/|rho1-rho2|	
ρ_2 cross Lhat.x	(ρ2y*(ρ1z-ρ2z)/|ρ1-ρ2|-ρ2z*(ρ1y-ρ2y)/|ρ1-ρ2|)		0
ρ2 cross Lhat.y	ρ2z*(ρ1x-ρ2x)/|ρ1-ρ2|-ρ2x*(ρ1z-ρ2z)/|ρ1-ρ2|		0
ρ2 cross Lhat.z	ρ2x*(ρ1y-ρ2y)/|ρ1-ρ2|-ρ2y*(ρ1x-ρ2x)/|ρ1-ρ2|		47,06473
|ρ2 cross Lhat|^2	sqrt(ρ2 cross Lhat.x^2+ρ2 cross Lhat.y^2+ρ2 cross Lhat.z^2)		**47,06473**
ρ1			
ρ_1 cross Lhat.x	(ρ1y*(ρ1z-ρ2z)/|ρ1-ρ2|-ρ1z*(ρ1y-ρ2y)/|ρ1-ρ2|)		0
ρ_1 cross Lhat.y	ρ1z*(ρ1x-ρ2x)/|ρ1-ρ2|-ρ1x*(ρ1z-ρ2z)/|ρ1-ρ2|		0
ρ_1 cross Lhat.z	ρ1x*(ρ1y-ρ2y)/|ρ1-ρ2|-ρ1y*(ρ1x-ρ2x)/|ρ1-ρ2|		47,06473
|ρ_1 cross Lhat|^2	sqrt(ρ1 cross Lhat.x^2+ρ1 cross Lhat.y^2+ρ1 cross Lhat.z^2)		**47,06473**

APPENDIX O

Solid Angle

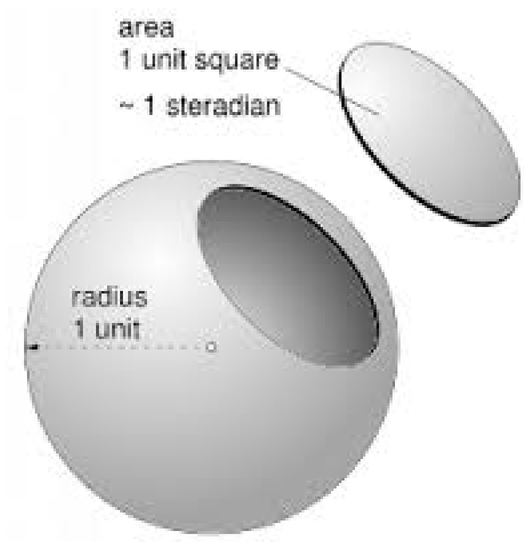

Figure O.1: Solid angle of 1 square unit, 1 steradian

$$A = r^2\Omega \tag{O.1}$$

where A=Area subtended by the solid angle

$$\Omega = 2\pi(1 - \cos\theta) \tag{O.2}$$

where Ω =Solid angle in steradians

Steradian as part of a sphere

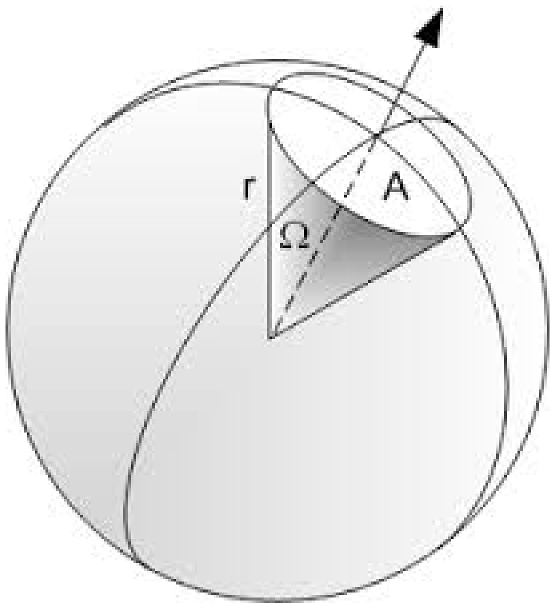

Figure O.2: Solid angle of 1 square unit, 1 steradian

$$1sr = \frac{1}{4\pi} \tag{O.3}$$

and

$$\Omega = \frac{A}{r^2} SR \tag{O.4}$$

where SR steradian units.

$$\Omega = 2[\arccos(\frac{\sin(\gamma)}{\sin\theta}) - \cos\theta \arccos(\frac{\tan\gamma}{\tan\theta})] \tag{O.5}$$

$$\tan\frac{1}{2}\Omega = \frac{\bar{a}\bar{b}\bar{c}}{\mathbf{abc} + (\bar{a}\dot{b})\mathbf{c} + (\bar{a}\dot{c})\mathbf{b} + (\dot{\bar{b}}c)\mathbf{a}} \tag{O.6}$$

the Oesterom version for a tetrahedron with base vertices a,b,c ,$\bar{a}, \bar{b}, \bar{c}$ edges from a,b,c to the apex angle Ω

APPENDIX P

Gravity Anomaly unification

P.1 Introduction

For 2 bodies with masses M,M_1 separated by r distance.

Gravity Newtonian force:
$f_p = G\rho\left(\frac{M,M1}{r^2}\right)$

$$\begin{aligned}\textbf{Gravitational constant: } G &= \frac{Nm^2}{kg^2}\\ \textbf{Density: } \rho &= \frac{kg}{m^3}\\ \text{N=Newton}&\\ \text{kg=kilogram}&\\ \text{m=meter}&\end{aligned} \tag{P.1}$$

P.2 Gravity potential f_p

In the expression for the gravity potential:

$$f_p = G\rho \int\limits_v \frac{dv}{r} \tag{P.2}$$

G has units : $\frac{Nm^2}{kg^2}$ ρ has units: $\frac{kg}{m^3}$ The integral nominator has units kg^3 and denominator m so finally the integral has units $\frac{kg}{m^3}$. Therefore we get:

$$f_p = G\rho m^2 = \frac{Nm^2 kg}{kg^2 m^3} m^2 = \frac{kg\frac{m}{sec^2} m^4 kg}{kg^2 m^3} = \frac{m^2}{sec^2} \tag{P.3}$$

P.3 Conclusions

Assuming that If we multiply the outcome by 1 outcome will not change, we get :

$$\frac{N}{m}\frac{sec^2}{kg} = 1 \tag{P.4}$$

and

$$\frac{N}{m}\frac{sec^2}{kg}\frac{m^2}{sec^2} = \frac{Nm}{kg} \tag{P.5}$$

The result units represent energy per unit mass, for the specified observation point and target.